Terms and Conditions of Use of Digitised Theses from Trinity College Library Dublin

Copyright statement

All material supplied by Trinity College Library is protected by copyright (under the Copyright and Related Rights Act, 2000 as amended) and other relevant Intellectual Property Rights. By accessing and using a Digitised Thesis from Trinity College Library you acknowledge that all Intellectual Property Rights in any Works supplied are the sole and exclusive property of the copyright and/or other IPR holder. Specific copyright holders may not be explicitly identified. Use of materials from other sources within a thesis should not be construed as a claim over them.

A non-exclusive, non-transferable licence is hereby granted to those using or reproducing, in whole or in part, the material for valid purposes, providing the copyright owners are acknowledged using the normal conventions. Where specific permission to use material is required, this is identified and such permission must be sought from the copyright holder or agency cited.

Liability statement

By using a Digitised Thesis, I accept that Trinity College Dublin bears no legal responsibility for the accuracy, legality or comprehensiveness of materials contained within the thesis, and that Trinity College Dublin accepts no liability for indirect, consequential, or incidental, damages or losses arising from use of the thesis for whatever reason. Information located in a thesis may be subject to specific use constraints, details of which may not be explicitly described. It is the responsibility of potential and actual users to be aware of such constraints and to abide by them. By making use of material from a digitised thesis, you accept these copyright and disclaimer provisions. Where it is brought to the attention of Trinity College Library that there may be a breach of copyright or other restraint, it is the policy to withdraw or take down access to a thesis while the issue is being resolved.

Access Agreement

By using a Digitised Thesis from Trinity College Library you are bound by the following Terms & Conditions. Please read them carefully.

I have read and I understand the following statement: All material supplied via a Digitised Thesis from Trinity College Library is protected by copyright and other intellectual property rights, and duplication or sale of all or part of any of a thesis is not permitted, except that material may be duplicated by you for your research use or for educational purposes in electronic or print form providing the copyright owners are acknowledged using the normal conventions. You must obtain permission for any other use. Electronic or print copies may not be offered, whether for sale or otherwise to anyone. This copy has been supplied on the understanding that it is copyright material and that no quotation from the thesis may be published without proper acknowledgement.

Aspects of Supramolecular Chemistry. Molecular Helicates and Coordination Polymers

Brian Conerney

B.Sc. *(Hons.)* (Rhodes)

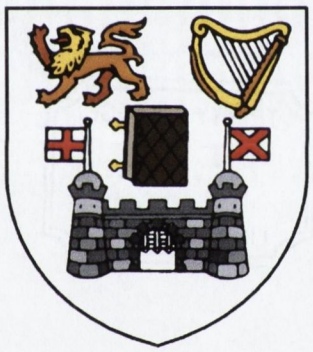

A thesis submitted to the University of Dublin for the degree of Doctor of Philosophy

Department of Chemistry

University of Dublin

August 2003

Declaration

This thesis has not been submitted as an exercise for a degree at any other University. Except where otherwise indicated, the work described herein has been carried out by the author alone. I, the undersigned, do also give permission to the Libraries of Trinity College, Dublin, to copy this thesis in whole or in part without further reference to me.

I give permission for the Library to lend or copy this thesis upon request.

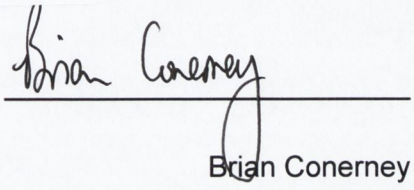

Brian Conerney

For Patricia, John and Lisa

"We choose to do these things, not because they are easy, but because they are hard, ... because that challenge is one that we are willing to accept, one we are unwilling to postpone"

John F. Kennedy
September 12, 1962

Acknowledgements

First and foremost I would like to express my gratitude to, Dr. Paul Kruger, for his supervision, encouragement and providing me the opportunity to study at Trinity.

I would like to thank Dr. Paul Jensen for his guidance and assistance provided to me on my "expedition" into the (often daunting!!) world of crystallography. A special mention must also go to Dr. Mark 'Woody' Nieuwenhuyzen at QUB for the structures solved before the CCD was working at TCD. I would also like to thank Dr. Tom McCabe for collecting data for me before Paul arrived.

Many thanks to all the academic staff in the Chemistry Department who have helped me get to this point. I am also indebted to the technical and secretarial staff, who have made life that bit easier! So to Fred, Patsy, John, Ed, Teresa, Seamus and the Cocker "techies", Corrinne, Tess and Helen thanks a million! Special thanks go to Dr. John O'Brien for his help with NMR and Dr. Martin Feeney for his help with ES-MS.

I would like to say a big thank you to all the members of the Kruger group, past and present. To the students Rob, Eithne, Murray, Sylvie, Karen, Michelle (×2!) Conchúir and the post docs Phil, Jensen and Fred, I say cheers okes!!

To all the other students and post docs in the department, especially the Gunnlaugsson and Draper groups I say thanks. A big thank you to Chris Fitchett for reading chapters so quickly in the final stages of this endeavour – much appreciated.

As far as the finances are concerned, I would like to acknowledge the Enterprise Ireland grant and the TCD College award, which I was fortunate enough to receive.

My friends who have helped me settle in Dublin and made my time here so enjoyable, many thanks must go to Gar, Tom, Joe, Rob, PJ & Clan (members of the "commentary tcheam"), Cags, Claire, Celine and Dan. To my mates from Malawi, Max and Gwynn many thanks for the last 15(!!) years.

A very special thanks must go to Aoife, who has put up with me for the last 3 years!

To my sister, Lisa, thanks for the support over the years and for the "top-ups" on my visits to see you!!

Finally I would like to thank Mom and Dad for their love and support over the years. It's has been a long ride and I think it's finally over!

Table of Contents

Declaration ii

Acknowledgements iv

Table of Contents v

Summary x

Abbreviations xii

Chapter One – Introduction. 1

1.1 Supramolecular chemistry. 2

1.1.1 Hydrogen-bonding. 2

1.2 Self-assembly. 5

1.2.1 Self-assembly in biological systems. 5

1.2.2 Self-assembly in unnatural systems. 6

1.3 Metallosupramolecular chemistry. 7

1.3.1 Rotaxanes. 8

1.3.2 Catenanes. 8

1.4 Molecular helicates. 10

1.4.1 Helicate components. 10

1.4.2 A brief introduction to double and triple helicates. 12

1.4.3 Linear nitrogen donating ligands for use in helicate formation. 12

1.4.4 Imine-based ligand systems. 16

1.5 Molecular architecture. 18

1.5.1 Design principles. 19

1.5.2 Molecular squares. 22

1.5.3 Molecular polyhedra - extension into the third dimension. 23

1.6 Polymeric frameworks. 26

1.6.1 'Crystal engineering' of coordination polymers. 26

1.6.2 Networks. 27

1.6.3 Interpenetration. 30

1.6.4 Metal-organic frameworks. 33

1.7 Solvothermal synthesis. 35

1.8 Present study. 37

Chapter Two – Synthesis and Characterisation of Molecular Helicates of Ag(I) and Cu(I) with C_2 and C_3 Symmetric Ligands. 38

Introduction 39

2.1 Preparation and characterisation of ligands. 40

2.1.1 Synthesis of *N,N',N''-tris*-pyridin-2-ylmethylene-4,4',4''-triaminotriphenyl-methane (**L3**). 41

2.1.2 Synthesis of *N,N',N''-tris*-phen-2-olmethylene-4,4',4''-triaminotriphenyl-methane (**H_3L4**). 43

2.1.3 Synthesis of *N,N'-bis*-pyridin-2-ylmethylene-4,4'-diaminodiphenylamine (**L5**). 44

2.1.3.1 Crystal structure of *N,N'-bis*-pyridin-2-ylmethylene-4,4'-diaminodiphenyl-amine (**L5**). 45

2.1.4 Synthesis of *N,N',N''-tris*-pyridin-2-ylmethylene-4,4',4''-triaminotriphenyl-amine (**L7**). 47

2.1.4.1 Crystal structure of *N,N',N''-tris*-pyridin-2-ylmethylene-4,4',4''-triaminotriphenylamine (**L7**). 48

2.1.5 Synthesis of *N,N',N''-tris*-phen-2-olmethylene-4,4',4''-triaminotriphenyl-amine (**H_3L8**). 51

2.1.5.1 Crystal structure of *N,N',N''-tris*-phen-2-olmethylene-4,4',4''-triaminotriphenyl-amine (**H_3L8**). 52

2.2 Complexation studies of L5 and L7 with Ag(I) and Cu(I) salts. 57

2.2.1 Complexation of *N,N'-bis*-pyridin-2-ylmethylene-4,4'-diaminodiphenylamine (**L5**) with Ag(I) salts. 57

2.2.2 Complexation of *N,N'-bis*-pyridin-2-ylmethylene-4,4'-diaminodiphenylamine (**L5**) with Cu(I) salts. 59

2.2.3 Complexation of *N,N',N''-tris*-pyridin-2-ylmethylene-4,4',4''-triaminotriphenylamine (**L7**) with Ag(I) salts. 61

2.2.4 Complexation of *N,N',N''-tris*-pyridin-2-ylmethylene-4,4',4''-triaminotriphenylamine (**L7**) with Cu(I) salts. 65

2.2.5 Preliminary UV-vis spectroscopic studies. 67

2.3 Conclusions. 68

Chapter Three – Coordination Polymers Incorporating 4,4'-Bipyridine. 70

Preamble. 71

Introduction....71

3.1 Reaction of Ru(II) with 2,2'-bipyridine, 2,2':4,4'':4',4'''-quaterpyridine (qpy)....72

3.1.1 Reaction of $Ru(2,2'\text{-bipy})_2Cl_2$ with qpy....72

3.1.2 Crystal structure of $[Ru(2,2'\text{-bipy})_2(qpy)][PF_6]_2 \cdot CH_3COCH_3$....73

3.1.3 Further complexation of $[Ru(2,2'\text{-bipy})_2(qpy)][PF_6]_2$....74

3.2 Reaction of Co(II) with 2,2'-bipyridine, 2,2':4,4'':4',4'''-quaterpyridine and 4,4'-bipyridine....75

3.2.1 Reaction of $Co(NO_3)_2$ with 2,2'-bipy and qpy....75

3.2.2 Reaction of $Co(NO_3)_2$ with 2,2'-bipy and 4,4'-bipy....76

3.2.3 Crystal structure of $[Co(4,4'\text{-bipy})_3(H_2O)_2][NO_3]_2 \cdot x(2,2'\text{-bipy}) \cdot y(4,4'\text{-bipy})$ (**1**)....77

3.2.4 Hydrothermal reaction of $Co(NO_3)_2$ with 4,4'-bipy (in the absence of 2,2'-bipy)....83

3.2.5 Crystal structure of $[Co(4,4'\text{-bipy})(H_2O)_4(4,4'\text{-bipy})_2][NO_3]_2 \cdot x(H_2O)$ (**2**)....83

3.3 Reaction of Ni(II) with 2,2'- and 4,4'-bipyridine....86

3.3.1 Reaction of $Ni(OAc)_2$ with 2,2'-bipy and 4,4'-bipy....86

3.3.2 Crystal structure of $[Ni(4,4'\text{-bipy})_2(OAc)_2(H_2O)_2] \cdot 2(H_2O) \cdot (MeOH)$ (**3**)....86

3.3.3 Reaction of $Ni(OAc)_2$ with 4,4'-bipy (in the absence of 2,2'-bipy)....90

3.3.4 Crystal structure of $[Ni(4,4'\text{-bipy})_2(OAc)_2(H_2O)_2]$ (**4**)....91

3.4 Reaction of Cu(II) with 4,4'-bipyridine....96

3.4.1 Hydrothermal reaction of $Cu(OAc)_2$ with 4,4'-bipy....96

3.4.2 Crystal structure of $Cu(4,4'\text{-bipy})(OAc)_2 \cdot 2.5H_2O$ (**5**)....96

3.5 Reaction of Zn(II) with 4,4'-bipyridine....101

3.4.1 Reaction of $Zn(OAc)_2$ with 4,4'-bipy....101

3.5.2 Crystal structure of $Zn(4,4'\text{-bipy})(OAc)_2$ (**6**)....102

3.6 Reaction of Cu(II) with and 4,4'-bipyridine in the presence of 1,4-benzenedicarboxylic acid....105

3.6.1 Hydrothermal reaction of $Cu(NO_3)_2$ with 4,4'-bipy and H_2bdc (1:1:2)....105

3.6.2 Crystal structure of $Cu(4,4'\text{-bipy})(NO_3)_2 \cdot xH_2O$ (**7**)....106

3.6.3 Crystal structure of $Cu(4,4'\text{-bipy})(NO_3)_2(H_2O)_2$ (**8**)....111

3.7 Conclusions....115

Chapter Four – Coordination Polymers of Cu(II) and Ni(II) Incorporating 4,4'-Bipyridine and 1,4-Benzenedicarboxylate..117

Introduction....118

4.1 Reaction of Cu(II) with 4,4'-bipyridine and 1,4-benzenedicarboxylic acid....119

4.1.1 Hydrothermal reaction of $Cu(NO_3)_2$ with 4,4'-bipy and H_2bdc (1:1:1)....119

4.1.2 Crystal structure of [Cu(4,4'-bipy)(bdc)(H_2bdc)]. (**9**) 120
4.1.3 Crystal structure of [Cu_4(4,4'-bipy)$_4$(bdc)$_3$(NO_3)$_2$(H_2O)$_2$] (**10**) 126
4.1.4 Crystal structure of [Cu(4,4'-bipy)(bdc)(NO_3)] (**11**) 139

4.2 Reaction of Ni(II) with 4,4'-bipyridine and 1,4-benzenedicarboxylic acid. 144
4.2.1 Hydrothermal reaction of $Ni(NO_3)_2$ with 4,4'-bipy and H_2bdc (1:1:1) 144
4.2.2 Crystal structure of [Ni(4,4'-bipy)(bdc)] (**12**). 144

4.3 Conclusions 148

Chapter Five – Materials & Methods, Experimental 151

5.1 Materials and methods 152
5.1.1 Reagents 152
5.1.2 Elemental analysis. 152
5.1.3 Nuclear magnetic resonance spectroscopy. 152
5.1.4 Infrared spectroscopy. 152
5.1.5 Electrospray mass spectrometry. 152
5.1.6 X-ray crystal diffraction. 153
5.1.7 Hydrothermal synthesis – acid digestion bomb 153

5.2 Experimental 154
5.2.1 Chapter 2. 154
N,N',N''-tris-pyridin-2-ylmethylene-4,4',4''-triaminotriphenylmethane (**L3**). 154
N,N',N''-tris-phen-2-olmethylene-4,4',4''-triaminotriphenylmethane (**H_3L4**) 155
N,N'-bis-pyridin-2-ylmethylene-4,4'-diaminodiphenylamine (**L5**). 155
tris(4-aminophenyl)amine. 156
N,N',N''-tris-pyridin-2-ylmethylene-4,4',4''-triaminotriphenylamine (**L7**). 156
N,N',N''-tris-phen-2-olmethylene-4,4',4''-triaminotriphenylamine (**H_3L8**) 156
Ag_3(**L7**)$_2$(PF_6)$_3$. 157
[Ag_2(**L5**)$_2$][BF_4]$_2$. 157
[Ag_2(**L5**)$_2$][PF_6]$_2$. 157
[Cu_2(**L5**)$_2$][BF_4]$_2$. 157
[Cu_2(**L5**)$_2$][PF_6]$_2$. 157
[Ag_3(**L7**)$_2$][BF_4]$_3$. 158
[Ag_3(**L7**)$_2$][PF_6]$_3$. 158
[Cu_3(**L7**)$_2$][BF_4]$_3$. 158
[Cu_3(**L7**)$_2$][PF_6]$_3$. 158
5.2.3 Chapter 3. 158
[Ru(2,2'-bipy)$_2$qpy][PF_6]$_2$ 158
Reaction of $Co(NO_3)_2 \cdot 6H_2O$ with 2,2'-bipy and qpy 159

Reaction of $Co(NO_3)_2 \cdot 6H_2O$ with 2,2'-bipy and 4,4'-bipy. (Structure **1**)..... 159
Hydrothermal reaction of $Co(NO_3)_2$ with 4,4'-bipy. (Structure **2**) 159
Reaction of $Ni(OAc)_2$ with 2,2'-bipy and 4,4'-bipy. (Structure **3**)..... 159
Reaction of $Ni(OAc)_2$ with 4,4'-bipy. (Structure **4**)..... 160
Reaction of $Cu(OAc)_2$ with 4,4'-bipy. (Structure **5**)..... 160
Reaction of $Zn(OAc)_2$ with 4,4'-bipy. (Structure **6**) 160
Hydrothermal reaction of $Cu(NO_3)_2 \cdot 3H_2O$ with H_2bdc and 4,4'-bipy.
(Structures **7** & **8**) 160
5.2.4 Chapter 4. 161
Hydrothermal reaction of $Cu(NO_3)_2$ with 4,4'-bipy and H_2bdc.
(Structures **9**, **10** & **11**)..... 161
Hydrothermal reaction of $Ni(NO_3)_2$ with 4,4'-bipy and H_2bdc. (Structure **12**) 161

Chapter Six – Future Work. 163

Future work..... 164

6.1 Molecular helicates. 164
6.1.1 Iterative development of dendrimer-like assemblies. 165
6.1.2 Small molecular entrapment. 165

6.2 Coordination Polymers..... 167

Appendix 168

Chapter 1..... 169

Chapter 2 – Ligand structures..... 171

Chapter 3..... 172

Chapter 4..... 174

Attached CD-ROM..... 176

Glossary 177

References 178

Summary

The research presented in this thesis lies within the general area of supramolecular and coordination chemistry. There are two facets to the work presented herein. Firstly, the syntheses and characterisation of novel helicate complexes are described. Secondly, the preparation and structural characterisation of novel coordination polymers is reported.

Chapter 2 details the synthesis of several novel Schiff's base ligands, with the view of employing them to form helicate species. The aim here was to extend a Schiff's base ligand family to incorporate C_3 symmetric ligands. To date, this field has been dominated by ligands possessing C_2 symmetry. The synthesis of two novel ligands (**L3** and **H_3L4**) based around a tetrahedral triphenylmethane bridging unit, to which are appended three bidentate coordination sites is described. However, these ligands are unstable in protic solvents, and so the central carbon atom of the bridging unit was replaced with a trigonal nitrogen atom (**L7** and **H_3L8**). The chemistry of these nitrogen bridge head systems, was first established through the formation of a C_2 symmetric analogue (**L5**). The crystal structures of each nitrogen-bridge head ligand is reported, as is their coordination to Ag(I) and Cu(I). The complexation of **L7** with Ag(I) was studied in detail through ^{1}H-NMR and ES-MS measurements. Complexiometric ^{1}H-NMR titrations of the metal salts with **L5**, and **L7** are also reported. Evidence from ^{1}H-NMR and ES-MS confirms that complexes formed with **L5** and **L7** have a metal-to-ligand ratio of 1:1 and 3:2, respectively.

Chapter 3 details the formation of first row transition metal containing coordination polymers. The initial goal of this work was to use the tetradentate ligand 2,2':4,4'':4',4'''-quaterpyridine (qpy) to form tetranuclear molecular squares. The successful formation and structural characterisation of a 'corner unit' of the square, $[Ru(2,2'\text{-bipy})_2(qpy)][PF_6]_2$, is reported. However, subsequent complexation in an attempt to form the molecular square proved problematic. Consequently, an alternative metal (Co(II)) was selected, and reacted with 2,2'-bipy and qpy. Analysis of the crystals by X-ray diffraction indicated that a polymeric structure had been formed. This polymeric structure was attributed to the presence of 4,4'-bipy. An identical product was obtained when the reaction was repeated with 4,4'-bipy substituted for qpy ($[Co(4,4'\text{-bipy})_3(H_2O)_2][NO_3]_2$ (**1**)). This provided the impetus for the preparation and structural characterisation of other novel coordination polymers. The structures of two novel Ni(II) coordination polymers ($[Ni(4,4'\text{-bipy})_2(OAc)_2(H_2O)_2]\cdot 2(H_2O)\cdot(MeOH)$ (**3**) and $[Ni(4,4'\text{-bipy})_2(OAc)_2(H_2O)_2]$ (**4**)) are reported. The hydrothermal synthesis of other first row transition metal coordination polymers is also reported in this chapter. The acetate salts of Cu(II), Ni(II) and Zn(II) were reacted hydrothermally with 4,4'-bipy to produce 1D

coordination polymers consisting of dimeric subunits, bridged by acetate groups. The common feature of the structures reported in Chapter 3 is that they all contain the linear bidentate ligand 4,4'-bipy, which acts as a linker unit along which polymeric chains extend.

Chapter 4 details the results obtained when nitrate salts of Cu(II) and Ni(II) were reacted with 4,4'-bipy and 1,4-benzendicarboxylic acid (H_2bdc). The rationale behind this combination was to employ a dicarboxylate moiety in an effort to link together the 1D polymeric chains of Cu(II) and Zn(II) reported in Chapter 3. The hydrothermal reaction of Cu(II) with 4,4'-bipy and H_2bdc, yielded three different crystalline products. The structure of ([Cu(4,4'-bipy)(bdc)(H_2bdc)] (**9**)) consists of a 2D coordination polymer, further connected into a 3D network of novel topology *via* hydrogen-bonding. Furthermore, three 3D networks interpenetrate, making the overall structure unique. The structure of ([Cu_4(4,4'-bipy)$_4$(bdc)$_3$(NO_3)$_2$(H_2O)$_2$] (**10**)), consists of an eight Cu(II) repeat unit, linked together in dimeric pairs to form an α-Po type network. Both chelating and bridging 1,4-benzenedicarboxylate (bdc) moieties are present in the structure, which forms networks that are doubly interpenetrated. The structure of ([Cu(4,4'-bipy)(bdc)(NO_3)] (**11**)) consists of a dimer containing polymeric chain which forms a 2D sheet. Nitrate anions coordinate to each of the metal centres in a sheet, and form a novel linkage between adjacent sheets. Although this connection has precedent in inorganic structures, no examples of this type of connection between metal/organic containing structures has been reported. The final compound reported in Chapter 4 is a Ni(II) containing 3D coordination polymer consisting of dimeric subunits of ([Ni(4,4'-bipy)(bdc)] (**12**)). The bdc groups are both bridging and chelating between the Ni(II) centres. The network formed is a doubly interpenetrated α-Po type system.

Abbreviations

1D	One-dimensional
^{1}H-NMR	Proton nuclear magnetic resonance spectroscopy
2,2'-bipy	2,2'-bipyridine
2D	Two-dimensional
3D	Three-dimensional
4,4'-bipy	4,4'-bipyridine
Å	Angstrom (10^{-10} m)
bdc	1,4-benzenedicarboxylate
CD_3CN	Deuterated acetonitrile
$CDCl_3$	Deuterated chloroform
$CHCl_3$	Chloroform
DCM	Dichloromethane
DMF	Dimethyl formamide
DMSO	Dimethyl sulfoxide
DNA	Deoxyribonucleic acid
dppp	Diphenylphosphine propane
ES-MS	Electrospray mass spectrometry
EtOH	Ethanol
g	Grams
H_2bdc	1,4-benzenedicarboxylic acid
hrs	Hours
IR	Infrared
L	Litres
M	Molar (mol/L)
m/z	Mass-to-charge ratio
mg	Milligrams
ml	Millilitres
MOF	Metal-organic framework
ng	Nanograms
NH_4PF_6	Ammonium hexafluorophosphate
nm	Nanometres
NO_3^-	Nitrate anion
OAc^-	Acetate anion
OTf^-	Trifluoromethansulfonate (triflate) anion
PF_6^-	Hexafluorophosphate anion

ppm	Parts per million
qpy	2,2':4,4'':4,4'''-quaterpyridine
RNA	Ribonucleic acid
SBU	Secondary building unit
TAPM	Triaminotriphenylmethane
terpy	Terpyridine
TMV	Tobacco Mosaic Virus
UV-vis	Ultra violet/visible spectroscopy
α-Po	α-polonium
δ	Chemical shift
μl	Microlitres
μm	Micrometres (microns)

Chapter One

Introduction.

1.1 Supramolecular chemistry.

Over the last twenty to thirty years an area of chemistry has developed that can be viewed as distinct from older or classical branches of chemistry. Supramolecular chemistry has been defined, by Lehn, as "chemistry beyond the molecule"[1] and has become a field of study in its own right. Lehn goes on to describe this field as "the chemistry of molecular assemblies and the intermolecular bond", concerning interactions *between* rather than *within* molecules.[2] This is different from the classical fields of chemistry where the properties and behaviour of like molecules are studied. The manner or architecture by which supramolecular systems are formed are a primary feature of study and involve the components being held together by non-covalent interactions. Essentially we can describe the field as the study of covalently bonded molecular building blocks held together in a predetermined fashion by non-covalent intermolecular forces.

The use of non-covalent interactions is widespread throughout Nature and much of the inspiration for designing supramolecular systems is drawn from studying the molecular interactions of larger biological species. This is reflected in the terminology used to describe supramolecular systems, frequently the interactions between molecules are described as host-guest or receptor-substrate. The types of interactions observed in supramolecular systems include: electrostatic interactions between oppositely charged species, hydrogen-bonding between complementary substituents, π–π interactions between aromatic rings, hydrophobic or solvatophilic interactions between appropriate functional groups and other donor acceptor interactions between Lewis donors and acceptors. Synthetic supramolecular chemistry often entails the generation of supramolecular systems through a pre-designed assembly of components, by employing the physico-chemical features of the previously mentioned intermolecular forces. The analogy of the building block in the formation of supramolecular systems coupled with the planned synthesis often means that these systems are frequently described as supramolecular architectures, where the molecular components are held together in a pre-determined arrangement with 'supramolecular glue', in the form of non-covalent forces.

1.1.1 Hydrogen-bonding.

One of the most prevalent non-covalent interactions employed both in Nature and by supramolecular chemists is the hydrogen-bond. However, what constitutes a hydrogen-bond? This is not a rhetorical question - currently a definitive answer does not exist. Ideas of what constitutes a hydrogen-bond are in a constant state of flux.[3, 4] Pauling in the 1940s gave the following definition "It has been recognised in recent

years that under certain conditions an atom of hydrogen is attracted by strong forces to two atoms, instead of only one, so it may be considered to be acting as a bond between them. This is called the *hydrogen-bond*. It is now recognised that [...] the hydrogen-bond is largely ionic in character and is formed only between the most electronegative atoms. [...] Although the hydrogen-bond is not a strong bond (its bond energy [...] being only about 5 kcal/mol*), it has great significance in determining the properties of substances."[5] Atkins provides a simple definition of the hydrogen-bond as "a link formed by a hydrogen atom lying between two strongly electronegative atoms".[6] Yet another definition was provided by Huyskens and co-workers, in 1991 "Specific interactions are short-range site-bounded cohesion forces that considerably weaken a given chemical bond of one of the partners. Hydrogen-bonding constitutes a particular case of specific interactions where the weakened chemical bond involves a hydrogen atom and a more electronegative one (in general O, N, S, halogens)".[7] These definitions are only a few of many definitions that have been proposed although most tend to refer to Pauling, a definition that was insightful and visionary when proposed.[3] For the purpose of this study the Pauling definition is adequate, however it should be borne in mind that in the intervening sixty years of chemical progress there are many examples (one being the C-H···O bond) of what are widely considered to be hydrogen-bonds that are precluded from Pauling's definition. There are a plethora of empirical definitions that usually reduce down to 'a hydrogen-bond exists where there is evidence that it exists'.[3] Insofar as this thesis is concerned a hydrogen-bond can be defined as a phenomenon of hydrogen and electronegative elements, as the hydrogen atom has no inner core of electrons, so the side of the atom facing away from the bond presents a virtually naked nucleus. This positive charge is attracted to the negative charge of an electronegative atom in a nearby molecule and because the hydrogen atom in a polar bond is electron-deficient on one side (*i.e.* the side opposite from the covalent bond) this side of the hydrogen atom can get quite close to a neighbouring electronegative atom (with a partial negative charge) and interact strongly with it (the closer it gets, the stronger the electrostatic attraction).[8] Frequently, in this body of work, the electrostatic interactions (hydrogen-bonds) occur between a water molecule and either a metal bonded ligand such as acetate or an adjacent water molecule. Figure 1.1 shows an example of hydrogen-bonds (dotted lines/multi-coloured line) ideal bond lengths and angles between water molecules are also included.

---

* 5 kcal/mol ~ 21 kJ/mol.

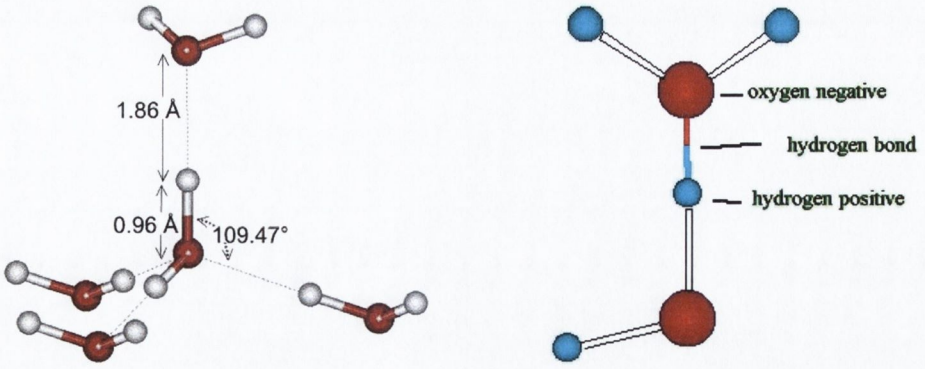

Figure 1.1 – Schematic representation of hydrogen-bonds between water molecules.

A subtle, yet important, point to note throughout this discussion is the fact that in order to achieve the formation of a hydrogen-bond both the electron deficient hydrogen atom and the electron rich oxygen atom must exist in the required orientation. This illustrates the concept of complementarity that is required for the formation of not only hydrogen-bonds, but for all non-covalent interactions between molecules. Another elegant example of this requirement is found in the base pairing in the deoxyribonucleic acid (DNA) double helix. The helix is composed of of two strands consisting of a phosphorylated sugar backbone, to which a series of purine and pyrimidine bases are connected. The strands generate a double helix by forming hydrogen-bonds between the bases. It is important to note that the four bases are arranged in such a manner that they form two complementary pairs. Adenine (A) forms two hydrogen-bonds with thymine (T) and guanine (G) complements cytosine (C) through the formation of three hydrogen-bonds. Figure 1.2 shows the interactions of the four bases.

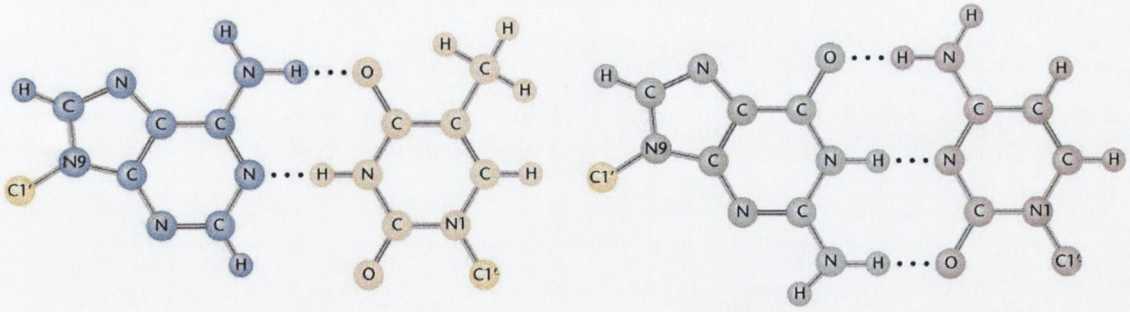

Figure 1.2 – Hydrogen-bonding between complementary base pairs in DNA.[9]

The complementarity extends from discrete base pairs throughout the whole helical structure, such that one strand (e.g. CCTTATA) is complementary to the other (e.g. GGAATAT).[10] The idea of complementarity in host-guest (receptor-substrate) chemistry can be traced from three concepts. Firstly, the recognition that molecules do not act if they do not bind. This was proposed by Ehrlich in 1906 and introduced the concept of a biological receptor. Secondly, Emil Fischer in 1894 recognised that binding must be selective and described the concept in the now familiar 'lock and key' image.

This laid the foundation for molecular recognition. Thirdly, the fact that selective binding must involve attraction or mutual affinity between host and guest. These three (essentially different) concepts were blended together over the years to give birth to the multidisciplinary field we now call supramolecular chemistry.[11] Steed and Atwood go on to say that "the binding sites must be spaced out on the host in such a way as to make it possible for them to interact with the guest in the binding conformation of the host molecule. If the host fulfils these criteria, it is said to be complementary".[11]

An inherent feature of complementary systems is the ability of either partner (the receptor or the substrate) to recognise one another. This leads to the concept of molecular recognition, which has its roots in the work of one of the forefathers of supramolecular chemistry, Charles Pedersen. The work of Pederson in the synthesis of crown ethers[12] laid the basis for the work done by fellow Nobel laureates Lehn (in forming cryptands[1, 2, 13]) and Cram (in host-guest elucidation[14]). The theory and practicalities of molecular recognition are far-reaching, and broad beyond the scope of this thesis. For further information the reader is directed to the many excellent reviews of this topic.[1, 2, 13, 14]

1.2 Self-assembly.

It was through the work in the spontaneous generation of inorganic helicates (Section 1.4) that Lehn and co-workers first introduced the concept of self-assembly.[15] Beyond the preorganisation (prepositioning) required in the formation of crown ethers, cryptands and other such complexes lies the design of systems that undergo self-organisation.[2] Lehn goes on to describe supramolecular self-assembly as "concerning the spontaneous association of either many or few components resulting in the generation of either discrete or oligomolecular supermolecules".[2]

Much of the inspiration behind the concept of self-assembly is drawn from biological systems.

1.2.1 Self-assembly in biological systems.

A favoured example of the phenomenon of self-assembly, in biological systems, is the tobacco mosaic virus (TMV), which is a helical virus particle 300 nm in length and 18 nm in diameter.[16] The viral particle consists of 2130 subunits each comprising 158 amino acids, which form a helical sheath around a single strand of ribonucleic acid (RNA), 6390 bases pairs in length. Figure 1.3 shows a schematic representation of this virus (the protein subunits are coloured blue). The mechanism of assembly of this virus has been studied extensively, and essentially involves the protein subunits forming a disk-shaped sub-assembly, which is transformed into a helical structure through the insertion of an RNA loop into the central hole of the protein disk. Additional protein disks

associate with the growing viral article, with each disk representing a double turn of the RNA helix.[16] The noncovalent interactions that hold the disk subassemblies together provide a facile route for the assembly or disassembly of the overall structure, due to the fact that the process is at or close to equilibrium. This means that the process is highly amenable to error-checking and if necessary self-correction.

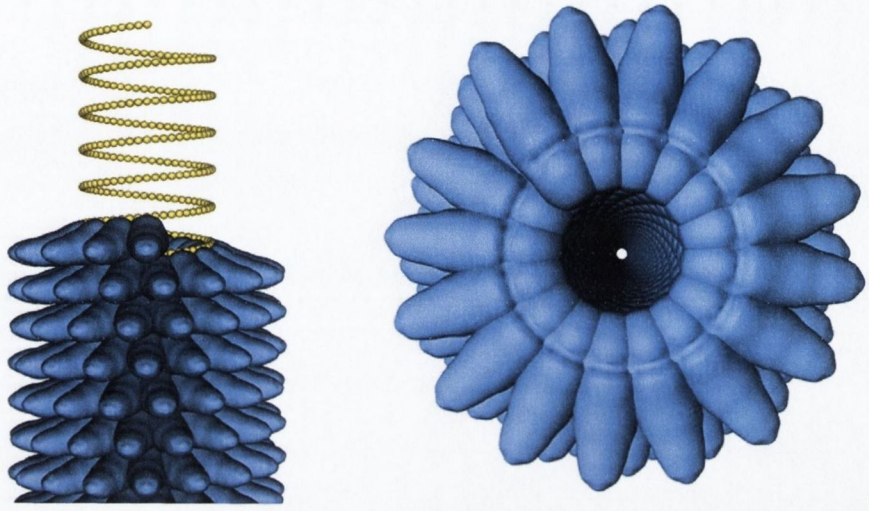

Figure 1.3 – Schematic representation of the tobacco mosaic virus.[17] (Note helical motif within the structure)

The above example demonstrates the ability of biological systems to employ the process of self-assembly to generate large ordered supramolecular arrays. It is important to keep in mind that Nature utilises a multitude of weak and easily reversible non-covalent interactions in this and many other self-assembling processes. It is from these kinds of examples that synthetic supramolecular chemists can draw inspiration.

1.2.2 Self-assembly in unnatural systems.

By analysing self-assembling biological systems we can learn several things. Firstly, self-assembling processes are economical by virtue of the fact that they are highly convergent. Secondly, the supramolecular assemblies can be rapidly, accurately and efficiently synthesised from relatively simple sub-units. Thirdly, the use of identical sub-units in the assembling process means keeping the diversity of interactions to a minimum. Finally, molecular recognition *via* many weak non-covalent bonding interactions leads to a reversible 'intelligent' synthetic pathway, which is self-checking and able to correct itself as and when required, and thus affords a product representing a thermodynamic minimum.[16]

There have been several attempts in the literature to define the term 'self-assembly'. Hamilton, in 1990, describes it as "the non-covalent interaction of two or more molecular subunits to form an aggregate whose novel structure and properties are determined by the nature and positioning of the components".[18] Whitesides and co-workers defined

self-assembly as "the spontaneous association of molecules under equilibrium conditions into stable, structured, well-defined aggregates joined by non-covalent bonds".[19] As far as this thesis is concerned, it will deal with self-assembling systems containing metal centres that are crucial in determining overall geometry of the superstructure (see Section 1.3 for further motivation for this). Stang and co-workers[20] have listed the following four points as common features of metal-mediated self-assembling systems:

(a) coordination bonds are utilised to hold self assembling units in position.

(b) assembly of subunits into larger aggregates is selective – the most stable aggregate is formed from cooperative binding of subunits.

(c) properties of the aggregates differ from those of the subunits and can be used to identify them from the subunits.

(d) aggregates formed are discrete rather than infinite.

This often precludes the formation of polymeric structures on the basis that the supermolecules formed are thermodynamically favoured and benefit from enthalpic and entropic effects.[20] (Although polymeric structures can be the desired product – see Section 1.6)

1.3 Metallosupramolecular chemistry.

The essential idea behind metallosupramolecular chemistry is to utilise the diverse possibilities, in terms of the photochemical, photophysical and electrochemical properties offered by transition metals. It is clear that the inclusion of metals into predominantly organic supramolecular structures increases the scope of this field tremendously. The controlled geometry around a metal centre allows metals to be used in a systematic manner as building blocks, responsible for connecting subunits in a controlled fashion. The metal will hold ligands together and will act as a centre orienting them in a given direction. In principle, the formation of any complex between a metal and a ligand is an assembly process that occurs spontaneously. The point to note is that the choice of both ligand and metal ion is crucial in producing the desired predefined architectures, in a controlled fashion. Metal ions have several properties that make them especially useful for applications in supramolecular assemblies:

(a) a set of coordination geometries

(b) a range of binding strengths from weak to very strong (from 2 kJ/mol to 250 kJ/mol), and of formation and dissociation kinetics, from labile to inert.[10]

(c) a variety of photochemical, electrochemical and magnetic properties.[8]

There are a plethora of examples of the use of metal ions in the formation of self-assembling supramolecular systems.

1.3.1 Rotaxanes.

One of the earlier examples of employing metal centres to form supramolecular assemblies is that of rotaxanes. Essentially a rotaxane consists of a linear molecule onto which is threaded a cyclic group. By controlling the constituents of both of the components, the rotaxane can be fine-tuned to allow the cyclic part to traverse along the shaft of the linear component, under certain specified conditions. There are many examples of these systems, some are completely organic in composition,[21, 22] and others have metal atoms located within the supermolecule. Such a metal containing rotaxane is shown in Figure 1.4. This compound was synthesised by Ogino and co-workers in 1981 and was spontaneously formed by the threading of α- or β-cyclodextrin onto a molecular thread, followed by capping the ends with a Co(III) complex.[23]

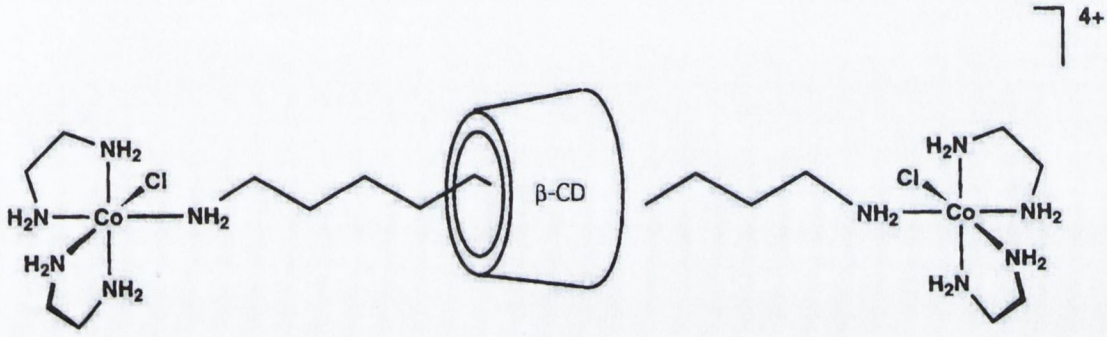

Figure 1.4 – Example of a self-assembling metal containing rotaxane.[23, 24]

1.3.2 Catenanes.

A catenane is a supermolecule consisting of two (or more) cyclic molecules that are interlinked. One of the methodologies employed in the synthesis of various supramolecular architectures is that of metal-templated synthesis. Sauvage successfully employed this technique in the formation of the organic catenane shown in Figure 1.5. Coordination of the phenanthroline groups to the Cu(I) centre allows them to be held in a predetermined fixed fashion whilst the remainder of the macrocycle is closed off. The metal is then removed leaving the organic catenane.

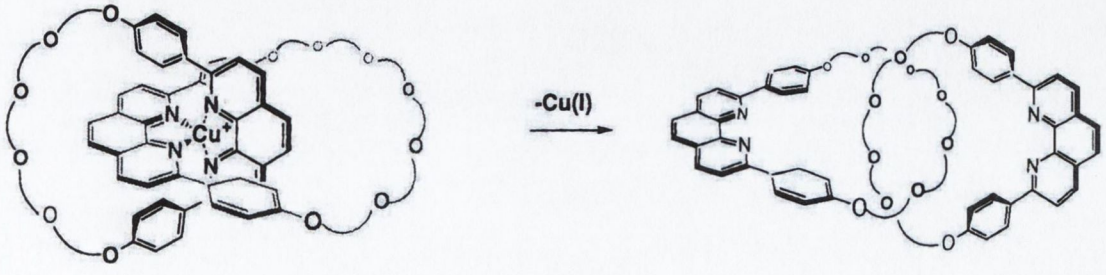

Figure 1.5 – Metal-templated synthesis of a catenane as reported by Sauvage and co-workers.[24]

There are also examples of catenane structures containing metal centres within the macrocycle, Fujita and co-workers[25] have shown that a large supramolecular architecture can self-assemble from the simple precursors ([A] and [B]) shown in Figure 1.6. It should be noted that the due to the reversible formation of pyridine-Pd(II) bonds, a rapid equilibrium exists between the [2]catenane ([C]) and the unlinked monomer ring ([D]). Confirmation that [C] had indeed been formed was given by various electrospray mass spectrometry (ES-MS) and nuclear magnetic resonance (NMR) data,[26, 27] this was complemented by an analogous compound made with Pt(II) which was fully characterised by X-ray crystallographic analysis. The mechanism of the interconversion between [C] and [D] has not been fully identified, although several have been proposed.

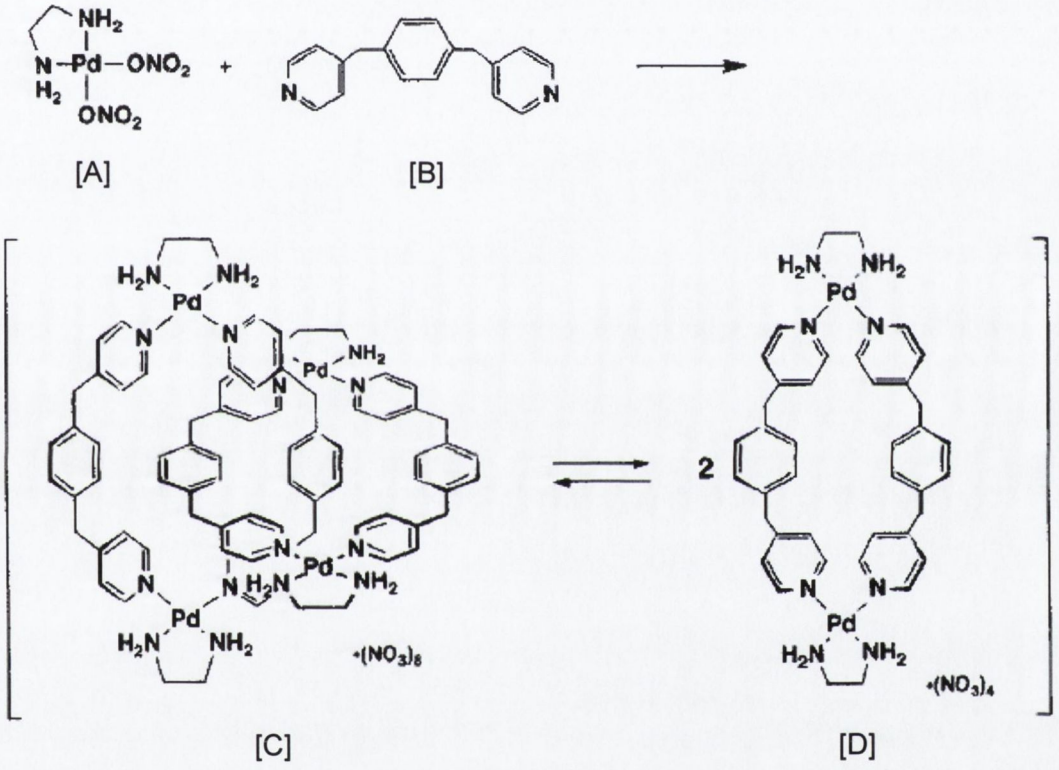

Figure 1.6 – Self-assembly of a [2]catenane as reported by Fujita and co-workers.[25]

Fujita has also shown that it is possible to utilise the concept of a "molecular lock" to "freeze" and "release" the equilibrium that exists between the catenane and the monocycle.[24, 27] This was how the crystallographic analysis was able to be performed on the Pt(II) counterpart system to that shown in Figure 1.6. The nature of the Pt(II)-pyridine coordination bond is such that under the correct conditions the irreversible nature of the Pt(II)-pyridine bond changes and becomes reversible.[24] A schematic of the process is shown in Figure 1.7. Initially, a molecular ring is formed that is locked. The lock is then released, by adding a salt (such as $NaNO_3$) and heating to 100 °C (process (a)). The system is then left in this state for 12 hrs, during which time the self-assembly of the interlocked rings occurs (process (b)). Finally, the framework is

locked together again, by removing the salt and cooling to form the catenane system (process(c)). Conveniently, the entire process can be followed through ^{1}H-NMR.[24]

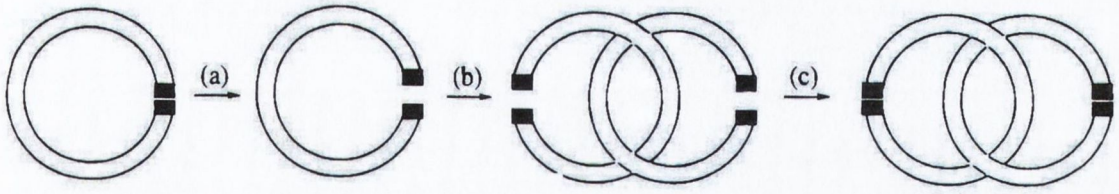

Figure 1.7 – Schematic representation of the procedure for the irreversible formation of a catenane from two complete rings using the molecular lock.[24] (Process (a): lock release (heating to 100 °C, in the presence of a salt). Process (b): self-assembly of interlocking rings. Process (c): locking of framework (removal of salt and cooling) to form the catenane.)

1.4 Molecular helicates.

A helix is a general structural motif that is found in both natural and unnatural structures.[28] There are many examples of the helical motif employed throughout biological systems, the most well known being DNA. DNA exists as a double helix, where the two strands are joined together through numerous hydrogen-bonds, between the base pairs on either strand.

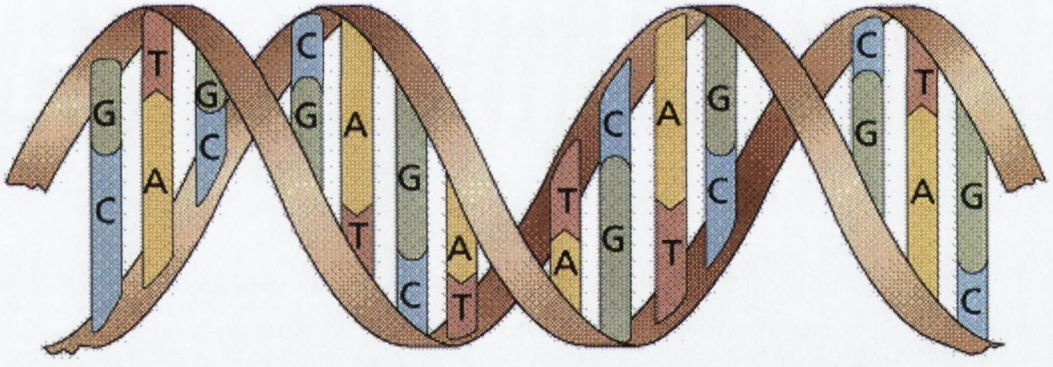

Figure 1.8 – Schematic representation of the B-DNA helical structure.

The hydrogen-bonding between individual base pairs is shown in Figure 1.2. The previous example of the TMV (Figure 1.3) also has a helical motif in its structure with the helical strand of RNA (represented by the yellow beads in Figure 1.3) being the backbone of the overall structure. Artificial structures can introduce helicity in various ways, conformational restrictions can be made of the macromolecules, inter- or intramolecular hydrogen-bonds, or coordination to metal ions.[28]

1.4.1 Helicate components.

Lehn introduced the term *helicate* in 1987[15] for metal complexes that contain two or more metal centres held together by one or more ligand strand.[15] The essential features of the helicate architecture are shown in Figure 1.9.

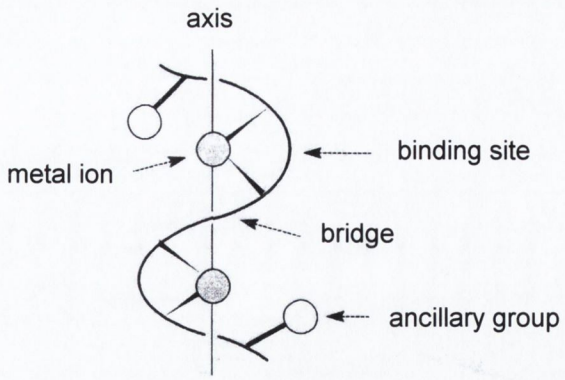

Figure 1.9 – Structural features of the helicate motif.[29]

As far as this report is concerned the helix motif is defined as: a coordination compound consisting of two or more metal centres, where all the ligand strands connecting two metal centres cross the metal-metal axis. An essential property of the helix as distinct from the non-helical arrangement is the possession chirality associated with a screw sense along a defined metal-metal axis.[30] Figure 1.10 shows the possible arrangements that could exist in the compound.

The structure in Figure 1.10(a) represents the nonhelical extreme that can form between two metals and two ligand strands. The alternative helical arrangement is shown schematically in Figure 1.10(b) and 1.10(c). As mentioned previously the nature of the chiral helicate means that there will exist two forms of the helicate. Structure (b) is represents the left-handed (M = Λ) helix, whilst (c) represents the right-handed (P = Δ) helix. It should be noted that the schematic representation shown in Figure 1.10 represent extreme forms of the complexes,[31] and that in reality the degree of twist associated with a helicate can vary.

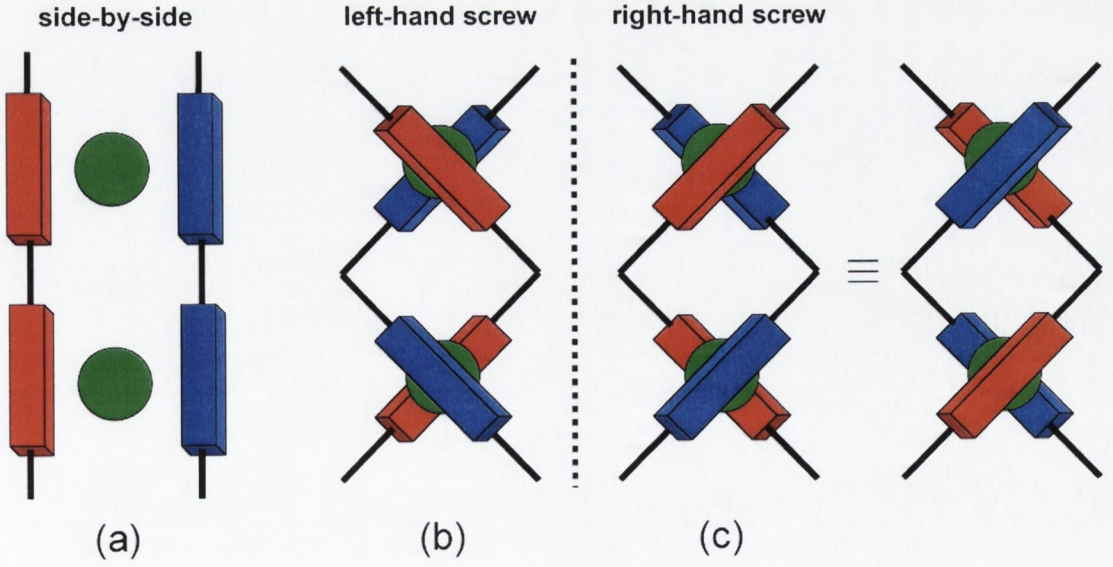

Figure 1.10 – (a) Nonhelical structure. (b) Left-handed helicate. (c) Right-handed helicate.[31]

1.4.2 A brief introduction to double and triple helicates.

By convention, a helicate containing two ligand strands linking a number of metal centres together is known as a double stranded helicate, or simply a double helicate. Similarly a helicate that has three ligand strands is known as a triple helicate. Often the number of metal centres is also mentioned, so the helicates shown in Figure 1.10(b) and (c) can be called examples of dinuclear double helicates since they possess two metal centres (dinuclear) and are double helicates (two strands).

Examples of double and triple helical complexes were known before Lehn formally introduced the term *helicate*. In 1976, Fuhrhop[32] and co-workers synthesised a zinc octaethyl formylbiliverdinate complex that in the presence of acid dimerised to form a dinuclear complex. X-ray structure analysis showed that the complex formed an overall helical structure. In 1980,[33] dinuclear complexes containing silver(I) and copper(I) were formed with imino/bipyridine ligands. Again X-ray structure determination showed the presence of a dinuclear double helix motif in the solid state. Various other dinuclear double helix structures were formed and characterised using similar ligand systems, such as the tetramethyl-substituted 2,2':6',2'':6'',2'''-quaterpyridine ligand.[34]

Triple stranded helical coordination complexes had been known since the 1970s. In 1978, Raymond[35] described the formation of dinuclear complexes of Fe(III) and Cr(III) with the rhodoturlic acid ligand as well as a *bis*(hydroxpyridine) derivative[36] (as an unnatural analogue to rhodoturlic acid).

1.4.3 Linear nitrogen donating ligands for use in helicate formation.

2,2'-Bipyridine (2,2'-bipy) is a bidentate ligand that has seen extensive use in the formation of helicates. The use of nitrogen donating groups in coordination chemistry is well-studied. The sp^2-hybridised nitrogen atom embedded in an aromatic (or any unsaturated) system acts as an excellent donor. Substitution at the 6 and 6' position on a 2,2'-bipy allows for functionalisation into *oligo*-type ligands, consisting of several 2,2'-bipy binding groups joined through a bridging group. It was these types of ligands that Lehn and co-workers[15, 37] used in the formation of their polynuclear double helicates shown in Figure 1.11.

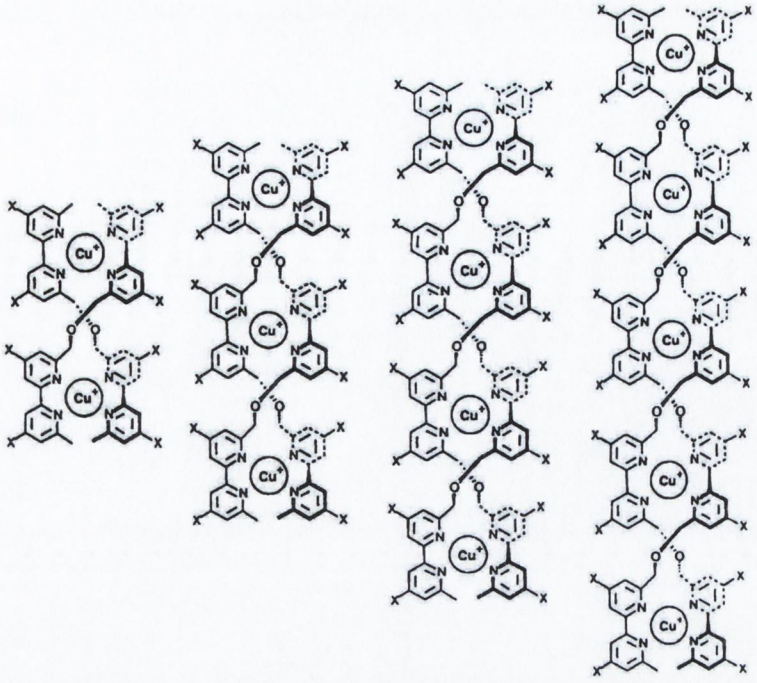

Figure 1.11 – Examples of the molecular helicates synthesised by Lehn and co-workers.[2]

There has been a large amount of work that has been carried out in the variation of functional groups within the ligands[28, 31, 38-40] shown in Figure 1.11. The common feature of all these (slightly different) ligands is that the helicate is formed by ligands wrapping themselves around a tetrahedral metal centre. By varying the bridging group and the binding site the helicate can be tuned to whatever desired properties are required of it.

An important point to remember whilst considering the synthesis of double and triple helicates (utilising oligonitrogen donor ligands) is that, just as the helicate is the desired product, the formation of the nonhelical form or meso-helicate[41] (side-by-side complex, mesocate[42]) is also possible.

One factor that can affect the formation of the helicate or the mesocate is the type of bridging unit within the ligand strand.[41] The three ligands shown in Figure 1.12 are all very similar ligands, the only differences between them is the number of bridging methylene groups, note that all the bipyridine units are connected through the 5-position. [A] has a single CH_2 bridging unit, [B] has three CH_2 bridging groups, whereas [C] has only two.

It has been noted that those ligands with an odd number of bridging CH_2 groups tend to form (almost exclusively) the achiral mesocate, whilst the ligands with an even number of CH_2 bridging units tend to form the chiral helicate.[28] The reason for this is that the preferred conformation of the alkyl chain is a zig-zag arrangement and when an odd number of methylene units is present, the overall molecule contains a mirror plane.

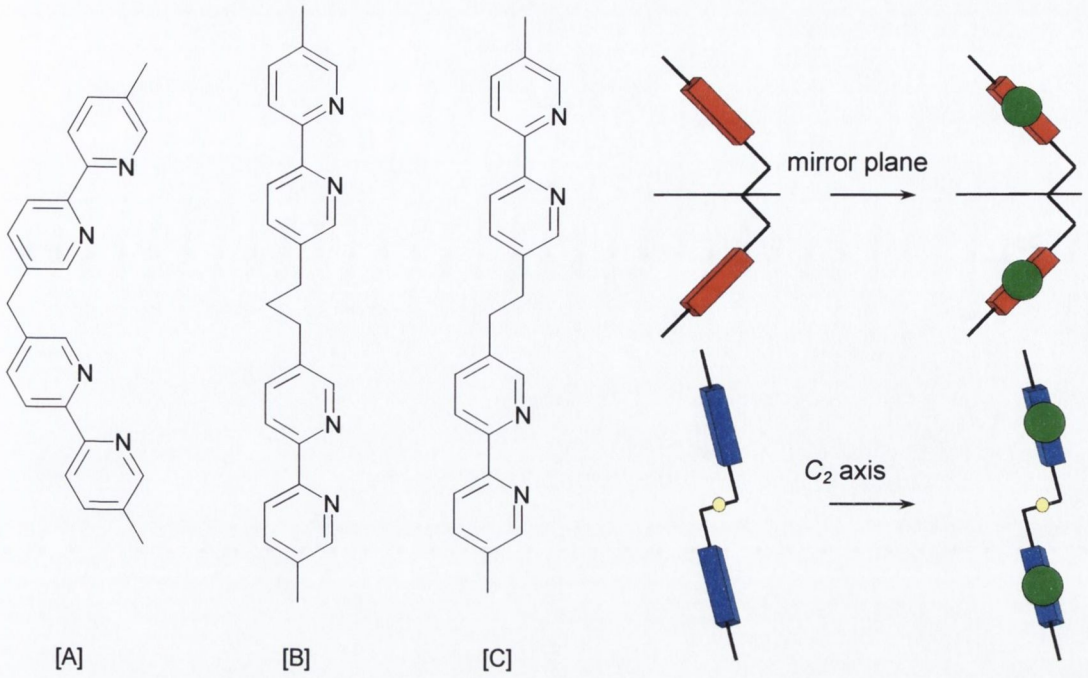

Figure 1.12 – *Left:* [A] single methylene bridged ligand, [B] triple methylene bridged ligand, [C] double methylene bridged ligand. *Right:* symmetry operators of methylene bridged ligands[28]

If this conformation is maintained through complexation to form a dinuclear complex it will force the formation of the mesocate. An even number of methylene units in the bridge results in a conformation that possesses a C_2 axis of symmetry, which upon complexation will yield the helicate.[28] This is shown in Figure 1.12.

Ligands also exist which possess different binding sites within the same strand. Figure 1.13 shows an example of a ligand strand[43] that has two different binding sites, and the Pd(II) complex it is able to form.[44, 45]

The ligand consists of two different metal binding sites, a terpyridine (terpy - tridentate - blue coloured) binding site as well as a bipyridine (bidentate – red coloured) binding site. Ligands with this arrangement are known as heterotopic ligands.[46] The arrangement of the ligand strands within the helicate means that there are different combinations to form a helicate. Should like binding sites (on each ligand) coordinate with a metal centre, the helicate is said to be aligned in a Head-to-Head manner.

A Head-to-Tail arrangement of a helicate is when heterotopic ligands align themselves so that different binding sites on each ligand strand are coordinated to a metal centre. This is schematically shown in Figure 1.14. (By this rationale, the heterotopic ligands in the Pd(II) complex shown in Figure 1.13(b) would therefore be in a Head-to-Tail arrangement.)

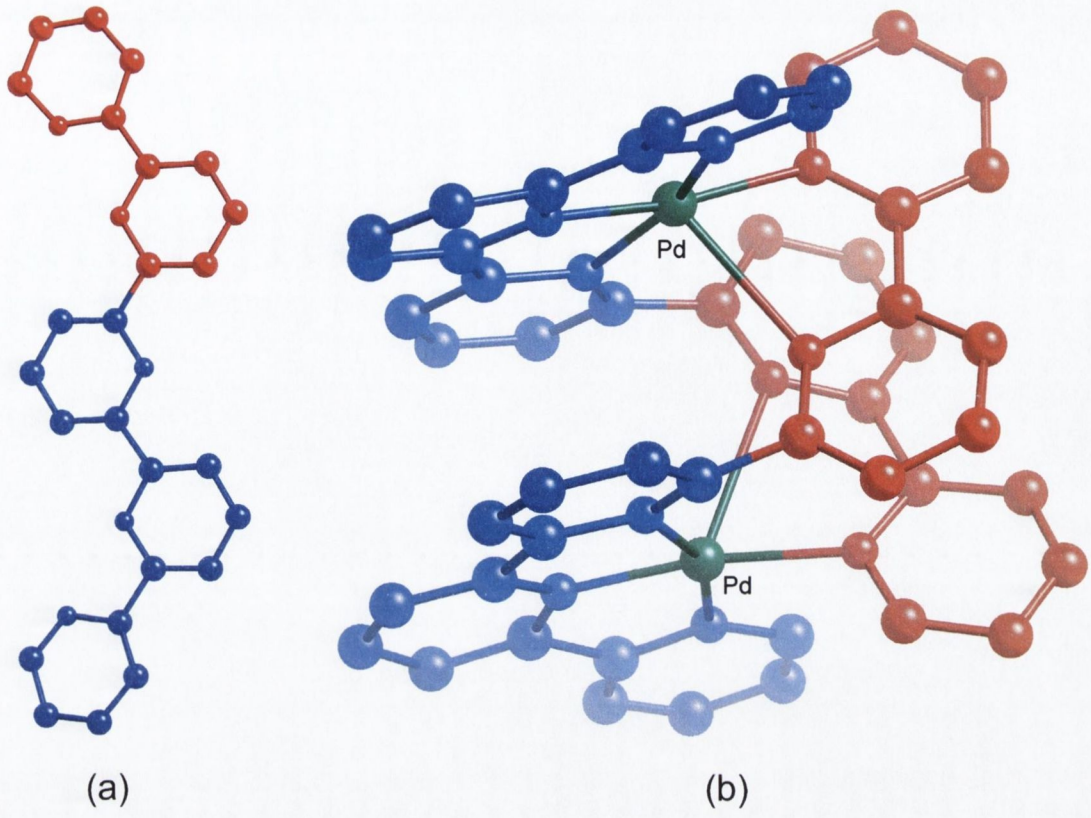

Figure 1.13 – (a) Quinquepyridine ligand strand with two different binding sites shown in different colours (2,2'-bipy binding site shown in red, terpy binding site shown in blue).[43]
(b) Dinuclear helicate Pd(II)-containing complex[44] formed.[†]

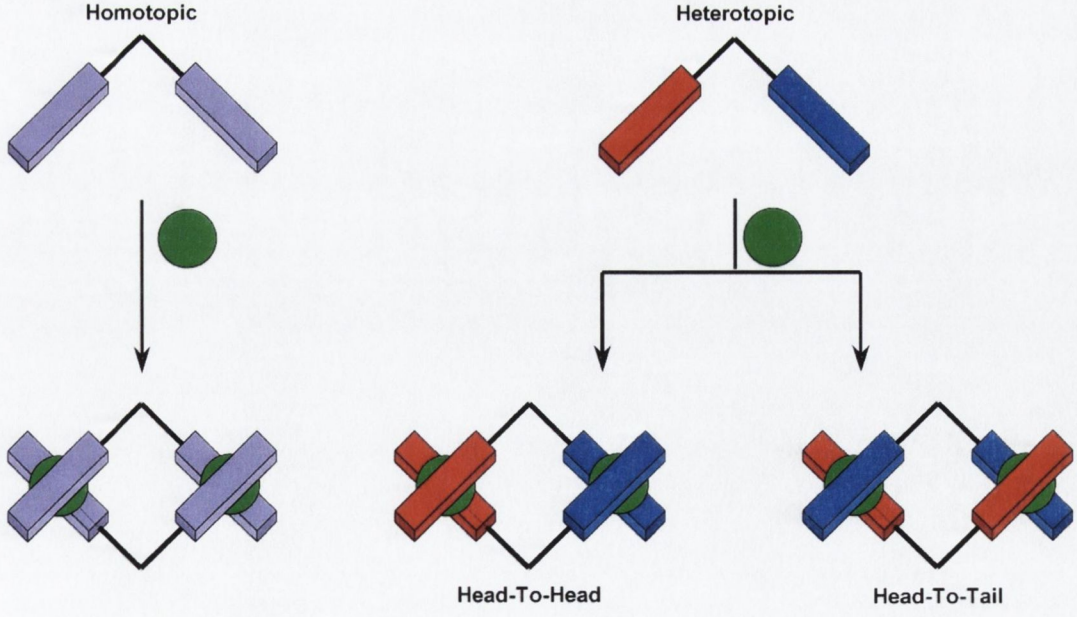

Figure 1.14 – Schematic showing homotopic and heterotopic ligand arrangement in helicate systems.[46]

[†] See Appendix for a space filling representation of this complex.

Much work has been done on synthesising heterotopic ligands for use in helicate formation.[45-49] The study of heterotopic ligands in the synthesis of molecular helicates is beyond the scope of this report, which is predominantly concerned with homotopic ligands.

1.4.4 Imine-based ligand systems.

Imine-based ligands are very easily synthesised, and are therefore readily available. Imines are formed in high yields by reacting aldehydes or ketones with amines.[50] A few examples of imine based ligand systems are shown in Figure 1.15. The ease of synthesis and abundance of starting compounds means that there are a plethora of possible imine ligands that can be formed.

Imine based ligand systems have seen extensive use in coordination chemistry, one of the first examples (Figure 1.15[A]) being that which McKenzie and co-workers used to form a dinuclear copper complex.[51] Although the term helicate was only introduced in 1987, the structure reported by McKenzie and co-workers, was reminiscent of what is today called a helicate.

Van Koten and co-workers used a similar ligand (Figure 1.15[B]) to that synthesised by McKenzie, except that a cyclohexane moiety was incorporated into the bridge between the imine groups. Upon complexation with two Ag(I) ions, a helicate is formed, although the author did not make a direct reference to the helical geometry of the complex.[52] (It is also interesting to note that van Koten reported coupling between the Ag(I) ion and the hydrogen of the imine.)

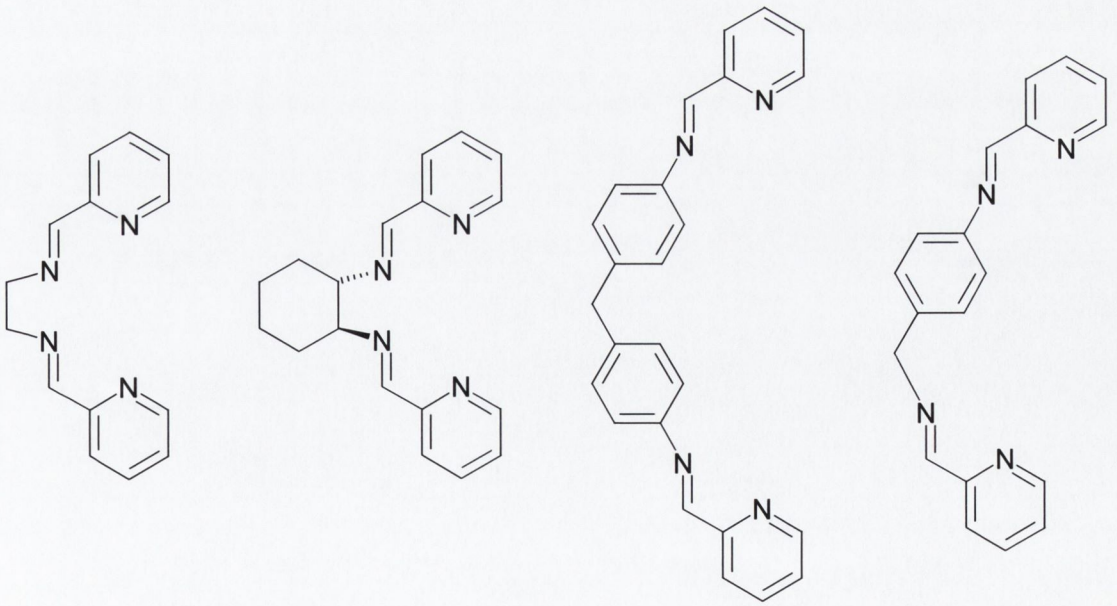

[A] [B] [C] [D]

Figure 1.15 – Imine containing ligand strands

Yoshida and co-workers have reported the synthesis of various imine containing helicate systems.[53, 54] Characterisation of these complexes have included using UV-vis titrations to establish the metal-to-ligand ratio within the helicate systems.[55]

Hannon has also reported the formation of various helicates and mesocates utilising imine based ligand systems. One of the first structures reported was a Ni(II) dinuclear triple helicate where the ligand was a pyridylimine system containing a methylene/diphenyl bridging unit (Figure 1.15[C]).

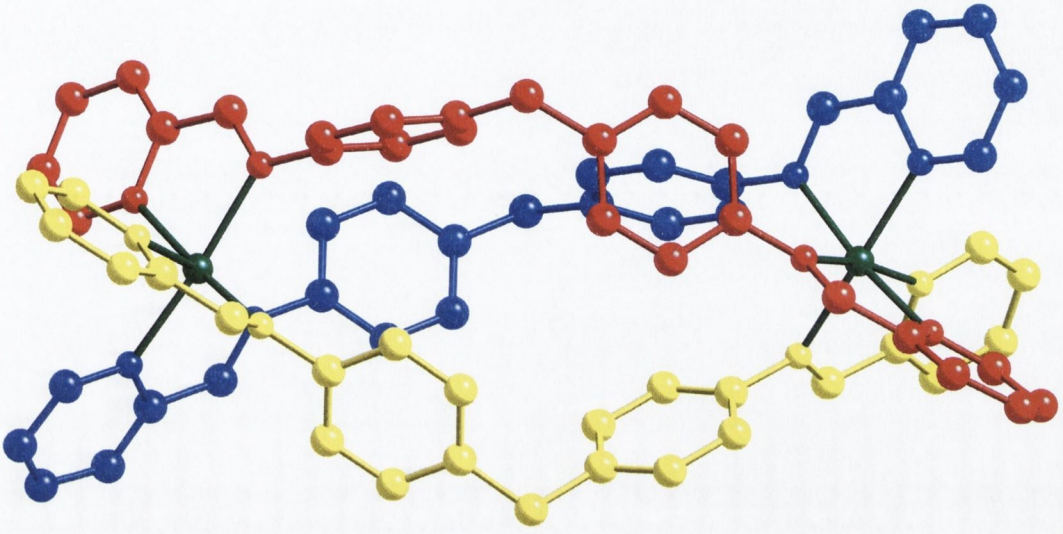

Figure 1.16 – Structure of a Ni(II) dinuclear triple helicate utilising an imine based ligand. (Each ligand strand shown in a different colour. Solvent molecules, counterions and hydrogen atoms omitted for clarity.)[50]

Work in the Kruger group in this area has involved the use the ligand shown in Figure 1.15[C], in the formation of both helicate and mesocate species. Complexation of this ligand with Cu(II) affords the helicate species, whilst complexation of Cu(I) with this ligand forms the mesocate species.[56] Functionalisation of this ligand, by altering the terminal pyridyl groups to phenolic moieties allows the formation of a ligand with both nitrogen- and oxygen-donating groups. The presence of the oxygen-donating group means that the charge balance can be completed without the need of counterions.[57] Recently Kruger and co-workers have reported the synthesis of the first dinuclear anion helicate species proving the versatility of this ligand system.[58]

Amongst the other helicates and mesocates reported by Hannon and co-workers[59-61] is a Ag(I) containing dinuclear double helicate. The ligand used is closely related to that shown in Figure 1.15[C] where a 1,1'-binapthalene derivative rather than a methylene/phenyl bridge is present. This has allowed for the stereoselective synthesis of one enantiomeric form of the helicate.[62] Non-symmetrical pyridylimine ligands have also been used in forming helicates. The ligand shown in Figure 1.15[D], which has a non-symmetrical geometry, has successfully been

complexed with Ag(I) metal to form a Head-to-Tail double helicate.[63] These types of ligands have proved highly popular with several groups utilising them in the ongoing study of helicate formation.[55, 64-66]

A closely related ligand system to that described above has been prepared by Williams and co-workers,[29, 67-69] where the imine moiety present in the ligand has been replaced by a benzimidazole group. The binding sites on the ligand strands remain bidentate with a pyridine ring providing the second coordination group to the metal. Figure 1.17 shows some of the ligands used in these helicates. The ligands incorporate bidentate and tridentate homotopic binding sites (Figure 1.17[A] and [B]) as well as a heterotopic ligand system – Figure 1.17[C].

Following on with the use of imidazole groups, other Schiff-base ligands where the pyridyl group has been replaced by an imidazole moiety have also been synthesised and complexed to form helicate structures. [66]

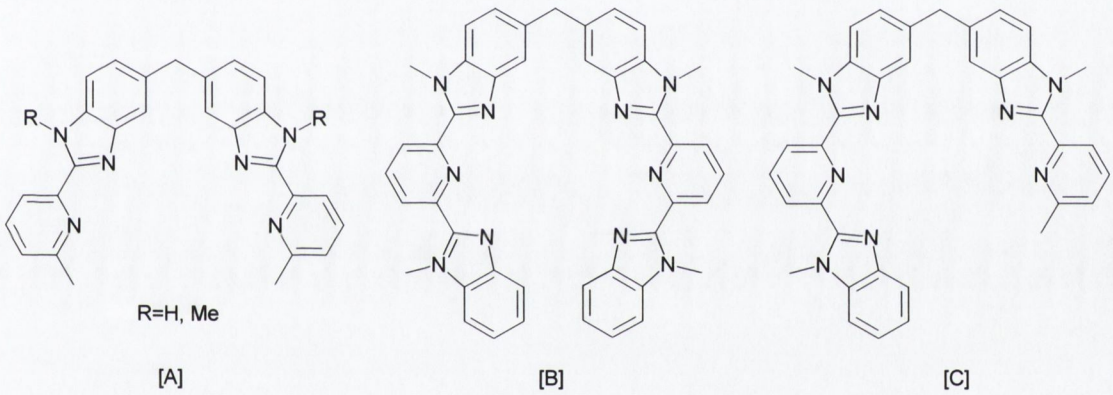

Figure 1.17 – Benzimidazole derivatives as ligands for helicate synthesis[29]

Clearly there are many permutations that are possible in the synthesis of imine-based ligands. The simple, easily controlled, step-wise construction of ligands along with the large array of available amines and aldehydes as starting materials means that the design of ligands is limited only by the imagination.

1.5 Molecular architecture.

The rapid growth in the field of supramolecular chemistry in recent years has allowed the synthetic chemist more control over larger molecules and supramolecular assemblies. The key to this has been the use of self-assembly in the construction of supermolecules. The concept of molecular architecture is derived from the synthesis of pre-designed macromolecules. In general the size of the assemblies that are being considered are in the 1 nm to 1 μm range, bringing them into the nanometre scale. Advances in this field of nanotechnology have broad applications in many fields.

The metallosupramolecular chemist can use the properties associated with metal ions together with the considerable range of ligands that are available to design and fine tune required features of the macromolecule. Vital to the synthesis of large macromolecules is the use of self-assembling systems. As previously stated (see Section 1.2.2) the use of so-called kinetically labile *'self-healing'*[20] coordination bonds between metals and ligands makes them ideal for large supermolecule synthesis. This report focuses on the formation of basic discrete geometric nanoscale shapes, for further information of the formation of multi-sided polygons and three dimensional polyhedra the reader is directed to several excellent reviews of this area.[20, 70-75]

1.5.1 Design principles.

The overall structural and functional characteristics are resultant from the information stored in their components. The presence of functional groups within subunits can dictate some of the overall properties of the macromolecule. The concept for generating structured architectures is through recognition derived self-assembly. As mentioned above, the synthetic chemist is able to vary both the metal centre and the orientation of the coordination sites of a ligand to achieve some control in the overall recognition ability of the subunits. Most commonly used binding components are nitrogen-containing heteroaryls, cyano-substituted aromatic ligands, *o*-catacholamides, hydroxamates and phosphorous-containing ligands.[20]

One of the approaches to design strategy is the so-called 'molecular library' model,[20] which was first applied by Verkade.[76] Fujita[25] extended this concept, and Stang[71, 77] systemised it.

Essentially this methodology employs rigid, highly directional multi-branched monodentate ligands, which bind to unsaturated metal complexes that have sites available for coordination to ligands. The principle behind the construction of any macrocyclic system can be broken down to that system consisting of any number of angular subunits (**A**) and linear bridging subunits (**L**). In the simplest case, where both the angular and linear subunits are ditopic (i.e. they have only two binding sites), then variation of the angle contained in **A** will result in the formation of convex molecular polygons,[20] this is shown in Figure 1.18.

The assembly of a planar triangle requires the combination of three angular subunits (each possessing a 60° turn) with three linear subunits (Figure 1.18(a)). A quadrangle can be constructed in several ways - that shown in Figure 1.18(b) consists of combining two different angular subunits. The sum of the angles contained between the angular subunits should add up to 180°. Similarly formation of a regular pentagon can be achieved by combining five linear subunits with five angular subunits that

possess an angle of 108°. A similar rationale can be applied in the formation of polygons containing higher numbers of sides.

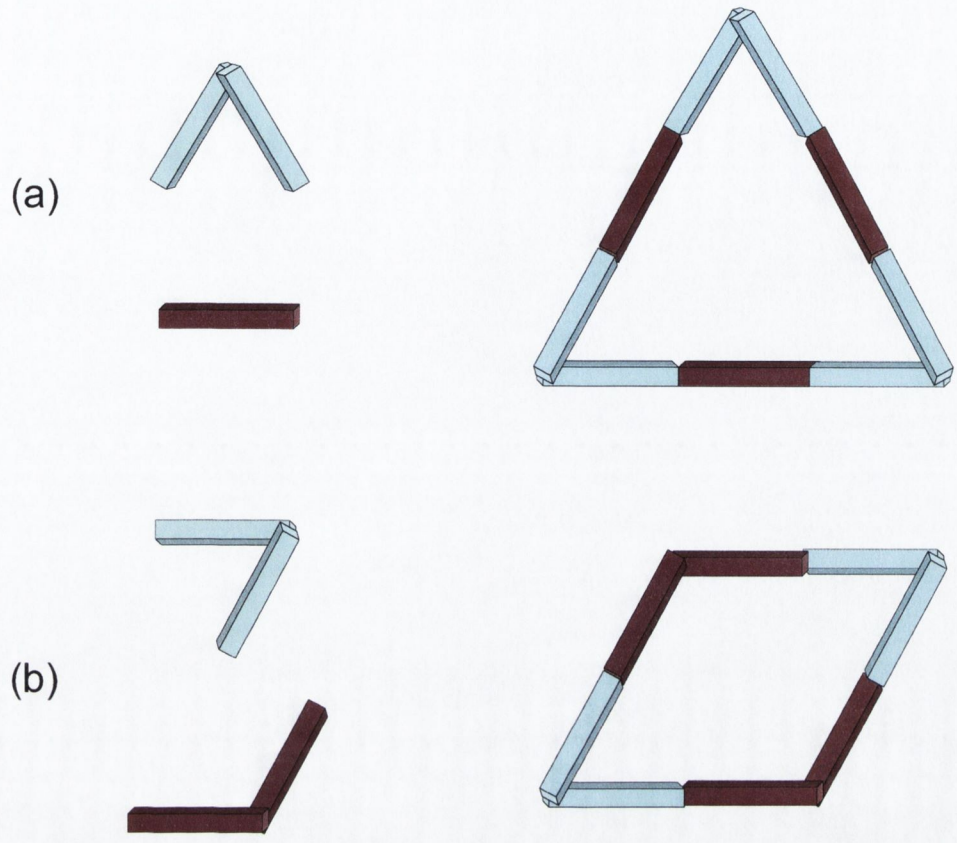

Figure 1.18 – Polygons formed from different angular and linear subunits. (a) Triangle formed from three angular subunits and three linear subunits. (b) Quadrangle formed from two sets of different angular subunits.[20]

One example of the formation of a molecular triangle is shown in Figure 1.19. Combination of $FeSO_4 \cdot 7H_2O$ with the ligand, in a 1:1 ratio immediately produced a deep violet colouration to the reaction mixture. Characterisation was done with ES-MS, and the presence of a trimeric species is accounted for by the formation of the triangular complex shown in Figure 1.19.[78] In this particular case, the angular subunit has the angle between terpyridyl binding sites set at approximately 60°, when combined with an octahedral metal centre (Fe^{2+}), which acts as a linear bridging subunit.

This example elegantly illustrates the concepts of ligands possessing inherent structural information as well as the self-assembly of macromolecules.

Whilst the subunits remain ditopic, the assemblies formed will generally be planar. Extending either one or both of the subunits' binding capability to three points of coordination, (i.e. a tritopic ligand) allows for the shape of the assembly to be extended into the third dimension. The same principle still applies in the formation of geometric polyhedra. This allows for the systematic formation of polyhedra such as tetrahedra, cubes and even higher faced polyhedra such as a dodecahedron. See Figure 1.20 for Stang's synthesis of a dodecahedron.[79]

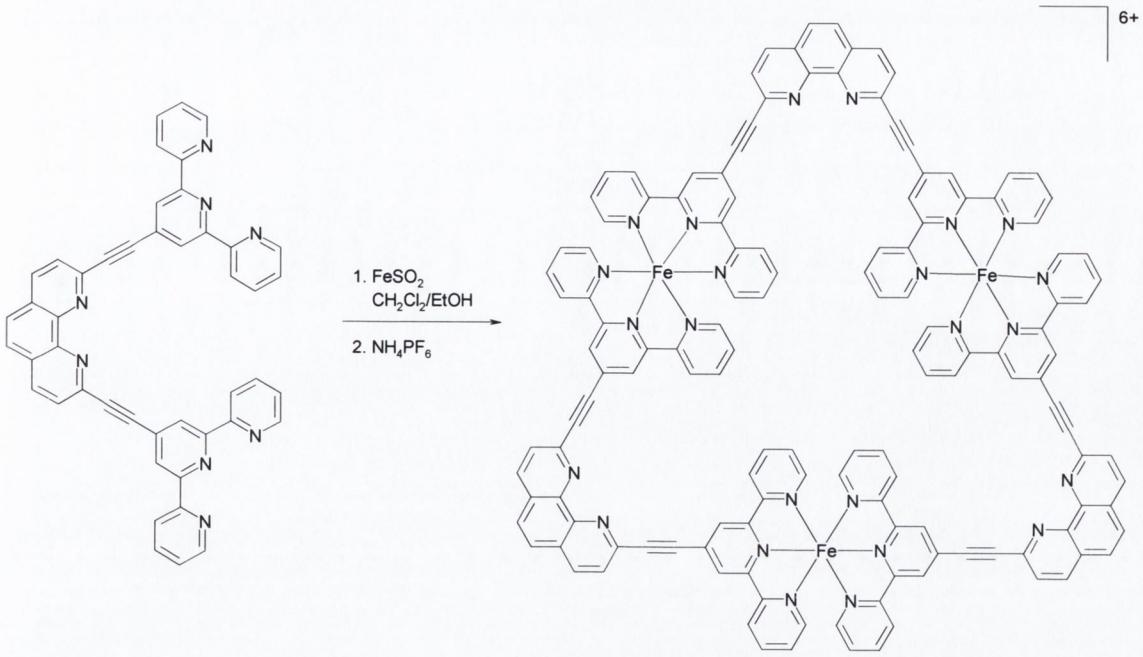

Figure 1.19 – Formation of a molecular triangle as reported by Ziessel and co-workers.[78]

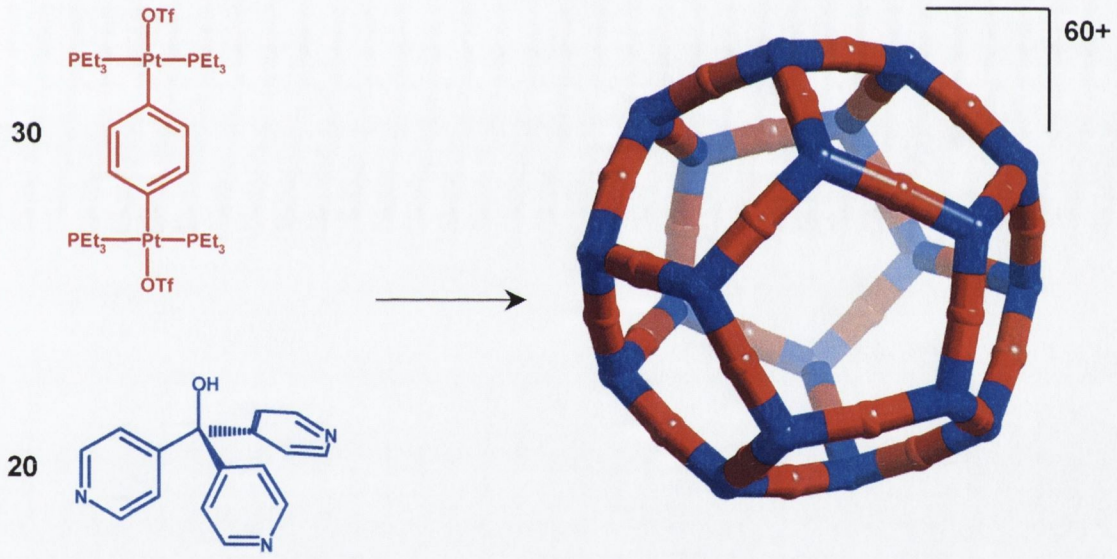

Figure 1.20 – Synthesis of a molecular dodecahedron ($[Pt_{60}L_{20}]^{60+}$), as reported by Stang and co-workers. [79]

The strength of this 'molecular library' approach lies in the possible combinations of linear and angular subunits. This 'combinatorial' approach means that one simply selects the desired angular and linear components (somewhat simple compounds), react them together, and allow the thermodynamically favoured product to form. Should the desired macromolecule not be formed, alternative subunits can be selected and the experiment repeated until the desired product has been obtained. This methodology allows for the formulation of combinatorial libraries from which building blocks can be selected.[20] It should be noted that it is paramount for the formation of

large architectures, that the angle(s) present within the angular subunit (**A**) remain constant throughout the assembly, this is assumed as an initial requirement of self-assembly (Section 1.2.2). In reality it is likely that there will be some deviation from the original binding angle, however, in most cases this is so slight that it can be ignored.[20]

1.5.2 Molecular squares.

Molecular squares represent one of the simplest macrocyclic assemblies that can be formed. Work carried out by Fujita and co-workers on the formation of dinuclear macrocycles has been previously mentioned (Section 1.3.2). Drawing on the fact that platinum and palladium tend to form tetracoordinate square planar complexes, Fujita and co-workers[80] reported the formation of the tetranuclear macrocyclic complex shown in Figure 1.21. It was also reported that the addition of the tetranuclear complex to an organic compound, 1,3,5-trimethoxybenzene, in a D_2O solution showed 'high field shifts' of the ^{1}H-NMR resonance peaks of the 1,3,5-trimethoxybenzene. This was attributed to the organic molecule being included into the cavity of the macrocycle.[80]

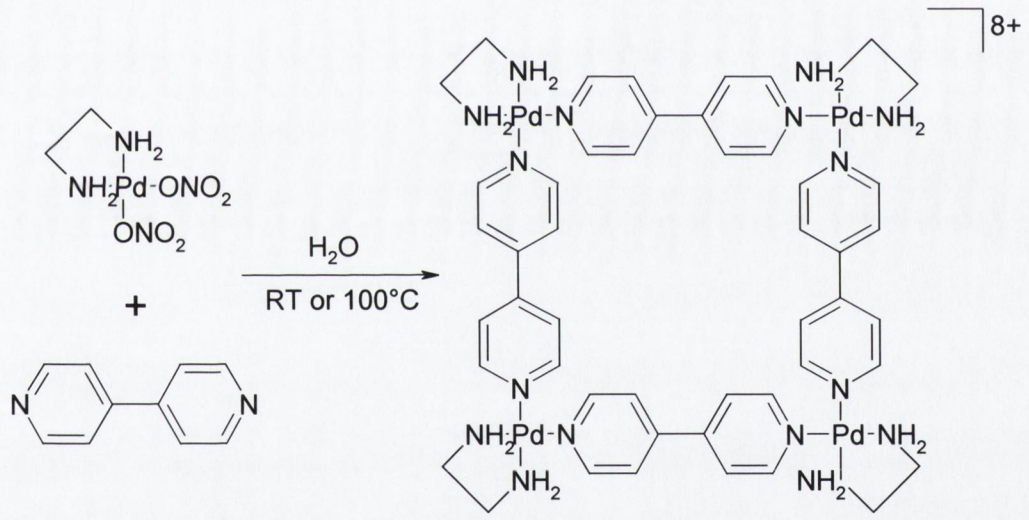

Figure 1.21 – Formation of a tetranuclear molecular square, as reported by Fujita and co-workers.[80]

In parallel with Fujita, Stang and co-workers,[81] have utilised building blocks containing lipophilic phosphine substituted and chelated bisphosphine platinum and palladium complexes to form molecular squares.[81]

The overall model used in the synthesis of these macromolecules employs a square planar metal centre coordinated to a linear bridging unit. Other examples of ditopic linear bridging units exist and these have been complexed with metal centres to form molecular squares.[82] The most obvious effect that changing the bridging unit will have is on the overall size of the cavity within the macrocycle. The nature of the bridging unit can also affect other physical properties of the aggregate. For example, a

highly conjugated fused aromatic system will tend to make the overall macromolecule more lipophilic in nature.

Along with those subunits described above there are many other angular subunits that have also been utilised in the synthesis of molecular squares. For example, an organometallic Pt-containing compound has been used as an angular subunit (Figure 1.22). This complex is also an example of a heterometallic molecular square.

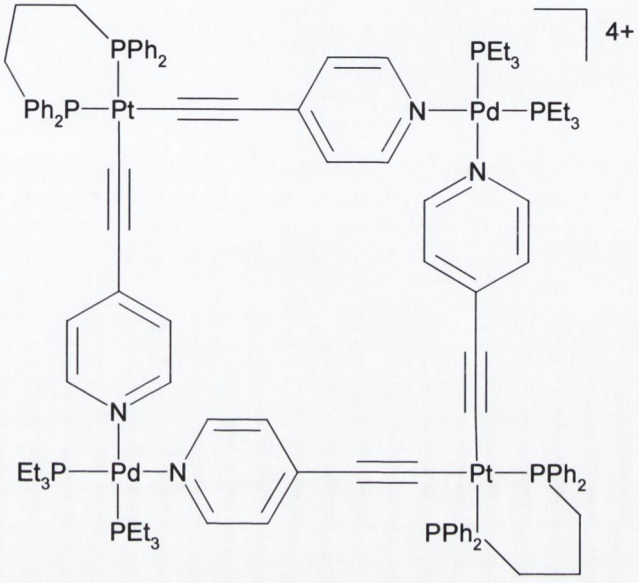

Figure 1.22 – An example of a heterometallic molecular square.[20]

For further elaboration on planar molecular squares the reader is referred to the large number of comprehensive reviews of this field.[20, 25, 70, 71, 75, 77]

1.5.3 Molecular polyhedra - extension into the third dimension.

As was mentioned above (Section 1.5.1), a tritopic angular subunit can be used to extend the geometric polygon to allow for the formation of three-dimensional polyhedra. One of the simplest platonic solids is a tetrahedron. The combination of four angular tritopic and six ditopic linear subunits will allow the formation of a tetrahedron shaped assembly.[20] Huttner and co-workers[83] reported the synthesis of a tetrahedral assembly utilising the 'molecular library' approach. The tritopic angular subunits consisted of an octahedral Fe(II) metal centre with three facial coordination sites blocked off by a tridentate phosphine ligand ($CH_3C(CH_2PPh_2)_3$). The linear bridging subunit which holds the tetrahedron together is the bidentate ligand fumaronitrile (NCC_2H_2CN). The preparation simply involved mixing the phosphine, $Fe(BF_4)_2 \cdot 6H_2O$ and fumaronitrile and allowing the system to self-assemble into the structure shown in Figure 1.23.

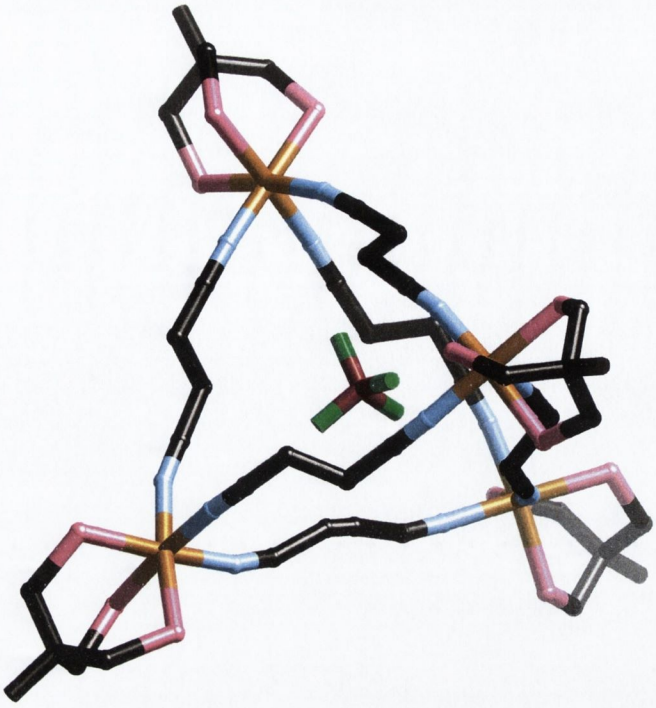

Figure 1.23 – Fe(II) containing molecular tetrahedron[83] (Fe-orange, P-pink; phenyl groups, hydrogens, solvent molecules and exterior counterions omitted for clarity)

An interesting feature of this assembly is that there is a single tetrafluoroborate anion encapsulated within the cavity of the tetrahedron. As can be seen the B-F bonds are pointing towards the iron centres, which may point to some kind of template-assisting in the assembly of this macromolecule.[20]

The cubic arrangement by definition requires eight corners perpendicular to each other. The first cubic system to be presented was the hydrocarbon parent species, the cubane, in 1964.[84, 85] Although there are examples of main group element-containing cubic systems[86-88] there are however, fewer transition metal-based self-assembled cubic systems.[20]

Thomas and co-workers[89] reported the formation of a cubic system comprising of eight octahedral corner units and twelve linear bridging units. The corner units consist of an octahedral ruthenium metal centre around which are positioned three 4,4'-bipyridine (4,4'-bipy) linear molecules and the remaining three coordination sites are occupied by the thiocrown ether [9]ane-S_3, which provide the corner itself. A reaction, in a non-coordinating medium, between [([9]ane-S_3)Ru(DMSO)Cl_2] with 4,4'-bipy in an 8:12 stoichiometry yielded a cubic arrangement. Characterisation was completed *via* ^{1}H-NMR spectroscopy, elemental analysis and ES-MS.[89]

The stepwise molecular library approach has successfully been applied to organometallic cubic structures. Rauchfuss and co-workers,[90-92] making use of the Prussian Blue type complexes,[93] have formed cubes consisting of molybdenum, cobalt

and rhodium metal centres held together by cyano bridges. One example is shown in Figure 1.24.

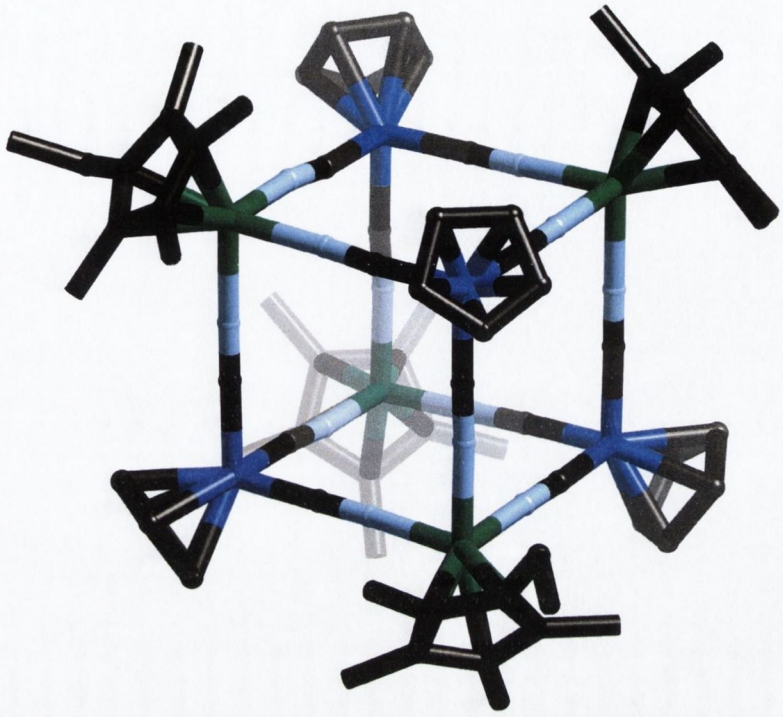

Figure 1.24 – Hetero-organometallic molecular cube[90] (Rh-green, Co-dark blue; hydrogens, solvent molecules and counterions omitted for clarity)

The cube is constructed systematically by initially forming the two-dimensional square and then extending to the third dimension, by removing blocking groups on the metal. Control of which metal centres are placed at which corner is also demonstrated by the authors, who also report the formation of the homometallic (solely Rh containing) square, as well as the Ru containing square.[90] The cube is not of perfect dimensions. The distance between two like metal centres within a face (e.g. the Rh-Rh distance) range from 7.1 Å (Co-Co) to 7.4 Å (Rh-Rh). The edge length (Co-Rh distance) is 5.1 Å and the angles between the cyano bridges vary from 85° to 95°, depending on metal centres. If one assumes an ideal cube whose angles are all 90°, and edges are 5.1 Å, the volume of the cavity is 132 $Å^3$.[90]

There are other examples of the synthesis of cubic shaped cages as well as higher polyhedra.[73, 94] These are beyond the scope of this thesis, however there are several excellent reviews of this area.[20, 70, 71, 77, 95]

It follows that the next logical step in the production of cage like structures is to make the step from forming discrete cubic entities to the formation of large networks consisting of interconnected cubes.

1.6 Polymeric frameworks.

The formation of large molecular frameworks is the natural progression from the controlled synthesis of discrete molecular cubes (or other polyhedra). Unblocking coordination sites around metal centres used in molecular squares or cubes allows for a polymeric system to develop. The term coordination polymer is used to describe a metal containing polymeric system where ligands are coordinated to metal centres. As with organic polymeric systems, solubility of coordination polymers can be limited and as a consequence, the solid-state properties of the coordination polymer are often the focus of attention. This means that structural analysis is heavily reliant on the formation of single crystals and X-ray crystallography. In fact, this is a benefit since physical and chemical properties of materials are largely dependent on their structure hence a measure of control over the structure allows for the manipulation of these solid-state properties. Desired properties of solids include magnetic (spin-crossover behaviour, long-range order), electrical (conductivity, semiconductivity, superconductivity), optical (transparency, non-linear optical behaviour), chemical (heterogeneous catalysis, solubility, topochemistry), and physical (microporosity, hardness) properties.[96] However, complete control (and predictability) of resultant physical and chemical properties remains, presently, an unattained objective.

1.6.1 'Crystal engineering' of coordination polymers.

Crystal engineering, essentially, aims to control the way in which molecules assemble in the solid state. The term implies that there is a measure of control over the resultant structure. The general idea behind crystal engineering has been around since the 1960s and is a very active area of research.[95, 97-107] The approach reported in 1990 by Hoskins and Robson,[108] describes the rational synthesis of new coordination polymers based on simple network prototypes. Robson's approach is to make an initial selection of a particular network (net) as a specific topological model on which to 'engineer' the structure.[109] In essence, a net is a topological concept and although some nets have real examples in the form of crystal structures, there are still many that have no real parallel and continue to provide a challenge to the crystal engineer. One example of this approach is the structure of diamond,[‡] which consists of tetrahedral carbon atoms connected together to give a simple 3D network. If the carbon atoms are replaced with tetrahedral metal centres (e.g. Cd(II)) and the C-C bonds with linear bridging ligands (e.g. cyanide), a new structure is formed ($[Cd(CN)_2]$) which has the same topology as diamond. In this case the C-C bonds of 1.54 Å are replaced with

[‡] See Appendix for a picture of the diamond network.

much longer Cd-CN-Cd bridges of 5.46 Å resulting in a very porous network and the structure actually consists of two identical interpenetrating networks.[108]

By controlling the geometry of metal ions and ligands it should be possible, in theory, to control the topology of the resulting network. The reality is, however, that molecules are often able to find different ways to link together depending on subtle factors such as choice of solvent or counter-ion. Different networks may also have the same nodal geometry but different topologies. In the example given above $[Cd(CN)_2]$ forms a diamond network, however there are other possible networks that might have formed, such as the lonsdaleite and quartz networks which also contain tetrahedral nodes.[§]

A polymorph of a structure contains the same chemical components but has a different packing mode in the solid-state. A similar situation exists for pseudopolymorphs, for which the chemical compositions differ only in the amount or type of solvent included. Polymorphism and pseudopolymorphism highlight the challenges presented to crystal engineers. Thus it is quite common to obtain unexpected results which are often more interesting than the original target structures.

1.6.2 Networks.

Twenty years ago, Wells[110] provided a survey of the simpler nets, however he noted that his compilation is not exhaustive, and that there does not exist an all-inclusive method of deriving nets. This has provided a useful catalogue of nets relevant to chemistry.

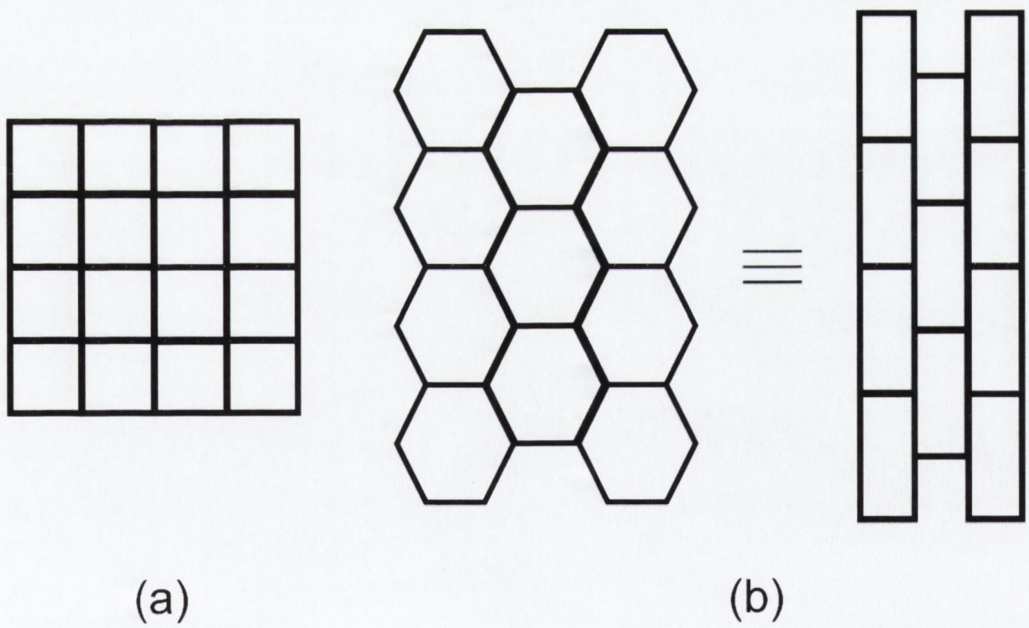

Figure 1.25 – (a) Schematic representation of the so-called (4,4) net. (b) Schematic representation of two geometrically different forms of the topologically equivalent (6,3) net.[111]

[§] See Appendix for a picture of the lonsdaleite and quartz networks.

One way to represent the topology or connectivity of a given net is in terms of the general symbol (n,p), where p is the number of connections to neighbouring nodes that radiate from any centre or node, and n is the number of nodes in the smallest closed circuits in the net. Thus, the number 6 in the symbol (6,3) indicates that the smallest complete circuits in the net are hexagons, and the number 3 indicates that each node is connected to three other nodes. Figure 1.25(b) shows two versions of the (6,3) net, which are geometrically different but topologically identical. This also illustrates the point that although nets may be geometrically deformed, provided no connections are broken, the topology is considered to remain unchanged.[111] A 'shortest circuit' is defined as the shortest circuit possible, which includes a given pair of links from a node. Thus, each pair of links from a node has a 'shortest circuit' associated with it. For each link emanating from a p-connected node there are (p-1) other links *via* which to return to the node. Hence for any node there are $p(p\text{-}1)/2$ 'shortest circuits'. The factor of $p(p\text{-}1)$ must be halved so that each 'shortest circuit' is not counted twice, since it does not matter from which direction the circuit is completed. As paradoxical as it may sound, the 'shortest circuits' for a given node are not necessarily all the same size. The (n,p) network notation strictly applies only when all the 'shortest circuits' originating from any node in the net are all n-gons (as is observed for the (6,3) network in Figure 1.25(b)).

When this is not the case the more complete Schläfli notation $n^{p(p\text{-}1)/2}$ should be used. In the network shown in Figure 1.25(a), four of the six 'shortest circuits' for each node involve four nodes (*cis* links[¶]), while the other two involve six nodes (*trans* links) In this case the complete Schläfli notation of $[4^4.6^2]$ should be used.[111] Wells simplified this to 4^4 or (4,4) by arbitrarily excluding circuits involving co-linear connections.[96]

The idea that nets can be topologically equivalent is useful when discussing networks. For example, the structure shown in Figure 1.26 is a hydrogen-bonded 2D network formed by large numbers of interconnected benzene-1,3,5-tricarboxylic acid (trimesic acid) molecules. This net is said to be topologically equivalent to the (6,3) net. Nodes within a net do not necessarily have to coincide with a particular atom within the structure. The nodes of the (6,3) net that can be used to represent the structure in Figure 1.26 are located in the centre of the benzene rings.

A number of 3D nets are often described by the names of materials displaying the relevant topology.

[¶] A *cis* link can be defined as a connector lying in a *cis* orientation to the connector traversed upon exiting the node. Similarly a *trans* link is a connector lying in a *trans* orientation to the exiting connector.

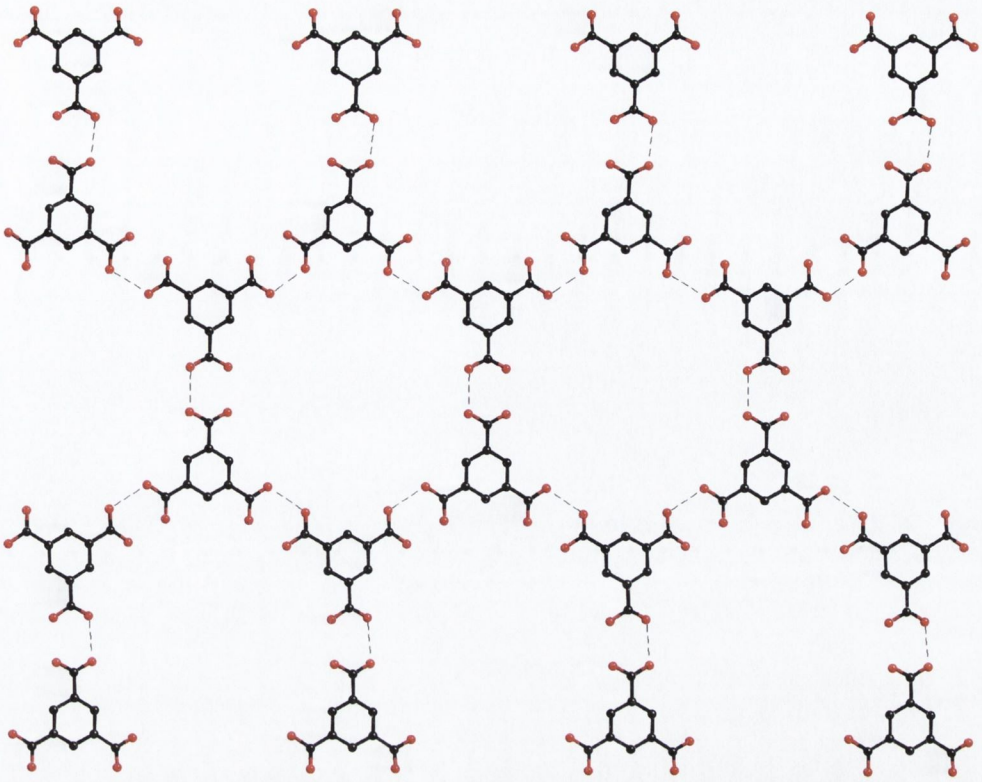

Figure 1.26 – Hydrogen-bonded network of trimesic acid molecules with a (6,3) topology. [112, 113]

Diamond, lonsdalite, and quartz have already been mentioned as examples of 3D nets with tetrahedral nodes. Another example is that of α-polonium (α-Po or NaCl), which contains six-connected octahedral nodes linked to form a cubic network (Figure 1.27(a)). There are a number of other simple 3D nets such as the NbO network shown in Figure 1.27(b), which contains square planar nodes with a 90° twist along each connection.

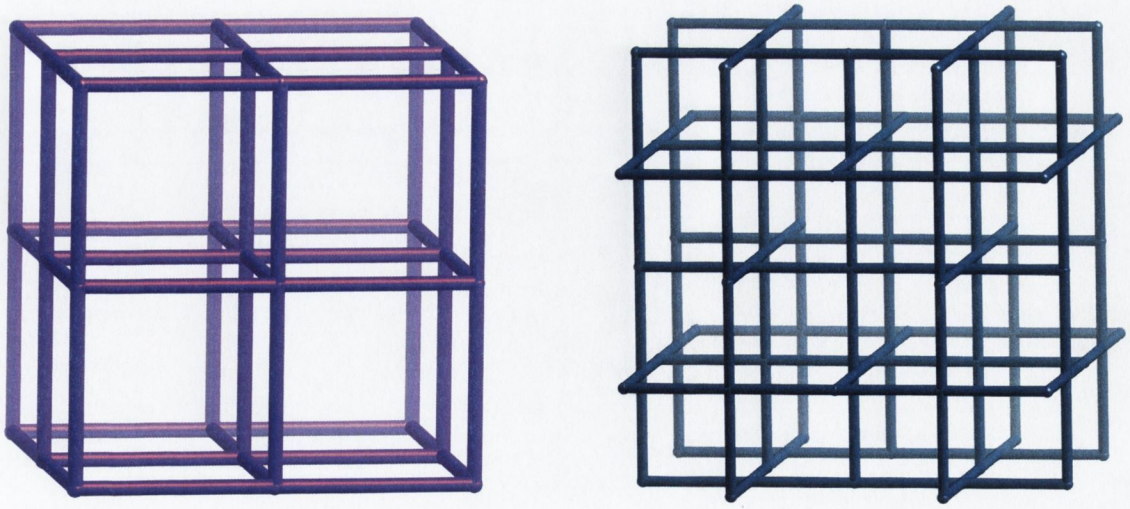

(a) (b)

Figure 1.27 – (a) α-Po (NaCl) type network consisting of six-connected nodes. (b) NbO type network consisting of four-connected square planar nodes arranged at right angles to each other.

Some networks contain more than one type of node connectivity. The rutile (TiO_2) network is one example that contains both octahedral six-connecting nodes and trigonal three-connecting nodes in the ratio 1:2 (Figure 1.28).

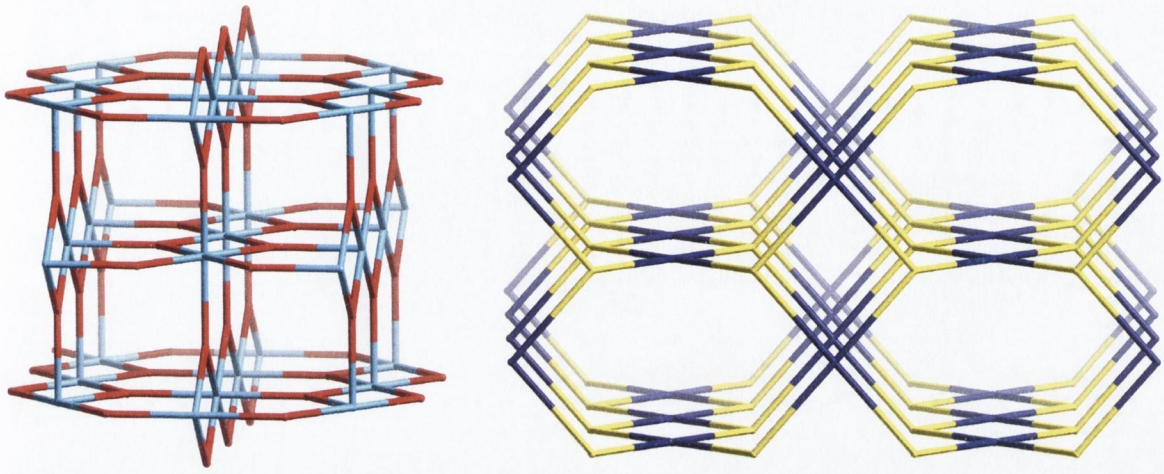

(a) (b)

Figure 1.28 – (a) Rutile (TiO_2) type network consisting of six- and three-connected nodes in a 1:2 ratio. (b) PtS type network consisting of both square planar and tetrahedral four-connected nodes

When applying the Schläfli notation to these networks the same principles apply (with regard to 'shortest circuits') but the two different nodes are dealt with separately. The many well-known simple 3D nets provide realistic targets for crystal engineers to model future materials upon.

1.6.3 Interpenetration.

Many coordination polymers contain cavities or voids within their networks. There are three main ways that such structures may maximize their packing efficiency. The first is intercalation, which means that other molecules, separate to the network, occupy the cavities. These may be charge-balancing ions, which are necessary for the formation of a charged network or they may be neutral molecules such as solvent. These can sometimes be replaced by other molecules, see the example given above (Section 1.6.2). The second is interdigitation, which may occur in 1D and 2D systems. In this case, protruding components of a network interlock with those of an adjacent network. This is similar to when one folds their hands together, hence the term 'interdigitation'. The other main way that coordination polymers maximize their packing efficiency is interpenetration. This occurs when two or more networks are entangled with each other such that they cannot be separated without the breaking of bonds. Rods of one network penetrate the rings of another and *vice versa*. Interpenetration is relatively uncommon in 1D systems and only two examples are known.[111] On the other hand, numerous examples of interpenetration have been observed for 2D and 3D systems and different topologies of interpenetration exist for each.[111] An example of 2D

networks showing inclined interpenetration is given in Figure 1.29. In this case an infinite number of parallel 2D sheets interpenetrate with another infinite set of parallel 2D sheets, which are inclined at an angle to those of the first set.

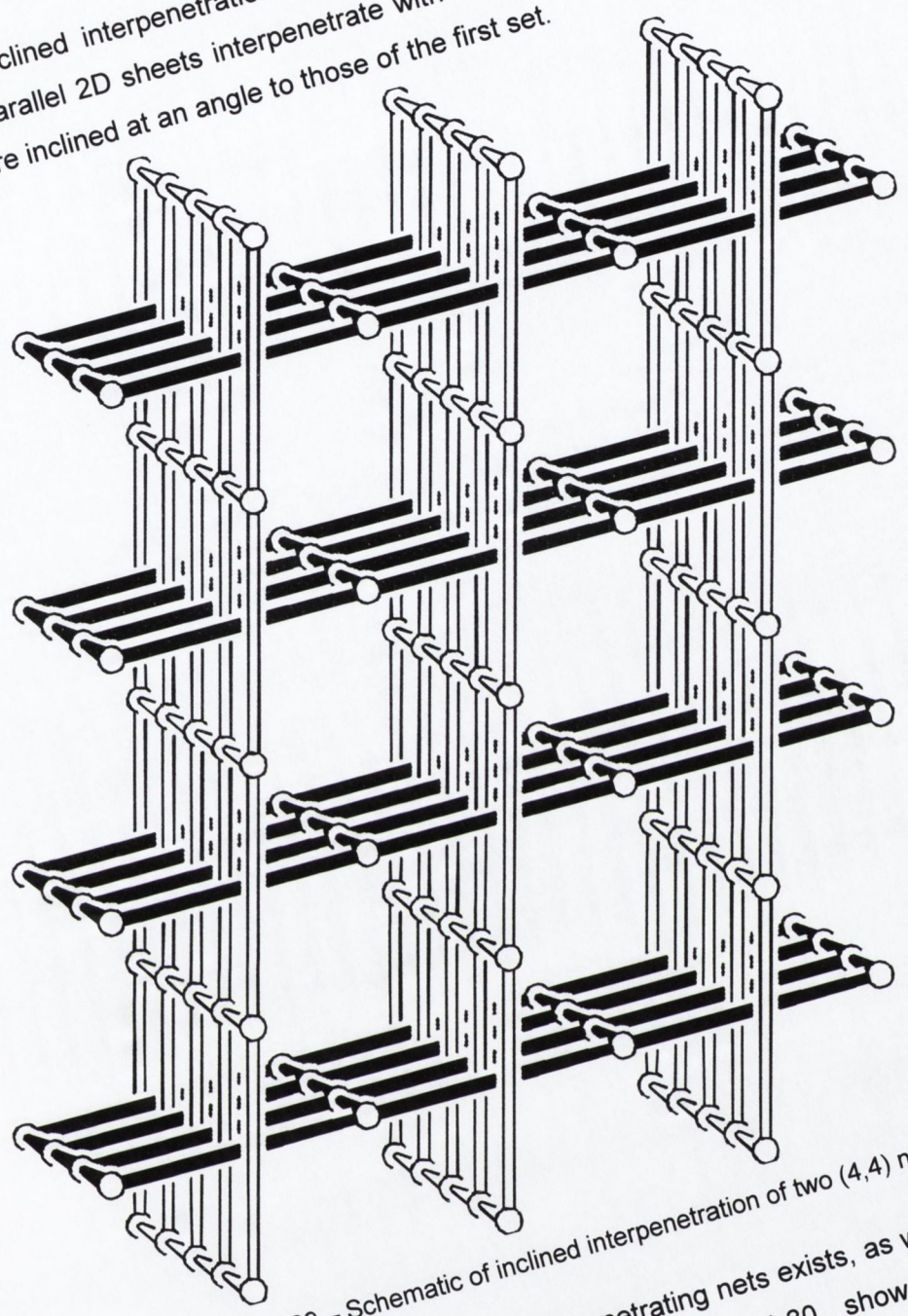

Figure 1.29 – Schematic of inclined interpenetration of two (4,4) networks.[111]

When a finite number of *n* interpenetrating nets exists, as with 3D networks, the term *n*-fold interpenetration applies.[111] Figure 1.30 shows schematically the interpenetration of two α-Po type networks. An actual example of two-fold interpenetration of 3D networks is shown in Figure 1.31, where each network consists of Co(II) metal centres connected by terepthalate bridges and 4,4'-bipy bridges.[114]

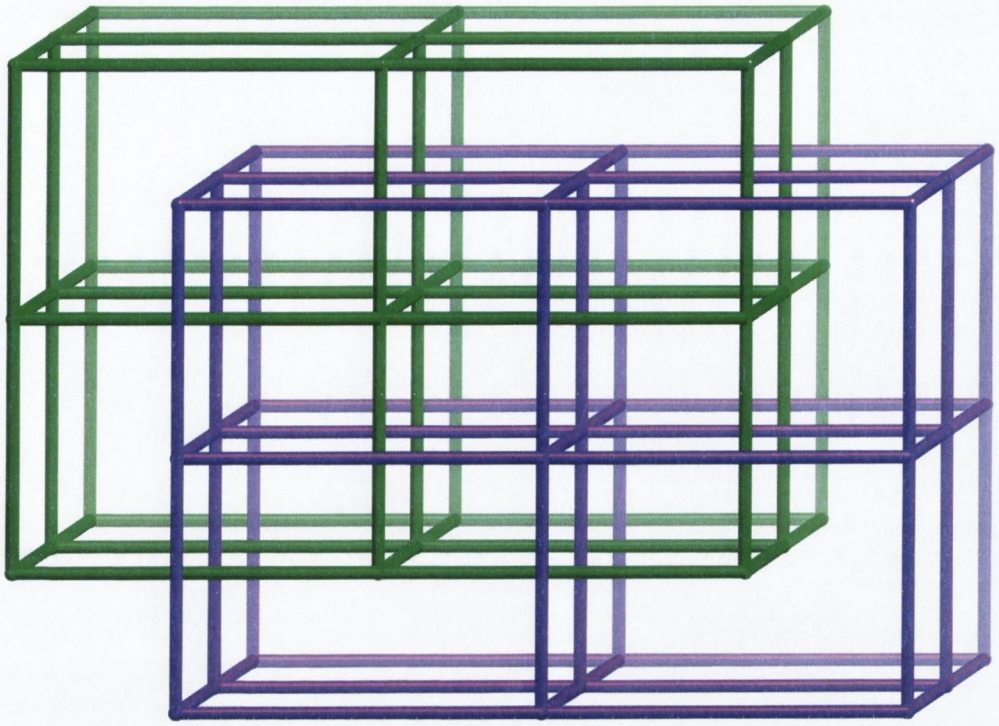

Figure 1.30 – Schematic representation of the interpenetration of two α-Po type networks.

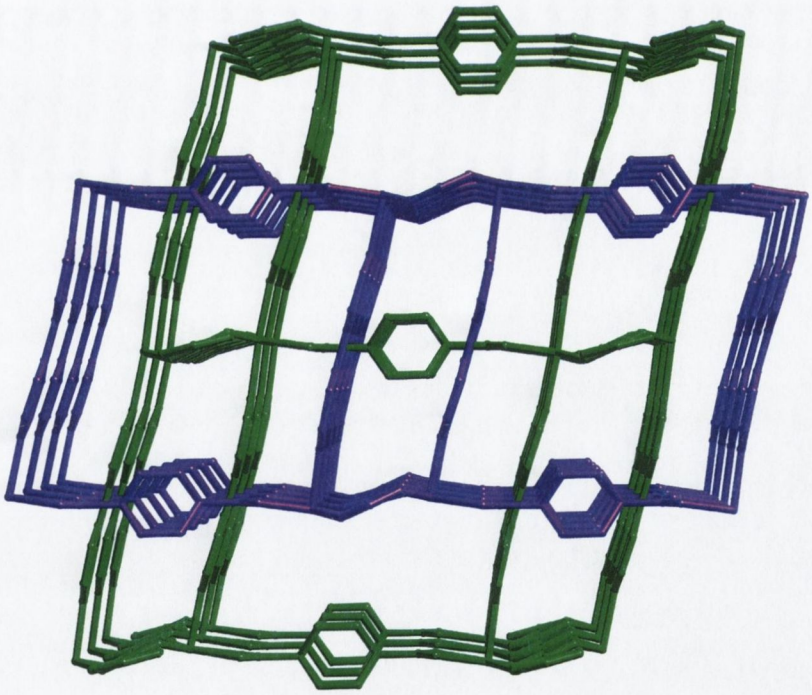

Figure 1.31 – Interpenetration of two 3D coordination polymers as reported by Chen and co-workers.[114] (Hydrogen atoms omitted for clarity)

Frequently synthetic procedures for the formation of coordination polymers involve high-pressure solvothermal techniques (see Section 1.7 below). The rate of cooling is often decisive in the formation of a crystalline product. Examples of interpenetrated networks are contained in this thesis.

1.6.4 Metal-organic frameworks.

One of the most promising applications of coordination polymer design is in the production of microporous materials. Coordination polymers offer various benefits over their inorganic rivals (e.g. zeolites) such as greater control over pore size and shape, as well as more gentle synthetic techniques. Until recently, the usefulness of these types of materials was limited by the loss of crystallinity after removal of guest solvent molecules from the lattice.

The approach adopted by Yaghi and co-workers, involves the formation of metal-organic frameworks (MOFs) by connecting so-called secondary building units (SBUs) together.[98, 115-117] The concept draws on the stability of metal carboxylate-containing 'clusters', of which two examples are shown in Figure 1.32.

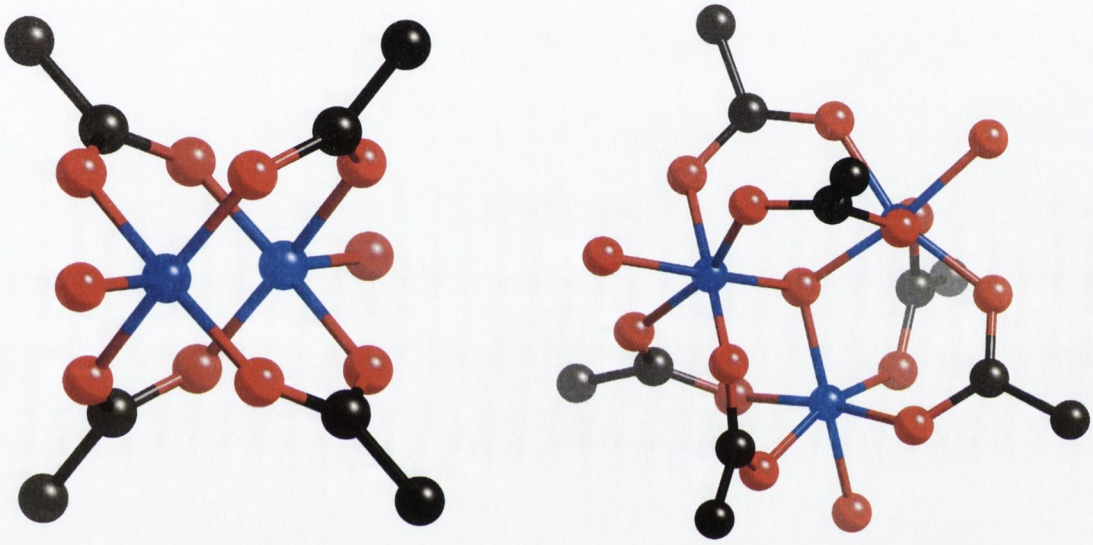

(a) (b)

Figure 1.32 – (a) 'Paddle-wheel' dinuclear carboxylate cluster. (b) Trinuclear carboxylate cluster.

Figure 1.32(a) shows the 'paddle-wheel' type of dinuclear carboxylate cluster, which contains four acetate groups coordinated to two metal centres. Figure 1.32(b) shows a trinuclear cluster where six acetate groups coordinate to three metal centres. Functionalisation of the acetate groups to include a second carboxylate coordination site allows for these clusters to be linked together. This is the approach adopted by Yaghi and co-workers. Figure 1.33 shows some of the carboxylate-containing ligands that have been used in the formation of various network systems, the actual number of carboxylate groups in each ligand ranges from two to four. Another feature of the ligands shown in Figure 1.33 is the difference in the distance between the carboxylate moieties. This bridge between carboxylates is an important feature as it allows a measure of control over the size of the cavities bound by the networks.

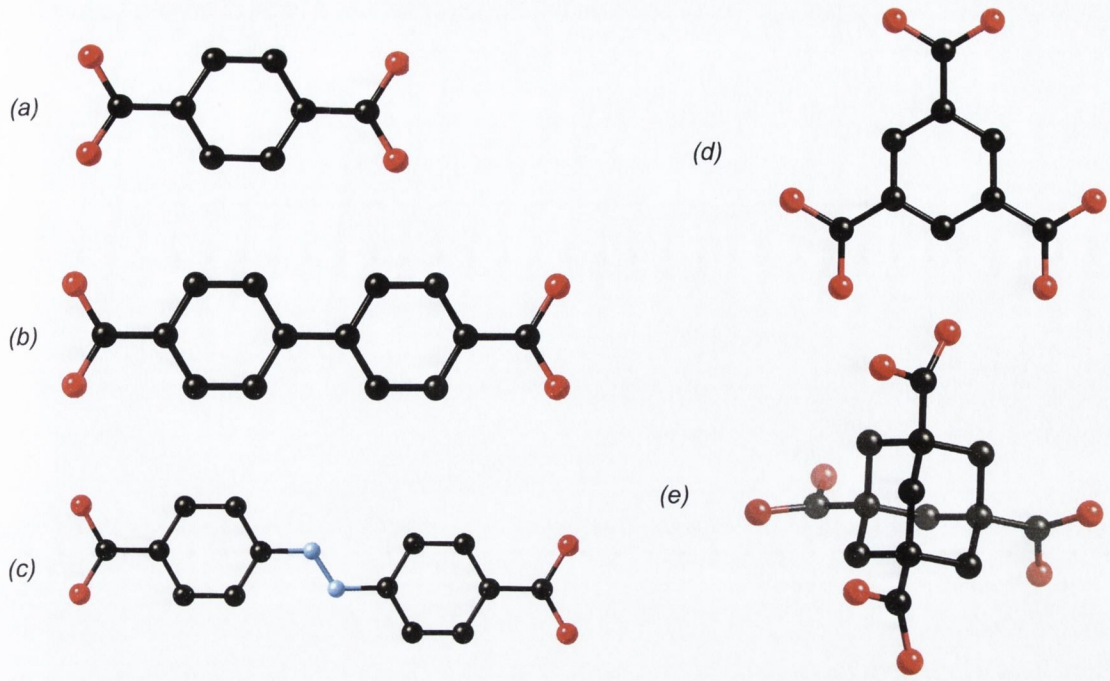

Figure 1.33 – Carboxylate-containing ligands for use in the formation of metal-organic-frameworks, as reported by Yaghi and co-workers.[98, 118]

Figure 1.34 shows the structures of a selection of porous coordination polymers (metal-organic frameworks) with the cativies highlighted in yellow. These MOFs consist of Zn-O-C clusters held together with different bridging groups. The length of the bridging unit determines the dimensions of the cavity and thus the porosity of the polymer. These compounds are prepared by combining $Zn(NO_3)_2 \cdot 5H_2O$ with the acid form of the carboxylate bridging unit (e.g. 1,4-benzendicarboxylic acid) in DMF and heating in a sealed vessel to between 85 and 105 °C, yielding the crystalline product.

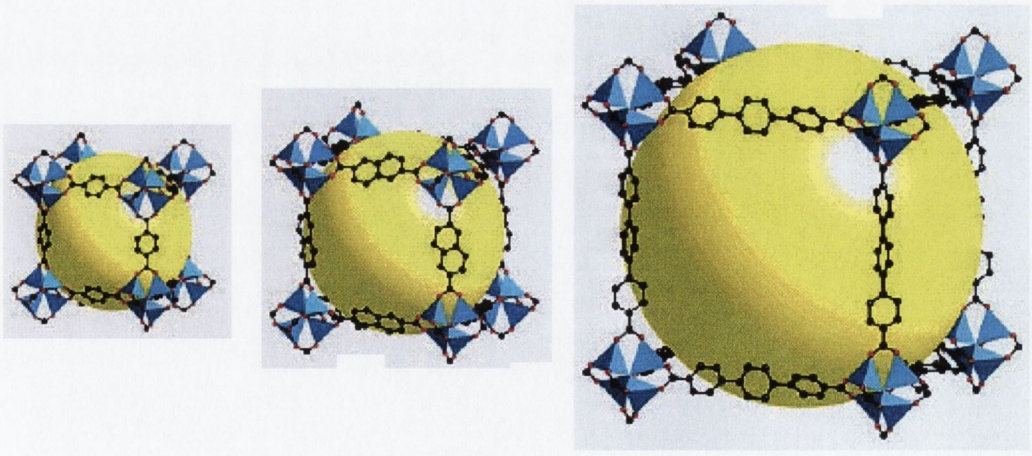

Figure 1.34 – A selection of zinc-containing metal-organic-frameworks of differing porosity.[117] Note the different bridging units used to expand the dimensions of the network.

An interesting point to note about these polymeric systems is that, somewhat surprisingly, the networks do not interpenetrate. This is significant since the volume of the cavities is so large.

Applications of these porous frameworks are currently being explored.[98, 116, 117] Research into the use of fuel cells as an alternative to combustion engines is a growing area of current study. One of the problems associated with fuel cells is the storage of hydrogen, which used as a fuel source. The fact that the MOF complexes form porous networks means that they may have a potential use in the storage of hydrogen for use in fuel cells.[119, 120] These MOFs have shown remarkable internal surface area properties indeed the current "world record" is held by a zinc-MOF, which has a specific surface area of approximately 3000 m^2g^{-1} compared to carbon nanotubes (200 m^2g^{-1}) and zeolites (700 m^2g^{-1}).[119, 121]

1.7 Solvothermal synthesis.

Solvothermal processes can be defined as chemical reactions or transformations in a solvent under supercritical conditions or near such a pressure-temperature domain.[122, 123] These processes have been mainly developed in the following scientific areas:

(a) the synthesis of new materials.

(b) the development of new processes for preparing functional materials.

(c) the shaping of materials (e.g. crystal growth).

Solvothermal processes therefore, are a powerful route for the preparation of novel materials. The development of this approach for materials synthesis has developed rapidly since the first international conference on solvothermal reactions was held, in 1994. Whilst various solvents have been studied, (including alcohols, liquid ammonia and NH_2NH_2) water has been the real driving force in solvothermal synthesis, so much so that the area of 'hydrothermal synthesis' has been developed. This technique has been very successful in the formation of new materials such as zeolites and aluminophosphates. The process, over the past ten years, has even found use in the production of artificial diamonds. Hydrothermal reactions have also been extensively applied to the synthesis of coordination complexes and clusters for the preparation of chemical sensors, microporous crystals, and magnetic materials. Much effort has been focused on the reaction of neutral donor ligands (such as 2,2'-bipy, pyrazine) with anionic ligands (such as carbonate, phosphate) in combination with a metal salt. This approach has returned a family of inorganic-organic hybrid materials such as those complexes mentioned above, reported by Yaghi and co-workers. In general, solvothermal processes have opened a fruitful route to the synthesis of novel materials, as well as improving the synthesis routes to already well-known materials such as

oxides and nitrides, by producing these compounds at temperatures and/or pressures much lower than those used in classical solid state chemistry. Knowledge is also gained from comparing the reaction products obtained by reacting identical systems at, for example, both room temperature and under solvothermal conditions. This has led to a better understanding of what is required to generate particular types of materials with specific compositions, structures, morphologies and, most importantly, properties. Finally, in addition to new materials it is an interesting aside to say that hydrothermal chemistry is currently attracting studies on the origin of life and/or environmental issues. It is hypothesised, for example, that rich hydrothermal reactions occurred in the sea and that all microorganisms have high-temperature ancestors. More and more evidence supports the idea of a hydrothermal origin to life, with micro-organisms found in hydrothermal vents (Figure 1.35).

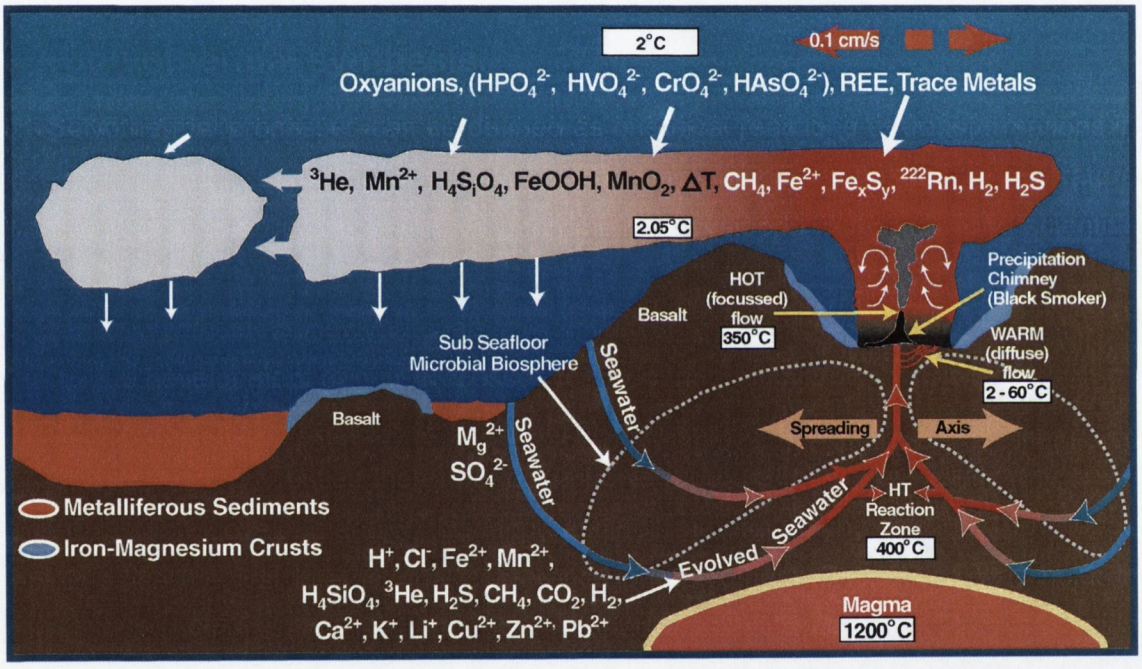

Figure 1.35 – Schematic of hydrothermal vent chemistry and a vent itself.[124]

A large number of novel materials have been synthesised from hydrothermal reactions. The increasing interest in hydrothermal synthesis derives from its advantages in terms of high reactivity of reactants and formation of metastable or unique condensed phases. The new materials it has returned have provoked significant interest in many fields such as photochemistry, catalysis and biology.

1.8 Present study.

This body of work is intended to both extend and develop previous work carried out, within the Kruger group, as well as open new routes of research in the area of coordination polymers. The candidate was involved in all aspects of X-ray structure determination at Trinity College Dublin. The final refinements were performed by the candidate, with assistance provided by Dr. Paul Jensen where necessary. Some crystallographic details, bond lengths and angles are given throughout the text, however full details (i.e. complete tables of bond lengths, angles, etc.) are available for all structures on the attached CD-ROM located at the back of this thesis.

Chapter 2 will concentrate specifically on the formation of novel metal-containing helicates incorporating the imine motif. The formation of a group of novel ligands for the preparation of helicates has been carried out. Some of the ligands reported are based around a C_3 symmetric backbone, and represent a shift away from previous C_2 symmetric ligand systems reported. Ligands with tridentate binding capability have also been synthesised and characterised. Complexation of the ligands with tetrahedral metal centres such as Ag(I) and Cu(I) has also been studied and is reported herein.

Chapter 3 details the attempt at the formation of a tetranuclear molecular box, which resulted in the construction of a coordination polymer. Development of other polymer systems, containing different metal centres is also reported. The interesting structures formed by these systems are studied by X-ray diffraction of single crystals, The predominant ligand used in the coordination polymers is 4,4'-bipy, since it has two coordination sites linearly disposed.

Chapter 4 contains results of compounds obtained by the hydrothermal reaction of metal salts with 4,4'-bipy in the presence of 1,4-benzenedicarboxylic acid. The general idea behind this area of work was to attempt to link 1D coordination polymers formed with the acetate salts of various metals together to form networks of higher dimensionality. Several different types of networks have been formed and the single crystal X-ray structures are described.

Chapter 5 provides the experimental details for the synthesis of the compounds described herein.

Chapter 6 is a brief description of avenues of future research that could be based on the work described in this thesis.

Chapter 2 – Ligand Structures

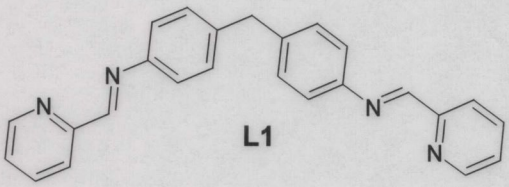

L1

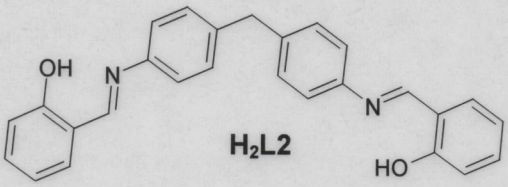

H_2L2

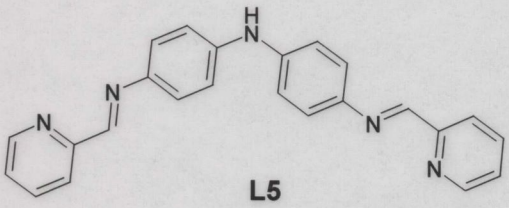

L5

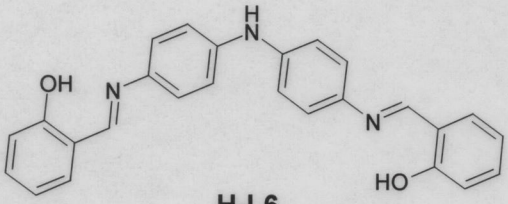

H_2L6

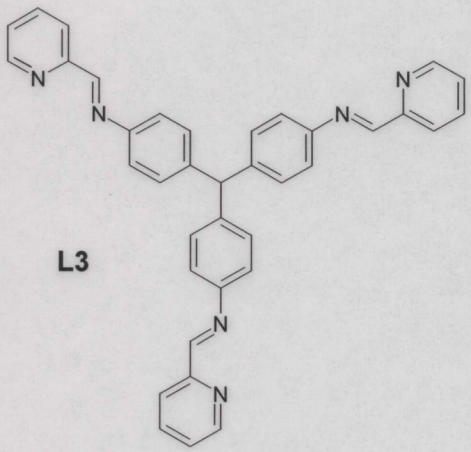

L3

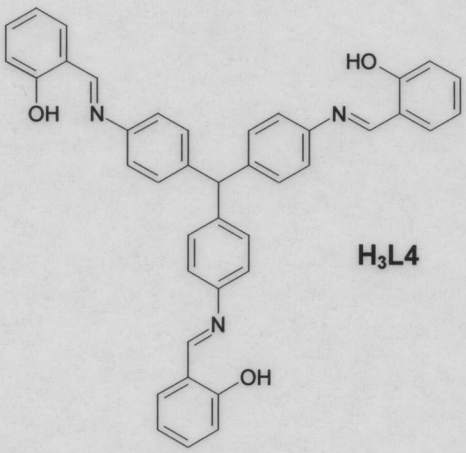

H_3L4

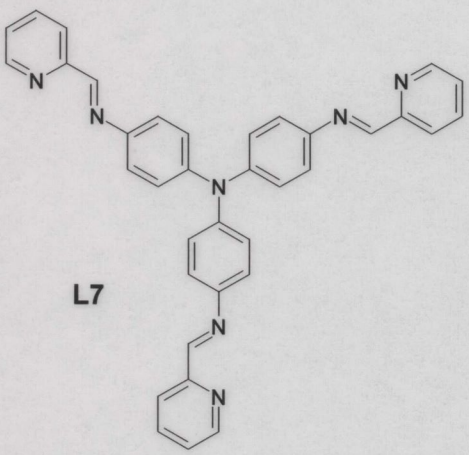

L7

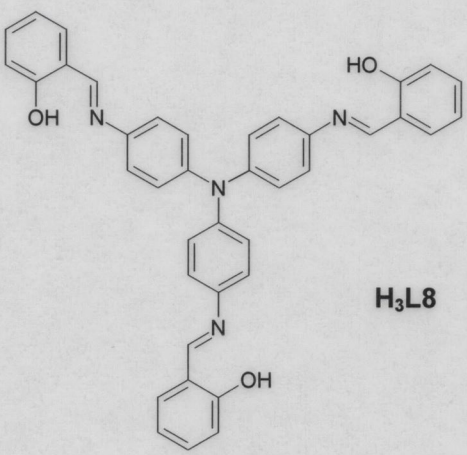

H_3L8

Chapter Two

Synthesis and Characterisation of Molecular Helicates of Ag(I) and Cu(I) with C_2 and C_3 Symmetric Ligands.

Introduction.

The formation of molecular helicates is a well established and highly topical area of current supramolecular research.[13, 28, 29, 31, 46] The synthesis of compounds containing the imine moiety is well understood and has a long established history.[125, 126] The imine functional group is characterised by the presence of a carbon-nitrogen double bond and is formed by a reversible nucleophilic addition reaction between a primary amine and an aldehyde or ketone.[125] (Figure 2.1)

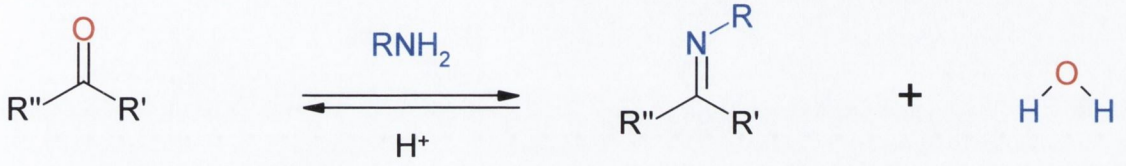

Figure 2.1 – Formation of the imine functional group.[125]

The reaction involves a nucleophilic attack of the carbonyl group by the lone-pair electrons of the amine, which leads to a dipolar tetrahedral intermediate. Proton transfer from the nitrogen to the oxygen then occurs, yielding a neutral carbinolamine species. The hydroxyl group is protonated by the acid catalyst. The nitrogen lone-pair electrons then expel water giving an iminium ion. Subsequent loss of H^+ from the nitrogen gives the neutral imine product. This reaction is normally an acid-catalysed process and studies have shown that the reaction rate is maximised in a weakly acidic pH of approximately 4.5.[125]

One of the earliest examples of the utilisation of imine based ligand systems in complexation with metals to form helical complexes is that shown by McKenzie and co-workers[51] who synthesised a copper containing dinuclear complex. Van Koten and co-workers[52] reported the synthesis of a Ag(I) helicates employing two bidentate pyridylimine ligands with the structure shown in Figure 1.15[A] and 1.15[B] (page 16). Amongst others, Hannon and co workers[55, 62, 127, 128] have reported the facile synthesis of ligands for use in the formation of molecular helicates.

One of the major benefits of using imine-based ligands in forming helicates is the basic synthetic techniques required for their formation. Work within the Kruger group has focused on the formation of molecular helicates composed of metal centres held together by imine containing ligand strands.[56-58] Figure 2.2 shows the core of the ligand strand that has been used as a template for the basis of the work reported here. The blue part of the molecule is the bridging unit, whilst the red parts are the terminal groups. By simply changing the starting reactants one can modify either group.

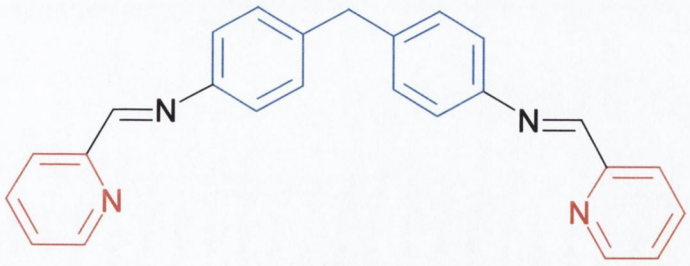

Figure 2.2 – *Bis*-imine template ligand used to form dinuclear double and triple helicates.[57]

Previous work within the Kruger group, involved varying the terminal groups to incorporate a phenol moiety. This was then reacted with the acetate salts of various transition metals to form either molecular helicates or the non-chiral so-called mesocates.[56-58]

An overwhelming feature of the work carried out to date in the area of molecular helicate formation is that all ligand systems consist of a series of linearly disposed coordination sites (with each site being either bi- or tridentate) giving a ligand strand with a primary C_2 axis of symmetry.[28] In an effort to address this situation and in an attempt to extend the scope of the work being carried out, it was decided to incorporate a third coordinating arm on the central bridging carbon. This would allow the formation of a ligand having its coordinating sites in a non-linear arrangement and possessing a C_3 axis of symmetry. Initial elementary computer modelling (HyperChem™[129]) showed that it may be possible to form a trinuclear double helicate, with this kind of ligand.

2.1 Preparation and characterisation of ligands.

The general synthetic pathway is shown in Figure 2.3 and has been well established for the formation of imine-based ligands. Varying the nature of the amines and aldehydes gives rise to a family of related ligand sets. Ligands **L1** and **H_2L2** have been previously synthesised and utilised in the formation of helicates.[57] The initial goal of this work was the synthesis of a 'three-armed' C_3 symmetric ligand, **L3.** This ligand has a methine spacer atom, between the phenyl pyridylimine coordinating arms. This represents the most obvious extension of the ligand family to incorporate a *tris*-chelating functionality. Both the pyridyl (**L3**) and phenolic (**H_3L4**) derivatives were synthesised, however, there were problems with the stability of these ligands, which will be elaborated on below. The spacer unit was changed from a carbon atom to a nitrogen atom. There were various reasons for this: Firstly, the introduction of a nitrogen atom altered the geometry of the spacer unit from a tetrahedral arrangement to a trigonal (planar) geometry. This would impact on the arrangement of the ligand strands within a helicate, as well as introducing the possibility of the formation of intermolecular interactions (through hydrogen-bond donor/acceptor interactions).

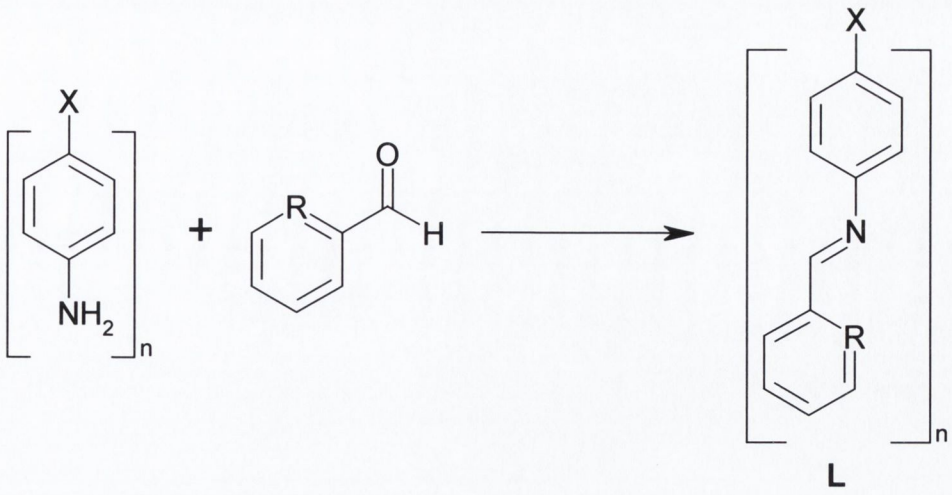

L

L1: n = 2, R = N, X = CH_2 **L5:** n = 2, R = N, X = NH

H_2L2: n = 2, R = C-OH, X = CH_2 **H_2L6:** n = 2, R = C-OH, X = NH

L3: n = 3, R = N, X = CH **L7:** n = 3, R = N, X = N

H_3L4: n = 3, R = C-OH, X = CH **H_3L8:** n = 3, R = C-OH, X = N

Figure 2.3 – General imine ligand synthetic pathway used in the current study.*

Secondly, the stability of the carbon-spacer containing molecules was questionable. It was observed that on standing in polar solvents the ligands degraded. It was hoped that the nitrogen-spacer group would introduce a greater degree of stability into the ligand system.

*2.1.1 Synthesis of N,N',N''-tris-pyridin-2-ylmethylene-4,4',4''-triaminotriphenyl-methane (**L3**).*

The novel ligand **L3** was prepared by adapting the Schiff's base condensation procedure used in synthesising the ligands **L1** and **L2**[57, 130] and using the triamine triaminotriphenylmethane (TAPM), which was prepared *via* a previously published method.[131, 132] Figure 2.4 shows the overall synthetic pathway for the formation of **L3**. Parafuchsin hydrochloride (**P1**) was reduced in the presence of Zn, by $Na_2S_2O_4$, in ethanol to produce the triamine, TAPM (**P2**). This was isolated as a black microcrystalline solid.

* See laminated pullout in Appendix for a handy reference for ligands.

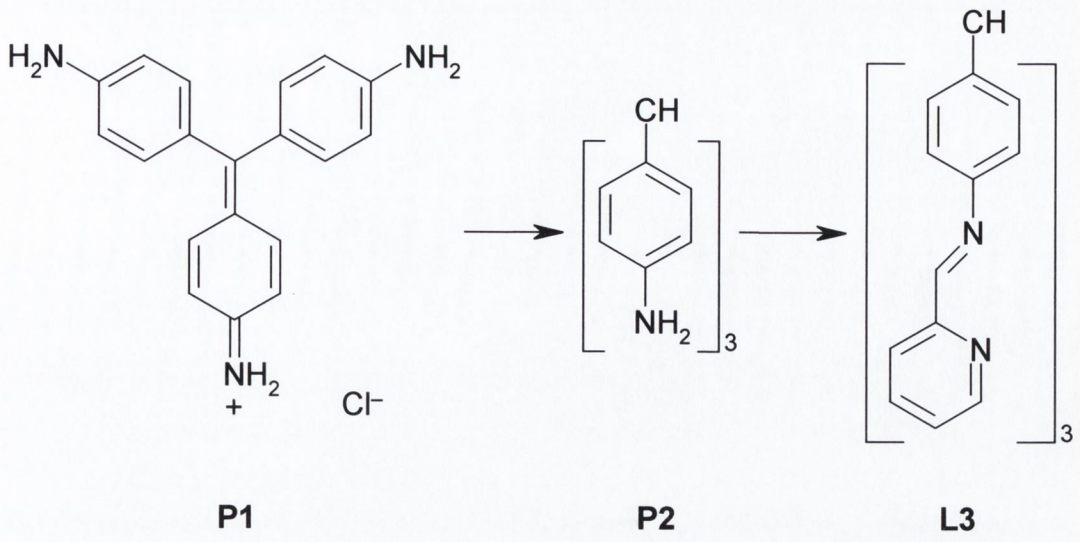

P1 **P2** **L3**

Figure 2.4 – Synthetic pathway for the formation of **L3**.

Under an argon atmosphere, TAPM (**P2**) was dissolved in chloroform, to which a 0.5 M chloroform solution of pyridine-2-carboxaldehyde was added and the mixture refluxed for 5 hrs. The reaction was then allowed to cool to room temperature and stirred overnight. Evaporation of solvent under reduced pressure yielded a dark brown solid. This modification of the published procedure[50] was required as degradation of the product was noted when the reaction was performed in solvents such as methanol, as the reaction turned a bright pink/magenta colour. Analysis of ^{1}H-NMR and ES-MS data was unable to ascertain the structure of the degradation product. Excessive broadening of the signals in the ^{1}H-NMR spectrum to the point where interpretation was impossible, along with unaccountable peaks being present in the ES-MS were characteristic of the degradation products. It is likely that the central spacer carbon atom loses its hydrogen and adopts a planar geometry, rather than the desired tetrahedral arrangement. Evidence for this is the colour of the degraded solution, which is similar to that seen when the (unreduced) parafuchsin hydrochloride is dissolved in alcoholic solvents. This reagent is used as a staining agent for microscopy, due to its strong colouration.[133]

When the reaction was performed under an inert atmosphere and in a chlorinated solvent, it proceeded more smoothly. The ligand was formed in good yield (80%) and elemental analysis (C:H:N) was consistent with the proposed structure. The IR spectrum indicated the presence of the imine group (1624 cm^{-1}). Figure 2.5 shows the ^{1}H-NMR spectrum of **L5** (Peaks are listed according to assignment shown on the structure).

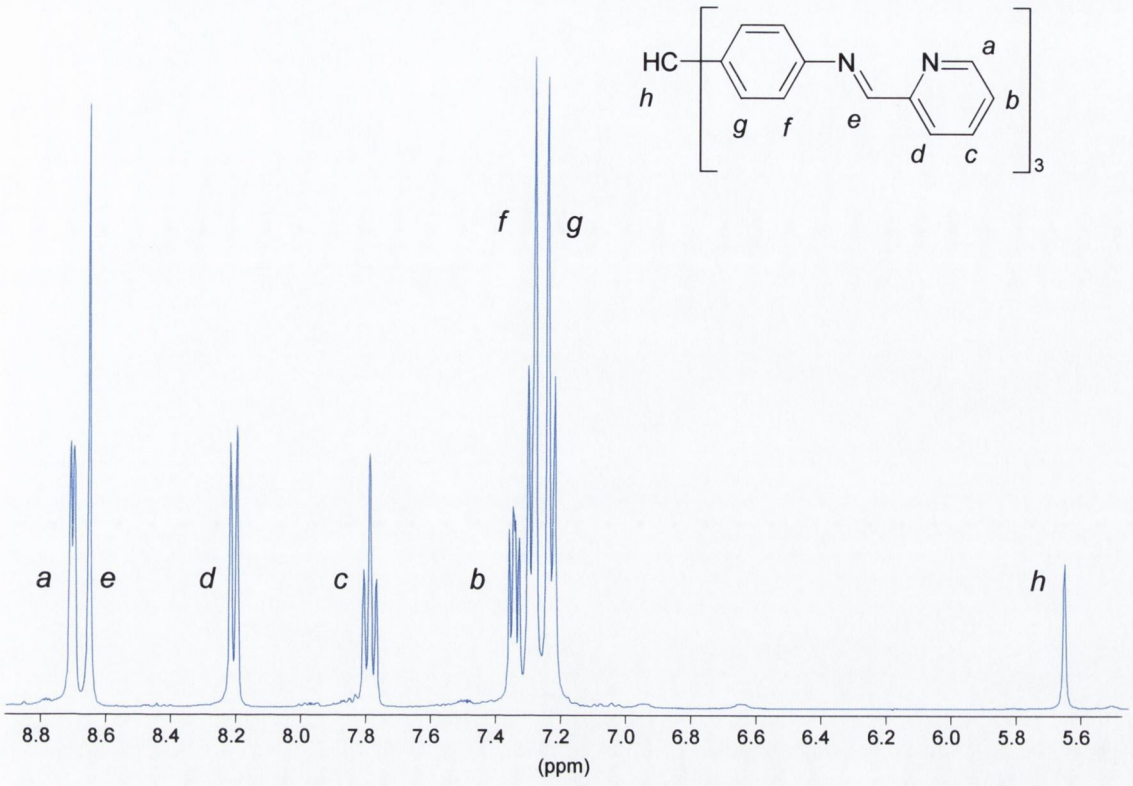

Figure 2.5 – ^{1}H-NMR ($CDCl_3$) and peak assignment for **L3**.

The mass spectrum was also consistent with the proposed structure as the molecular ion at *m/z* = 557.03 was noted. There were no other species observed in solution.

*2.1.2 Synthesis of N,N',N''-tris-phen-2-olmethylene-4,4',4''-triaminotriphenyl-methane (**H_3L4**).*

One of the benefits to this synthetic route is that by simply altering the aldehyde used as a starting reagent one can extend this family of ligands. Just as had been done previously,[57] pyridine-2-carboxaldehyde could be substituted for salicylaldehyde which would allow for the formation of a ligand strand with a different coordinating group.

H_3L4 was prepared in the same manner as **L3**, except with the pyridine-2-carboxaldehyde substituted by salicyaldehyde. Salicyaldehyde was added to the triamine (**P2**) in chloroform and stirred for 4 days, after which the mixture was dried ($MgSO_4$), filtered and evaporated to dryness, giving a yellow/brown powder. The ligand was formed in good yield (76%) and elemental analysis was consistent with the proposed structure. IR analysis showed the presence of the imine group (1618 cm^{-1}). Figure 2.6 shows the ^{1}H-NMR spectrum along with the peak assignments.

Initial complexation reactions of **H_3L4** with $Zn(OAc)_2$ were monitored by UV-vis complexiometric titrations showed promise (see Section 2.2.5), however the stability of both the **L3** and **H_3L4** ligands in the alcoholic solvent regimes used made reproducibility difficult.

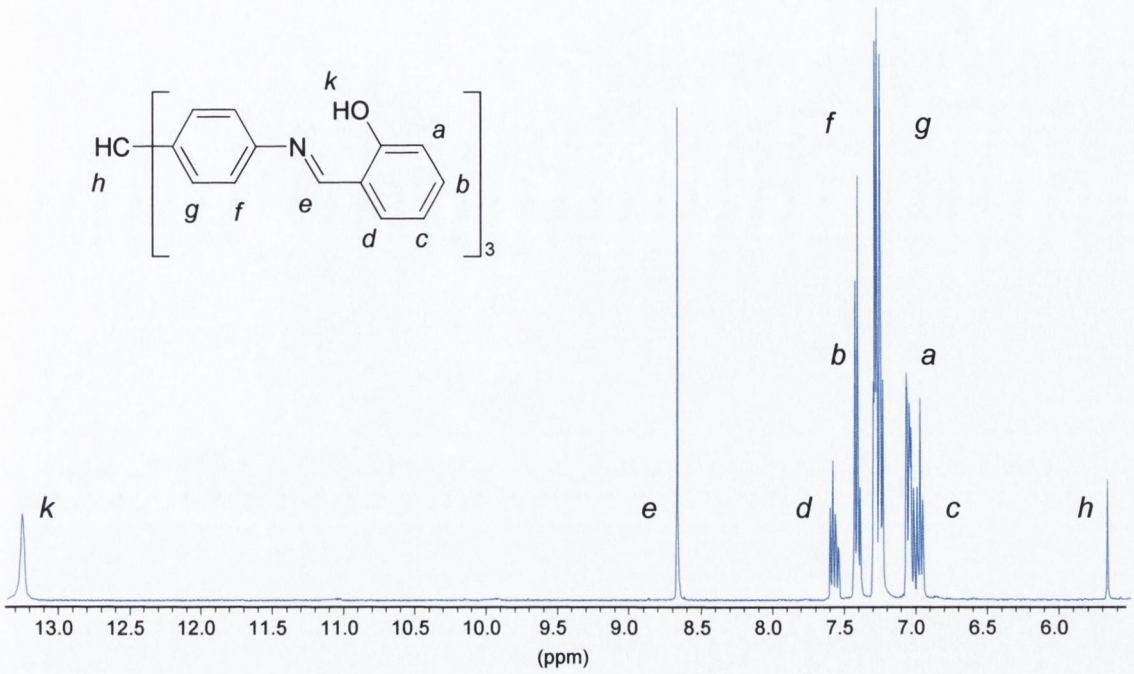

Figure 2.6 – ^{1}H-NMR ($CDCl_3$) and peak assignment for **H_3L4**.

*2.1.3 Synthesis of N,N'-bis-pyridin-2-ylmethylene-4,4'-diaminodiphenylamine (**L5**).*

Although the initial results of complexation of **H_3L4** with Zn(II) were encouraging, the stability of the ligands in solution was less than satisfactory. A potential resolution to this problem was to change the spacer atom from carbon to nitrogen. The synthesis of the nitrogen-atom-spacer containing ligands was to be carried out in the same vein as the carbon containing ones. The rationale behind this was to prepare the *bis*-coordinating ligand **L5** in order to extend the family of 'two-armed' ligands, and to verify that complexation with various metals would still occur. Once this had been established, the ligand family could then be extended to incorporate the 'three-armed' ligands (**L7** and **H_3L8**).

L5 was prepared from diaminodiphenylamine (**P3**), which is available commercially as an 85% technical grade sulfate salt ($NH(Ph\text{-}NH_2)_2 \cdot H_2SO_4$), so purification was required. **P3** was recrystallised in water by refluxing (with activated charcoal), then filtering whilst hot and allowing to cool slowly, yielding a grey powder. This was suspended in water and a few drops of concentrated H_2SO_4 added. A methanolic solution (4 ml) of pyridine-2-carboxaldehyde was then added and the mixture stirred overnight. The mixture was adjusted to pH 7 with 2 M NaOH, extracted with DCM (~50 ml), evaporated to dryness under reduced pressure, yielding a light brown solid. This solid was then recrystallised from hot ethanol, yielding a golden-yellow crystalline solid. Microanalytical data was consistent with the proposed structure (Figure 2.7). ES-MS indicated a molecular ion (*m/z* = 378.17), which is expected for the

protonated species $[C_{24}H_{20}N_6]^+$. IR spectroscopy indicated the presence of an imine moiety (1621 cm^{-1}) and ^{1}H-NMR data were consistent with the proposed structure (Figure 2.6).

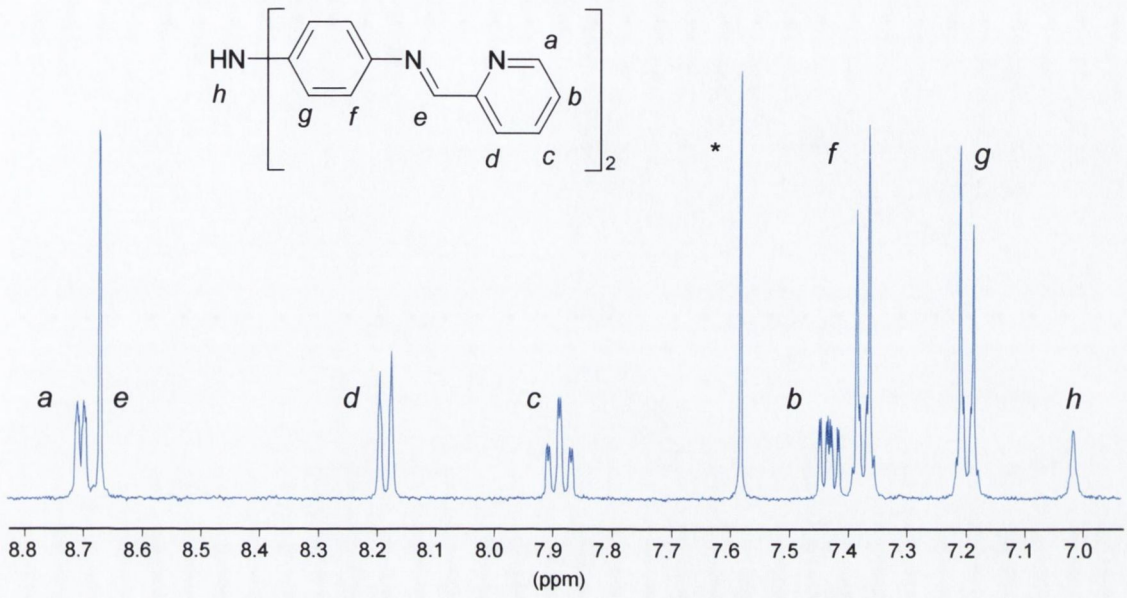

Figure 2.7 – ^{1}H-NMR ($CDCl_3$) spectrum and peak assignment for **L5**.
(* denotes residual $CHCl_3$)

*2.1.3.1 Crystal structure of N,N'-bis-pyridin-2-ylmethylene-4,4'-diaminodiphenyl-amine (**L5**).*

Crystals suitable for a structure determination by single crystal X-ray diffraction, were obtained after a recrystallisation from ethanol.[†] Figure 2.8 shows the molecular structure and numbering diagram for **L5**.

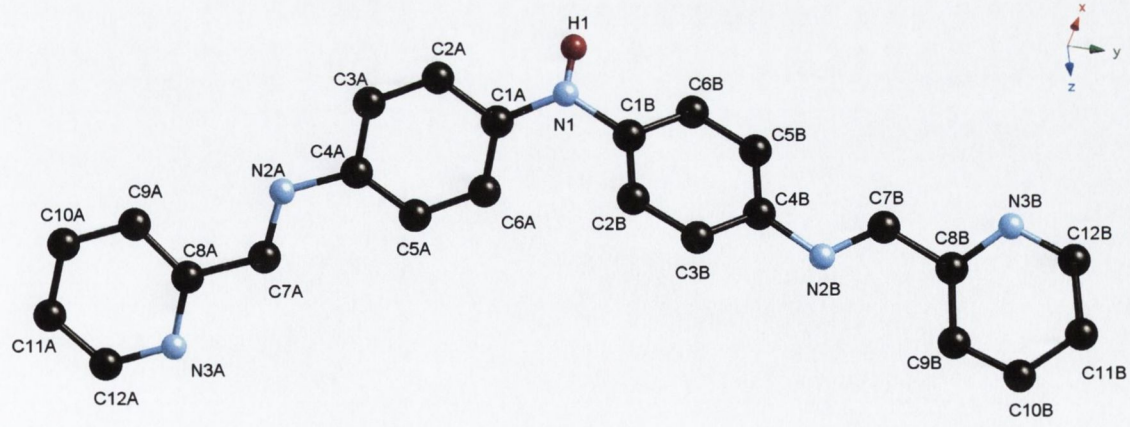

Figure 2.8 – Molecular structure and atomic labelling diagram for **L5**. (Some hydrogen atoms omitted for clarity)

[†] The crystals described in this chapter were initially grown in collaboration with Conchúir MacGloinn, a final year undergraduate student working under the supervision of the candidate.

The structure of **L5** consists of a planar (secondary) amine bridging unit with two coordinating 'arms' attached. Table 2.1 shows selected bond lengths and angles for **L5**. The central amine shows some distortion from regular trigonal geometry, with angles of 114(2)°, 119(2)°, and 125.4(3)° for C1B–N1–H1, C1A–N1–H1 and C1A–N1–C1B respectively. The phenyl rings of either 'arm' are twisted relative to the plane of the bridging nitrogen (N1). The 'A-arm' has a torsion angle of 20.7(5)° (C1B–N1–C1A–C6A), whilst the 'B-arm' has a twist of 42.7(5)° (C1A–N1–C1B–C2B). The pyridylimine groups are also twisted with respect to the phenyl rings, by 18.2(5)° on one 'arm' (C5A–C4A–N2A–C7A) and 27.6(5)° on the other (C5B–C4B–N2B–C7B).

Table 2.1 – Selected bond lengths (Å) and angles (°) for **L5**.

N(1) – C1A	1.392(4)	C1A – N1 – C1B	125.6(3)
N(1) – C1B	1.398(4)	C7A – N2A – C4A	120.8(3)
N(1) – H1	0.88(3)	C7B – N2B – C4B	118.6(3)
N(2A) – C7A	1.253(5)	C1B – N1 – C1A – C6A	20.7(5)
C(7A) – C8A	1.488(5)	C1A – N1 – C1B – C2B	42.7(5)
N(2B) – C7B	1.274(4)	C5A – C4A – N2A – C7A	18.2(5)
C(7B) – C8B	1.469(5)	C5B – C4B – N2B – C7B	27.6(5)

The pyridyl and imine nitrogen atoms are orientated *trans* to each other, a common orientation for pyridylimine ligands[134-138] as this minimizes electron repulsion between them whilst maintaining conjugation.

The packing of this ligand shows a marked difference to that of **L1**,[139] which has a methylene spacer group between the phenyl rings. **L1** utilises π-interactions to stack multiple molecules on top of one another, creating virtual 'columns' of π-stacked ligands, although there are no interactions between adjacent stacks. **L5** on the other hand has a hydrogen-bond between the central amine hydrogen and a pyridyl amine nitrogen (H1···N3B 2.17(4) Å, N1···N3B 3.037(4) Å). This bond links adjacent molecules to form a 1D infinite helical chain spiralling about the two-fold screw axis down the *b* axis. Figure 2.9 shows the hydrogen-bonded (red and white dashed bonds) chain of **L5** molecules.

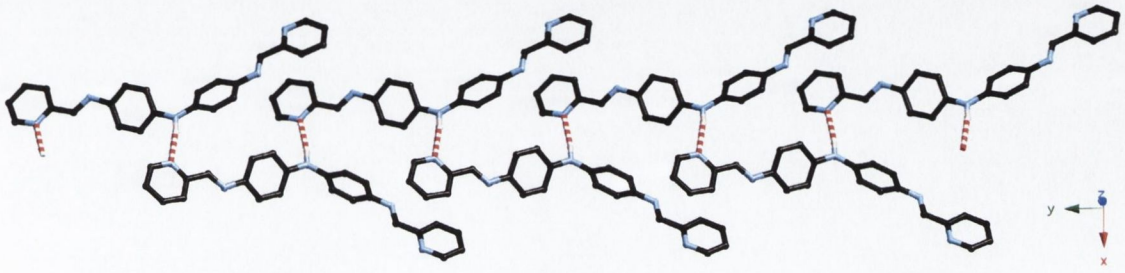

Figure 2.9 – Packing diagram for **L5** showing hydrogen-bonded 1D helical chain arrangement.

Since the structure is centrosymmetric both left and right-handed helical chains are present with those of opposite handedness related by inversion and glide plane symmetry. There is also an interaction between pyridyl rings on adjacent molecules. Although the rings do not completely overlap, one side of the pyridyl ring on the 'B-arm' of one molecule overlaps with the pyridyl ring on the 'A-arm' on an adjacent molecule. There is evidence for π-π interactions insofar as the carbon-carbon distance between the rings is within the tolerance for observed π-interactions (C10B–C8A 3.337(5) Å, C9B–C9A 3.415(5) Å).

*2.1.4 Synthesis of N,N',N''-tris-pyridin-2-ylmethylene-4,4',4''-triaminotriphenyl-amine (**L7**).*

L7 was prepared from the triamine *tris*(4-aminophenyl)amine. It in turn was prepared from *tris*(4-nitrophenyl)amine by reduction with hydrazine monohydrate and palladium on carbon,[140] this was followed by a Schiff base condensation of the triamine with pyridine-2-carboxaldehyde in degassed DCM. The product was recrystallised from warm ethanol and yielded an orange powder. The ligand was formed in good yield (72%) and elemental analysis indicated that **L7** had indeed been formed. The IR spectrum indicated the presence of the imine group (1625 cm^{-1}). ES-MS indicated the presence of a single molecular ion with a peak of *m/z* = 558.24, consistent with the protonated species $[C_{36}H_{28}N_7]^+$. Figure 2.10 shows the ^{1}H-NMR spectrum of **L7**, along with the peak assignment.

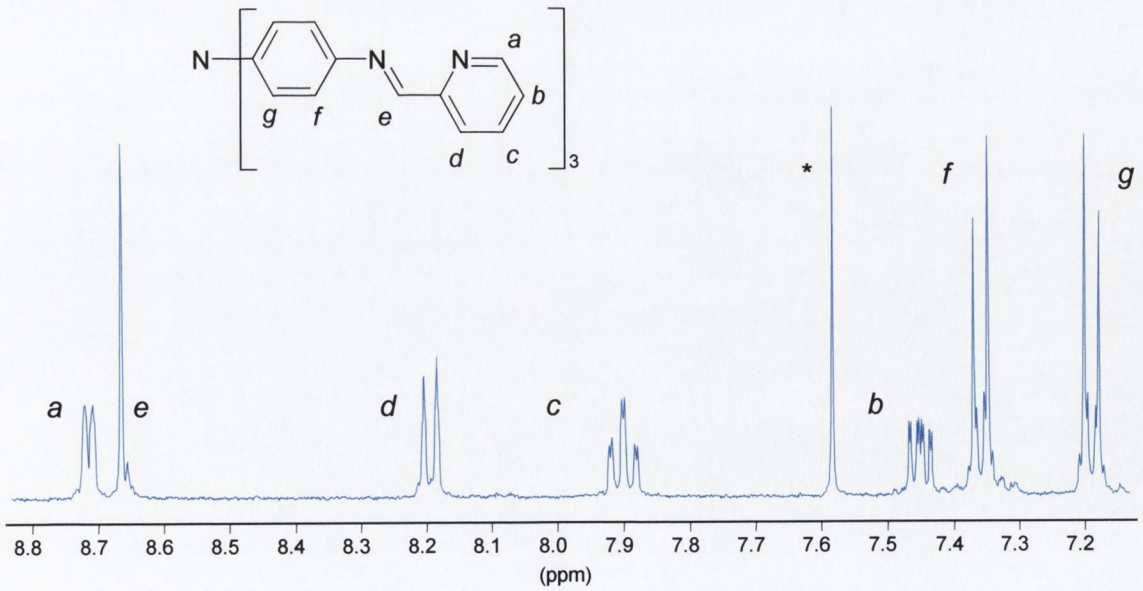

Figure 2.10 – ^{1}H-NMR ($CDCl_3$) spectrum and peak assignment for **L7**.
(* denotes residual $CHCl_3$)

*2.1.4.1 Crystal structure of N,N',N''-tris-pyridin-2-ylmethylene-4,4',4''-triaminotriphenylamine (**L7**).*

Crystals (orange plates) suitable for a structure determination by single crystal X-ray diffraction were obtained by recrystallising the crude powder from hot toluene. Figure 2.11 shows the molecular structure and numbering scheme for **L7**.

The structure of this ligand consists of a planar (tertiary) amine-bridging unit to which three coordinating 'arms' are attached. The central amine shows only marginal distortion from a regular trigonal geometry. The aromatic ring of each arm is twisted relative to the plane of the spacer amine. Table 2.2 lists selected bond lengths and angles for this structure.

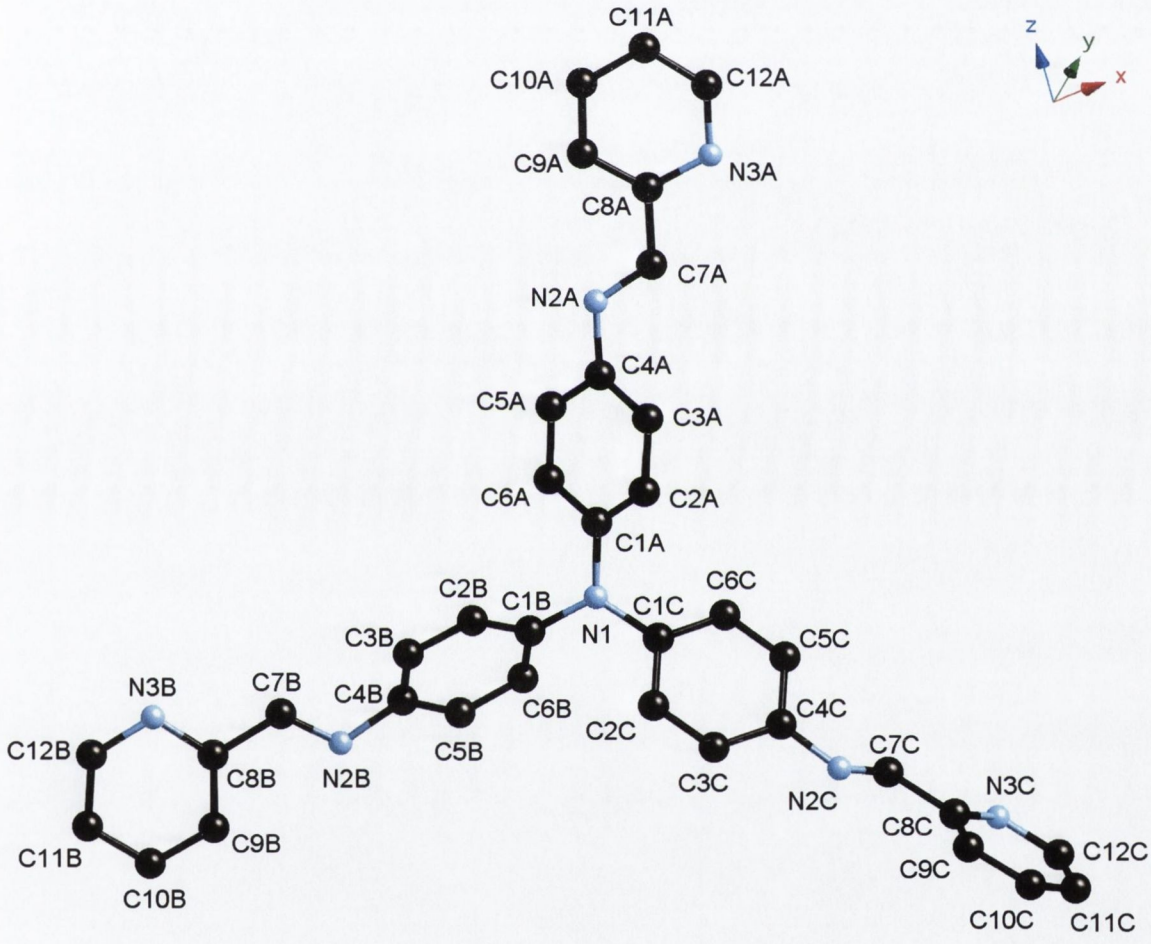

Figure 2.11 – Molecular structure and atomic labelling diagram for **L7**. (Hydrogen atoms and toluene molecules omitted for clarity)

The twisted arrangement of the arms around the nitrogen spacer atom is similar to the blades of a propeller. Torsions angles between the central amine and the aromatic rings of each arm are listed in Table 2.2. As in the **L5** structure, the pyridylimine groups are twisted with respect to the aminophenyl groups, and pyridyl nitrogen (N3) lies in a *trans* arrangement relative to the imine nitrogen (N2).

Table 2.2 – Selected bond lengths (Å) and angles (°) for **L7**.

N1 – C1A	1.416(9)	C1A – N1 – C1B	119.0(6)
N1 – C1B	1.426(9)	C1A – N1 – C1C	121.3(6)
N1 – C1C	1.406(9)	C1B – N1 – C1C	119.7(6)
N2A – C7A	1.289(9)	C4A – N2A – C7A	121.2(7)
N2B – C7B	1.261(9)	C4B – N2B – C7B	118.0(7)
N2B – C7B	1.248(9)	C4C – N2C – C7C	119.2(7)
C7A – C8A	1.468(11)	C6A – C1A – N1 – C1B	32(1)
C7B – C8B	1.483(10)	C2A – C1A – N1 – C1C	31(1)
C7C – C8C	1.484(11)	C2B – C1B – N1 – C1A	53(1)
N3B ··· H3A^{i}	2.6080	C6B – C1B – N1 – C1C	54(1)
N3B ··· C3A^{i}	3.42(1)	C6C – C1C – N1 – C1A	38(1)
N3C ··· H6C^{ii}	2.5713	C2C – C1C – N1 – C1B	35(1)
N3C ··· C6C^{ii}	3.46(1)		

Symmetry Codes: *i* = –x, -y, 2-z; *ii* = 1-x, 1-y, 1-z.

The packing of this molecule is understandably different to that seen in **L5**. The trigonal planar nature of the central spacer nitrogen (N1) dictates the overall geometry of the molecule. (Figure 2.12(a) shows schematically the orientation of each molecule in addition to the crystal the packing of four **L7** molecules and the hydrogen bonds between them.) Each molecule has four hydrogen bonds linking to adjacent molecules and in so doing forms a 1D hydrogen-bonded chain. The molecules align themselves such that there are two hydrogen bonds between the 'C-arms' of adjacent molecules (N3C···H6C). This can clearly be seen in Figure 2.12(b) where the purple and white dashed lines represent hydrogen bonds between the red and green **L7** molecules. An inversion centre relates the two molecules, and so in the red and green molecules, the other 'arms' lie in an opposite orientation to each other.

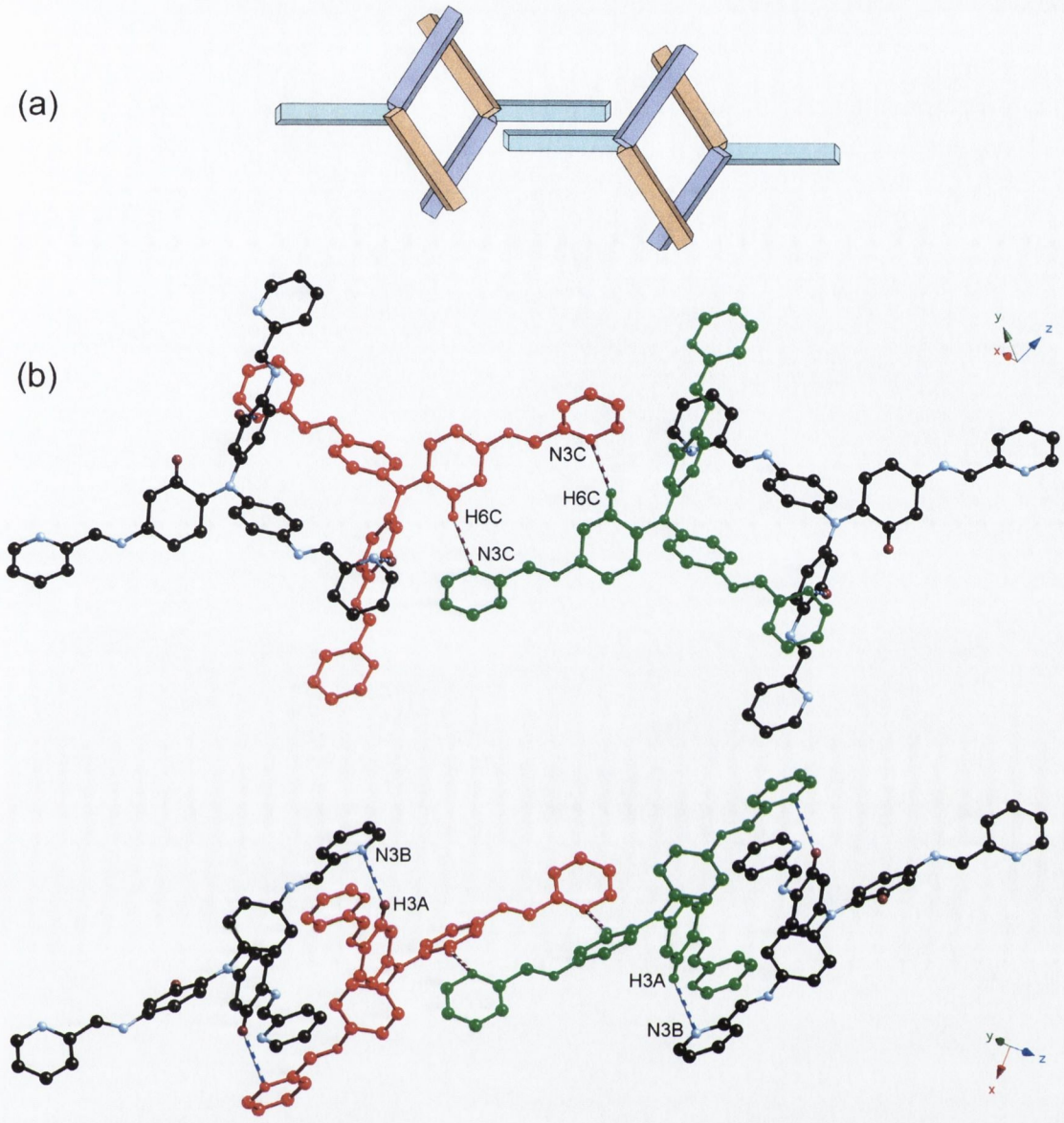

Figure 2.12 – (a) Schematic representation of the way in which **L7** associates in the solid state. The blue block represents the 'C-arm', purple the 'B-arm' and orange the 'A-arm'. (b) Crystal packing of **L7** and hydrogen-bonding between molecules.

Figure 2.12(b) shows additional hydrogen-bonds between the 'A-' and 'B-arms', bond distances are listed in Table 2.2. The hydrogen-bonded chain that forms extends in the (11-1) direction. Adjacent chains are related through inversion and lie in a parallel fashion. This orientation allow for voids within the packing, which are occupied by solvent (toluene) molecules.

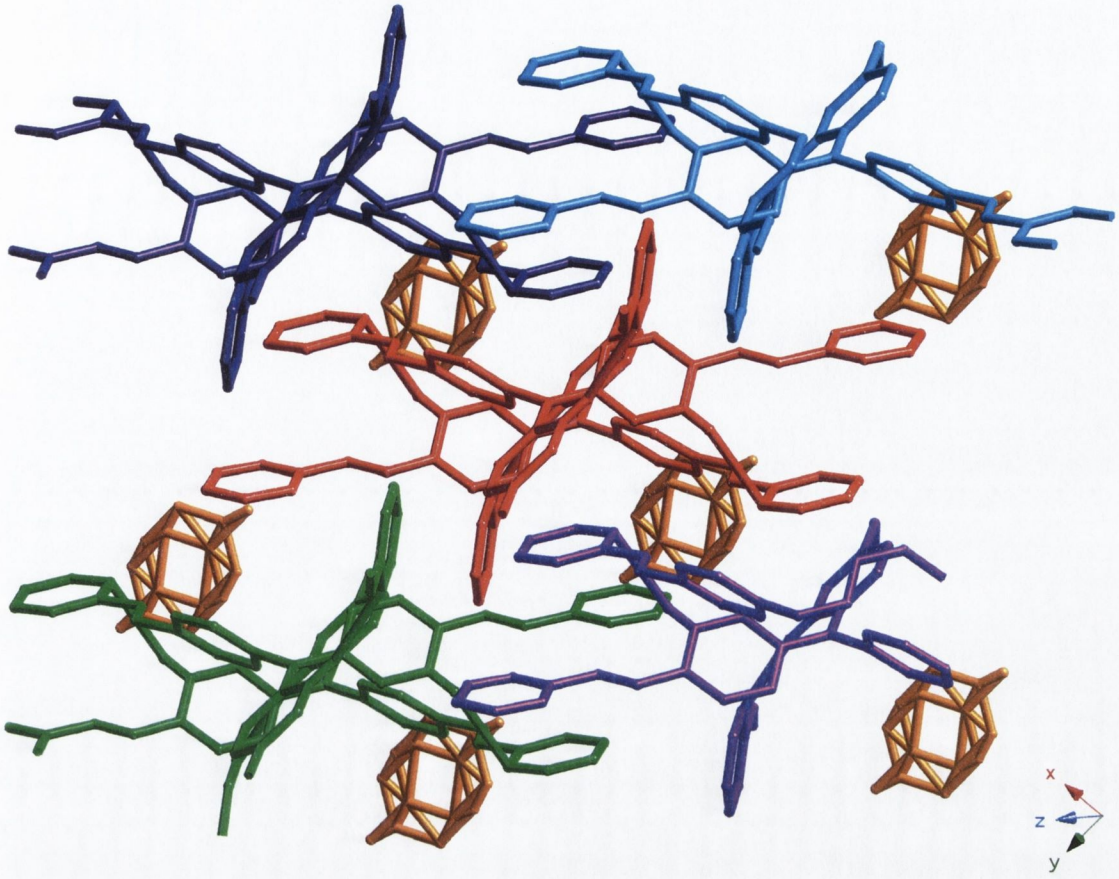

Figure 2.13 – Packing diagram of **L7**, viewed in the (11-1) direction. (Unconnected chains in different colours. Disordered toluene molecules are shown in orange, hydrogen atoms omitted for clarity.)

The toluene molecules are disordered over two sites, which are related by an inversion centre. Figure 2.13 shows the hydrogen-bonded chains as viewed along the (11-1) direction. Different chains are shown in different colours, and the disordered toluene molecules can clearly be seen.

*2.1.5 Synthesis of N,N',N''-tris-phen-2-olmethylene-4,4',4''-triaminotriphenyl-amine (**H_3L8**).*

H_3L8 was again prepared from the triamine *tris*(4-aminophenyl)amine, which was formed as described in Section 2.1.4. The ligand itself was formed *via* a Schiff base condensation on the *tris*(4-aminophenyl)amine with salicylaldehyde in degassed DCM. The ligand was isolated as a brown powder, in much lower yield than was seen for **L7** (54%). Elemental analysis indicated that **H_3L8** had been formed, further confirmation was provided by the mass spectrum, which showed peaks at *m/z* = 603.27 and 302.12 which are indicative of the ions $[C_{39}H_{31}N_4O_3]^+$ and $[C_{39}H_{32}N_4O_3]^{2+}$ respectively. The IR spectrum was collected and indicated the presence of the imine group (1615 cm^{-1}). The ^{1}H-NMR spectrum is shown in Figure 2.14 along with peak assignments.

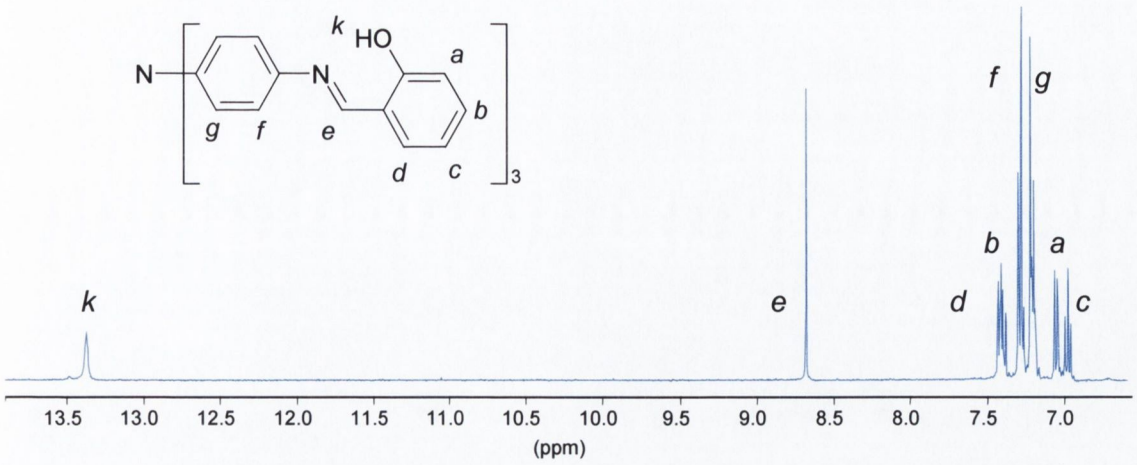

Figure 2.14 – ^{1}H-NMR ($CDCl_3$) spectrum and peak assignments for **H_3L8**.

*2.1.5.1 Crystal structure of N,N',N''-tris-phen-2-olmethylene-4,4',4''-triaminotriphenyl-amine (**H_3L8**).*

Successive recrystallisations from ethanol and toluene yielded orange crystals suitable for a structure determination *via* single crystal X-ray diffraction.

As might be expected, the structure of this ligand is simliar to **L7**. The overall shape of the molecule is trigonal planar, with the arms twisted relative to each other in a propeller arrangement. Figure 2.15 shows the molecular structure and atom numbering for this molecule. The most noticeable feature of this molecule is the arrangement of the phenol groups at the terminus of each 'arm'. Unlike the pyridyl groups in **L5** and **L7**, they are able to form an intramolecular hydrogen bond. This accounts for the orientation of the OH groups, which are *cis* to the imino-nitrogen atoms (N2). Table 2.3 lists selected bond lengths and angles for **H_3L8**, including both intramolecular hydrogen bonds and intermolecular close contacts.

Packing of this molecule is similar to **L7**, although there are some marked differences. The most obvious difference is the presence of *three* intermolecular close contacts. These are represented as dashed lines (blue and white, red and white, green and white) between the molecules shown in Figure 2.16. Two of the contacts (O1A···H12C (blue dashed) and O1B···H11C (red dashed)) allow for the formation of a 2D 'layer' of interconnected molecules, this can be seen in Figure 2.16, where the red, cyan, blue and purple molecules are connected to form a single 'layer'. The remaining close contact (O1C···H3A (green dashed)) connects two 'layers' together to form a sheet. Figure 2.16 also shows the two layers, the green and yellow molecules lie in a plane below that formed by the red, cyan, blue and purple molecules.

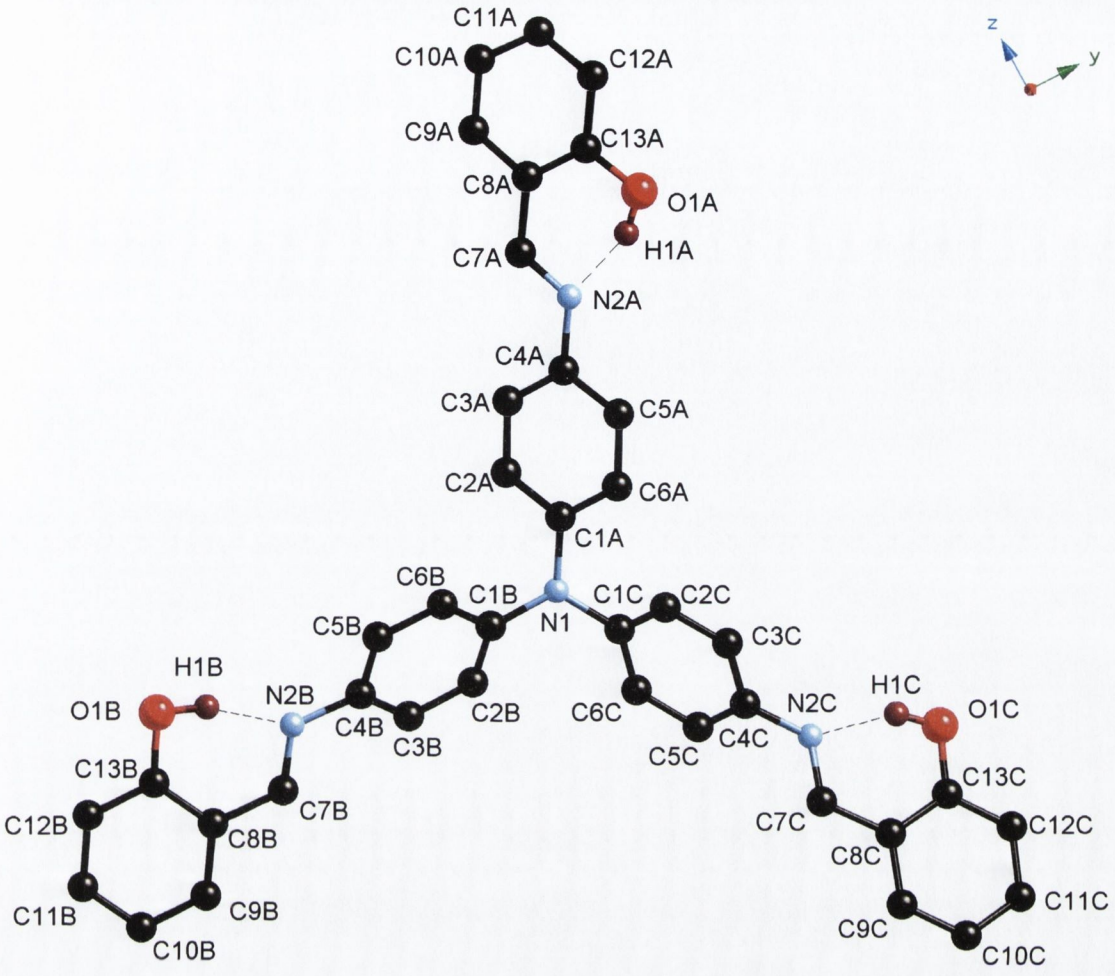

Figure 2.15 – Molecular structure and atomic labelling diagram for **H_3L8**.
(Aromatic and imine hydrogen atoms omitted for clarity)

As is observed in **L7**, there are voids between molecules, which are occupied by toluene molecules. Figure 2.17 shows the positioning of the toluene molecules (orange molecules) in an interconnected sheet. In fact the toluene molecules lie in the planes defined by the 'layers' mentioned above. Molecules of toluene lie in each layer in an alternate arrangement, so the toluene molecules to the extreme left of Figure 2.17 are in the lower layer of the sheet, the next molecules towards the right are in the upper layer and so on.

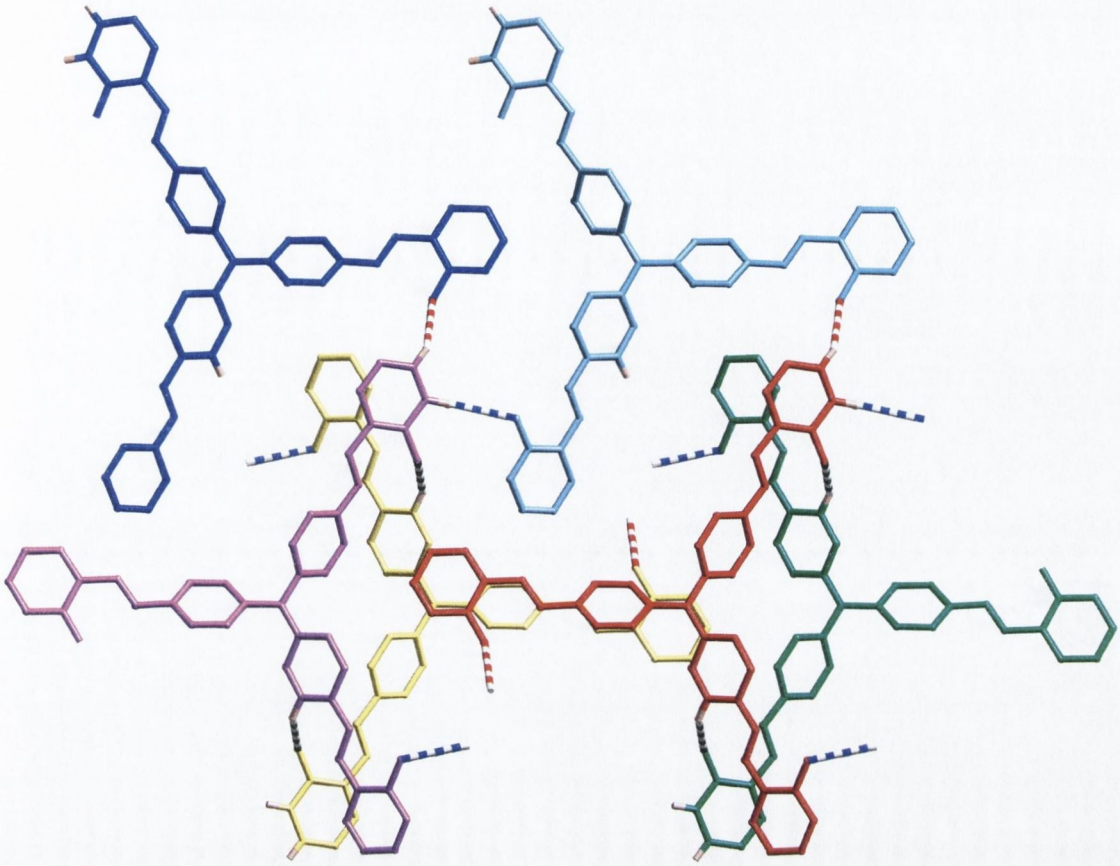

Figure 2.16 – Crystal packing of **H_3L8** and hydrogen-bonding (blue and white dashed, and red and white dashed) between molecules within a 'sheet'.

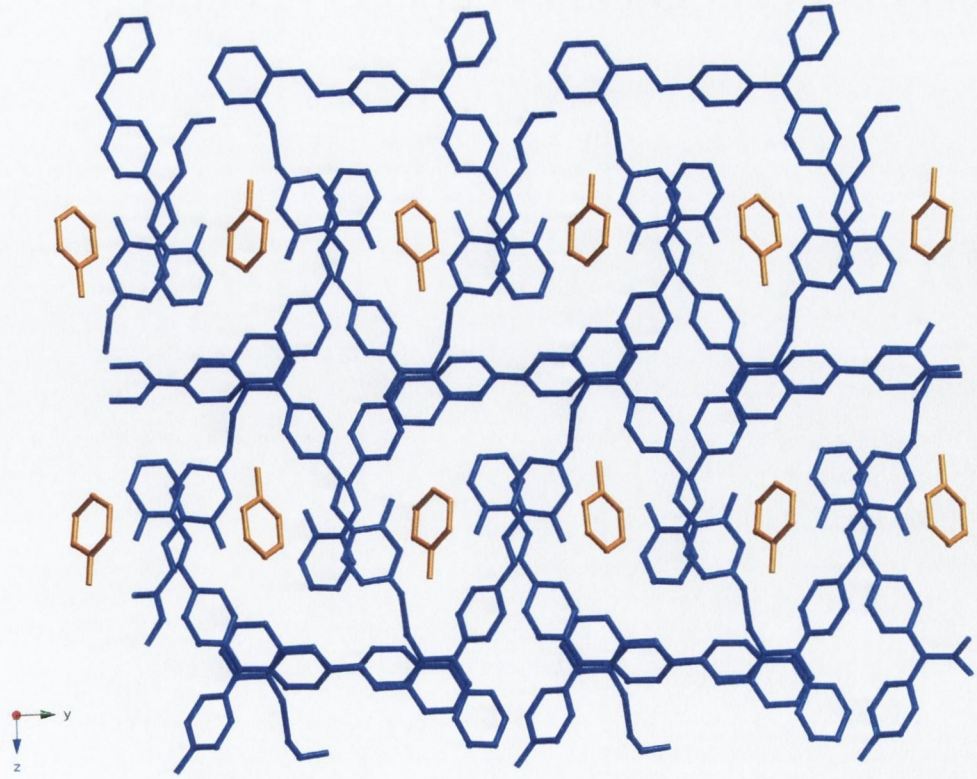

Figure 2.17 – Crystal packing of a 'sheet' of **H_3L8** (toluene molecules shown in orange).

Table 2.3 – Selected bond lengths (Å) and angles (°) for **H_3L8**.

N1 – C1A	1.415(2)	C1A – N1 – C1B	119.8(2)
N1 – C1B	1.415(2)	C1A – N1 – C1C	119.9(2)
N1 – C1C	1.419(2)	C1B – N1 – C1C	120.2(2)
N2A – C7A	1.282(3)	C4A – N2A – C7A	121.4(2)
N2B – C7B	1.258(3)	C4B – N2B – C7B	120.9(2)
N2C – C7C	1.281(3)	C4C – N2C – C7C	121.9(2)
N2A ··· H1A	1.77(2)	O1A – H1A – N2A	154(2)
N2A ··· O1A	2.589(2)	O1B – H1B – N2B	162(2)
N2B ··· H1B	1.67(2)	O1C – H1C – N2C	150(2)
N2B ··· O1B	2.608(2)	C2A – C1A – N1 – C1B	40.4(3)
N2C ··· H1C	1.80(2)	C6A – C1A – N1 – C1C	37.6(3)
N2C ··· O1C	2.583(2)	C6B – C1B – N1 – C1A	34.7(3)
O1A ··· H12C^{i}	2.71(2)	C2B – C1B – N1 – C1C	39.8(3)
O1A ··· C12C^{i}	3.611(3)	C2C – C1C – N1 – C1A	50.9(3)
O1B ··· H11C^{ii}	2.63(2)	C6C – C1C – N1 – C1B	47.6(3)
O1B ··· C11C^{ii}	3.351(3)		
O1C ··· H3A^{iii}	2.48(2)		
O1C ··· C3A^{iii}	3.174(3)		

Symmetry Codes: *i* = ½+x, -½-y, ½+z; *ii* = ½+x, ½-y, ½+z ; *iii* = 1-x, -y, -z.

The overall packing of sheets within the structure is shown in Figure 2.18. These sheets clearly stack in a plane that is offset to any of the planes defining the unit cell. Within individual sheets, inversion centres and two-fold screw axes relate layers to each other. The same relationships apply between sheets. Figure 2.18 has the unit cell marked (blue dashed lines) and the positions of the inversion centres (within the cell) can clearly be seen.

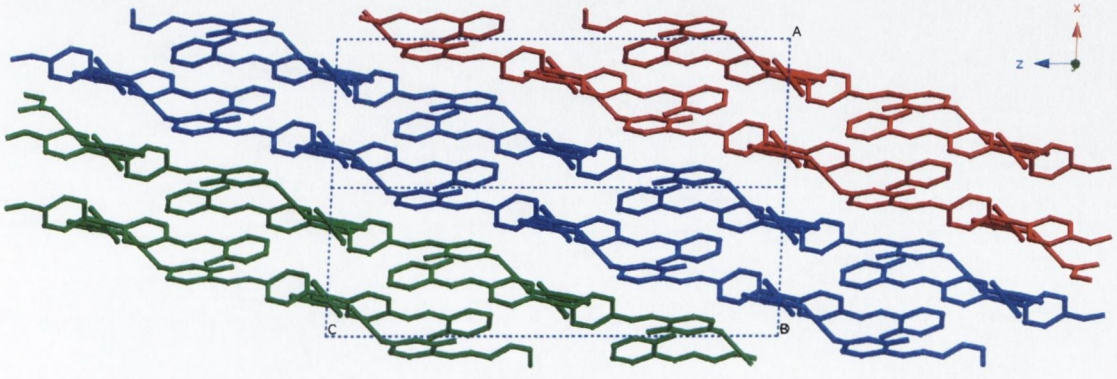

Figure 2.18 – Crystal packing of several 'sheets' of **H_3L8**. (View along *b*-axis, dashed line indicates cell.)

Table 2.4 – Crystal data for **L5**, **L7** and **H_3L8**.

Compound	**L5**	**L7**	**H_3L8**
Chemical Formula	$C_{24}H_{19}N_5$	$C_{39.5}H_{31}N_7$	$C_{46}H_{38}N_4O_3$
Formula Weight	377.44	603.71	694.80
Crystal System	Monoclinic	Triclinic	Monoclinic
Space Group	$P2_1/c$	$P\text{-}1$	$P2_1/n$
a /Å	11.742(1)	10.133(1)	8.662(1)
b /Å	15.627(1)	11.055(1)	8.662(1)
c /Å	10.924(1)	16.685(1)	26.49(1)
α /°	90.00	70.954(2)	90.00
β /°	101.205(2)	75.751(2)	92.425(2)
γ /°	90.00	74.992(2)	90.00
V /Å^3	1966.3(3)	1679.7(2)	3616.4(5)
Z	4	2	4
D_{calc} /g cm^{-3}	1.275	1.194	1.276
μ(Mo-K$_\alpha$) /mm^{-1}	0.078	0.073	0.081
T /K	153(2)	153(2)	153(2)
Crystal Size max /mm	0.33	0.25	0.40
mid /mm	0.23	0.20	0.20
min /mm	0.04	0.08	0.09
$2\theta_{max}$	45.0	40.0	50
Min/Max Trans. Factor	0.816/1.000	0.641/1.000	0.661/1.000
R_{int}	0.0611	0.0796	0.0477
R_1, wR_2 [I>2σ(I)][a]	0.0663, 0.1281	0.0987, 0.2723	0.0540, 0.1239
R_1, wR_2 (all data)	0.0902, 0.1378	0.1400, 0.3087	0.0884, 0.1382
Reflections: collected	8855	8330	20599
unique	2563	3144	6377
observed	2023	2049	4057

[a] $R_1 = \Sigma||F_o| - |F_c||/\Sigma|F_o|$, $wR_2 = [\Sigma w(F_o^2 - F_c^2)^2/\Sigma w(F_o^2)^2]^{1/2}$

2.2 Complexation studies of L5 and L7 with Ag(I) and Cu(I) salts.

*2.2.1 Complexation of N,N'-bis-pyridin-2-ylmethylene-4,4'-diaminodiphenylamine (**L5**) with Ag(I) salts.*

The solution chemistry involved in the reaction of **L5** with two Ag(I) salts (BF_4^- and PF_6^-) was studied predominantly through ^{1}H-NMR complexiometric titrations.[141] It was noted that treatment of a DCM solution of **L5** with a MeCN solution of Ag(I) led to the formation of a deep red coloured solution. Due to solubility constraints, a mixture of solvents was used in all titrations. A solution of **L5** was made up in 4:1 CD_3CN-$CDCl_3$ and the ^{1}H-NMR spectrum collected. Successive additions of 20 μl aliquots of an Ag(I) solution, containing 0.5 equivalents, were made and spectra collected after each addition. Figure 2.19 shows the spectra of successive additions of the Ag(I) solution to **L5**. In Figure 2.19, spectrum *(i)* represents the uncoordinated ligand. Upon the first addition of Ag(I) (spectrum *(ii)*) the solution turned from a bright yellow to a red colour, indicative of complexation. This is confirmed by the corresponding shifts in each proton resonance. Unfortunately further addition of Ag(I) resulted in excessive broadening of all proton signals, making distinction of individual resonances difficult.

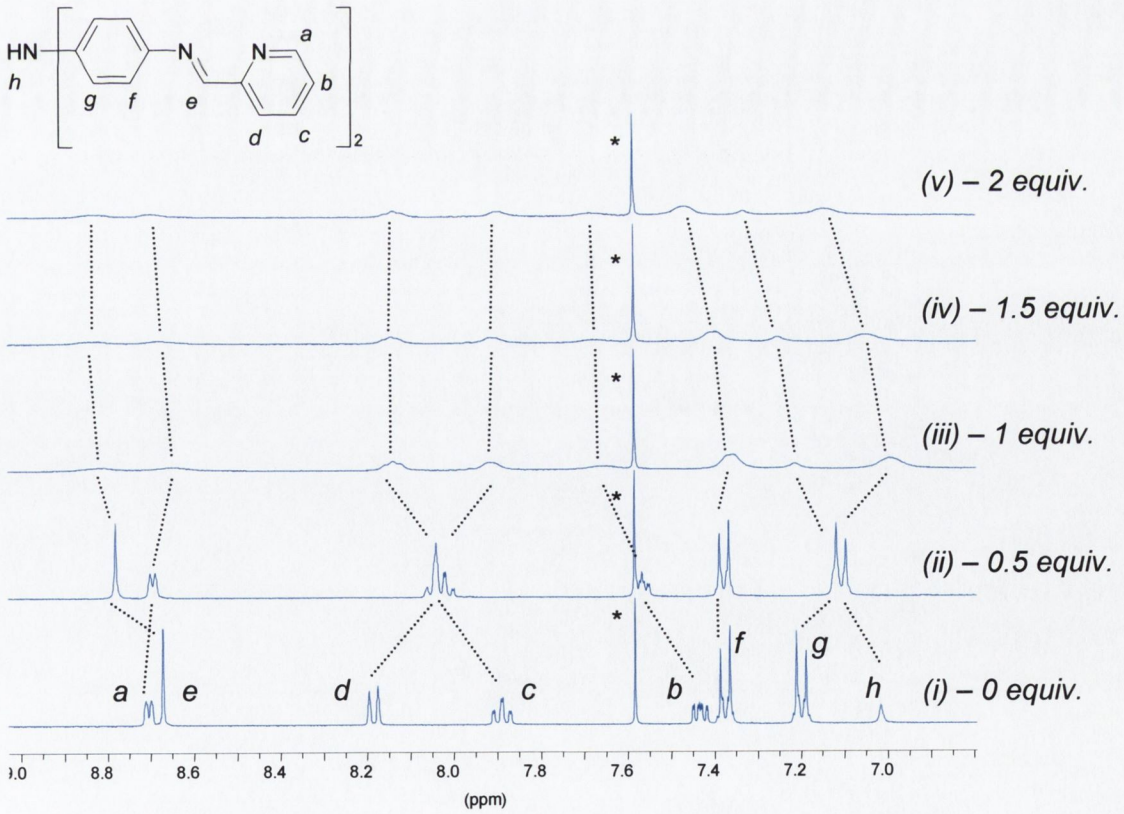

Figure 2.19 – ^{1}H-NMR ($CDCl_3$) of successive additions of $AgBF_4$ to **L5**.
(* denotes residual $CHCl_3$)

The broadening of proton resonances of ligands upon complexation seen in Figure 2.19, is a feature that has been reported previously for helicate systems.[28, 62, 127] The broadening is indicative of fluxional processes occurring within solution. This peak broadening was noted during complexation of **L5** with both the $AgBF_4$ and $AgPF_6$. This broadening of resonance peaks is evidence that complexation has occurred. Further evidence was provided by mass spectrometry. Samples of the titration solutions were taken and analysed by ES-MS. Figure 2.20 shows the spectrum obtained from the complexiometric titration of **L5** with $AgBF_4$. The mass spectrum did indicate the presence of an $[Ag_2(\mathbf{L5})_2]^{2+}$ species. The largest peak is at *m/z* = 485.09, which is magnified in the inset figure shown in Figure 2.20. A spacing of *m/z* 0.5 between the peaks within the cluster corresponds to the presence of a +2 charged complex, and the overall pattern of the isotopic distribution is consistent with that predicted by the MassLynx™ program[142] (top spectrum of inset) for the species $[Ag_2(\mathbf{L5})_2]^{2+}$.

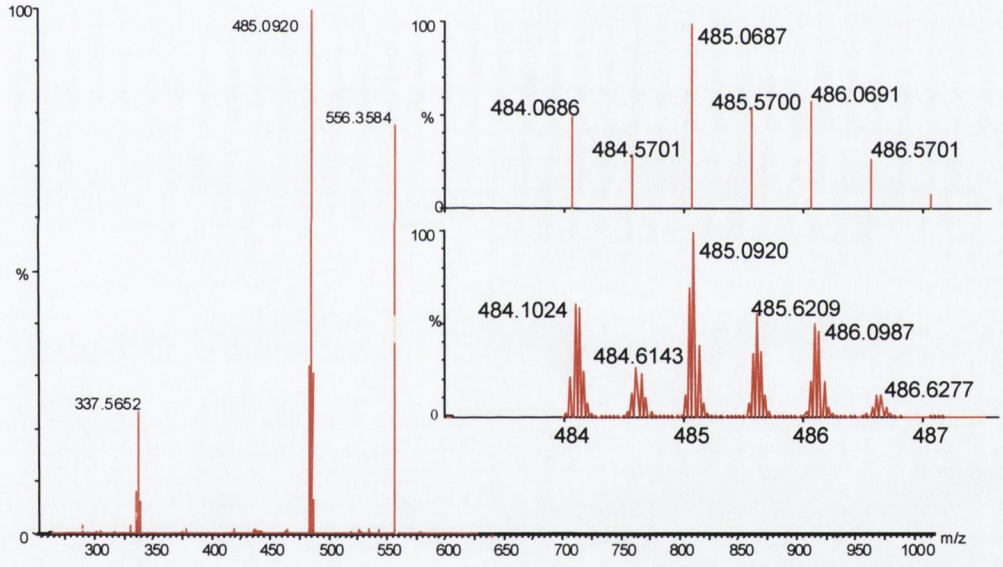

Figure 2.20 – Mass spectrum from the solution of $AgBF_4$/**L5** complexiometric titration. Inset: *Top* – predicted spectrum for $[Ag_2(\mathbf{L5})_2]^{2+}$. *Bottom* – actual spectrum obtained.

There are two other peaks in the spectrum, the peak at *m/z* = 556.36, can be accounted for by the addition of an internal standard for the calculation of the accurate mass peaks in the spectrum. The peak at *m/z* = 337.57 corresponds to the species $[Ag_2(\mathbf{L5})(MeCN)_2]^{2+}$.

The data presented above is evidence for the existence of the Ag(I) containing dinuclear double helicate species $[Ag_2(\mathbf{L5})_2]^{2+}$. It has not been fully ascertained whether this species exists as the helicate or the mesocate. The fluxional nature of the compound in solution, as shown by the broadening of proton resonances, suggest that the helicate and mesocate could both be present in solution. Variable temperature

^{1}H-NMR would assist in the isolation and identification of each species, however, at present this technique is not available at TCD.

*2.2.2 Complexation of N,N'-bis-pyridin-2-ylmethylene-4,4'-diaminodiphenylamine (**L5**) with Cu(I) salts.*

As was the case in the study of the reaction of **L5** with Ag(I), the complexation of Cu(I) with **L5** was studied *via* complexiometric ^{1}H-NMR titrations. The source of Cu(I) was from $Cu(MeCN)_4PF_6$, which was prepared from literature methods.[143] The same solvent regime was used (4:1, $CD_3CN/CDCl_3$) and a similar protocol followed.

A solution of the **L5** was made in 4:1 CD_3CN-$CDCl_3$ and the ^{1}H-NMR spectrum collected. Successive additions of 20 μl aliquots of a Cu(I) solution, containing 0.5 equivalents, were made and spectra collected after each addition. Figure 2.21 shows the ^{1}H-NMR spectra of successive additions of the Cu(I) solution to **L5**.

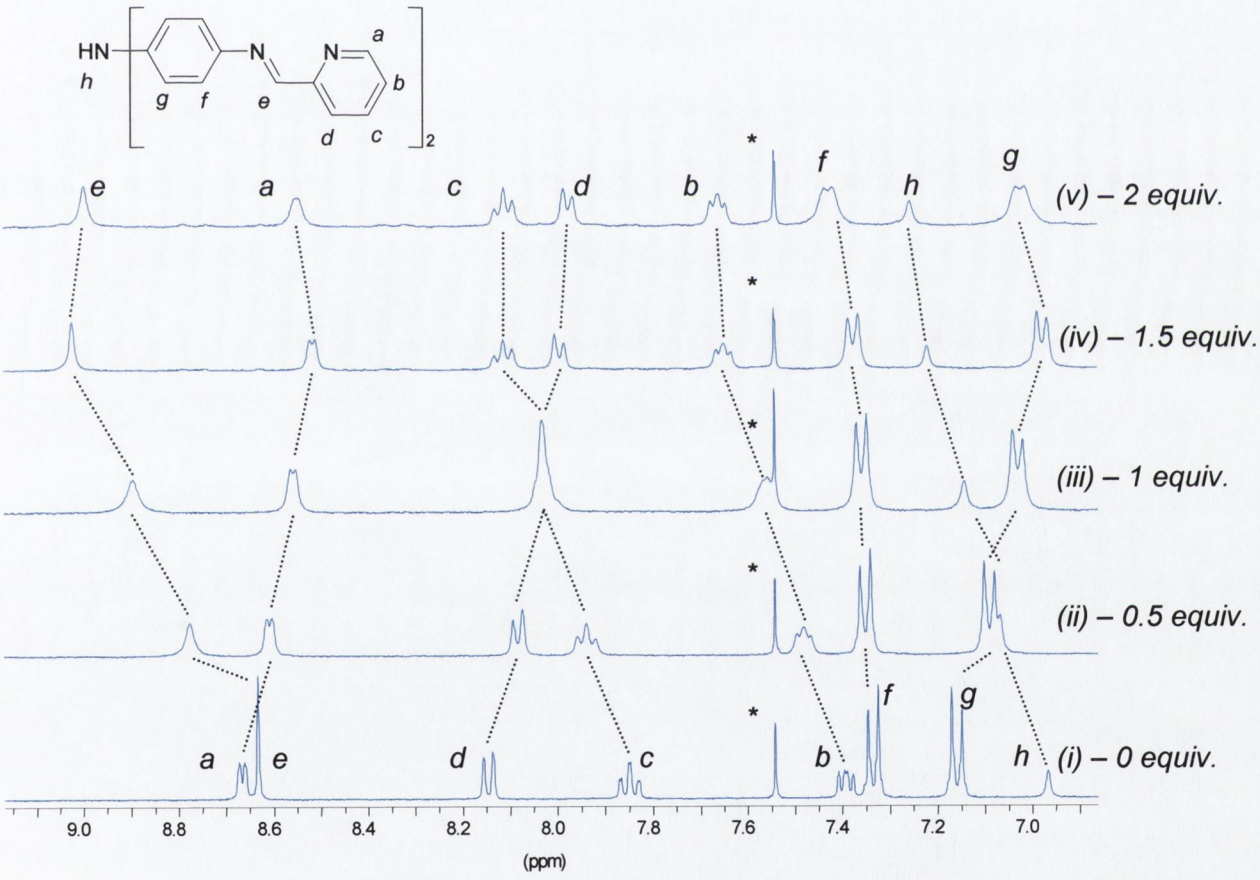

Figure 2.21 – ^{1}H-NMR ($CDCl_3$) of successive additions of $Cu(MeCN)_4PF_6$ to **L5**.
(* denotes residual $CHCl_3$. See Appendix for a molar plot for this experiment.)

As can be clearly seen from the spectra, upon addition of Cu(I), there is an appreciable change in the chemical shifts of each resonance. It should also be noted here that the solubility of $Cu(MeCN)_4PF_6$ in the quantity of solvent being used (2 ml) was considerably lower than the silver counterpart. This resulted in a cloudy solution being formed (although the mixture was sonicated in an effort to homogenise the

suspension). A consequence of this is that it is likely that the calculated concentration would be slightly higher than the actual solution concentration. Nevertheless, the resultant ^{1}H-NMR spectra are well defined and allow for facile interpretation. As Cu(I) is added, the overall trend of the peak movement can be noted. Peaks *a*, *d*, and *g* all experience an upfield shift, the movement of *a*, is *ca.* 0.11 ppm, whilst *d* and *g* experience shifts of 0.17 and 0.13 ppm, respectively. The remaining peaks all experience a downfield shift upon Cu(I) addition. The degree of shift varies from marginal (*f ca.* 0.04 ppm) through to large (*e ca.* 0.37 ppm). However the most important point to note is that after the addition of 1 equivalent of Cu(I) the peaks all become broad. This is evidence of fluxional behaviour, the fact that this occurs after the addition of one equivalent of Cu(I) is consistent with previous work where a combination of transient species have been seen to form.[55] The fluxional processes occurring in the solution are shown by the broadening of the resonances. Unlike the complexation with Ag(I), after further addition of Cu(I) (1.5 and 2 equivalents), the peak broadening diminishes and the peak resolution sharpens. This is consistent with the stabilisation of species within solution. Figure 2.22 shows the mass spectrum of a sample of the complexiometric titration solution the complex, as well as a magnification of the peak at *m/z* = 440.07.

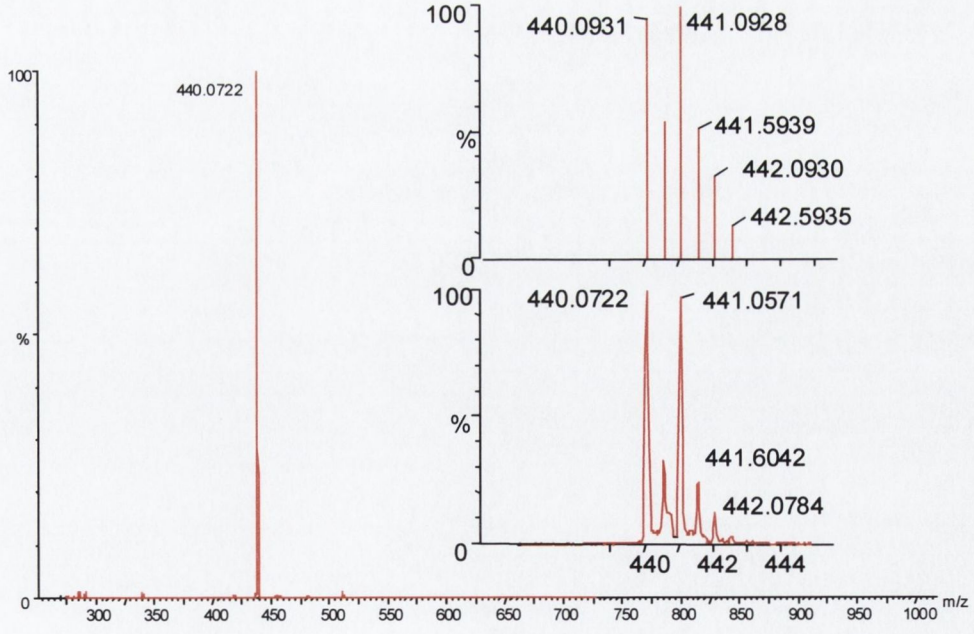

Figure 2.22 – Mass spectrum from the solution of $Cu(MeCN)_4PF_6$/**L5** complexiometric titration. Inset: *Top* – predicted spectrum for $[Cu_2(\mathbf{L5})_2]^{2+}$. *Bottom* – actual spectrum obtained.

There are no other peaks observed in this spectrum and the isotopic abundance distribution of the peak at *m/z* = 440.07 suggests a +2 charged species of the form $[Cu_2(\mathbf{L5})_2]^{2+}$. As was the case in the Ag(I) complexation, whether the $[Cu_2(\mathbf{L5})_2]^{2+}$

complex exists as the helicate or mesocate cannot be determined on the basis of the evidence above. The broadening of the proton resonances after the addition of one equivalent of Cu(I) (rather than at 0.5 equivalents) might be rationalised by the low solubility of $Cu(MeCN)_4PF_6$ in the solvent regime used. This would cause the actual concentration of Cu(I) to lag behind the calculated concentration, and so complexation would appear to occur (indicated by a decrease in peak broadening) at a (calculated) concentration of 1.5 – 2.0 equivalents of Cu(I) added (Figure 2.21).

It should also be noted that there was no effect on complexation from the counterion. Similar titration and ES-MS results were obtained for both hexafluorophosphate and tetrafluoroborate salts of Cu(I) and Ag(I).

*2.2.3 Complexation of N,N',N''-tris-pyridin-2-ylmethylene-4,4',4''-triaminotriphenylamine (**L7**) with Ag(I) salts.*

Treatment of a DCM solution of **L7** with a MeCN solution of $AgPF_6$ in a 2:3 ratio of ligand to metal, led to the formation of a deep red-coloured solution. Addition of a saturated methanolic solution of NH_4PF_6 to the reaction mixture gave an orange coloured precipitate. This was collected and dried *in vacuo*. Microanalytical data indicated that an $[Ag_3(\mathbf{L7})_2](PF_6)_3$ complex had been formed in good yield (55%). Confirmation of this came from ES-MS of the compound, which showed the presence of a peak at *m/z* = 479.76, with an isotopic abundance consistent with an $[Ag_3(\mathbf{L7})_2]^{3+}$ species in solution. The ^{1}H-NMR spectrum of the complex is well defined and allows facile interpretation, which is indicative of a highly symmetrical species. A major feature of this complexation reaction is that there is no evidence (in the ^{1}H-NMR spectrum) of any ligand dissociation or fluxional processes under these conditions.[144] This is in contrast to previously reported behaviour of C_2 symmetric ligand systems.[28, 55, 127]

As was the case for **L5**, the solution chemistry of **L7** with Ag(I) was further studied *via* a complexiometric ^{1}H-NMR titration. The same solvent system was used, but additions of Ag(I) contained only 0.118 equivalents and continued until approximately 2.3 equivalents had been added. Upon the first addition of $AgPF_6$, the colour of the ligand solution was again seen to change from a bright orange to a deep red, indicative of the complexation of Ag(I) by **L7**.

Successive spectra were collected and these are shown in Figure 2.23, along with the peak assignments. Spectrum *(i)* is the spectrum of the free ligand **L7** and the spectra above *(i)* are collected after successive additions of 0.118 equivalents of $AgPF_6$ to the ligand solution.

Upon addition of Ag(I), the signals from protons *b*, *c* and *e* are observed to shift downfield by approximately 0.25 ppm. The pyridyl proton *d* shifts upfield by a similar amount. Signals from protons *a*, *f* and *g* shift the least but do experience both up- and

downfield movement. The pyridyl proton *a* experiences only a marginal shift of approximately 0.02 ppm, whilst the phenyl protons (*f* and *g*) of the central aromatic ring shift downfield and upfield by 0.06 and 0.10 ppm, respectively.

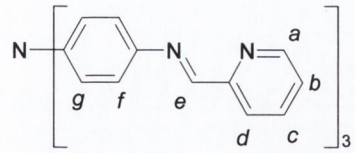

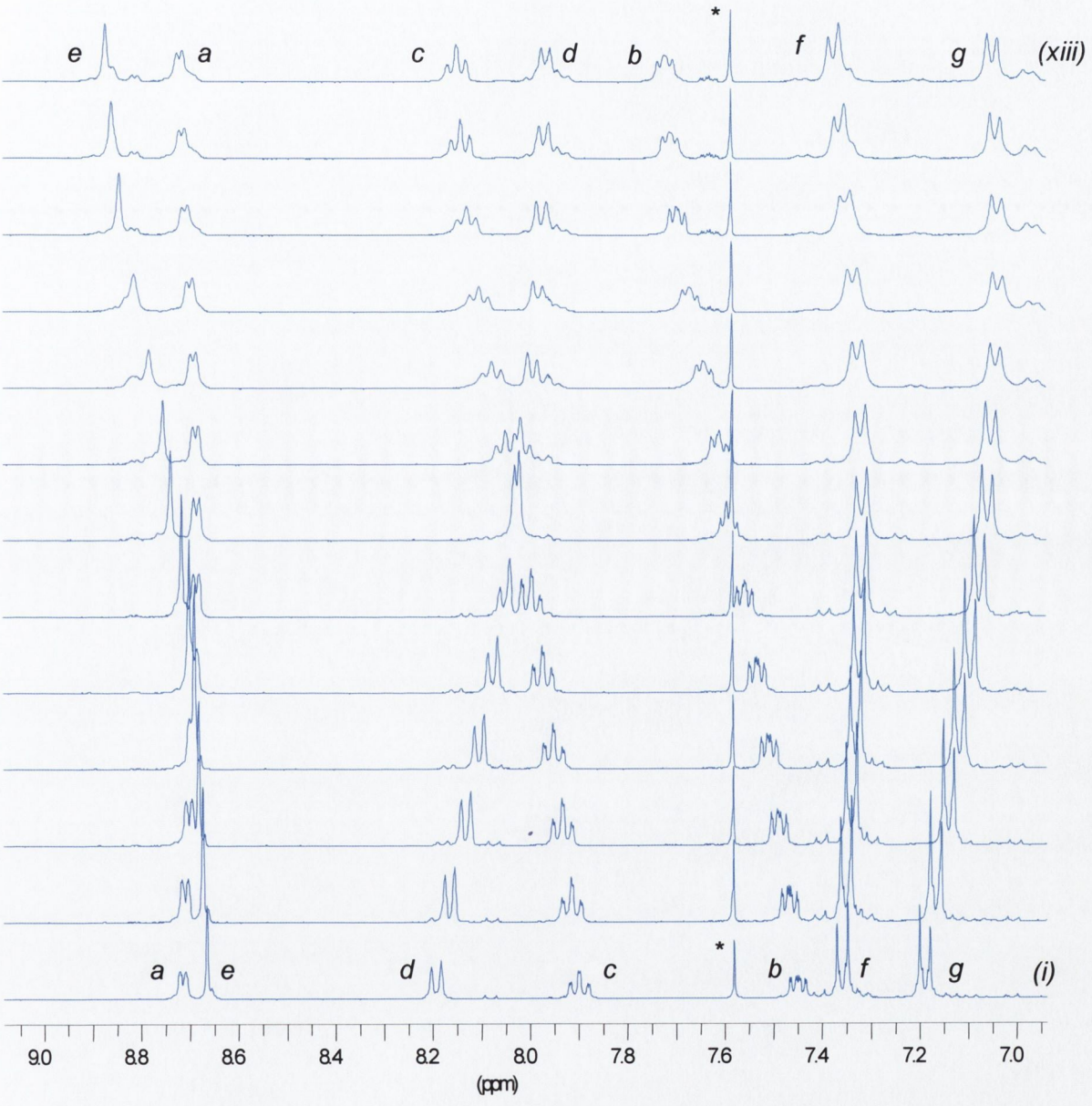

Figure 2.23 – ^{1}H-NMR ($CDCl_3$) of successive additions of 0.118 equivalents of $AgPF_6$ to **L7**. (* denotes residual $CHCl_3$. Spectrum *(i)* 0 equivalents Ag(I) added, spectrum *(xiii)* 1.416 equivalents Ag(I) added.)

An important feature to note regarding this experiment is that after a certain amount of Ag(I) (*ca.* 1.5 equivalents; the top spectrum shown in Figure 2.23) has been added, there is little or no further movement in the chemical shifts of all the protons. A

plot of the change in chemical shift ($\Delta\delta$) against amount of Ag(I) added (in equivalents) clearly illustrates this point (Figure 2.24).

These observations can be rationalised in following way: Upon addition of Ag(I), coordination within the pyridylimine binding site occurs, which causes a disruption of the micro-electronic environment that the protons exist in. This change in the shielding of the protons causes changes in the resonance peaks associated with each proton. Successive additions of Ag(I) lead firstly to an $[Ag_2(\mathbf{L7})_2]^{2+}$ dinuclear complex with a 1:1 stoichiometry. This can be seen in the ^{1}H-NMR spectrum by the broadening of the peaks, which is indicative of the formation of transient species within the solution. As can also be seen in Figure 2.24 there is a slight inflection point (at *ca.* 1.0 equivalents of Ag(I) added) in the movement of the signals from protons *a*, *f* and *g*. This could possibly be accounted for by the through-space effects those protons may begin to experience as the neighbouring ligand strand approaches.

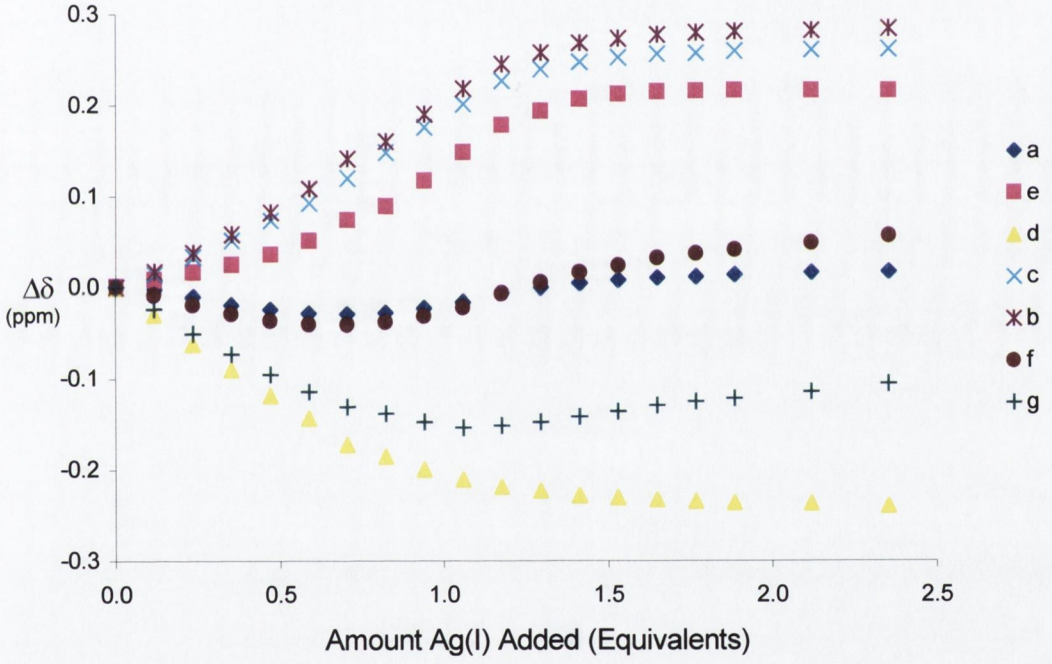

Figure 2.24 – Molar plot of change in chemical shift ($\Delta\delta$) against successive additions of $AgPF_6$ to **L7**.

Further addition of Ag(I) up to and beyond 1.5 equivalents allows for the generation of an $[Ag_3(\mathbf{L7})_2]^{3+}$ species, which is robust in the presence of excess Ag(I), as characterised by the well resolved peaks in the ^{1}H-NMR spectrum.

Further evidence for the formation of a 3:2 metal to ligand complex is given by the mass spectrum of the titration solution. Figure 2.25 shows mass spectrum along with a magnification of the molecular ion peak (*m/z* = 479.76). The isotopic distribution indicates a complex that contains three Ag(I) atoms and corresponds to the species

$[Ag_3(\mathbf{L7})_2]^{3+}$. The two inset spectra are the predicted spectrum[142] (inset top) and the actual spectrum collected (inset bottom)

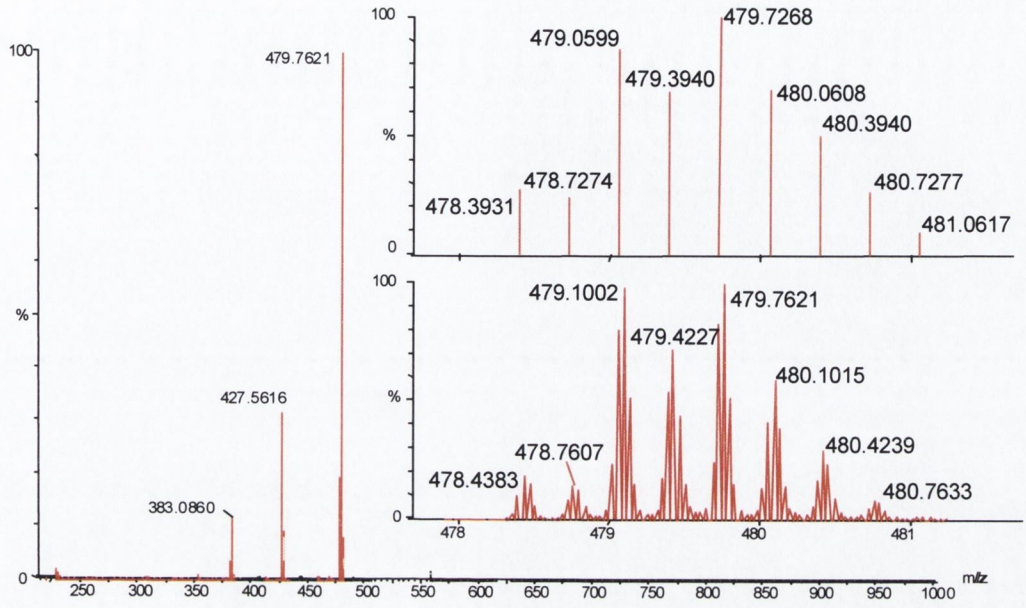

Figure 2.25 – Mass spectrum from the solution of $AgPF_6$/**L7** complexiometric titration. Inset: *Top* – predicted spectrum for $[Ag_3(\mathbf{L7})_2]^{3+}$. *Bottom* – actual spectrum obtained.

There are two other peaks present in the spectrum, both of which can be accounted for by fragmentation species, a feature that has been reported previously in ES mass spectra.[145] The peak at *m/z* = 427.56 corresponds to the $[Ag_2(\mathbf{L7})(MeCN)_2]^{2+}$ species, whilst the peak at *m/z* = 383.09 corresponds to a species containing the ligand fragment **L7'**[‡] to give $[Ag_2(\mathbf{L7'})(MeCN)_2]^{2+}$.

What does $[Ag_3(\mathbf{L7})_2]^{3+}$ look like? Based on the evidence proposed above and, preliminary molecular modelling,[129] it is proposed that the complex will be helical in nature. The helical nature of the complex is reflected in each arm, as they crossover the Ag-Ag axis. As mentioned in the introduction, helical complexes based upon C_2-symmetric ligand types may exist in either a helical form (*rac*-isomer) or as a mesocate (*meso*-isomer, the ligands do not cross the metal-metal axis), and may interconvert between each (as evidenced by their fluxional behaviour in solution). Whilst this is an option here, the three-armed nature of the complex ensures that a helical species must exist even if the *meso*-isomer is formed i.e. it is impossible to coordinate three arms without at least two arms crossing the Ag-Ag axis. Figure 2.26 shows molecular models, (generated by HyperChem™[129]) of both possible isomers of the complex. Figure 2.26(a) shows the *rac*-isomer, along with arrows depicting the helical

[‡] **L7'** is a fragment of **L7** corresponding to the loss of a pyridyl group (**L7'** = $C_{30}H_{24}N_6$)

moieties within the complex, note how *each* ligand strand crosses over the Ag-Ag axis. Contrasting this Figure 2.26(b) shows the *meso*-isomer where both helical (indicated by the arrow) and non-helical (indicated by the crossed arrows) moieties are present. In this case note how *only one* ligand 'arm' (from each ligand) crosses the Ag-Ag axis. Irrespectively, the meso-isomer must always retain a helical strand.

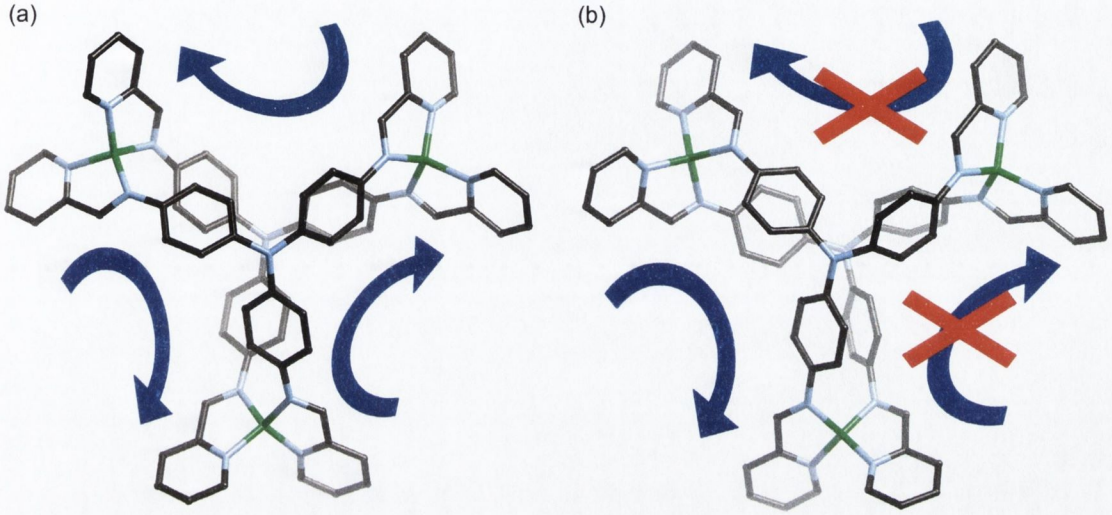

Figure 2.26 – (a) HyperChem[129] model of the *rac*-$[Ag_3(\mathbf{L7})_2]^{3+}$ isomer. Note all ligand strands cross Ag-Ag axes. (b) HyperChem[129] model of the *meso*-$[Ag_3(\mathbf{L7})_2]^{3+}$ isomer. Note only one ligand arm (from each ligand) crosses the Ag-Ag axis.

*2.2.4 Complexation of N,N',N''-tris-pyridin-2-ylmethylene-4,4',4''-triaminotriphenylamine (**L7**) with Cu(I) salts.*

An acetonitrile solution of $Cu(MeCN)_4PF_6$ was reacted with **L7** and excess methanolic NH_4PF_6 added. A brown precipitate formed, which was collected. However microanalytical data could not be matched to a complex analogous to that seen for the reaction of Ag(I) with **L7**. A complexiometric ^{1}H-NMR titration was performed in an effort to gain an insight into what was occurring. The same solvent regime was used as in previous titrations, and the spectra are shown in Figure 2.27.

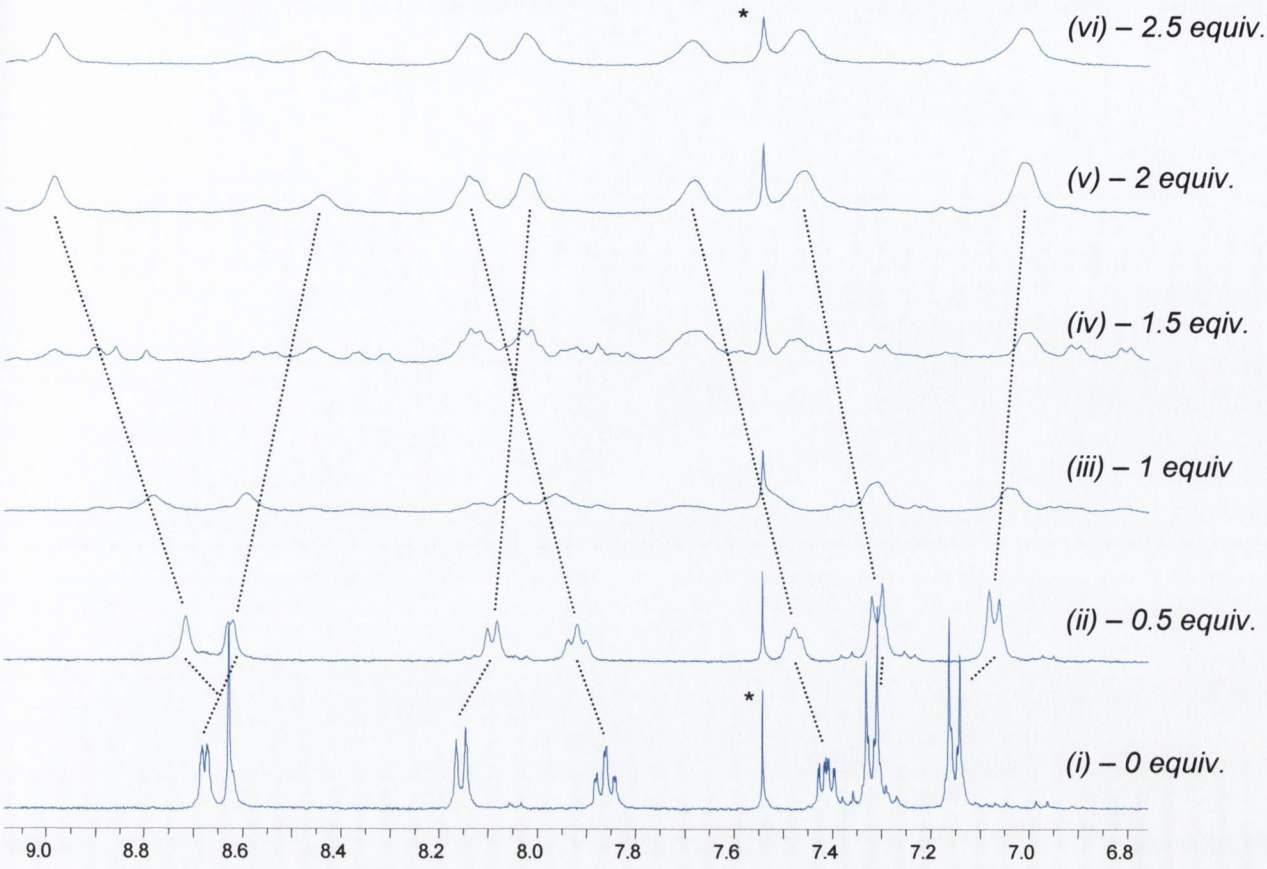

Figure 2.27 – ^{1}H-NMR of successive additions of $Cu(MeCN)_4PF_6$ to **L7**.
(* denotes residual $CHCl_3$)

As can clearly be seen, there is excessive broadening of the resonance peaks upon addition of Cu(I). This (as before) is indicative of multiple species within the solution, and is a result the fluxional nature of species forming and breaking up, unlike the previous reaction (between Ag(I) and **L7**) the ^{1}H-NMR spectrum does not display a decrease in peak broadening after the addition of excess Cu(I). This suggests there are several species in solution, which is confirmed by the mass spectrum of the titration mixture, which is shown in Figure 2.28. The peak at *m/z* = 435.07 is consistent with a 3:2 metal-to-ligand complex. A magnification of this peak is shown in the inset along with the predicted spectrum for the species $[Cu_3(\mathbf{L7})_2]^{3+}$. This is clear evidence that the Cu(I) complex with **L7** is analogous to the Ag(I) complex described above. As was the case in the complexation of Ag(I) to **L7**, other species are present in solution, the ^{1}H-NMR spectra shown in Figure 2.27 confirm this. There are two other peaks that are labelled in the mass spectrum, which can be accounted for. The peak at *m/z* = 382.59 corresponds to the species $[Cu_2(\mathbf{L7})(MeCN)_2]^{2+}$, whilst the peak at *m/z* = 290.38 corresponds to the tri-nuclear species $[Cu_3(\mathbf{L7})(MeCN)_3]^{3+}$.

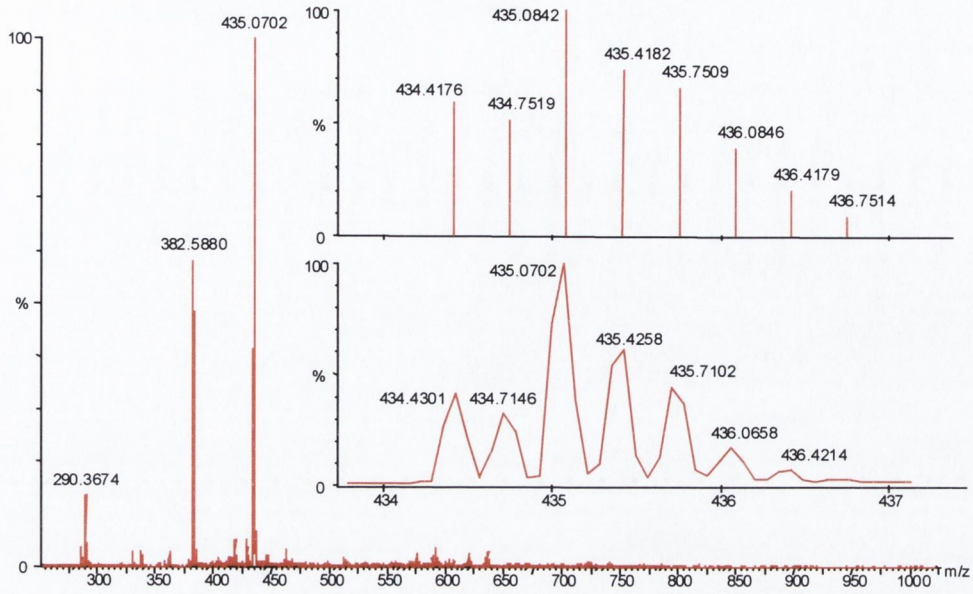

Figure 2.28 – Mass spectrum from the solution of $Cu(MeCN)_4PF_6$/**L7** complexiometric titration. Inset: *Top* – predicted spectrum for $[Cu_3(\mathbf{L7})_2]^{3+}$. *Bottom* – actual spectrum obtained.

Unlike the Ag(I) case, there are a large number of very small peaks in the baseline of this titration solution, which, when magnified and analysed, can be accounted for by species that contain varying of metal-to-ligand ratios (identified by the isotopic distribution patterns). It is likely that it is these complexes that are the source of the broadening of the proton resonances in the ^{1}H-NMR.

2.2.5 Preliminary UV-vis spectroscopic studies.

As was mentioned in Section 2.1.2 preliminary results from UV-vis complexiometric titrations of Zn(II) with **H_3L4** indicated the formation of a $[Zn_3(\mathbf{L4})_2]$ species. Further titrations of the **L7** ligand with metal salts were performed, and preliminary results are reported in this section.

The procedure followed was similar to that used in the ^{1}H-NMR titrations described in previous sections. A 10 ml solution of **L7** was made up in 4:1 CH_3CN-$CHCl_3$ and the UV-vis spectrum collected. Successive additions of 10 µl aliquots of an Ag(I) solution, each containing 0.25 equivalents, were made and spectra collected after each addition. Figure 2.29 shows the spectra of successive additions of the Ag(I) solution to **L7**. Upon addition of Ag(I), a hypochromic shift is observed in the peak at 412 nm. This peak is most probably due to a ligand-based transition, most likely of $\pi \rightarrow \pi^*$ origin. Concurrently, a hyperchromic shift is observed at 494 nm, as indicated in Figure 2.29. The presence of a clear isosbestic point at 442 nm is also apparent.

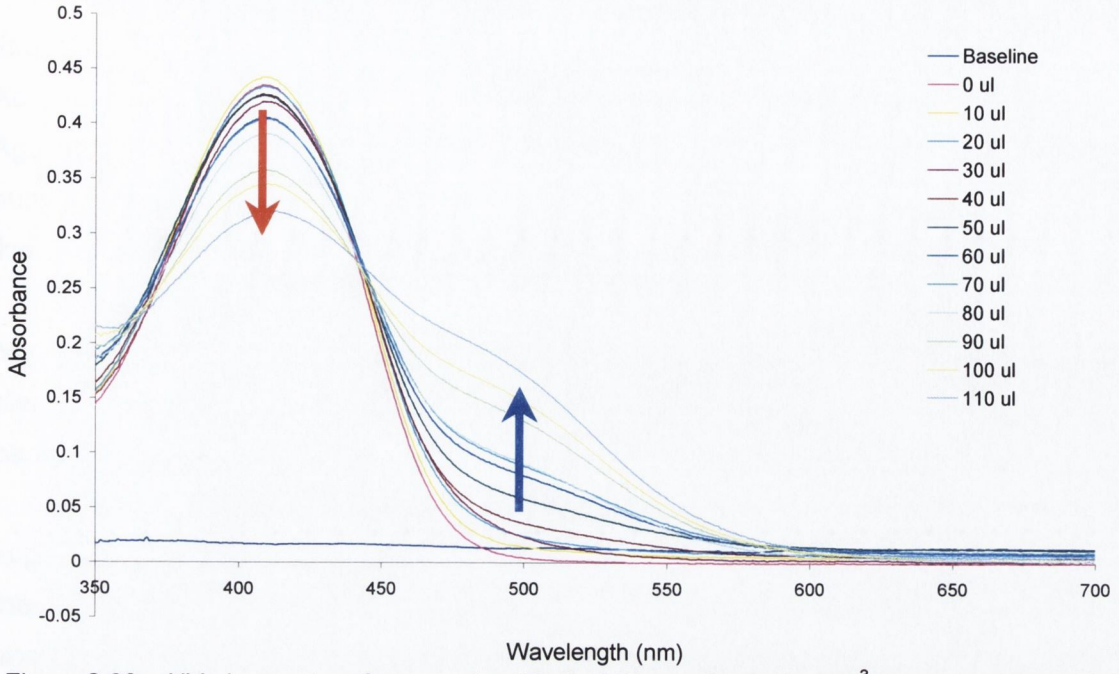

Figure 2.29 – UV-vis spectra of successive 10 µl additions of a 7.18×10^{-3} M solution of $AgPF_6$ to a 2.87×10^{-5} M solution of **L7**. (Red arrow shows decrease of absorbance at 412 nm, blue arrow shows increase of absorbance at 494 nm. Each 10 µl aliquot contains 0.25 equivalents of Ag(I))

The formation of the peak at 494 nm is most likely to be due to metal-to-ligand charge transfer between Ag(I) and **L7** on complexation

It should be noted that these results are preliminary and further work needs to be carried out, in order to ascertain the exact nature of the species present.

2.3 Conclusions.

As a result of this study, a novel series of Schiff's base ligands have been synthesised and characterised. Previous work[57] has been extended in the formation of ligands with a new bridging group, as well as addition of a third 'coordinating arm'. The ligands have been characterised by ^{1}H-NMR, ES-MS, IR and in some cases, single crystal X-ray crystallography. The instability of the **L3** ligand in protic solvents, was overcome by changing the backbone of the ligand to include a nitrogen bridging atom. These ligands (**L5** and **L7**) have proved more robust in terms of stability within protic solvents.

Complexation of the ligands with the tetrahedral metal ions Ag(I) and Cu(I) was studied *via* complexiometric ^{1}H-NMR titrations and ES-MS. In the case of **L5**, although the mass spectrum showed the presence of a $[M_2(\mathbf{L5})_2]^{2+}$ species, whether the helicate or mesocate form exists, remains to be proven. Previous studies have shown that variable temperature ^{1}H-NMR studies could clarify this issue, however this facility is not currently available at TCD.

The complexation of **L7** with Ag(I) and Cu(I) was also studied *via* ^{1}H-NMR titrations and ES-MS. Clearly there is evidence of the formation of $[M_3(\mathbf{L7})_2]^{3+}$ species. As was shown in Section 2.2.3 a trinuclear species may contain a helicate moiety. Again the formation of the mesocate form is indeed possible, however due to the number of coordinating arms, should a mesocate form exist between two metal centres, the helicate form will exist between the remaining metal centre.[144]

There remains a great deal of scope with regards to the continuation of this work. As has been mentioned, variable temperature ^{1}H-NMR studies could assist in identifying the helicate or mesocate species, currently we are seeking a collaborative partnership to persue this.[146]

Crystallisation of the helical complexes, would provide further information, especially in the trinuclear systems, as to whether the *rac*- or *meso*-isomer is present in the solid state. To date all attempts to crystallise these complexes have remained unsuccessful, however crystallisations are ongoing.

A further feature of the helicate architecture is the inherent chirality present in the system. The chirality of the helicate systems formed herein, has yet to be studied. All the work reported in this chapter has involved racemic mixtures, although collaboration with Lacour[146] is being undertaken to utilise work involved in isolating enantiomers by using chiral anions as a resolving agent.[147]

Chapter Three

Coordination Polymers Incorporating 4,4'-Bipyridine.

Preamble.

The work presented in the following chapter represents how serendipitous discoveries change the direction of scientific research. Initially, work was to focus on (amongst other things) the synthesis of a tetranuclear 'molecular square'. However, an initial product was a 4,4'-bipy containing coordination polymer. This developed into a study of the synthesis and structural characterisation of various coordination polymers, which is reported herein.

Introduction.

A recent trend in metallosupramolecular chemistry has involved the controlled synthesis of metallo-aggregates such as rotaxanes,[24, 148] catenanes,[25] helicates,[2, 15] molecular polygons and polyhedra.[20, 70, 81] The formation of metal containing molecular squares is a much-studied area.[81, 149-151] In an effort to extend this work further, we intended to utilise the tetradentate ligand 2,2':4,4'':4',4'''-quaterpyridine (qpy) shown in Figure 3.1 as an angular bridging unit. This ligand had previously been synthesised by Baker and co-workers[152] and has three coordination sites, one bidentate and two monodentate.

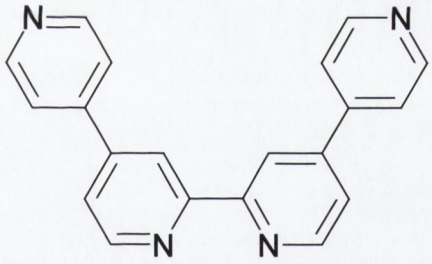

Figure 3.1 – 2,2':4,4'':4',4'''-Quaterpyridine ligand, first synthesised by Baker and co-workers.[152]

This ligand is able to chelate to a metal centre in a similar way to 2,2'-bipy, whilst still having the ability to coordinate through the remaining pyridyl groups to two other metal centres. It was envisaged that a molecular square utilising this ligand would have the appearance of the structure shown in Figure 3.2(a). This compound would consist of two octahedral Ru(II) metal centres, each coordinated to two 2,2'-bipy molecules and one quaterpyridine ligand. Two square planar Pd(II) metal centres are coordinated to the monodentate pyridyl groups on the quaterpyridine ligand. Figure 3.2(b) shows the structure of a similar molecular square, however in this case the Pd(II) metals have been replaced with two octahedral Ru(II) metal centres. This forms a molecular square, which would be able to encapsulate a single PF_6^- anion within the cavity (see Appendix for a Hyperchem™[129] molecular model of this compound). (Obviously there would be other counter-ions present in the system, which

we propose would reside around the aggregate. The point of this modelling is to demonstrate that the target molecular square is potentially attainable on steric grounds.)

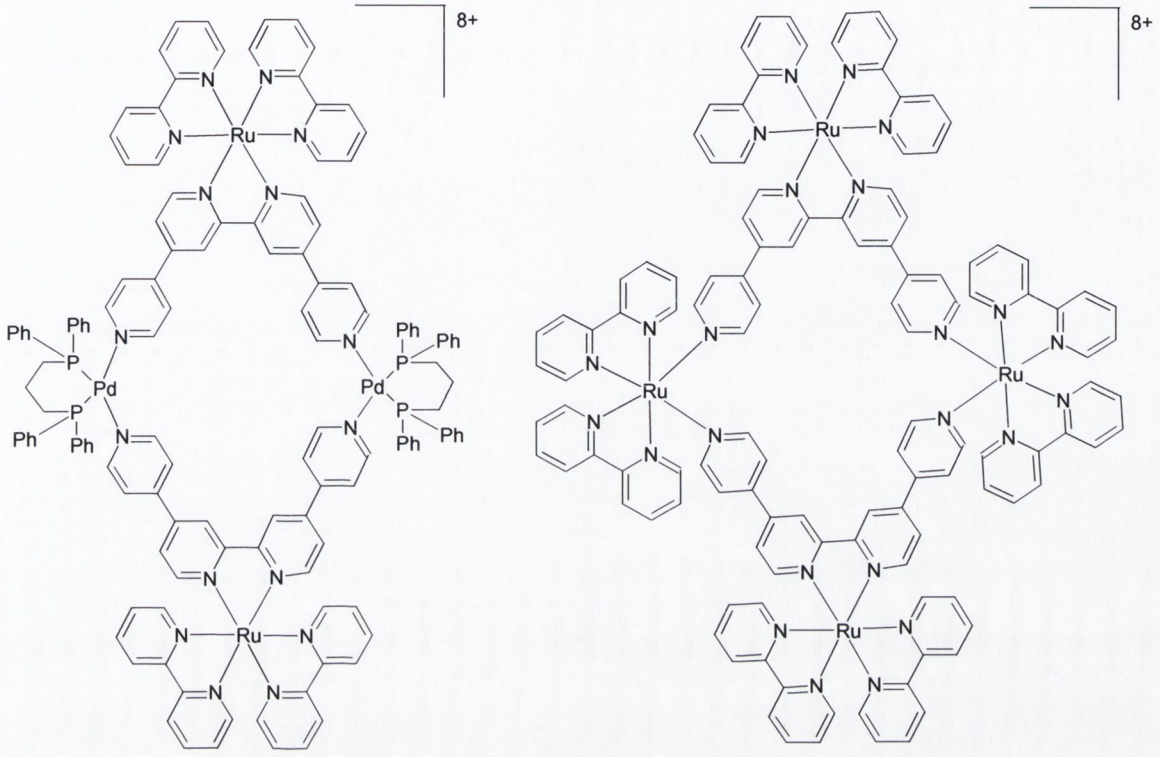

Figure 3.2 – (a) Proposed Ru_2Pd_2 containing structure of a tetranuclear molecular square. (b) Proposed Ru_4 containing structure of a tetranuclear molecular square.

3.1 Reaction of Ru(II) with 2,2'-bipyridine, 2,2':4,4'':4',4'''-quaterpyridine (qpy).

The chemistry of polypyridyl ruthenium complexes is well-documented area of research.[153] The stable oxidative properties of ruthenium make it an ideal candidate for use in the synthesis of molecular squares.

3.1.1 Reaction of Ru(2,2'-bipy)$_2$Cl$_2$ with qpy.

Ru(2,2'-bipy)$_2$Cl$_2$ was prepared by a modification of previously published methods.[154] Ru(2,2'-bipy)$_2$Cl$_2$ was reacted with one equivalent of qpy in a 1:1 mixture of EtOH and water. Addition of aqueous NH_4PF_6 yielded an orange/red precipitate. ^{1}H-NMR analysis of the crude precipitate indicated the presence of impurities (starting reagents) so a purification of the product *via* ion-exchange chromatography was made. Characterisation by was made ^{1}H-NMR and ES-MS analyses.

3.1.2 Crystal structure of $[Ru(2,2'\text{-bipy})_2(qpy)][PF_6]_2 \cdot CH_3COCH_3$.

Crystals of $[Ru(qpy)(2,2'\text{-bipy})_2][PF_6]_2 \cdot CH_3COCH_3$ were formed by slow evaporation of an acetonitrile solution of the compound. The crystal structure was obtained by Dr. Mark Nieuwenhuyzen at Queen's University, Belfast.* The ruthenium centre adopts an octahedral geometry, and has two 2,2'-bipy molecules and a single qpy ligand chelating to it. Figure 3.3 shows the molecular structure of a single molecule.

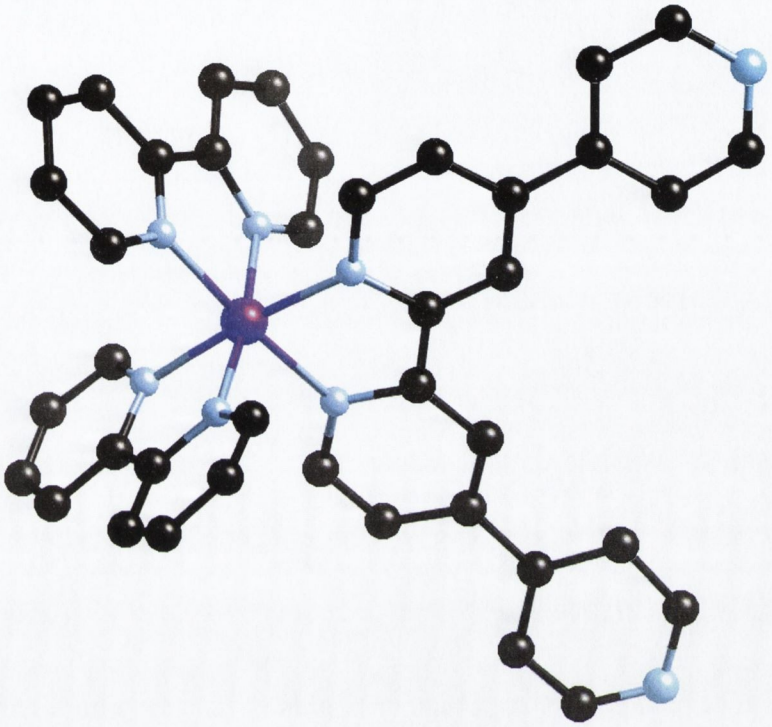

Figure 3.3 – Crystal structure of $[Ru\ (2,2'\text{-bpy})_2(qpy)]^{2+}$ (Δ-isomer shown, solvent molecules, hydrogen atoms, and counter-ions omitted for clarity)

The hexafluorophosphate anions, acetone molecules and hydrogen atoms are omitted from Figure 3.3 for clarity. The presence of acetone in the structure can be attributed to its use in the chromatography. Therefore acetone was present in the purified product prior to recrystallisation. The non-coordinating pyridyl groups in the qpy molecule are twisted slightly along the carbon-carbon bond between the rings giving rise to torsions angles of approximately 20°. The structure is centric so both Δ and Λ enantiomers are present in equal quantities. The structure shown in Figure 3.3 is the Δ enantiomer. Although individual complexes are chiral no attempt was made to resolve enantiomers and thus racemic mixtures were used in further reactions. Therefore any aggregates formed with this complex would likely contain diastereomeric mixtures.

* See Appendix for a listing of crystallographic data for this compound.

3.1.3 Further complexation of $[Ru(2,2'\text{-bipy})_2(qpy)][PF_6]_2$.

Once the corner unit $(Ru(2,2'\text{-bipy})_2(qpy)]^{2+}$) of the molecular square had been synthesised an attempt to form the entire square could be made. To this end, $[Ru(2,2'\text{-bipy})_2(qpy)][PF_6]_2$ was reacted with $Pd(dppp)(OTf)_2$ (dppp = diphenylphosphine propane, OTf = triflate) in degassed nitromethane. The aromatic section (δ 7 – 9 ppm) of the ^{1}H-NMR spectrum was extremely complicated, since proton resonances from three different aromatic systems were present. Ion-exchange chromatography (Section 5.2.3, page 157) was unable to yield a pure product. The main problem with analysis of this compound was the overlapping of resonance peaks in the ^{1}H-NMR spectrum. This problem could be overcome by altering the ligands coordinated to the Pd(II) centre. If the dppp ligand were substituted by a ligand that contained no aromatic rings, such as diaminoethane (en), the ^{1}H-NMR spectrum would be less overlapped and more open to interpretation. During the course of this work Thomas and co-workers reported the synthesis of the $[[Ru(2,2'\text{-bipy})_2(qpy)]_2[Pd(en)_2]_2]^{8+}$ species.[155] The characterisation of the complex was made with elemental analysis, FAB-MS and ^{1}H-NMR and UV-vis spectroscopy. Luminescence and absorption titrations on the complex found minor changes in the emission intensity with selected guest molecules.[155] Although Thomas and co-workers reported the formation of small crystals with the hexafluorophosphate salt of the complex, the crystals were highly unstable even at reduced temperatures.

Since a crystal structure of the molecular square species is highly desirable, it was decided (in the present study) to begin altering the components of the system in search of a stable product suitable for single crystal X-ray diffraction. The first option taken was to alter the metal centres of the complex.

3.2 Reaction of Co(II) with 2,2'-bipyridine, 2,2':4,4'':4',4'''-quaterpyridine and 4,4'-bipyridine.

As an initial attempt at utilising an alternative metal in the formation of a molecular square, a first row transition metal was selected. For reasons of convenience Co(II) was used in the attempted formation of the corner unit. The synthesis of 2,2'-bipy and Co(II)/(III) containing complexes have been reported.[156-158] One drawback to the use of Co(II) (d^7) paramagnetic complexes means that analysis by ^{1}H-NMR of any products formed with Co(II) present would be difficult. However one of the reasons behind altering the metal centre is to promote crystallisation, and to therefore allow analysis by single crystal X-ray diffraction.

3.2.1 Reaction of $Co(NO_3)_2$ with 2,2'-bipy and qpy.

An aqueous solution of 2,2'-bipy and $Co(NO_3)_2$, was reacted with a methanolic solution of qpy in an overall ratio of 2:1:1. After several days a few (~5 or 6) small orange prismatic crystals formed. IR spectroscopy indicated the presence of aromatic rings systems as well as nitrate anions (1328 cm^{-1}). This was consistent with a potential $[Co(2,2'\text{-bipy})_n(qpy)]^{2+}$ (*n = 1 or 2*) complex. The crystal structure was obtained by Dr. Mark Nieuwenhuyzen at Queen's University, Belfast. Preliminary results showed a structure containing no quaterpyridine ligands, however there were a large number of disordered molecules (nitrate, solvent, starting reagents) within the crystal lattice, but none that could be interpreted as qpy. Figure 3.4 shows a model of the initial structure, the disordered guest molecules, solvent and counter-ions are omitted from the figure for clarity (they reside in the voids bound by the Co/4,4'-bipy network). Clearly the desired $[Co(qpy)(2,2'\text{-bipy})]^{2+}$ molecule is not present. In fact the complex forms 1D coordination polymeric chains, which are hydrogen-bonded together to form a 2D sheet.

The presence of 4,4'-bipy in the structure was initially puzzling, but can be attributed to an impurity in the sample of qpy used in the reaction. This is probable, especially as the alternative (that the carbon-carbon bond linking the two 4,4'-bipy groups together was broken) is unlikely under the mild conditions the reaction was performed. Analysis of the qpy sample by thin-layer chromatography and ^{1}H-NMR, indicated that residual 4,4'-bipy was present in the qpy sample used as a reagent. This is consistent with only a small amount of product being obtained.

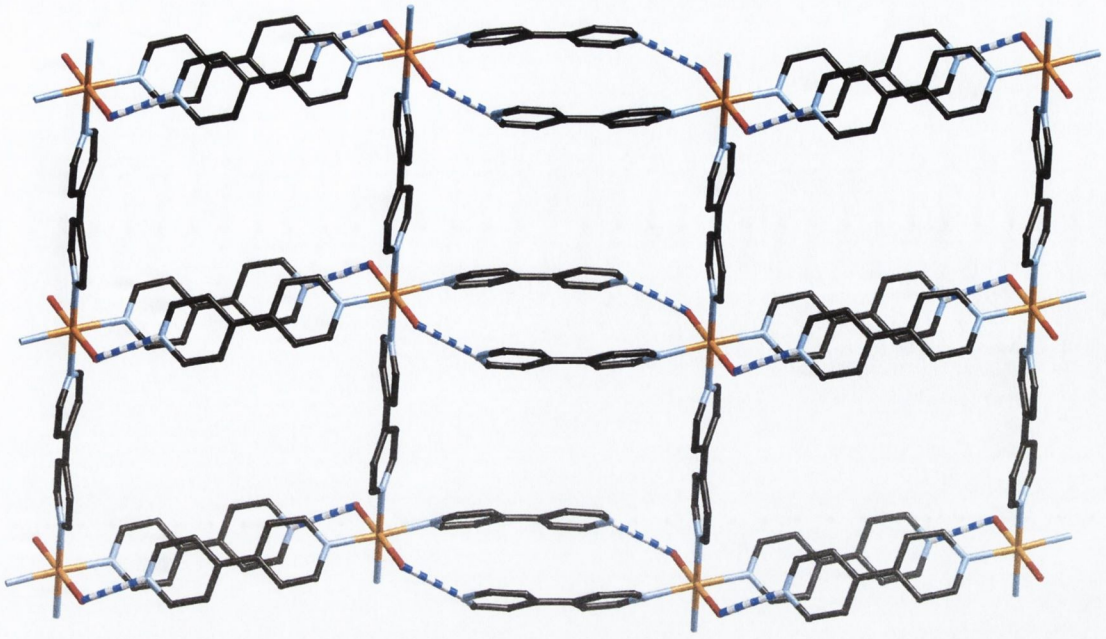

Figure 3.4 – Initial structure obtained from X-ray diffraction analysis of crystals formed by reacting $Co(NO_3)_2$, 2,2'-bipy and qpy. (Expected formula – $[Co(2,2'\text{-bipy})_2(qpy)]^{2+}$. Solvent and disordered guest molecules removed for clarity, refinement factor $R_1 = 0.134$)

An attempt to replicate the structure shown in Figure 3.4 was undertaken. The reaction was altered such that qpy was substituted by 4,4'-bipy (see Section 3.2.2). The quantity of 2,2'-bipy present in the reaction mixture was, initially, not altered (although the reaction was also repeated in the absence of 2,2'-bipy – see Section 3.2.4).

3.2.2 Reaction of $Co(NO_3)_2$ with 2,2'-bipy and 4,4'-bipy.

An aqueous solution of 2,2'-bipy and $Co(NO_3)_2$, was reacted with a methanolic solution of 4,4'-bipy in an overall ratio of 2:1:1. Orange prismatic crystals formed over a period of three days, which were collected by filtration. As expected, the yield of crystals for this reaction (322mg) was considerably higher than the equivalent reaction using qpy which contained the 4,4'-bipy impurity. Again, IR analysis showed the presence of aromatic pyridyl ring systems, as well as nitrate anions. In fact the IR spectrum obtained was almost identical to that obtained for the reaction with qpy. A crystal was selected for analysis by X-ray diffraction, and data collected by Dr. Tom McCabe at Trinity College, Dublin. The same unit cell was obtained, indicating the same structure. Refinement of the model from the original solution against this new data yielded a slightly better result. The raw frames were indicative of a disordered structure. A selection of crystals from the same batch displayed similar diffraction patterns, as did crystals from repeat reaction batches.

*3.2.3 Crystal structure of [Co(4,4'-bipy)$_3$(H$_2$O)$_2$][NO$_3$]$_2$·x(2,2'-bipy)·y(4,4'-bipy) (**1**).*

A direct consequence of the relatively poor data obtained from these crystals is that the integrated data are not very consistent ($R_{(int)}$ = 0.139). This, combined with the problems associated with modelling highly disordered moieties, means that a satisfactory refinement is difficult to achieve. Crystallographic data for this compound are listed in Table 3.1. The structure was refined in the monoclinic space group *C2/c*. Figure 3.5 shows the molecular structure surrounding a single Co atom and the atomic labelling of the coordinating ligands.

This structure consists of a 1D coordination polymer, which is extended into a second dimension through hydrogen-bonds between 1D chains. Figure 3.5 shows the molecular structure and atomic labelling of the repeating unit within each chain. The chain extends along the crystallographic *b* axis with the metal centres connected by 4,4'-bipy ligands. Each Co(II) centre sits on a twofold rotation axis and adopts a marginally distorted octahedral geometry. Table 3.1 lists selected bond lengths, distances and angles for **1**. All like donors are in a *trans* arrangement to each other.

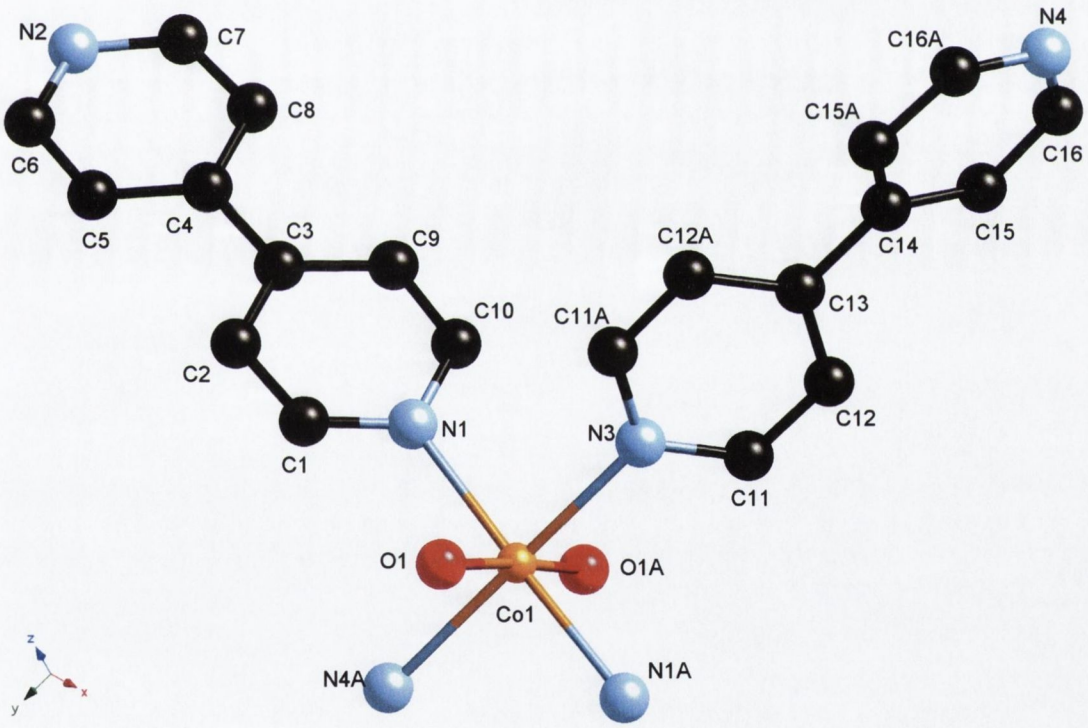

Figure 3.5 – Molecular structure and atomic labelling diagram for **1**. (Hydrogen atoms, nitrate and disordered molecules omitted for clarity)

Table 3.1 – Crystallographic data for **1** and **2**.

Compound	**1**	**2**
Chemical Formula	$C_{56}H_{24}N_{10}O_6Co$	$C_{30}H_{24}N_{7.5}O_{11.5}Co$
Formula Weight	991.78	732.50
Crystal System	Monoclinic	Triclinic
Space Group	*C*2/*c*	*P*-1
a /Å	17.752(2)	10.8229(7)
b /Å	11.439(1)	11.3604(7)
c /Å	24.448(3)	15.2080(9)
α /°	90	77.047 (1)
β /°	94.096(2)	84.486(1)
γ /°	90	78.024(1)
V /Å^3	4951.6(9)	1780.2(2)
Z	4	2
D_{calc} /g cm^{-3}	1.330	1.549
μ(Mo-K$_\alpha$) /mm^{-1}	0.409	0.549
T /K	173(2)	173(2)
Crystal Size max /mm	0.28	0.50
mid /mm	0.15	0.30
min /mm	0.10	0.15
$2\theta_{max}$	40.00	56.66
Min/Max Trans. Factor	n/a‡	0.839/1.000
R_{int}	0.1074	0.0247
R_1, wR_2 [I>2σ(I)][a]	0.1045, 0.2697	0.0859, 0.2391
R_1, wR_2 (all data)	0.1241, 0.2755	0.0971, 0.2483
Reflections: collected	13374	19959
unique	2298	7899
observed	1787	6638

[a] $R_1 = \Sigma||F_o| - |F_c||/\Sigma|F_o|$, $wR_2 = [\Sigma w(F_o^2 - F_c^2)^2/\Sigma w(F_o^2)^2]^{1/2}$

‡ No absorption correction was applied to this data.

Table 3.2 – Selected bond lengths (Å), distances (Å) and angles (°) for **1**.

Co1 – N1	2.178(5)	N1 – Co1 – N3	90.9(2)
Co1 – N3	2.233(7)	N1 – Co1 – O1	92.7(2)
Co1 – O1	2.063(4)	N3 – Co1 – O1	88.0(1)
Co1 – O1A^{i}	2.062(4)	O1 – Co1 – O1A^{i}	176.0(2)
Co1 – N4A^{ii}	2.161(6)	N1 – Co1 – N1A^{i}	178.2(3)
Co1 – N1A^{i}	2.178(5)	N3 – Co1 – N4A^{ii}	180
O1 ··· N2^{iii}	2.789(7)	Co1 – O1 – N2^{iv}	115.8(2)
C10 ··· N2^{iv}	3.191(9)	C12 – C13 – C14 – C15	30.1(5)

Symmetry Codes: *i* = ½+x, ½-y, 2-z; *ii* = x, 1+y, z; *iii* = x, 1-y, ½+z; *iv* = -x, 1-y, 2-z.

The bridging 4,4'-bipy ligands are twisted along the central bond between the pyridyl rings. This gives rise to a torsion angle of 30.1(5)° between the rings. This is in contrast to the pyridyl rings of the monodentate 4,4'-bipy ligands which are almost co-planar. Figure 3.6 shows a portion of a 1D polymeric chain formed through the bidentate 4,4'-bipy ligands.

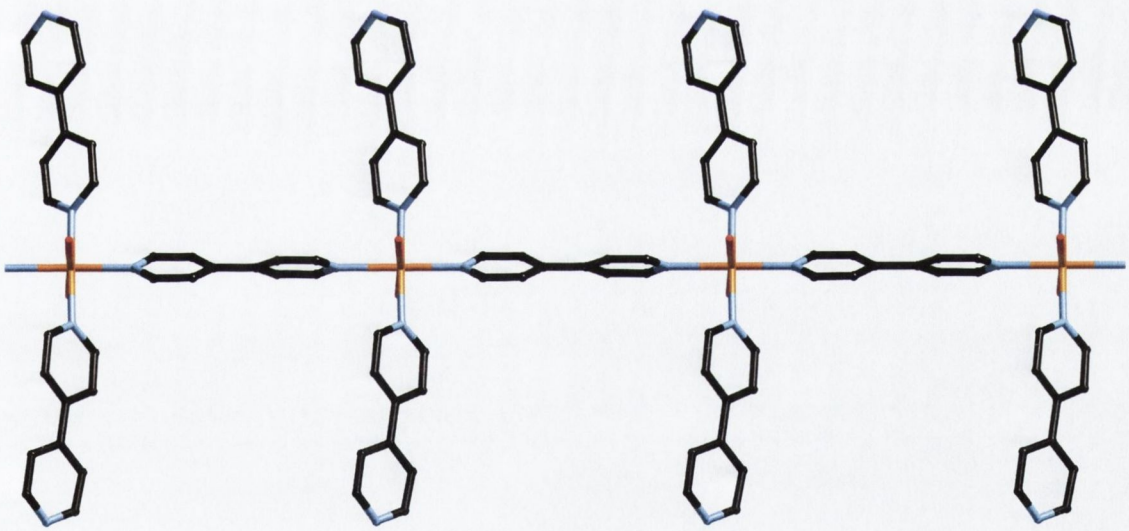

Figure 3.6 – A section of a 1D polymeric chain of **1**. (Chain extends along the *b* axis. Hydrogen atoms, nitrate and disordered molecules omitted for clarity)

Adjacent chains lie in a parallel arrangement and are related by inversion centres, twofold rotation axes and twofold screw axes. There is a hydrogen-bond between the uncoordinated nitrogen of a monodentate 4,4'-bipy (N2) and a coordinated water molecule (O1) on an adjacent chain. This hydrogen-bond is shown as a blue and white dashed bond in Figure 3.7. The 'stacked' orientation of the 4,4'-bipy molecules allows for π-interactions between the two ligands (C10···N2A 3.191(9) Å).

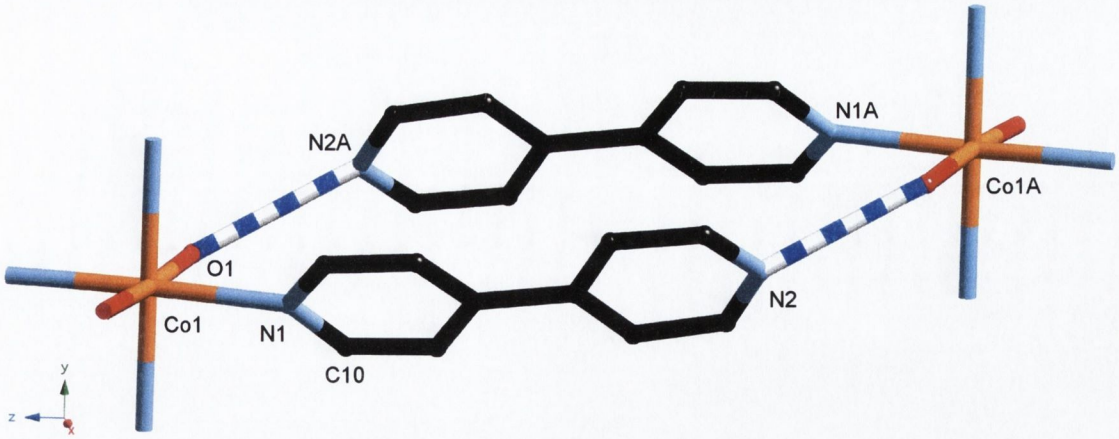

Figure 3.7 – Hydrogen-bonding (blue and white dashed bond) and π-stacking between two adjacent 1D polymeric chains of **1**.

These double 4,4'-bipy/H_2O hydrogen-bond bridges, as shown in Figure 3.7, connects 1D polymeric chains in 2D (4,4) grid networks. The two 4,4'-bipy molecules involved in each hydrogen-bonds connection are related by an inversion centre located midway between the relevant metal centres. This connection within the 2D sheets bridges the metal centres along the crystallographic *c* axis. Figure 3.8 shows three coloured chains (yellow, green, and red) linked by hydrogen-bonds and π-interactions as described above. The grid-like (4,4) topology of the network can clearly be seen. The metal-to-metal distance between adjacent chains is approximately 12.43 Å.

2D sheets of **1** (as shown in Figure 3.8) stack together in a staggered arrangement. Figure 3.9(a) shows three 2D polymeric sheets packing together, as viewed along the crystallographic *b* axis. Twofold screw axes lie perpendicular to the page in between the sheets. Figure 3.9(b) shows the same three sheets of **1** viewed along the crystallographic *a* axis, The staggered arrangement of adjacent sheets can clearly be seen since the central red sheet is offset by *b*/2 with respect to the green and purple sheets.

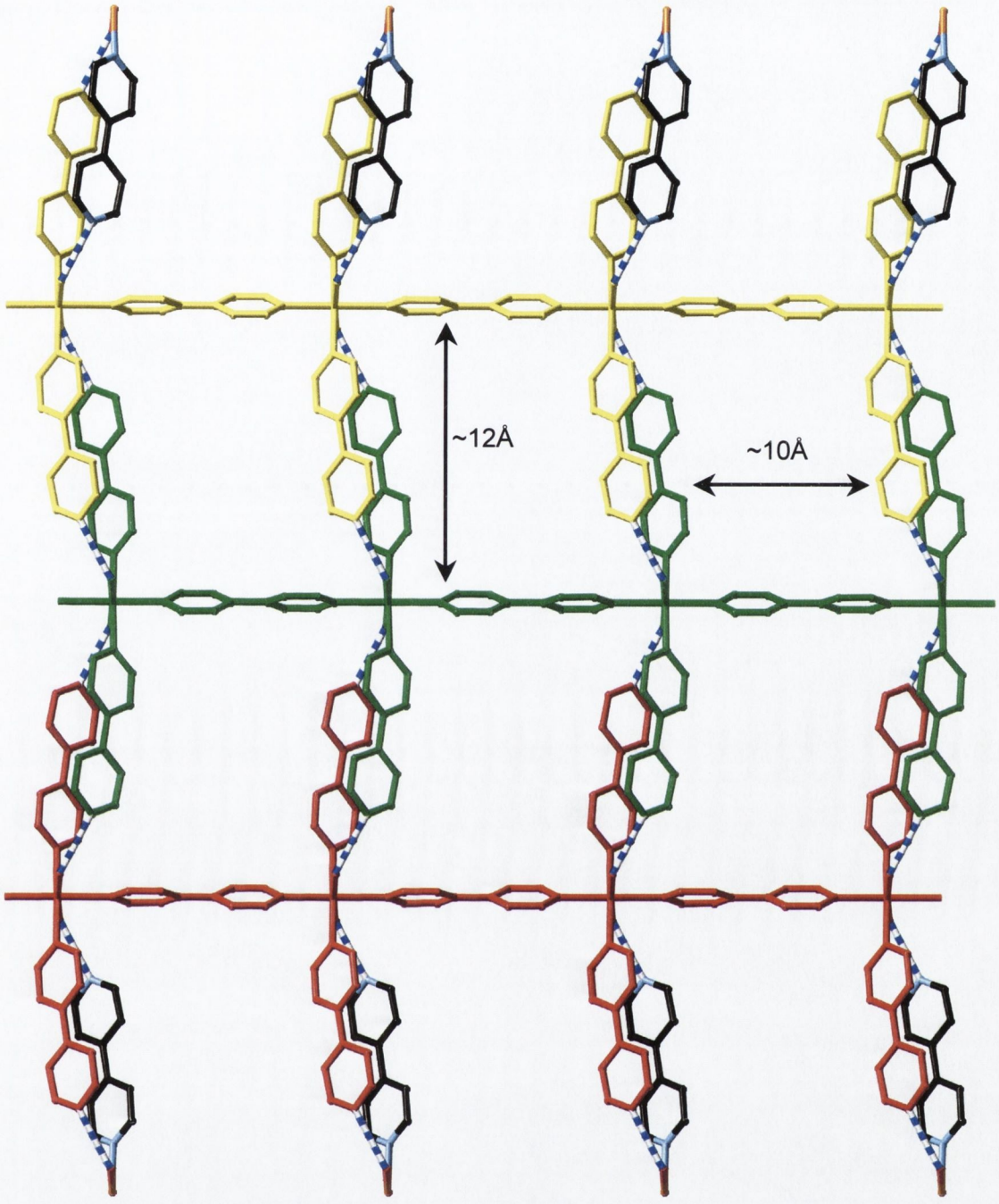

Figure 3.8 –Hydrogen-bonding and π-interactions between three 1D polymeric chains (yellow, green, and red) of **1** form a (4,4) 2D sheet. (View along the *a* axis, hydrogen atoms, nitrate and solvent molecules omitted for clarity)

The voids that exist both within a single sheet and between adjacent sheets are large enough such that other molecules are able to occupy them. Although these molecules have not been refined fully and are not shown, it is clear that they consist of reactants (2,2'-bipy or 4,4'-bipy) nitrate anions and lattice water molecules. As is to be

expected there is a high degree of disorder to these groups, and this is a major factor in the poor quality of the refinement (R_1 = 0.107).[§]

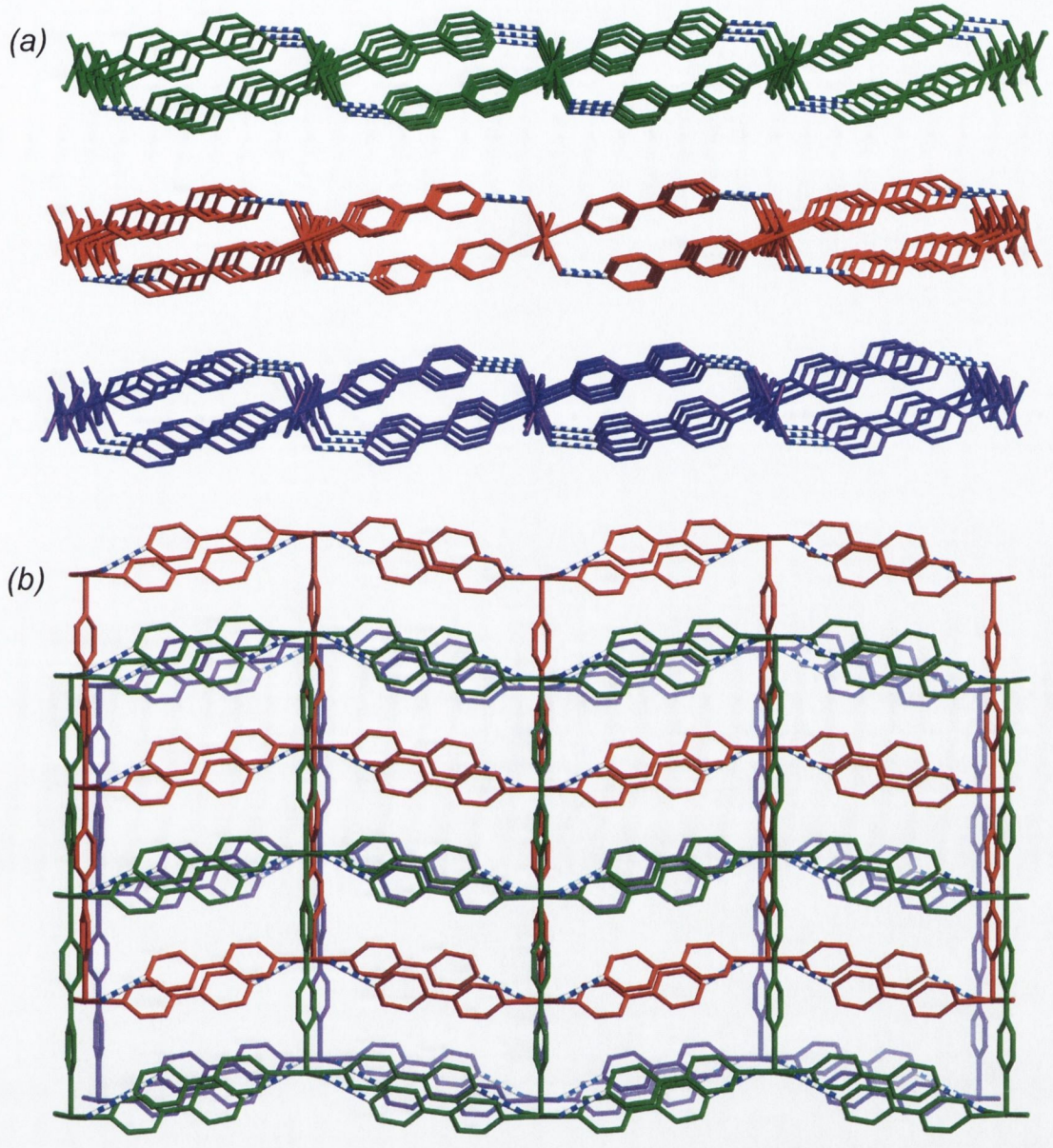

Figure 3.9 – Packing arrangement of three 2D sheets of **1**. (a) View along the *b* axis, twofold screw axes lie between sheets. (b) View along the *a* axis, the staggered arrangement of the sheets is evident as the red sheet is easily visible between the green and purple sheets. (Hydrogen atoms, nitrate and solvent molecules omitted for clarity)

The structure of compound **1** is exactly the same as the structure obtained from the crystals formed in the reaction of Co(II) with 2,2'-bipy and qpy (although the disordered molecules from each crystal have not been modelled, the 2D sheets are the same). Somewhat surprisingly a search of the Cambridge Structural Database (CSD)[112,

[§] An electronic version of the structure of **1** (as well as the other structures in this thesis) is saved on the CD at the back of this thesis for the readers perusal. See Appendix for details.

[113, 159] revealed that this particular structure, has not been reported, although the highly disordered 'guest' molecules make refining a model to accurately fit the data a decidedly challenging task. It was at this point that the research in the present study turned towards coordination polymers

Recently there has been much interest focussed on the controlled fabrication of coordination polymers.[104, 107-109, 160] These materials are synthesised with a view to creating new materials with applications such as molecular sieves and catalysts. There has been a large amount of work done in recent years utilising linear pyridyl-donor ligands for the synthesis of coordination polymers.[161-166] Variation of the ligand (e.g. pyrazine[162, 167], 4,4'-bipy, 1,2-*bis*(4-pyridyl)ethane, 1.3-*bis*(4-pyridyl)propane) allows the dimensions of the cavity bound by the ligands to be altered.[164] The use of 4,4'-bipy as a linker unit, joining metal centres is well documented.[163, 168-173]

3.2.4 Hydrothermal reaction of $Co(NO_3)_2$ with 4,4'-bipy (in the absence of 2,2'-bipy).

The use of solvothermal synthetic techniques was introduced in Chapter 1, and has seen a sharp increase in popularity in recent years[122, 174, 175] especially in the formation of coordination polymers. It was encouraging that the coordination polymer formed in the reaction of Co(II) with 2,2'-bipy and 4,4'-bipy (**1**) had not been previously reported. Subsequently, it was decided to remove the 2,2'-bipy from the reaction mixture, as it (seemingly) had no major effect on the resultant crystal structure. Furthermore the reaction was to be conducted under hydrothermal conditions.

An aqueous mixture of $Co(NO_3)_2$ and 4,4'-bipy was placed in a 46 ml Teflon®-lined stainless steel vessel, and placed in an oven. A standard heat-cooling cycle was then run.[¶] Upon opening, large orange crystals were separated from a solid black residue. However these were not suitable for analysis by X-ray diffraction as they were too large and not of high enough quality. A portion of the mother liquor was filtered and allowed to stand overnight whereupon, small orange crystals formed that were suitable for a structure determination by X-ray diffraction. The IR spectra of both crystalline products were virtually identical.

*3.2.5 Crystal structure of $[Co(4,4'\text{-bipy})(H_2O)_4(4,4'\text{-bipy})_2][NO_3]_2 \cdot x(H_2O)$ (**2**).*

The structure of **2** is similar to the structure of **1** described above. The Co(II) centre adopts an octahedral geometry and has 4,4'-bipy and water molecules coordinated to it. However, in this case there are two 4,4'-bipy molecules and four water molecules coordinated to each Co(II). Figure 3.10 shows the molecular structure of the asymmetric unit as well as the labelling of atoms. Crystallographic data are given in Table 3.1.

[¶] See Chapter 5, Section 5.1.7 (page 152) for full details.

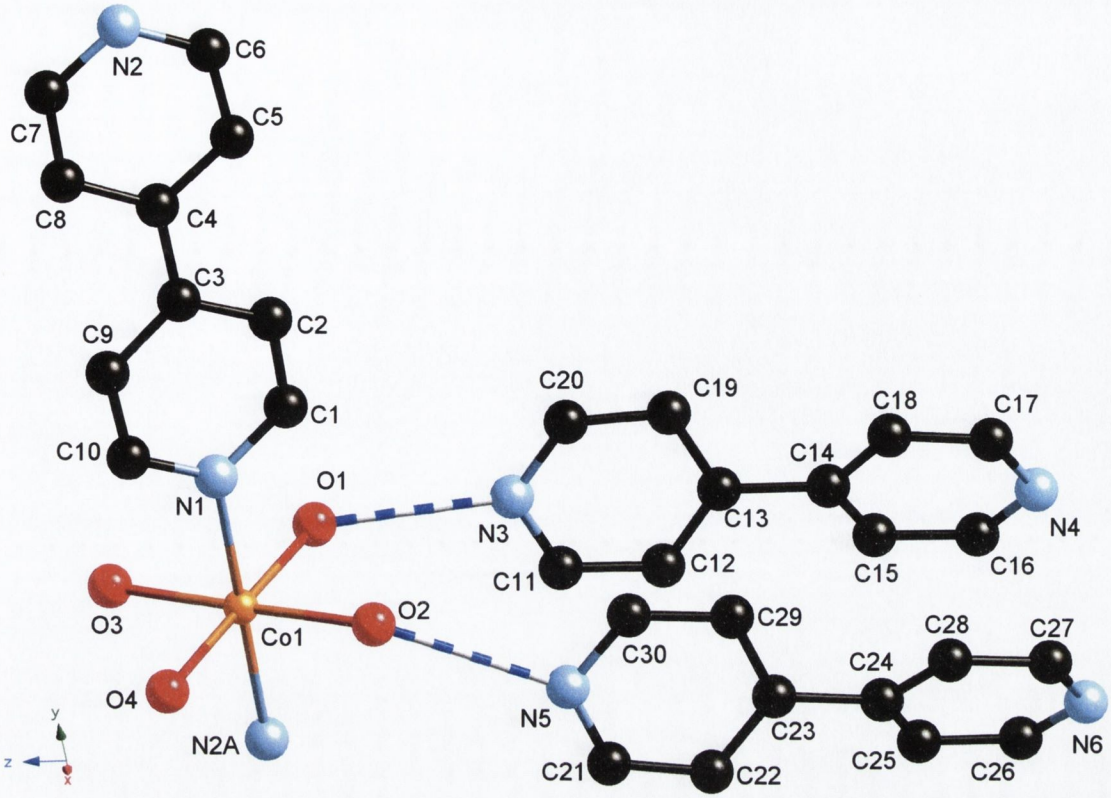

Figure 3.10 – Molecular structure and atomic labelling diagram for **2**. (Hydrogen atoms, nitrate and solvent molecules omitted for clarity)

This compound, like **1**, is a one dimensional coordination polymer, which has short contacts to bidentate groups that then extend the structure into a hydrogen-bonded two-dimensional sheet. The one-dimensional chain consists of Co(II) centres linked through 4,4'-bipy molecules. These axial 4,4'-bipy groups have a rather reduced torsion angle of the pyridyl rings (7.1(7)°), when compared to that seen in **1** (30.1(5)°). Each of the four equatorial waters are hydrogen-bonded (blue and white dashed bonds) to an uncoordinated nitrogen atom of a 4,4'-bipy molecule, which effectively 'links' metal centres. This has the overall effect of increasing the metal-metal distance in this direction compared to that of **1**. The 'linking' 4,4'-bipy molecules are close enough that π-interactions are evident between the rings (C16···C26 3.392(9) Å). Both hydrogen-bonded 4,4'-bipy molecules have a definite twist along the central bond, with torsions angles of 24.0(8)° and 33.9(7)° between each pyridyl ring. Selected bond lengths and angles for **2** are shown in Table 3.3.

Table 3.3 – Selected bond lengths (Å), distances (Å) and angles (°) for **2**.

Co1 – N1	2.127(3)	N1 – Co1 – O1	91.8(2)
Co1 – N2A^{i}	2.127(3)	N1 – Co1 – O2	87.1(2)
Co1 – O1	2.092(3)	N1 – Co1 – O3	91.9(2)
Co1 – O2	2.098(3)	N1 – Co1 – O4	89.4(2)
Co1 – O3	2.086(3)	N1 – Co1 – N2A^{i}	178.7(2)
Co1 – O4	2.083(3)	Co1 – O1 – N3	128.5(2)
O1 ··· N3	2.712(6)	Co1 – O2 – N5	138.1(2)
O2 ··· N5	2.790(5)	Co1 – O3 – N4^{ii}	138.3(2)
O3 ··· N4^{ii}	2.776(6)	Co1 – O4 – N6^{ii}	122.3(2)
O4 ··· N6^{ii}	2.735(6)	C2 – C3 – C4 – C5	7.1(7)
C16 ··· C26	3.392(9)	C12 – C13 – C14 – C15	24.0(8)
		C22 – C23 – C24 – C25	33.9(7)

Symmetry Codes: *i* = x, 1+y, z; *ii* = x, y, -1+z.

Figure 3.11 is a packing diagram of this compound, which shows how a single sheet is held together. The 1D polymeric chains are coloured (yellow, red, purple and green), whilst the other 'bridging' 4,4'-bipys are shown in standard colours. The metal-to-metal distance across this 'bridge' of 15.21 Å is somewhat longer than the corresponding metal-metal distance in **1**, of 12.43 Å.

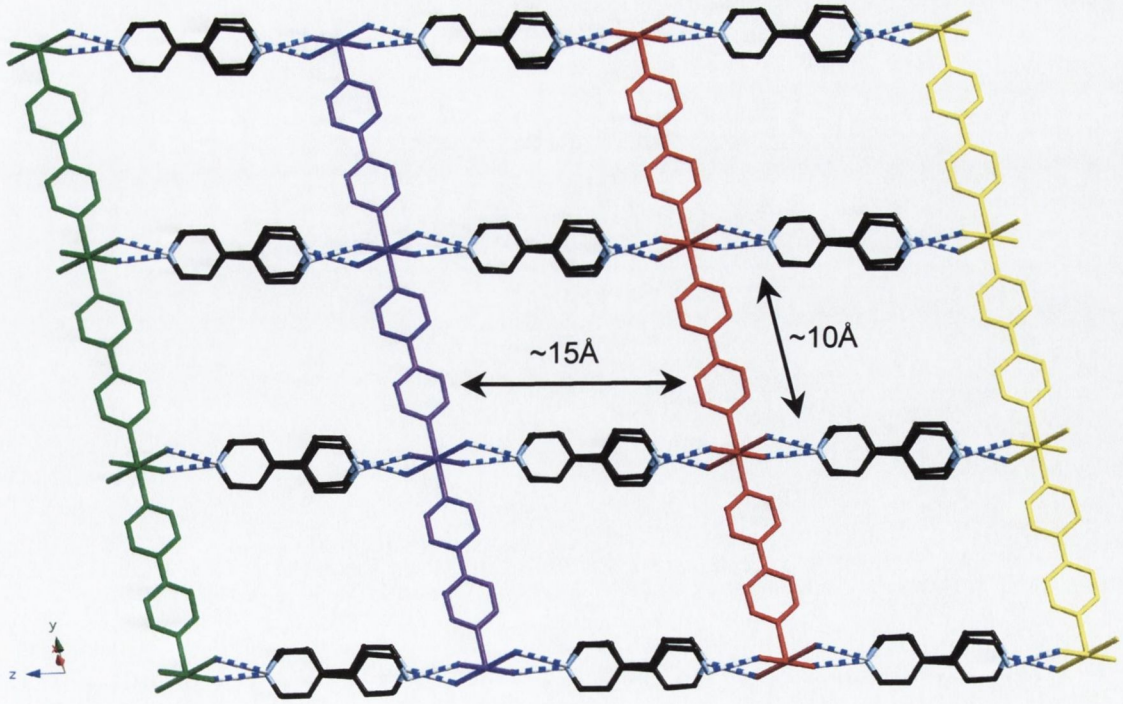

Figure 3.11 – Packing diagram for **2**. Note different bridging mode of 4,4'-bipy in linking coloured 1D chains together as compared to that seen in **1**(Figure 3.8). (Hydrogen atoms, nitrate and solvent molecules omitted for clarity)

An interesting feature of this compound is that unlike **1** there are no 2,2'- or 4,4'-bipy molecules encapsulated in the lattice. However there are nitrate anions and water molecules present, and these are disordered. During the course of investigation into this compound, a publication by Lu and co-workers[176] reported the exact same structure. The publication included a description of the hydrogen-bonded network of nitrate anions, and water molecules that are present in the cavities of the network. Initial work into the formation of nanofibers from this compound was also reported in this communication.

3.3 Reaction of Ni(II) with 2,2'- and 4,4'-bipyridine.

There are several examples of Ni(II) containing coordination polymers.[168, 177-179] Following the interesting structures obtained with Co(II), it was decided to alter the metal centre in order to see if similar or new networks could be formed. Since 2,2'-bipy was included in the analogous Co(II) reaction it was decided to include it again with Ni(II). Whilst the nitrate salt of Co(II) was used in the reactions described above, in the present reactions the acetate salt of Ni(II) was used. The main reason for this change was that the Ni(II) acetate (OAc) salt was readily available. Also, various Ni(II)/4,4'-bipy containing coordination polymers with nitrates used as counter-ions have been reported.[105, 179-183]

3.3.1 Reaction of $Ni(OAc)_2$ with 2,2'-bipy and 4,4'-bipy.

$Ni(OAc)_2$ and 2,2'-bipy were reacted in a 1:1 ratio in aqueous solution with a resultant colour change from green to blue. A methanolic solution of 1 equivalent of 4,4'-bipy was added. After several days and upon evaporation a low yield of pale blue crystals formed, which were suitable for a single crystal X-ray diffraction study. The crystals were unstable out of the mother liquor. The IR spectrum showed the presence of an acetate group (ν_{as}(C–O) 1578, ν_s(C–O) 1409 cm^{-1}) as well as bipy and water molecules. Microanalytical data was consistent with the structure below.

*3.3.2 Crystal structure of $[Ni(4,4'\text{-bipy})_2(OAc)_2(H_2O)_2]\cdot 2(H_2O)\cdot(MeOH)$ (**3**).*

This structure was refined in the *C*2/*c* space group and crystallographic details for **3** are given in Table 3.4. The structure of **3** is markedly different to previously described structures **1** and **2**. It is not a coordination polymer since there are no coordination linkages to form polymeric chains. Rather, the structure exists as discrete molecules that have a number of short contacts, which form a 2D hydrogen-bonded network. Figure 3.12 shows the individual Ni(II) molecules and numbering of the atoms within it.

Table 3.4 – Crystallographic data for **3** and **4**.

Compound	**3**	**4**
Chemical Formula	$C_{26}H_{30}N_4O_{12}Ni$	$C_{14}H_{18}N_2O_6Ni$
Formula Weight	649.25	369.01
Crystal System	Monoclinic	Monoclinic
Space Group	*C*2/*c*	*C*2/*c*
a /Å	24.998(3)	18.276(4)
b /Å	7.1312(9)	13.071(3)
c /Å	18.218(2)	6.770(1)
α /°	90	90.00
β /°	116.602(2)	101.97(3)
γ /°	90	90.00
V /Å^3	2904.0(7)	1582.1(6)
Z	4	4
D_{calc} /g cm^{-3}	1.485	1.549
μ(Mo-K$_\alpha$) /mm^{-1}	0.738	1.258
T /K	173(2)	153(2)
Crystal Size max /mm	0.30	0.15
mid /mm	0.10	0.08
min /mm	0.05	0.07
$2\theta_{max}$	56.56	56.72
Min/Max Trans. Factor	0.858/1.000	0.835/1.000
R_{int}	0.0937	0.0397
R_1, wR_2 [I>2σ(I)][a]	0.0657, 0.1712	0.0375, 0.0852
R_1, wR_2 (all data)	0.0835, 0.1811	0.0473, 0.0888
Reflections: collected	11368	15387
unique	2094	2019
observed	1607	1694

[a] $R_1 = \Sigma||F_o| - |F_c||/\Sigma|F_o|$, $wR_2 = [\Sigma w(F_o^2 - F_c^2)^2/\Sigma w(F_o^2)^2]^{1/2}$

The metal centre sits on an inversion centre, and as a consequence only half of the atoms shown (excluding those attached through hydrogen-bonding) in Figure 3.12 are unique. The Ni(II) centre adopts an octahedral geometry, with two 4,4'-bipy molecules occupying axial positions and four oxygen atoms coordinating at the equatorial positions around the metal. Two of the equatorial oxygen atoms belong to acetate groups, whilst the other two are coordinated water molecules, with like donors arranged *trans* to each other, leading to the inversion symmetry. Selected bond lengths and angles are given in Table 3.5.

As well as intramolecular hydrogen-bonds between the uncoordinated acetate oxygens and the coordinated water molecules (O2···O3 2.655(6) Å, shown as pink and white dashed bond in Figure 3.12), there are a number of other non-covalent interactions that form a network structure. The coordinated water molecule O3 hydrogen-bonds to the uncoordinated nitrogen atom N2 of 4,4'-bipy ligand on an adjacent complex. This interaction is shown in Figure 3.12 as a red and white dashed bond.

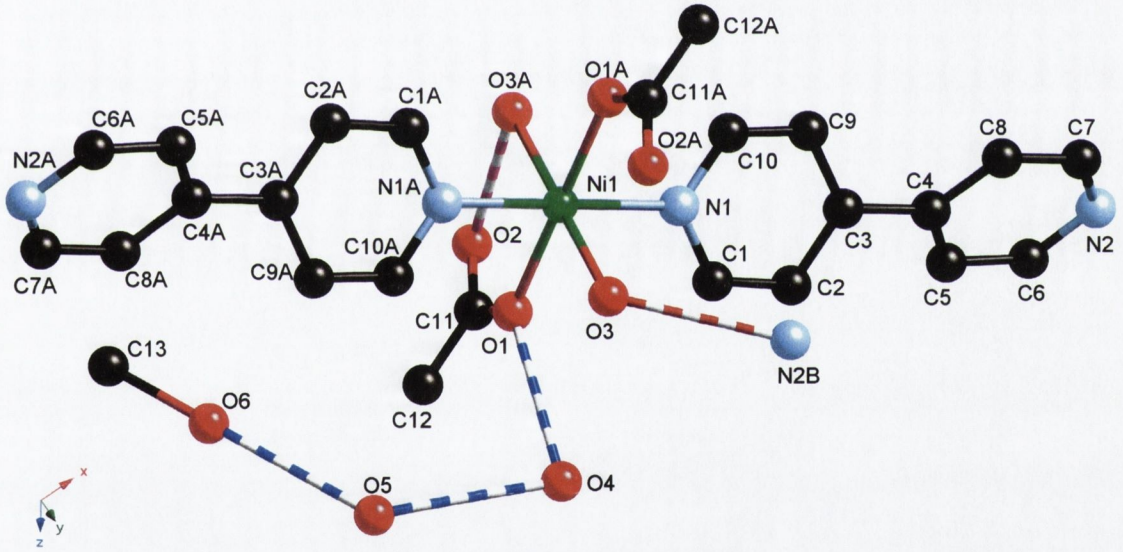

Figure 3.12 – Molecular structure and atomic labelling diagram for **3**. Hydrogen-bonds designated by dashed bonds. (Pink and white correspond to intramolecular O···O, red and white correspond to N···O and blue and white correspond to intermolecular O···O. Hydrogen atoms omitted for clarity)

These connections link individual molecules to form a 2D hydrogen-bonded sheet, which is shown in Figure 3.13. Reinforcing this arrangement is the presence of π-interactions between the aromatic rings of adjacent 4,4'-bipy molecules, as can be seen in Figure 3.13 (N2···C1 3.185(6) Å).

Table 3.5 – Selected bond lengths (Å), distances (Å) and angles (°) for **3**.

Ni1 – N1	2.099(4)	N1 – Ni1 – O1	90.1(2)
Ni1 – O1	2.067(3)	N1 – Ni1 – O3	92.5(2)
Ni1 – O3	2.062(4)	N1 – Ni1 – N1A^{i}	180.0
C11 – O1	1.277(8)	O1 – Ni1 – O3	86.8(2)
C11 – O2	1.278(8)	O1 – Ni1 – O1A^{i}	180.00
O1 ··· O4^{ii}	2.839(5)	O3 – Ni1 – O3A^{i}	180.0(2)
O4 ··· O5	2.918(9)	C2 – C3 – C4 – C5	38.4(7)
O5 ··· O6	2.890(2)	O3 – H3B ··· N2B^{iii}	129(9)
O3 ··· N2B^{iii}	2.798(6)		
H3B ··· N2B^{iii}	2.19(8)		
N2 ··· C1^{iv}	3.185(7)		

Symmetry Codes: *i* = -x, -y, -z; *ii* = x, y, -1+z; *ii* = x, -1+y, z; *iii* = ½-x, -½+y, ½-z; *iv* = ½-x, ½+y, ½-z.

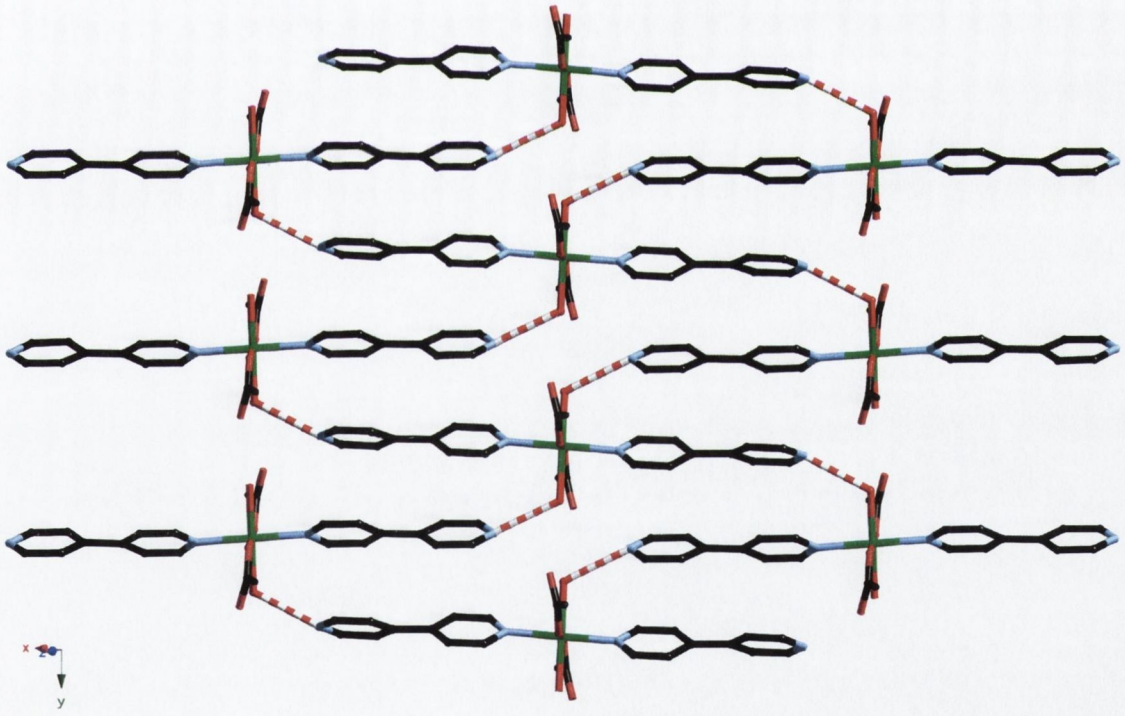

Figure 3.13 – Packing diagram showing a single 2D hydrogen-bonded sheet of **3**. Note π-stacking of 4,4'-bipy groups. (Red and white dashed bonds correspond to hydrogen-bonds, hydrogen atoms omitted for clarity)

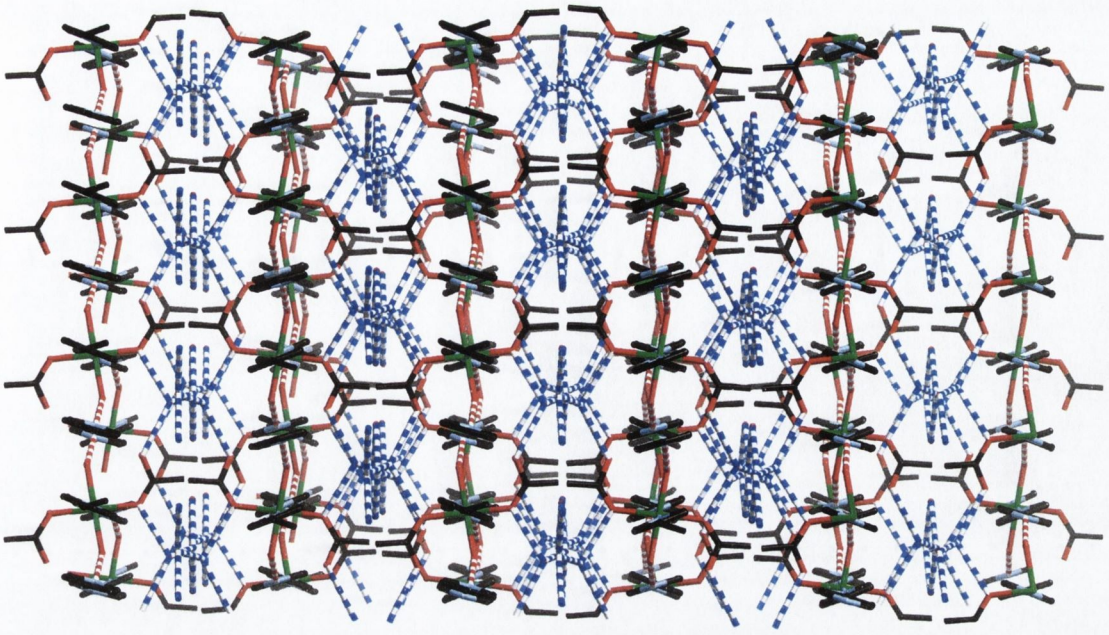

Figure 3.14 – Packing diagram showing hydrogen-bonded lattice water network within **3**. (Blue and white dashed bonds correspond to hydrogen-bonds between methanol, water molecules and coordinated acetate oxygens. View along (101) direction, hydrogen atoms omitted for clarity)

As can also be seen in Figure 3.12, there are hydrogen-bonds between coordinated acetate and lattice solvent molecules (blue and white dashed bonds). These form a network, which consists of water and MeOH molecules. As the 2D hydrogen-bonded sheets pack together, the network of solvent molecules occupies the channels that form in the structure and link the 2D sheets into a 3D network. Figure 3.14 shows this network, where lattice solvent molecules are joined together *via* blue and white dashed bonds.

Clearly the subtle change of counter-ion from nitrate (in **1** and **2**) to acetate (in **3**) has had a dramatic effect on the structure formed. As far as can be ascertained, the structure of **3** has not been previously reported.

3.3.3 Reaction of $Ni(OAc)_2$ with 4,4'-bipy (in the absence of 2,2'-bipy).

The reaction was also repeated in the absence of 2,2'-bipy. A methanolic solution of 4,4'-bipy was reacted with an aqueous solution of $Ni(OAc)_2$ in a 1:1 ratio. Blue needles formed upon evaporation of the reaction mixture. A crystal suitable for a structural determination by X-ray diffraction was extracted from the mother liquor before the product was filtered. The IR spectrum confirmed the presence of the acetate group (ν_{as}(C–O) 1552, ν_s(C–O) 1409 cm^{-1}). Microanalytical data for **4** was consistent with the structure below.

*3.3.4 Crystal structure of [Ni(4,4'-bipy)$_2$(OAc)$_2$(H$_2$O)$_2$] (**4**).*

Data for this structure were collected at Trinity College. Automatic cell indexing failed and inspection of the raw frames indicated that non-merohedral twinning might be present. This was confirmed by the GEMINI program[184] which was able to index two twin domains to the data. The structure solution was obtained using the data from only one component of the twin. As expected the refinement was poor (R_1 = 0.116, high residual peaks) since it did not take into account the overlapping peaks from the other domain. The raw data was then re-integrated by Dr. Simon Parsons at the University of Edinburgh, with a beta-test version of the latest Bruker SAINT integrating program, and an absorption correction performed using the TWINABS program.[185] These programs generate an HKLF5-type data file, which contains an assignment for each reflection that associates it with a twin component parameter included in the solution instruction file. The initial solution was then refined against the re-integrated data in HKLF5 format, which gave an excellent refinement (R_1 = 0.038). Crystallographic data for **4** are listed in Table 3.4.

The structure of **4** is quite different to the previously described Ni(II) structure **3**, since there is only one 4,4'-bipy per Ni(II) and no lattice solvent molecules. The coordination sphere of the Ni(II) centre, however is very similar to that of **3**, as shown in Figure 3.15. The Ni(II) centre adopts an octahedral geometry with only slight distortion. 4,4'-Bipy ligands coordinate in the axial positions on the Ni(II) centre. Two water molecules and two acetate groups occupy the equatorial positions with the same orientation (i.e. *trans* to each other) as was seen in **3**. Selected bond lengths and angles are given in Table 3.6. The bidentate 4,4'-bipy ligand links the metal centres to form of a 1D coordination polymer, which extends along the (110) direction.

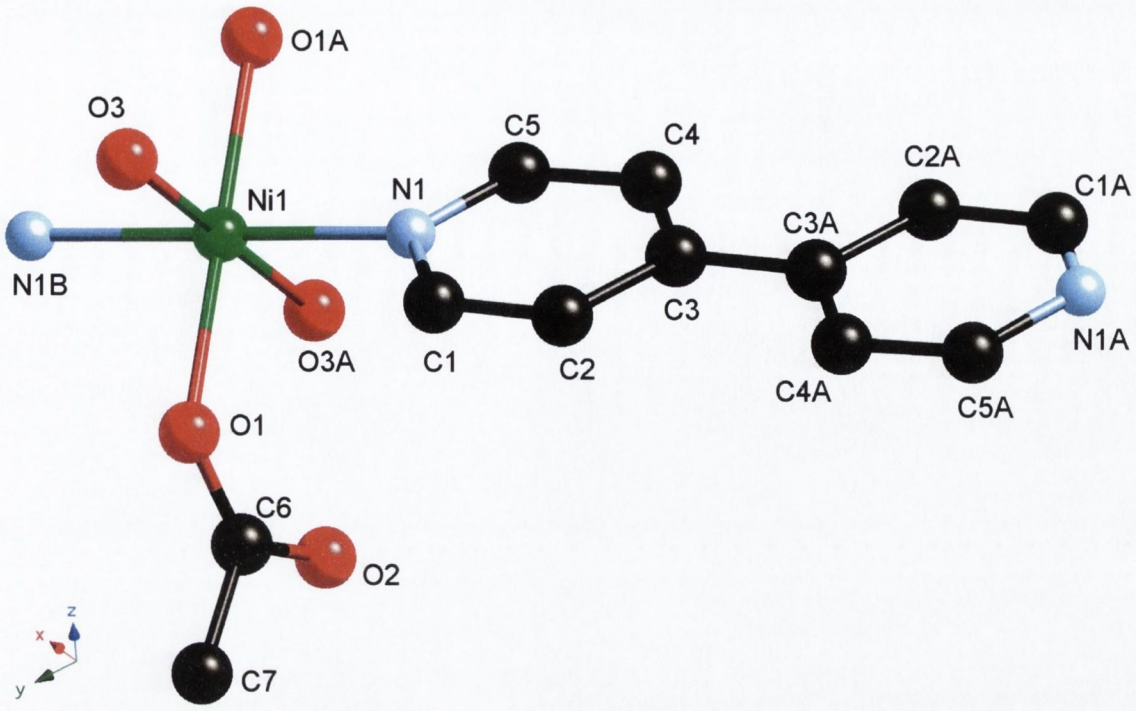

Figure 3.15 – Molecular structure and atomic labelling diagram for **4**. (4,4'-Bipy and acetate hydrogen atoms omitted for clarity)

Table 3.6 – Selected bond lengths (Å), distances (Å) and angles (°) for **4**.

Ni1 – N1	2.071(2)	N1 – Ni1 – O1	89.29(7)
Ni1 – O1	2.068(2)	N1 – Ni1 – O3	88.48(8)
Ni1 – O3	2.101(2)	O1 – Ni1 – O3	91.73(7)
O3 – H3A	0.84(3)	O1 – C6 – O2	125.2(2)
O3 – H3B	0.86(3)	O3 – H3B ··· O2	168(3)
O3 ··· O2	2.645(3)	O3 – H3A ··· $O2^{ii}$	152(3)
H3B ··· O2	1.79(3)		
O3 ··· $O2^{ii}$	2.851(3)		
H3A ··· $O2^{ii}$	2.07(3)		
C4 ··· $C4^{iii}$	3.3916(6)		

Symmetry Codes: *i* = ½-x, 1½-y, -z; *ii* = ½-x, 1½-y, 1-z; *iii* = x, 1-y, ½-z.

There are two unique hydrogen-bonds present in **4**. An intramolecular hydrogen-bond exists between the coordinated water molecule (O3) and the uncoordinated oxygen of the acetate group (O3···O2 2.645(3) Å, H3B···O2 1.79(3) Å). The second hydrogen-bond (intermolecular) exists between the coordinated water molecule (O3) and the uncoordinated oxygen of an acetate group on an adjacent Ni(II) polymeric chain (O3···O2A 2.851(3)Å, H3A···O2A 2.07(3)Å). Figure 3.12 shows both intra- (purple and white dashed) and intermolecular (blue and white dashed)

hydrogen-bonds. These short contacts have the effect of linking the chains together, and forming a hydrogen-bonded 2D (4,4) sheet network.

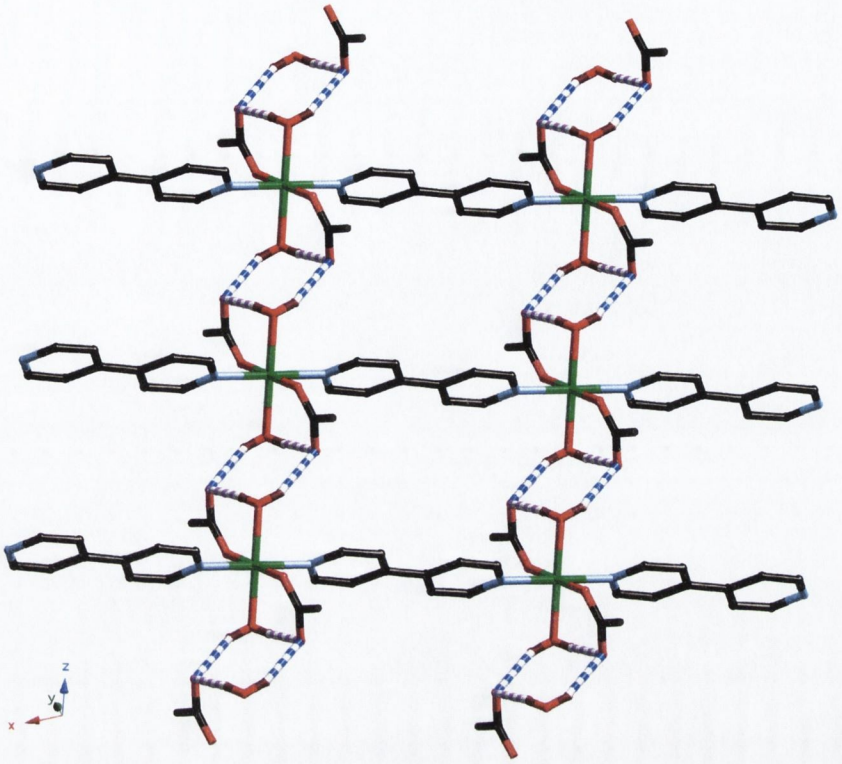

Figure 3.16 – Packing diagram showing intra- and intermolecular hydrogen-bonds present in a single 2D sheet of **4**. (4,4'-Bipy hydrogen atoms omitted for clarity)

The metal-to-metal distance across the hydrogen-bond bridge is approximately 6.77 Å. This combined with the metal-to-metal distance across the 4,4'-bipy bridge of approximately 11.2 Å gives large windows in the sheets, which can clearly be seen in Figure 3.16. The size of these windows allows each to be penetrated by a 4,4'-bipy ligand of another sheet. The overall result is two sets of parallel sheets interpenetrating each other at an angle of 71°. Figure 3.17 shows the mode of inclined interpenetration of these sheets. The red sheets run parallel to each other with each of them interpenetrated by the blue sheets, and *vice versa*. π-interactions (C4···C4A 3.3916(6) Å) give stacks of 4,4'-bipy ligands down the *c* axis with alternate 4,4'-bipys belonging to two different sheets (Figure 3.17). These π-interactions contribute to the stability of this structure. Interpenetrated sheets are related through twofold rotation and screw axes, which lie halfway between interpenetrated sheets.

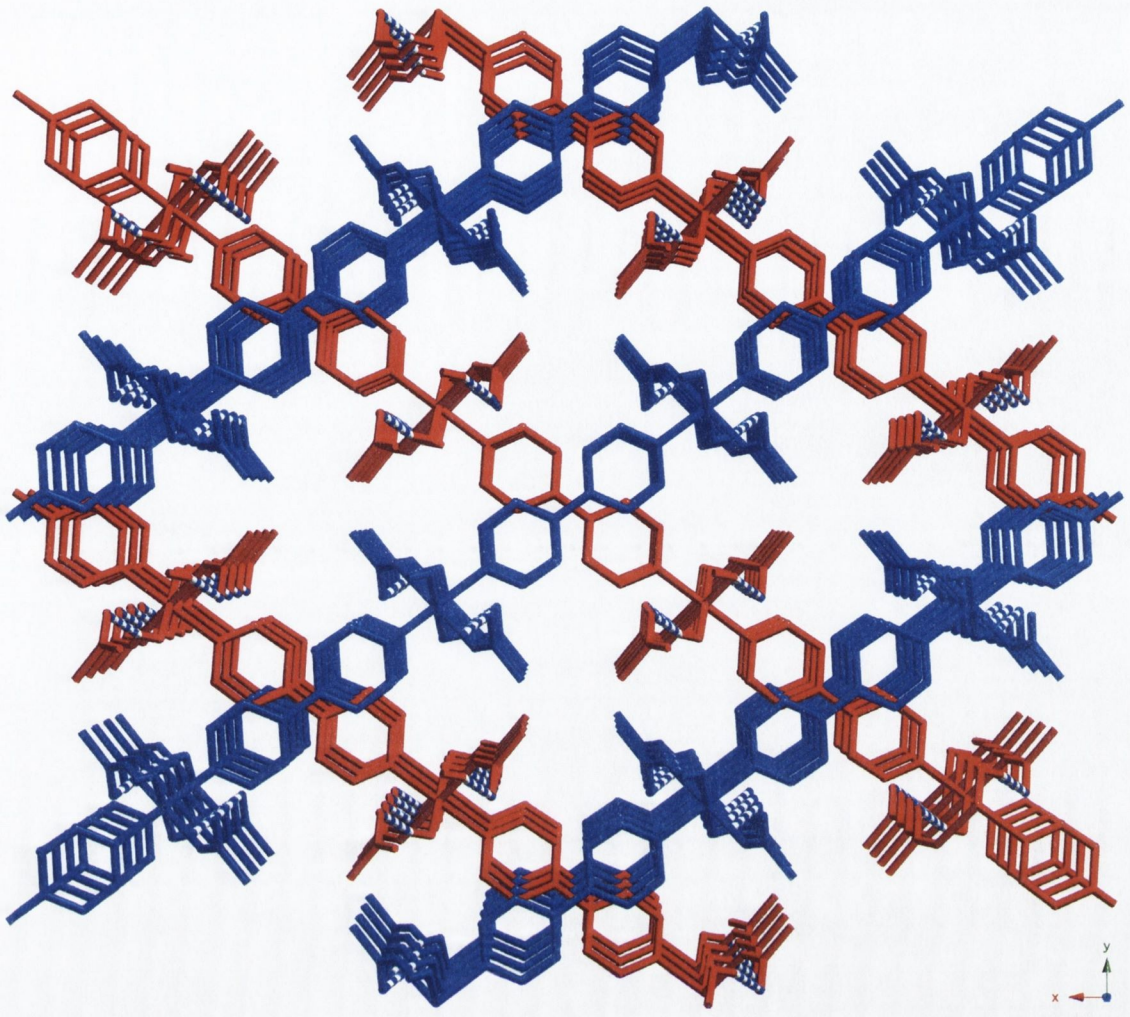

Figure 3.17 – Packing diagram showing the inclined interpenetration of hydrogen-bonded sheets of **4**. Note the proximity of the 4,4'-bipy groups on interpenetrated sheets. (View along the *c* axis, hydrogen atoms omitted for clarity)

The methyl groups of the acetates in **4** all point into the channels formed by the inclined interpenetrating sheets. This situation is in contrast to that observed for the related compound $[Co(4,4'\text{-bipy})(OAc)_2(H_2O)_2]$[186] in which solvent molecules occupy the channels formed by the inclined sheets interpenetrating at 63°. The coordination sphere of the Co(II) is the same as that observed for Ni(II) in **4**, however the acetate moieties in this structure do not form the intramolecular hydrogen-bond seen in **4**. The different orientation of the acetates, with the methyl groups lying within the plane of the sheet, allows intermolecular hydrogen-bonding to connect the interpenetrated 2D sheets into a 3D network. (Figure 3.18)

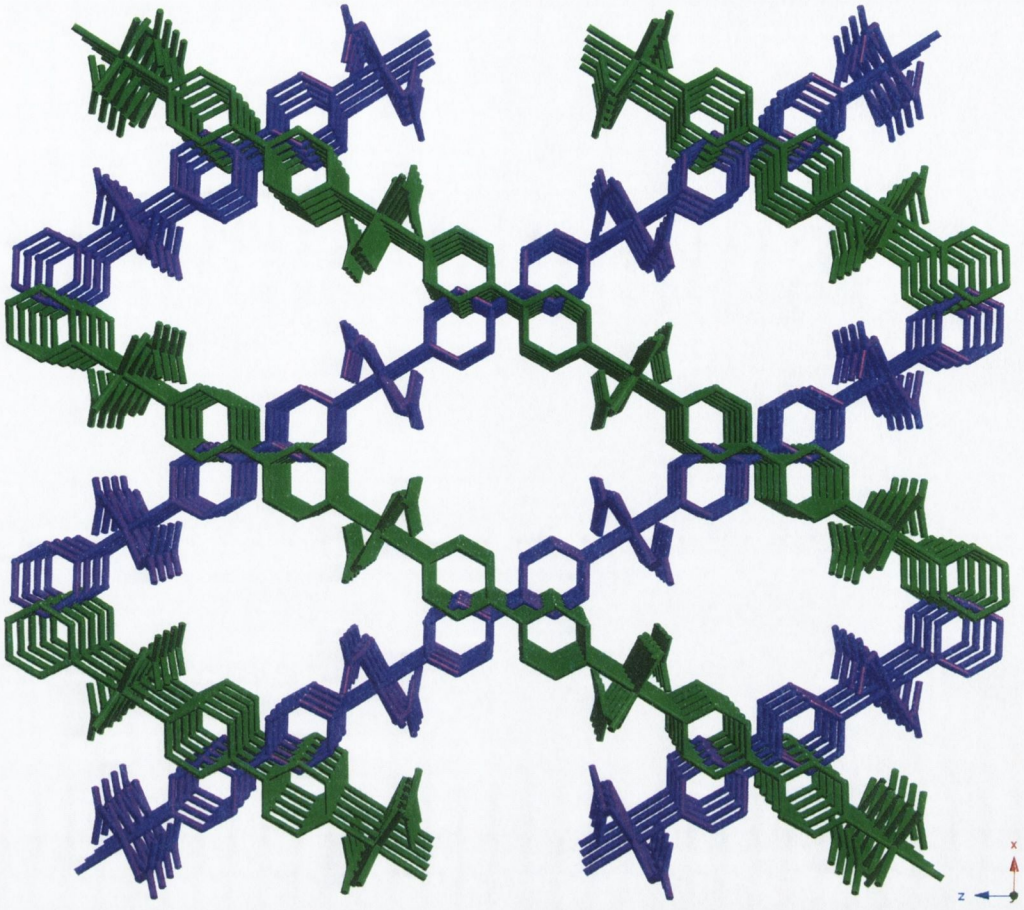

Figure 3.18 – Inclined interpenetration of 2D sheets of $[Co(4,4'\text{-bipy})(OAc)_2(H_2O)_2]$.[186]
(Hydrogen-bonds, lattice solvent molecules and hydrogen atoms omitted for clarity)

Considering the widespread use of 4,4'-bipy in transition metal chemistry, it is surprising that the structures of neither **3** nor **4** are known in the literature.[112, 113, 159] It is interesting that the presence of 2,2'-bipy in the reaction has an effect on the product, even though it is not included in the product. This could be due to $Ni(2,2'\text{-bipy})_n$ species effectively increasing the 4,4'-bipy to Ni(II) ratio or there may also be templating effects. Comparison of the reactions which form **4** and $[Co(4,4'\text{-bipy})(OAc)_2(H_2O)_2]$[186] shows that subtle changes in conditions can cause different polymeric structures to form from the same components. The only difference in the synthesis (apart from the metal ion) is the solvent system, with methanolic solutions used for the Co(II) compound compared to aqueous methanol solutions used for **4**.

A search of the CSD for compounds containing both 4,4'-bipy and acetate ions revealed only two structures containing first row transition metals (both with Co(II)).[186, 187] Therefore it was decided to investigate this particular combination of ligands with other first row transition metals.

3.4 Reaction of Cu(II) with 4,4'-bipyridine.

The formation of copper-containing coordination polymers of varying dimensions is well documented.[95, 162, 166, 173, 188-194] The lack of Cu(II) structures containing both 4,4'-bipy and acetate in the literature provides justification for its use in the present study.

3.4.1 Hydrothermal reaction of $Cu(OAc)_2$ with 4,4'-bipy.

An aqueous mixture of $Cu(OAc)_2$ and 4,4'-bipy was placed in a Teflon®-lined stainless steel vessel, and placed in an oven. A standard heat-cooling cycle was then run. Upon opening the reaction vessel, it was noted that there were two main products: blue crystals (110mg) were mixed in with a pale blue precipitate. Over time the crystals were observed to lose crystallinity, due to the loss of water. This was confirmed by TGA, with the sample gradually losing 10% of the sample weight over a 15 min time period at 30 °C, corresponding to the loss of the water molecules in the lattice. This problem is likely to have affected the sample sent for elemental analysis at UCD. Nevertheless, the data provided by microanalysis indicated that 4,4'-bipy and acetate moieties were present in a 1:2 ratio. This is consistent with the X-ray structure discussed below. The IR spectra of both the amorphous powder and crystalline products were similar and showed the presence of an acetate moiety (ν_{as}(C–O) 1584, ν_s(C–O) 1414 cm^{-1}). A single crystal suitable for analysis by X-ray diffraction was obtained, and a structural determination was made.

*3.4.2 Crystal structure of $Cu(4,4'\text{-bipy})(OAc)_2 \cdot 2.5H_2O$ (**5**).*

This structure was refined in the monoclinic space group *C*2/*c* and crystallographic data are given in Table 3.8. The structure of **5** contains a neutral copper acetate dimer sub-unit. Figure 3.19 shows the atomic numbering scheme and atom connectivity of this dimer. The dimer is the repeat unit of a 1D coordination polymer that extends along the crystallographic *b* axis. The 1D polymer is centred along a two-fold rotation axis located midway between the copper centres of each dimer. Each copper centre adopts a distorted square-based pyramidal geometry. Selected bond lengths and angles are given in Table 3.8. Unlike the 'paddle-wheel' copper acetate dimer,[195] where all acetates adopt a bridging mode that utilises both oxygen atoms, the acetates in **5** coordinate with two different modes. One acetate bridges between copper centres *via* a single oxygen atom, whilst the other is monodentate. The oxygen atom of the bridging acetate (O1) occupies a basal position on one of the copper atoms (Cu1) and an axial position on the other (Cu1A). The Cu1–O1–Cu1A angle is 101.9(2)° giving a Cu1–Cu1A distance of approximately 3.4 Å.

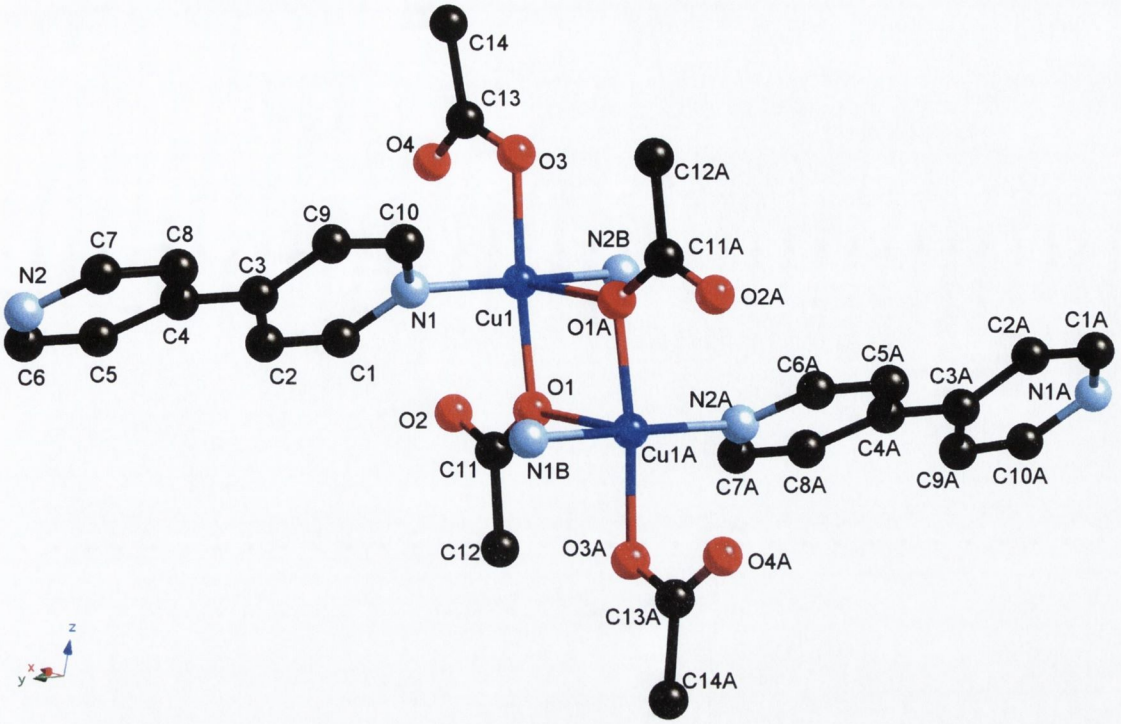

Figure 3.19 – Molecular structure and atomic labelling diagram for the dimeric unit of **5**. (Hydrogen atoms and solvent molecules omitted for clarity)

Two 4,4'-bipy ligands are coordinated to each copper centre in *trans* positions of the basal plane and link the dimer units into 1D chains. The 4,4'-bipys also form face-to-face π-interactions as shown in Figure 3.20, with the closest π–interactions (N2···C7 3.407(6) Å) being similar to the copper-copper distance within dimers. Dimeric chains of **5** are packed together in a parallel manner, with adjacent polymers related by inversion centres and two-fold screw axes.

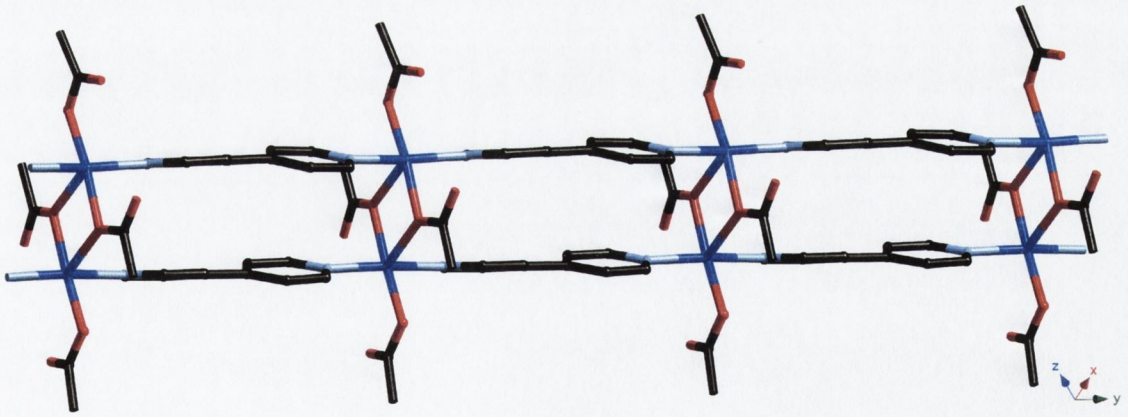

Figure 3.20 – Single polymeric chain of **5**, showing the acetate bridging and π-stacking of 4,4'-bipy molecules within the chain. (Hydrogen atoms and solvent molecules omitted for clarity)

Table 3.7 – Crystallographic data for **5** and **6**.

Compound	**5**	**6**
Chemical Formula	$C_{14}H_{14}N_2O_{6.5}Cu$	$C_{14}H_{14}N_2O_4Zn$
Formula Weight	377.81	339.64
Crystal System	Monoclinic	Triclinic
Space Group	*C*2/*c*	*P*-1
a /Å	16.758(4)	7.942(3)
b /Å	11.135(3)	9.106(3)
c /Å	17.341(4)	10.593(3)
α /°	90.00	109.296(4)
β /°	100.395(3)	99.716(4)
γ /°	90.00	101.034(4)
V /Å^3	3182.7(14)	687.0(4)
Z	8	2
D_{calc} /g cm^{-3}	1.577	1.642
μ(Mo-K$_\alpha$) /mm^{-1}	1.408	1.804
T /K	153(2)	153(2)
Crystal Size max /mm	0.38	0.48
mid /mm	0.15	0.05
min /mm	0.10	0.05
$2\theta_{max}$	56.54	56.4
Min/Max Trans. Factor	0.894/1.000	0.658/1.000
R_{int}	0.0507	0.0943
R_1, wR_2 [I>2σ(I)][a]	0.0641, 0.1501	0.0582, 0.1338
R_1, wR_2 (all data)	0.0842, 0.1562	0.0733, 0.1402
Reflections: collected	14022	7698
unique	3685	3046
observed	2901	2390

[a] $R_1 = \Sigma||F_o| - |F_c||/\Sigma|F_o|$, $wR_2 = [\Sigma w(F_o^2 - F_c^2)^2/\Sigma w(F_o^2)^2]^{1/2}$

Table 3.8 – Selected bond lengths (Å), distances (Å) and angles (°) for **5**.

Cu1 – O1	1.971(3)	O3 – Cu1 – N1	89.3(2)
Cu1 – O3	1.954(3)	O1 – Cu1 – N1	89.7(2)
Cu1 – N1	2.018(4)	O3 – Cu1 – O1	172.6(2)
Cu1 – N2B^{i}	2.025(4)	O3 – Cu1 – O1A^{ii}	94.6(2)
Cu1 – O1A^{ii}	2.426(3)	O1 – Cu1 – O1A^{ii}	78.1(2)
C11 – O1	1.282(6)	O3 – Cu1 – N2B^{i}	90.5(2)
C11 – O2	1.228(6)	O1 – Cu1 – N2B^{i}	91.4(2)
C13 – O3	1.272(6)	N1 – Cu1 – N2B^{i}	173.8(2)
C13 – O4	1.237(6)	N1 – Cu1 – O1A^{ii}	92.9(2)
N2 ·· C7^{ii}	3.407(6)	Cu1 – O1 – Cu1A^{ii}	101.9(2)
		C11 – O1 – Cu1	114.6(3)
		C11 – O1 – Cu1A^{ii}	143.3(3)
		C13 – O3 – Cu1	113.0(3)
		C(2) – C(3) – C(4) – C(5)	16.3(8)

Symmetry Codes: *i* = x, 1+y, z; *ii* = -x, y, -½-z.

Water molecules occupy the voids between polymeric chains and form hydrogen-bonds with the uncoordinated oxygen atoms (O2 and O4) of the acetate groups. Figure 3.21 shows a packing diagram of the polymeric chains as viewed down the crystallographic *b* axis. The lattice water network is depicted by the dashed lines.

Figure 3.22 shows in detail the hydrogen-bonded network that exists between the water molecules. The extraneous parts of the coordination polymers have been rendered as transluent for clarity (4,4'-bipy molecules, *etc*). The required symmetry operators can be found in Table 3.9.

Oxygen, O5, was refined at full occupancy, whilst oxygen atoms O6, O7, and O8 were refined at half occupancy. The proximity of O7 to O8 (0.86(1) Å) means that they can not both be present at the same time. As a consequence of the half occupancy of the three oxygen atoms the connectivity of the network can exist in two 'states'. These are shown in Figure 3.22 where the atoms O6, O7, and O8 represent the positions of the atoms half of the time and the hydrogen-bonds are shown as red and white dashes. The atoms O6(iii), O7(iii), and O8(iii) represent the atom positions during the remaining time. The hydrogen-bonds in this case are shown as blue and red dashes. Table 3.9 lists the bond lengths for the water network found in **5**. The hydrogen-bonds between O5 and its nearest symmetry relative (O5(i)···O5(ii); dashed), and O5 and O2 (O5(i)···O2(i); dashed) exist in all cases as both O5 and O2 are fully occupied.

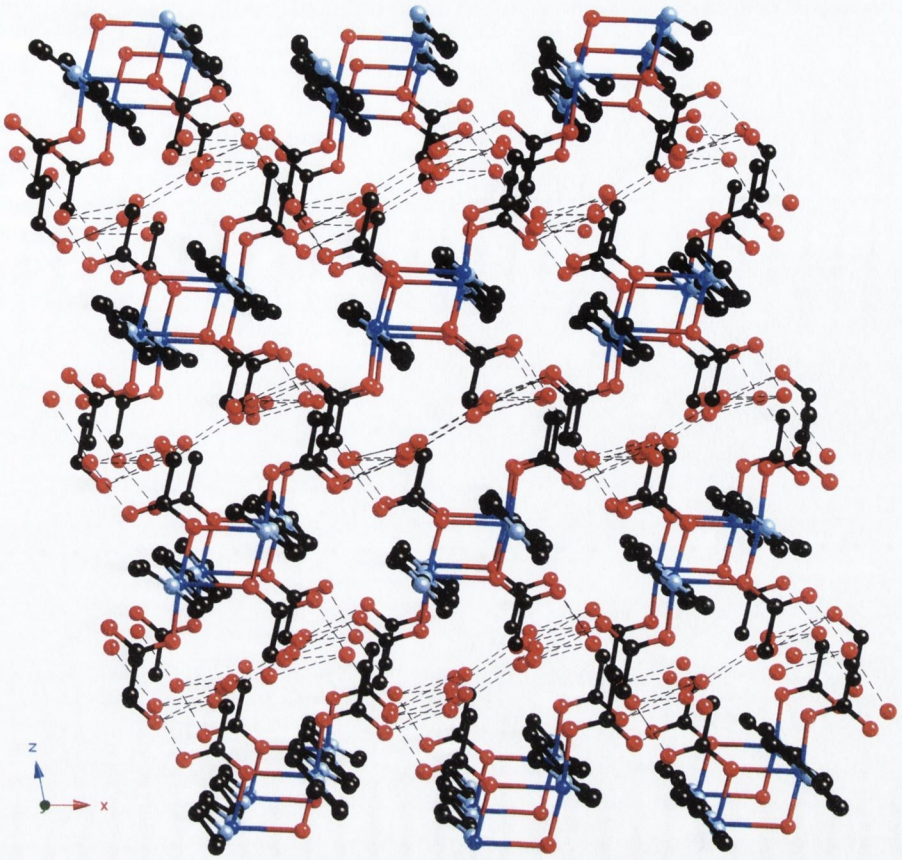

Figure 3.21 – Packing diagram for **5**. Hydrogen-bonds represented by dashed lines. Polymeric chains extend perpendicular to the page. (View along the *b* axis)

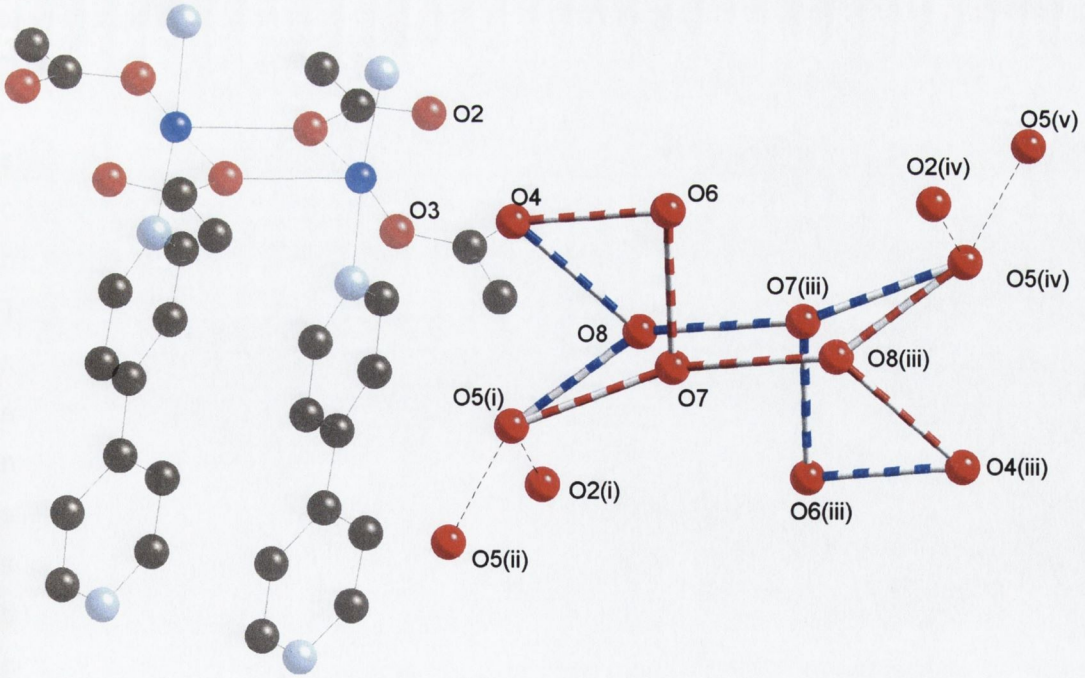

Figure 3.22 – Hydrogen-bonded lattice water network of **5**. Copper containing dimeric unit shown as translucent for orientation purposes. Oxygen atoms O6, O7 and O8 refined at half occupancy. Blue and red dashed bonds represent the alternate positions of hydrogen-bonds, thin dashed lines represent fully occupied hydrogen-bonds. (Hydrogen atoms omitted for clarity, symmetry codes listed in Table 3.8)

Table 3.9 – Bond distances (Å) of hydrogen-bonded water network.

O2 ··· O5	2.855(6)	O8 ··· $O5^{i}$	2.75(2)
O4 ··· O6	2.776(9)	$O5^{i}$ ··· $O5^{ii}$	2.81(2)
O4 ··· O8	2.91(2)	$O5^{i}$ ··· $O2^{i}$	2.855(6)
O6 ··· O7	2.87(2)	O7 ··· $O8^{iii}$	3.04(2)
O7 ··· $O5^{i}$	2.99(2)		

Symmetry Codes: *i* = ½-x, -½+y, -½-z; *ii* = x, -y, ½+z; *iii* = 1-x, -y, -z;

As stated in Chapter 1, one of the reasons behind the synthesis of coordination polymers is the potential for interesting magnetic properties. Magnetic coupling between metal centres can be dependent on various factors.[8] Typically, ligand bridges between metal centres, as is the case for **5**, assist with this coupling. To this end, the magnetic properties of a crystalline sample were analysed by Dr. Boujemaa Moubaraki and Prof. Keith Murray at Monash University. The compound displayed extremely weak antiferromagnetic behaviour and will not be discussed further.

3.5 Reaction of Zn(II) with 4,4'-bipyridine.

The use of Zn(II) in the formation of coordination polymers is well documented,[173, 196-200] and thus it was the next metal of choice. As was the case for Cu(II), the acetate salt of Zn(II) was selected.

3.4.1 Reaction of $Zn(OAc)_2$ with 4,4'-bipy.

An aqueous mixture of $Zn(OAc)_2$ and 4,4'-bipy was placed in a Telfon®-lined stainless steel vessel, and given a standard heat-cooling cycle. When the bomb was opened after the heat cycle there was no solid product at all. However, colourless needles grew from the reaction solution upon standing over a period of several days. The reaction was also performed at ambient conditions, similar to the Ni(II) reactions. A methanolic solution of 4,4'-bipy was added to an aqueous solution of $Zn(OAc)_2$ and the mixture stirred for two days, during which time a white precipitate formed. Stirring of the mixture was halted and over the next several days the reaction mixture was then left to stand, during which time the precipitate settled, and colourless crystals formed at the surface of the reaction solution, as evaporation occurred. Microanalytical data of both the amorphous precipitate and crystalline product were the same and indicative of a compound with the formula $[Zn(4,4'\text{-bipy})(OAc)_2]$. The IR spectra for both sets of crystals (i.e. those formed after the hydrothermal reaction and the non-hydrothermal reaction) as well as the white precipitate were identical, and were indicate the presence of acetate ((ν_{as}(C–O) 1586, ν_s(C–O) 1422 cm^{-1}). A crystal suitable for a structural

determination by single crystal X-ray diffraction was selected and the structure determined.

*3.5.2 Crystal structure of Zn(4,4'-bipy)(OAc)$_2$ (**6**)*

The structure of **6** is isostructural with a previously published Co(II)/4,4'-bipy structure[187]. Crystallographic data for **6** are given in Table 3.7. In a similar fashion to **5**, this 1D coordination polymer consists of dimeric sub-units, which act as repeat units. Figure 3.23 shows the atomic numbering scheme and atom connectivity of this dimer. The dimer has an inversion centre located midway between the zinc centres.

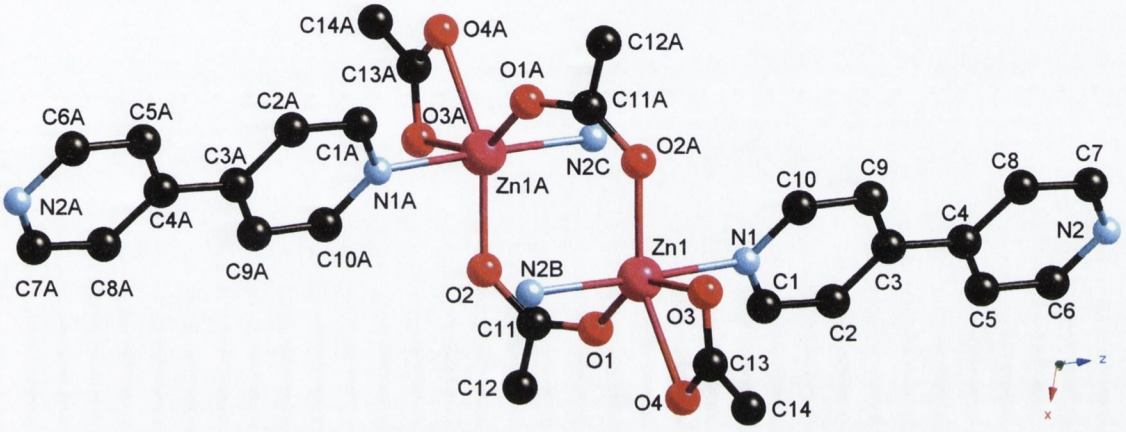

Figure 3.23 – Molecular structure and atomic labelling diagram for **6**.
(Hydrogen atoms omitted for clarity)

The Zn(II) centres show significant distortion from octahedral geometry. Selected bond lengths and angles are given in Table 3.10. Whilst the anions are identical to the copper structure mentioned previously (**5**) the modes of coordination are different. One of the acetate groups bridges between the two zinc centres, utilising both oxygen atoms, in contrast to the single atom bridges in **5**. The other acetate chelates to the metal ion, forming a four-membered Zn–O–C–O ring, with a bite angle, O3–Zn1–O4, of 58(1)° unlike that of the Cu(II) structure, which is monodentate. The different mode of bridging (compared to the copper analogue) results in the internuclear distance (Zn1 – Zn1A 3.945 Å) being greater in this dimer. Two 4,4'-bipy ligands bridge between adjacent Zn(II) dimers forming face-to-face π-interactions. Figure 3.24 shows a single polymeric chain.

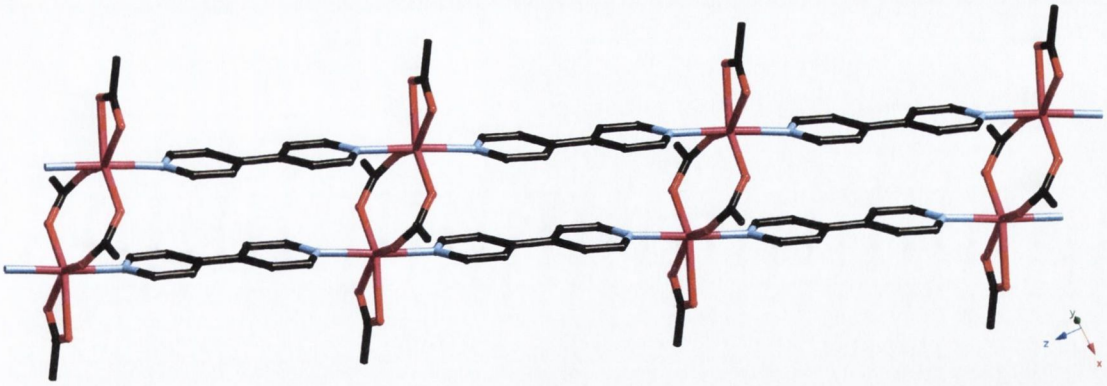

Figure 3.24 – Single polymeric chain showing offset stacking of Zn(II) dimers. (Hydrogen atoms omitted for clarity)

The linking of the zinc acetate dimer units, which results in an offset stacking arrangement of the 4,4'-bipy groups, means that the closest π–interactions (C3···C3 3.559(8) Å) are significantly shorter than the zinc-zinc distance.

Table 3.10 – Selected bond lengths (Å), distances (Å) and angles (°) for **6**.

Zn1 – O1	2.016(3)	O1 – Zn1 – N1	86.2(1)
Zn1 – O2A^{i}	2.027(3)	O2A^{i} – Zn1 – N1	87.3(1)
Zn1 – O3	2.164(3)	O3 – Zn1 – N1	92.4(1)
Zn1 – O4	2.298(3)	N2B^{ii} – Zn1 – N1	176.7(2)
Zn1 – N2B^{ii}	2.173(3)	O3 – Zn1 – O4	58.1(1)
Zn1 – N1	2.180(3)	N1 – Zn1 – O4	91.8(1)
C11 – O1	1.264(5)	C11 – O1 – Zn1	136.8(3)
C11 – O2	1.249(5)	C11 – O2 – Zn1	93.5(3)
C13 – O3	1.252(5)	C13 – O4 – Zn1	87.6(3)
C13 – O4	1.244(5)	O2 – C11 – O1	125.8(4)
O3 ··· H8^{iii}	2.353	C13 – O3 ··· H8^{iii}	136.6
O3 ··· H9^{iii}	2.440	C13 – O3 ··· H9^{iii}	131.6
O4 ··· H5^{iv}	2.569	H8^{iii} ··· O3 ··· H9^{iii}	51.0
O4 ··· H6^{iv}	2.658	C13 – O4 ··· H5^{iv}	151.0
C3 ··· C3^{v}	3.559(8)	C13 – O4 ··· H6^{iv}	147.1
		H5^{iv} ··· O4 ··· H6^{iv}	52.1

Symmetry Codes: *i* = -1-x, -y, -1-z; *ii* = x, y-1, z-1; *iii* = -1-x, 1-y, -z; *iv* = -x, 1-y, -z; *v* = -1-x, -y, -z.

Dimeric polymer chains are packed in a parallel fashion, with adjacent polymers being related by inversion centres. C–H···O hydrogen bonds exist between the oxygen atoms of the chelating acetate group (O3 and O4) and the hydrogens of 4,4'-bipy on adjacent polymeric chains (H8/H9, and H5/H6). The bond lengths and angles for these

contacts are listed in Table 3.10. These hydrogen-bonds link 1D chains together to form a 3D hydrogen-bonded network. Figure 3.25 shows the packing of the 1D polymers.

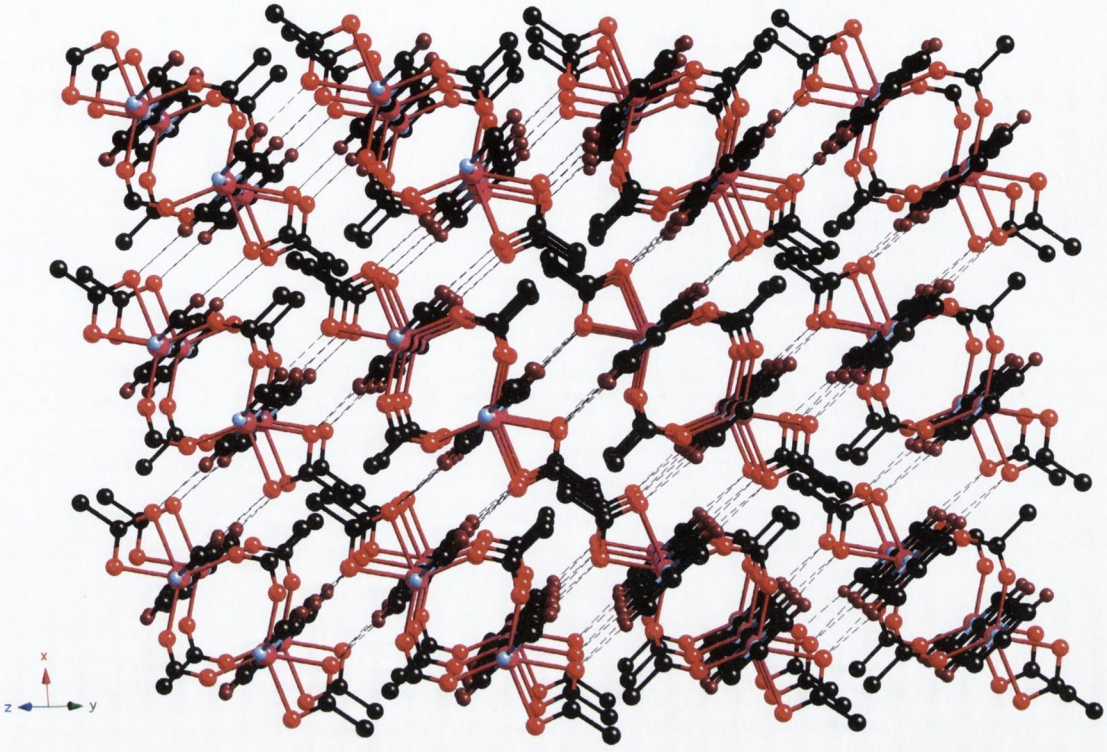

Figure 3.25 – Packing diagram for **6**. Hydrogen-bonds represented by dashed lines. Polymeric chains extend perpendicular to the page. (View along the (011) direction, non hydrogen-bonding hydrogen atoms omitted for clarity)

The structure contains no solvent molecules within the lattice. The 1D polymeric chains extend along the (011) direction.

The structures of **5** and **6** are closely related. The formation of 1D dimeric polymer chains is a common feature of both structures, as is the parallel packing of the chains. Although each structure has acetate groups coordinating to the metal centres in two different modes, the main differences between the two structures are the coordinating modes of the acetate ligands. The disposition of the uncoordinated acetate oxygens in **5** appears to favour inclusion of lattice water through hydrogen-bonding, a feature absent in **6**.

3.6 Reaction of Cu(II) with and 4,4'-bipyridine in the presence of 1,4-benzenedicarboxylic acid.

The structures described in the current chapter have all incorporated the bidentate ligand 4,4'-bipy. There is a large body of work utilising this ligand in the formation of coordination polymers.[173, 187, 189, 192, 201-208] Other widely used ligand systems include oxygen donor carboxylate ligands. The use of mono-, di- and tri-carboxylate containing ligands is well documented.[98, 115-117, 209-212] Coordination polymers that contain *both* 4,4'-bipy and carboxylate as ligands are somewhat rarer.[213] In an effort to redress this situation, it was decided to use hydrothermal synthetic techniques to form coordination polymers that contain both 4,4'-bipy and a di-carboxylate ligand (1,4-benzenedicarboxylate (bdc)).

The structures described in the remainder of the current chapter do not contain 1,4-benzendicarboxylic acid (H_2bdc) or the deprotonated form (bdc), even though it was used in the synthesis. Products containing both 4,4'-bipy and bdc (or H_2bdc) will be reported in Chapter 4 of this thesis. Repetition of the reactions reported here, in the absence of H_2bdc did not yield any crystalline products. This appears to indicate that bdc is involved in some manner in determining the product, although the exact nature of its involvement is not, as yet, understood.

3.6.1 Hydrothermal reaction of $Cu(NO_3)_2$ with 4,4'-bipy and H_2bdc (1:1:2).

An aqueous mixture of $Cu(NO_3)_2$, 4,4'-bipy and H_2bdc was placed in a Teflon®-lined stainless steel vessel, and placed in an oven. A standard heating cycle, was then run. Upon opening the reaction vessel, it was noted that there was a mixture of products. There was a large amount of amorphous white powder mixed in with a pale blue powder. There were also two different types of crystals present. There were royal blue prisms (**7**) and pale green/blue blocks (**8**). The yield of the crystalline products was extremely low (< 1% of the reaction mixture) and only amounted to a matter of tens of crystals. As a consequence there was an insufficient quantity of crystals to perform microanalysis, or IR spectroscopy. The royal blue crystals (**7**) were unstable and lost crystallinity when removed from the mother liquor. However, the crystals that were present were of sufficient quality to analyse by X-ray diffraction, and structural determinations were made for both compounds.

*3.6.2 Crystal structure of Cu(4,4'-bipy)$(NO_3)_2 \cdot xH_2O$ (**7**).*

Crystallographic details for this structure are listed in Table 3.11. The structure was refined in the orthorhombic space group *Fddd*. The atomic structure of the coordination sphere of the Cu(II) metal centre is shown in Figure 3.26.

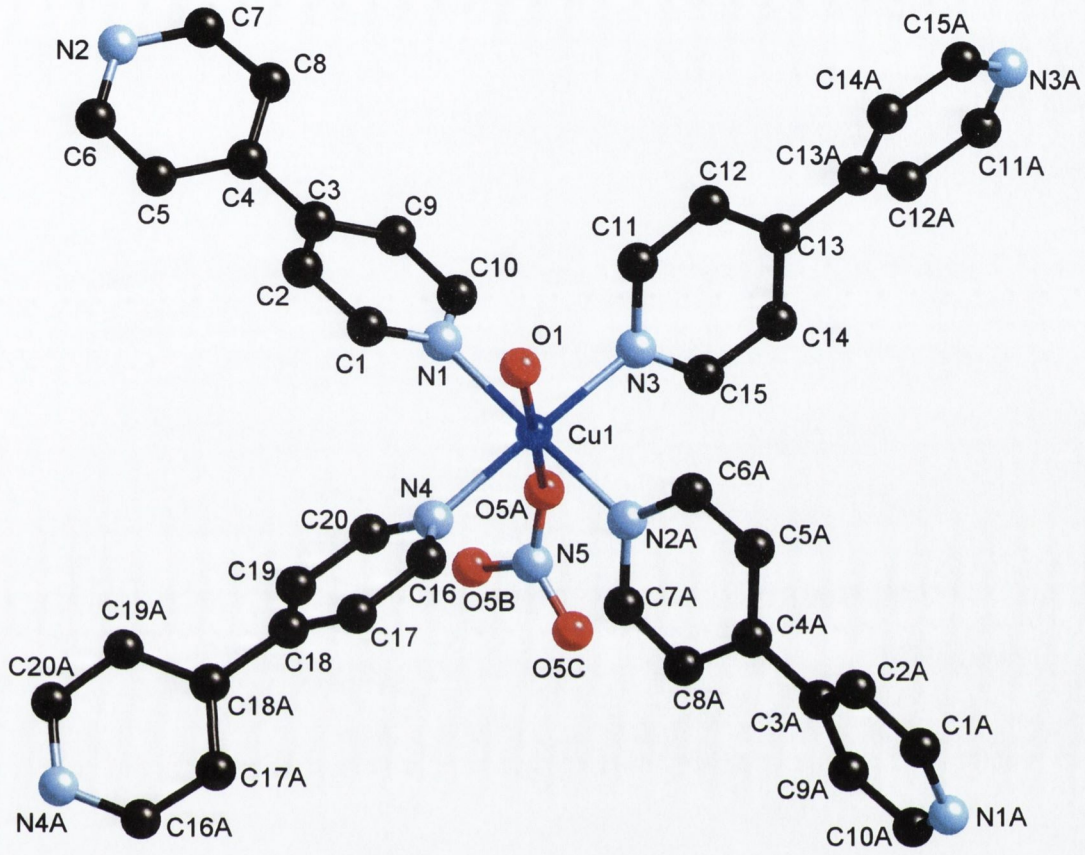

Figure 3.26 – Molecular structure and atomic labelling diagram for the Cu(II) centre of **7**. (Lattice water molecules, counter-ions and hydrogen atoms omitted for clarity)

The Cu(II) centre in this structure adopts an octahedral geometry, which shows typical Jahn-Teller distortion. There are four 4,4'-bipy molecules coordinated to each metal centre, in the equatorial positions (Cu–N, 2.03–2.05 Å). Oxygen atoms, both of which, have been refined at full occupancy, occupy the axial positions. One of the oxygen atoms (O1) is the oxygen on a water molecule. Although the other oxygen atom (O5A) has full occupancy, it has been modelled in two parts. One half has the oxygen being a water molecule, and the other has the oxygen being part of a nitrate anion, which has been refined at half occupancy. Selected bond lengths and angles for this compound are listed in Table 3.12.

Table 3.11 – Crystallographic data for **7** and **8**.

Compound	**7**	**8**
Chemical Formula	$C_{20}H_{16}CuN_6O_{13.75}$	$C_{20}H_{20}N_6O_8Cu$
Formula Weight	623.93	535.96
Crystal System	Orthorhombic	Triclinic
Space Group	*Fddd*	*P*-1
a /Å	14.649(2)	6.976(1)
b /Å	41.999(5)	12.115(1)
c /Å	42.040(5)	12.792(1)
α /°	90.00	96.916(2)
β /°	90.00	97.632(2)
γ /°	90.00	96.233(2)
V /Å^3	25865(6)	1055.13(16)
Z	32	2
D_{calc} /g cm^{-3}	1.126	1.687
μ(Mo-K$_\alpha$) /mm^{-1}	0.716	1.099
T /K	153(2)	153(2)
Crystal Size max /mm	0.50	0.25
mid /mm	0.45	0.15
min /mm	0.25	0.10
$2\theta_{max}$	50.14	46.56
Min/Max Trans. Factor	0.827/1.000	0.799/1.000
R_{int}	0.0618	0.0421
R_1, wR_2 [I>2σ(I)][a]	0.0953, 0.2891	0.0358, 0.0724
R_1, wR_2 (all data)	0.1173, 0.2970	0.0494, 0.0767
Reflections: collected	65923	7253
unique	5747	3040
observed	4149	2375

[a] $R_1 = \Sigma||F_o| - |F_c||/\Sigma|F_o|$, $wR_2 = [\Sigma w(F_o^2 - F_c^2)^2/\Sigma w(F_o^2)^2]^{1/2}$

Table 3.12 – Selected bond lengths (Å) and angles (°) for **7**.

Cu1 – N1	2.041(5)	N1 – Cu1 – N3	90.6(2)
Cu1 – N3	2.032(5)	N1 – Cu1 – N4	89.9(29)
Cu1 – N4	2.044(5)	N1 – Cu1 – O1	88.6(2)
Cu1 – O1	2.423(5)	N1 – Cu1 – O5A	88.6(2)
Cu1 – O5A	2.465(5)	N1 – Cu1 – N2^{i}	178.2(2)
Cu1 – N2A^{i}	2.039(5)	O1 – Cu1 – O5A	177.2(2)
		C2 – C3 – C4 – C5	33.8(9)
		C12 – C13 – C13^{ii} – C14^{ii}	32.8(4)
		C17 – C18 – C18^{iii} – C17^{iii}	57(1)

Symmetry Codes: *i* = ¾+x, -y, -¼+z; *ii* = ¼-x, ¼-y, z; *iii* = -¼-x, ¾-y, z.

The overall packing of this structure gives two highly unusual 3D polymeric, interpenetrated, networks. The metal centres act as square-planar nodes, which are connected within the network by bidentate 4,4'-bipy ligands. A single network is composed of octanuclear rhombic units, as shown in Figure 3.27(a).

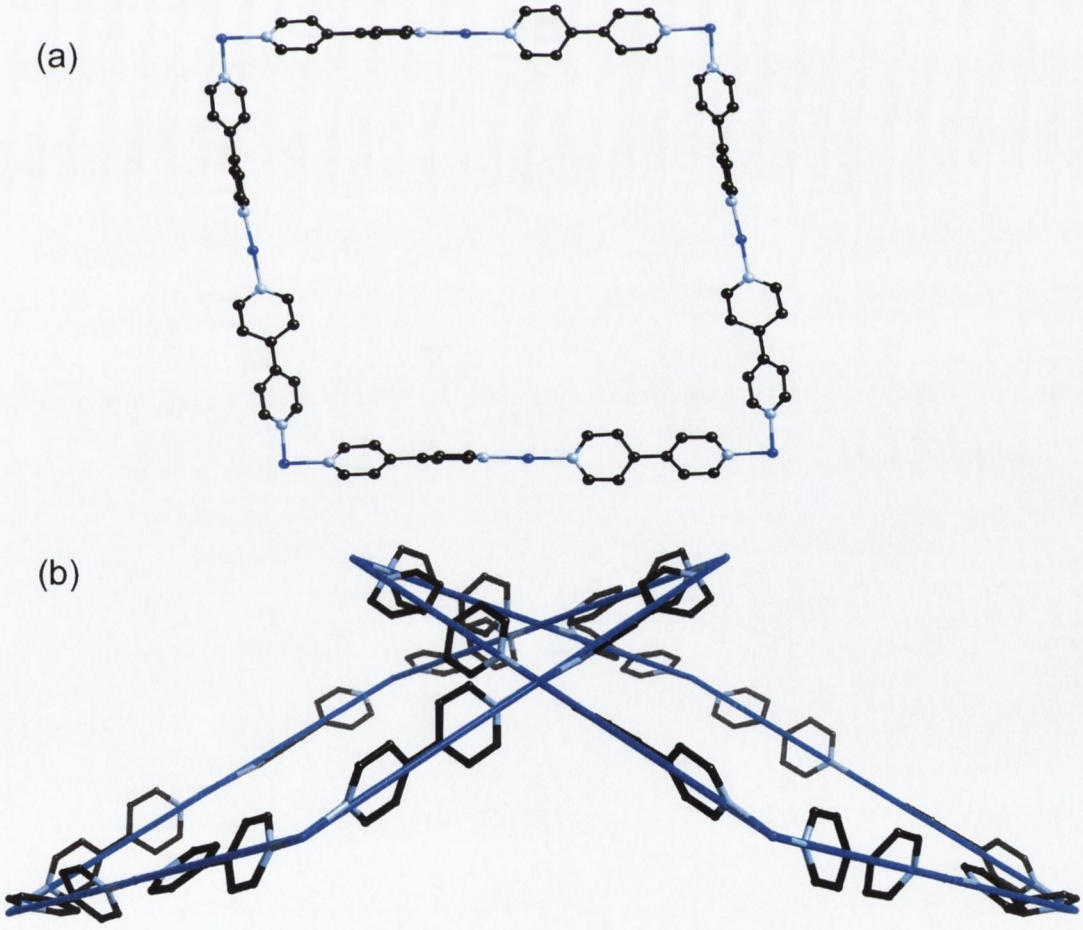

Figure 3.27 – (a) Single octanuclear rhombic unit. (b) Fused rhombic units. The 4-membered ring formed by two fused rhombic units is clearly puckered.

As the Cu(II) centres act as square planar nodes, the rhombic units bound by eight metal centres are fused together in an inclined arrangement, this is shown in Figure 3.27(b). This allows for the formation of circuits containing four nodes, which are highly folded (see Figure 3.27(b)) and have an inter-nodal distance of *ca.* 11.1Å. The larger eight-membered rhombic circuits have a diagonal ratio (long/short diagonal) of *ca.* 1.115. Figure 3.28 is a schematic diagram showing the two interpenetrated networks.

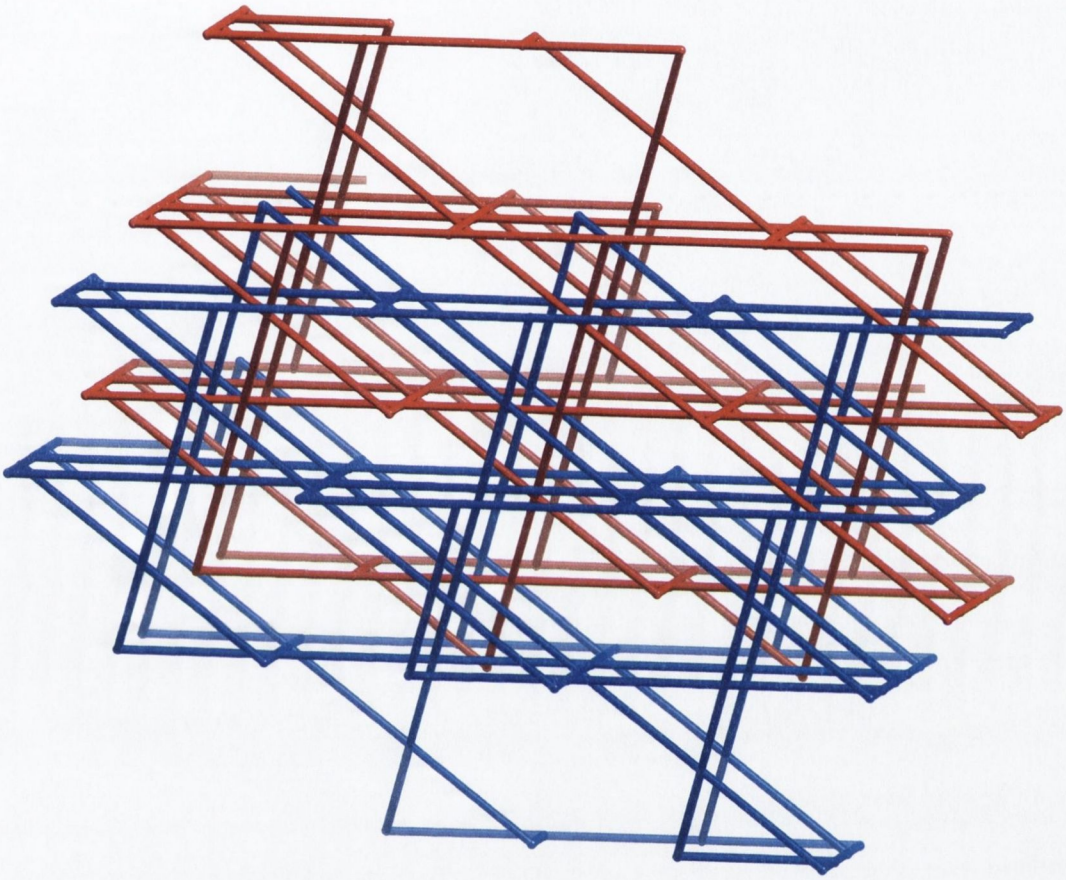

Figure 3.28 – Schematic representation of the two interpenetrated networks formed in **7**.

The topology of this network is unusual. It has only one kind of node with the Schläfli symbol $[4^2.8^4]$. This network topology has been previously reported, by Batten and co-workers[111] for structures reported by Ermer and co-workers,[214] and Bishop and co-workers.[215-217] The structures reported by these groups contained networks of diol-containing molecules connected *via* hydrogen-bonds. During the course of this study, Ciani and co-workers[218] reported an example of a coordination polymer with this network topology which is very similar to the structure **7**. In fact, the network composition (Cu(II) metal centres and 4,4'-bipy molecules) in their example is exactly the same as **7**. However, the reported coordination polymer contains triflate anions, which are coordinated to the Cu(II) centres in axial positions *c.f.* water and nitrate in **7**. Another important feature of the structure reported by Ciani and co-workers, compared to that of **7** is the interpenetration of one net through the other. The connectors of one

network pass through the centres of the voids of the other network. This 'symmetrical interpenetration' means that there is a high degree of symmetry in the crystallographic system, and the structure refines in the tetragonal space group $I4_1/acd$. In the structure of **7**, the connectors of one network do not pass through the centres of the voids of the second network, and as a consequence the interpenetration is not 'symmetrical'. This gives rise to lower symmetry (*Fddd*) for the structure of **7**. Figure 3.29 shows the interpenetration of both **7** (Figure 3.29(a)) and that network reported by Ciani and co-workers (Figure 3.29(b)).

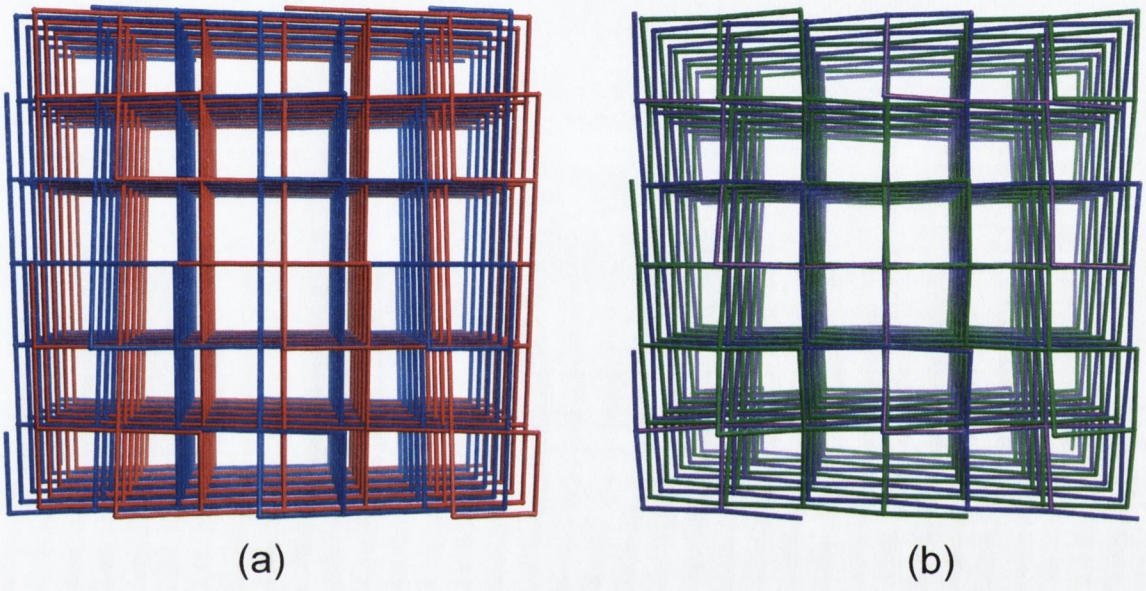

Figure 3.29 – (a) Interpenetation of two ($4^2 8^4$) networks in **7**. (b) Interpenetration of two networks (same topology) as reported by Ciani and co-workers.[218] Note the offset nature of the interpenetration of **7**, whilst the two networks are arranged 'symmetrically' in (b).

An interesting feature of the structure reported by Ciani is that solvent molecules within the lattice can be exchanged without disrupting the network. Indeed, Ciani and co-workers propose that the network displays elastic properties in stretching and contracting as guest molecules are introduced.[218] Experiments of this type are yet to be made on **7**.

*3.6.3 Crystal structure of Cu(4,4'-bipy)$(NO_3)_2(H_2O)_2$ (**8**).*

The structure of **8** was refined in the *P*-1 space group and crystallographic details are given in Table 3.11. The overall structure consists of a copper-containing monomeric subunit, which hydrogen-bonds to adjacent monomers to form a 2D sheet. Figure 3.30 shows the copper-containing asymmetric unit and the atomic labelling.

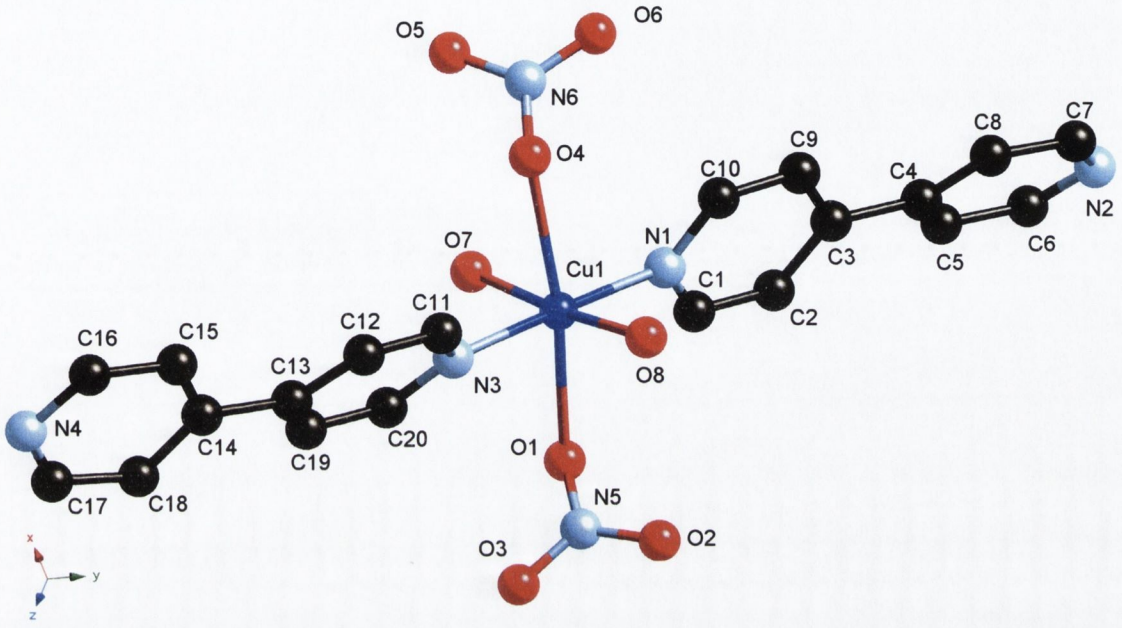

Figure 3.30 – Molecular structure and atomic labelling diagram for **8**. (Hydrogen atoms omitted for clarity)

Selected bond lengths and angles for **8** are given in Table 3.13(a). The Cu(II) centre adopts an octahedral geometry, with Jahn-Teller distortion. The equatorial positions around the Cu(II) are occupied by two 4,4'-bipy ligands and two water molecules, with like donors in a *trans* arrangement to each other. The axial positions are occupied by nitrate anions coordinated *via* a single oxygen atom. The lengths of these bonds are considerably longer than those of the equatorial ligands. One axial bond (Cu1–O(4) 2.522(2) Å) is also significantly longer than the other (Cu1–O(1) 2.438(2) Å).

Table 3.13(a) – Selected bond lengths (Å) and angles (°) for **8**.

Cu1 – O1	2.438(2)	O1 – Cu1 – N1	90.06(9)
Cu1 – O4	2.522(2)	O1 – Cu1 – N3	88.33(9)
Cu1 – N1	2.007(2)	O1 – Cu1 – O7	87.81(9)
Cu1 – N3	2.012(2)	O1 – Cu1 – O8	97.75(9)
Cu1 – O7	1.963(2)	O1 – Cu1 – O4	172.51(8)
Cu1 – O8	1.961(2)	O4 – Cu1 – N1	95.49(9)
N5 – O1	1.262(3)	O4 – Cu1 – N3	86.16(9)
N5 – O2	1.257(3)	O4 – Cu1 – O7	87.06(9)
N5 – O3	1.240(3)	O4 – Cu1 – O8	87.46(9)
N6 – O4	1.266(3)	N1 – Cu1 – N3	178.3(1)
N6 – O5	1.249(3)	N1 – Cu1 – O7	91.2(1)
N6 – O6	1.240(3)	N1 – Cu1 – O8	88.3(1)
		N3 – Cu1 – O7	89.3(1)
		N3 – Cu1 – O8	91.4(1)
		O7 – Cu1 – O8	174.4(1)
		C2 – C3 – C4 – C5	21.7(5)
		C12 – C13 – C14 – C15	15.8(5)

The monomeric units in this structure are very similar to those of the $[Ni(4,4'\text{-bipy})_2(OAc)_2(H_2O)_2]$ (**3**) complex with nitrates replacing the acetates. Like **3**, the monomeric units hydrogen-bond together to form a (4,4) 2D network. In **3**, 'single' bipy-water hydrogen-bond bridges give the (4,4) 2D network (see Figure 3.13, page 88). In **8**, however, there are 'double' bipy-water hydrogen-bond bridges (O7···N2 2.725(3) Å, O8···N4 2.700(3) Å) between metal centres giving 1D chains. These are cross-linked by 'double' water-nitrate hydrogen-bond bridges (O2···O7 2.729(3) Å, O5···O8 2.734(3) Å) to give the (4,4) 2D network as shown in Figure 3.30. Face-to-face π-interactions also occur between adjacent 4,4'-bipy molecules (N(2)···C(20) 3.229(4) Å) within the sheets, as they do in **3**, giving infinite stacks down the *a* axis. Unlike **3**, no lattice solvent molecules reside between the hydrogen-bonded sheets in **8**. The sheets are, therefore, much closer together than those of **3** as shown in Figure 3.31. Several close C–H···O contacts also occur within the structure between the bipy protons and nitrate oxygen atoms. The majority of these interactions are between adjacent sheets while some are intramolecular or within sheets. (See Table 3.13(b) for all hydrogen-bond lengths and angles).

Table 3.13(b) – Selected hydrogen-bond distances (Å) and angles (°) for **8**.

O2 ··· H7A^{i}	1.893(5)	O5 ··· H10	2.412
O2 ··· O7^{i}	2.729(3)	O5 ··· C10	3.117(4)
O5 ··· H8A^{ii}	1.918(10)	O3 ··· H6^{vii}	2.546
O5 ··· O8^{ii}	2.734(3)	O3 ··· C6^{vii}	3.232(4)
H7B ··· N2^{iii}	1.896(8)	O3 ··· H18^{viii}	2.551
O2 ··· H7A^{i}	1.893(5)	O3 ··· C18^{viii}	3.295(4)
O2 ··· O7^{i}	2.729(3)	O1 ··· H18^{viii}	2.575
O5 ··· H8A^{ii}	1.918(10)	O1 ··· C18^{viii}	3.365(4)
O5 ··· O8^{ii}	2.734(3)		
H7B ··· N2^{iii}	1.896(8)		
O7 ··· N2^{iii}	2.725(3)	O2 ··· H7A^{i} – O7^{i}	173(3)
H8B ··· N4^{iv}	1.869(8)	O5 ··· H8A^{ii} – O8^{ii}	164(3)
O8 ··· N4^{iv}	2.700(3)	O7 – H7B ··· N2^{iii}	169(4)
N2 ··· C20^{iv}	3.229(4)	O8 – H8B ··· N4^{iv}	169(4)
O4 ··· H12^{v}	2.389	O4 ··· H12^{v} – C12^{v}	174.6
O4 ··· C12^{v}	3.335(4)	O4 ··· H15^{v} – C15^{v}	145.6
O4 ··· H15^{v}	2.611	O6 ··· H8^{vi} – C8^{vi}	143.6
O4 ··· C15^{v}	3.437(4)	O6 ··· H9^{vi} – C9^{vi}	176.1
O6 ··· H8^{vi}	2.499	O5 ··· H10 – C10	130.8
O6 ··· C8^{vi}	3.313(4)	O3 ··· H6^{vii} – C6^{vii}	129.2
O6 ··· H9^{vi}	2.424	O3 ··· H18^{viii} – C18^{viii}	135.3
O6 ··· C9^{vi}	3.372(4)	O1 ··· H18^{viii} – C18^{viii}	140.7

Symmetry Codes: *i* = 1+x, y, z; *ii* = -1+x, y, z; *iii* = x, 1+y, z; *iv* = x, -1+y, z; *v* = -x, -1-y, 1-z; *vi* = -1-x, -2-y, 1-z; *vii* = 1+x, 1+y, z; *viii* = -x, -1-y, -z.

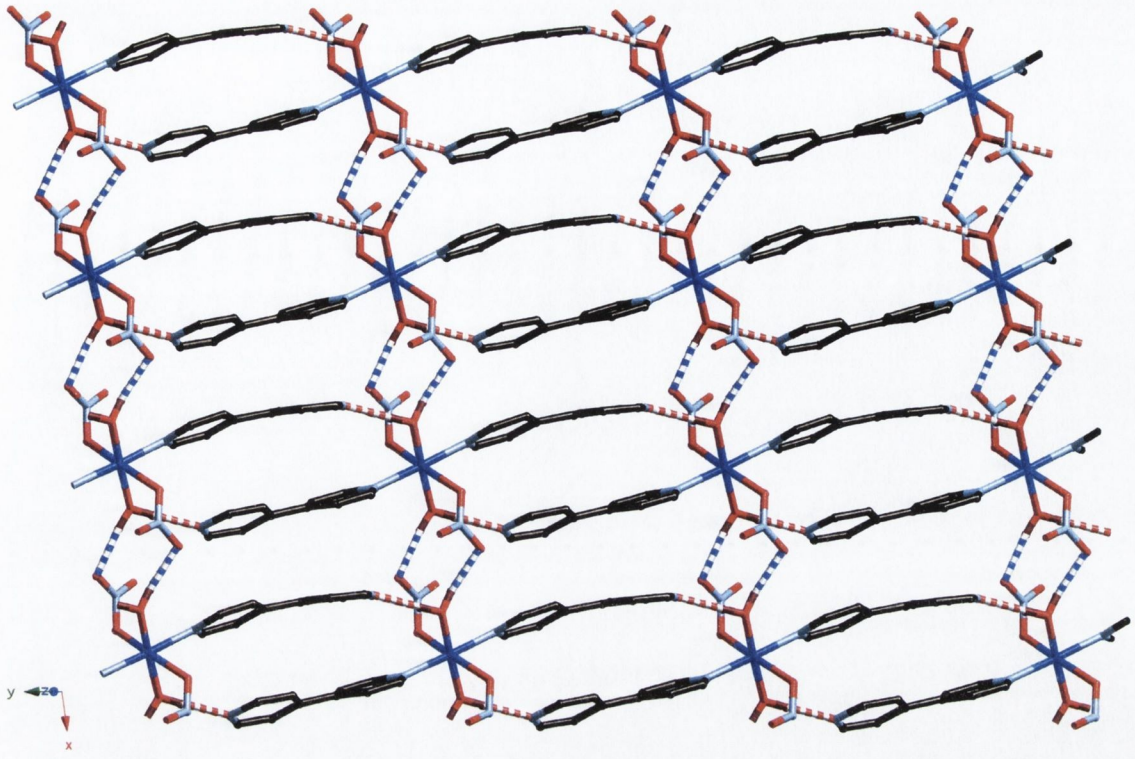

Figure 3.31 – A single 2D sheet of **8** formed by intermolecular hydrogen-bonds. (Hydrogen atoms omitted for clarity)

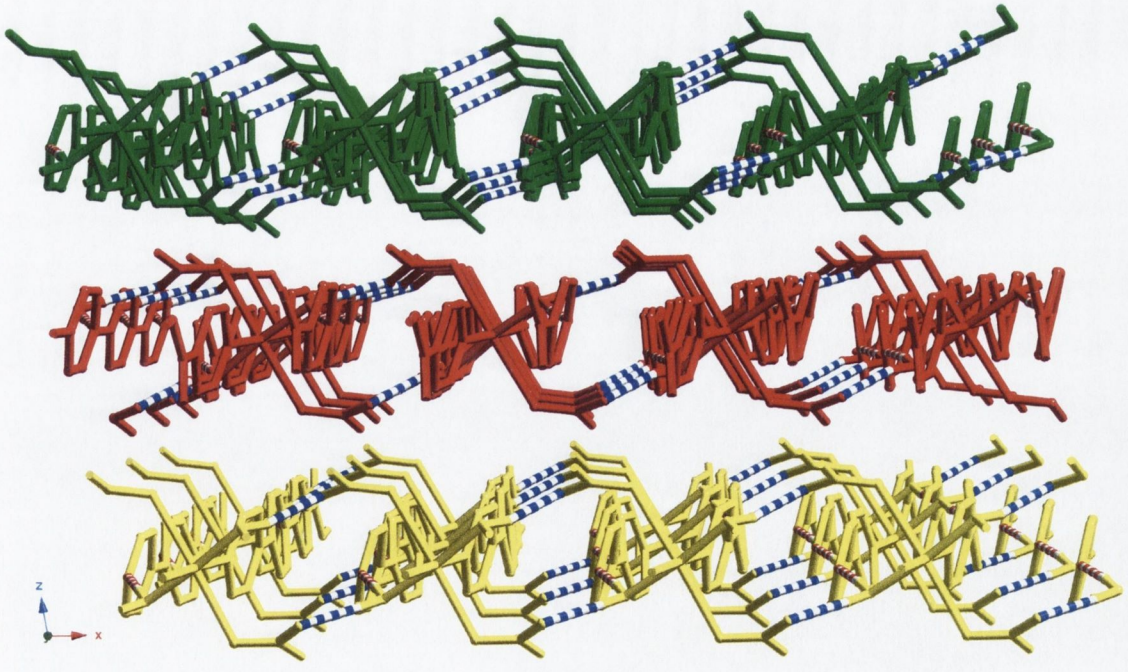

Figure 3.32 – Packing diagram showing multiple 2D Sheets of **8**. The C-H···O contacts between sheets are not shown. (View along the *b* axis)

3.7 Conclusions.

As a result of this study several novel coordination compounds with interesting structures have been synthesised. The use of hydrothermal synthetic techniques can give coordination polymers with both subtle or marked differences to those synthesised by non-hydrothermal techniques.

The initial interest in coordination polymers in the present study was a result of work towards the formation of a 'molecular square'. Changing the metal centre from Ru(II) to Co(II) in the reaction with qpy afforded a novel polymeric structure. The presence of 4,4'-bipy in the structure can be attributed to an impurity of 4,4'-bipy in the sample of qpy used in the reaction, since a second reaction where qpy was substituted by 4,4'-bipy yielded exactly the same structure. Although the structure of **2** was reported during the course of this study, the differences in the structures of **1** and **2** are good examples of the subtle differences between structures that can be present when different synthetic techniques are used.

The presence of 2,2'-bipy appears to have some influence on the structures of the Ni(II) containing compounds **3** and **4**, although the exact mode of interaction is not understood. Structure **3** forms a hydrogen-bonded network of monomeric sub-units, whilst **4** forms a polymeric network. Both the structures are novel and, coupled with the only difference in synthesis being the presence or absence of 2,2'-bipy in the reaction mixture, warrants further investigation.

The structures **5** and **6** are similar. Both form 1D polymeric chains composed of metal containing dimer sub-units. The mode of acetate bridging between the metal centres is different, with **5** having a single oxygen atom of the acetate group bridging, whilst the Zn(II) complex, **6**, showed the bridging mode seen in the classical 'paddle wheel' type acetate complex.

The presence of 1,4-benzenedicarboxylic acid in the reaction described in section 3.4 has a definite influence on the novel structures of **7** and **8** obtained in this reaction. Although a particularly low yield of crystalline product was obtained, the structures of the crystals are interesting and markedly different. Structure **7** forms a doubly interpenetrated 3D coordination polymer. Although the topology of the network has been know for some time,[111, 214-217] it was only very recently reported for a coordination polymer by Ciani and co-workers.[218] The orientation of the two interpenetrated networks seen in **7** is quite different to that seen in the structure reported by Ciani and co-workers. Furthermore, the instability of the crystals means that further analysis may prove challenging. Another product of the same reaction was **8**, which has a structure reminiscent of **3**. There is no coordination polymer linkage, rather

a collection of hydrogen-bonds between discreet monomeric units, which form 2D hydrogen-bonded sheets.

The presence of H_2bdc in the reaction mixture appears to have some kind of influence on the structures obtained. The exact nature of this influence clearly requires further investigation. What is clear though, is that in the absence of H_2bdc in the reaction mixture none of the crystalline products described in section 3.4 are obtained. Variation of the ratio of H_2bdc present yields a different set of crystalline products that are described in the following chapter.

Refinement of the synthetic techniques to yield pure crystalline products is an important avenue of research to pursue. The results published by Ciani and co-workers[218] are encouraging with regard to the potential of **7** to contain and exchange various guest molecules.

Chapter Four

Coordination Polymers of Cu(II) and Ni(II) Incorporating 4,4'-Bipyridine and 1,4-Benzenedicarboxylate.

Introduction

The previous chapter discussed various structures that contained 4,4'-bipy, which has two linearly disposed coordination sites. Also mentioned was another linear *bis*-coordinating ligand 1,4-benzenedicarboxylate (bdc). The use of oxygen donor coordination ligands in the formation of coordination polymers is well documented in the literature.[116, 175, 210, 212, 219, 220] As was mentioned in Chapter 1 the approach that Yaghi and co-workers have adopted is to form rigid Secondary Building Units (SBUs), which consist of a metal centre with several carboxylate ligands coordinated to it, essentially forming a metal-carboxylate cluster. This approach has two main advantages to it. Firstly, the coordinating ligands (functionalised carboxylates) provide the counter charge required for a neutral SBU, this also means that the voids in a resultant polymeric network are not occupied by counterions. Secondly, the geometry of the SBUs (e.g. 'paddle-wheel' or 'tri-nuclear oxylate') 'stiffen' the overall network, making it robust towards dissociation. Yaghi and co-workers have been successful in generating materials that are able to retain the framework whilst allowing exchange of guests within the cavities.[98, 116]

The approach adopted in the current chapter was to effectively link the 1D coordination polymers formed in the previous chapter together to form either 2D sheets or 3D networks. In the previous chapter several complexes were formed which incorporated a mono-acetate anion, in the structure. Functionalisation of the acetate group should allow multiple carboxylate groups to be attached to a central scaffold. Figure 4.1 shows two possible carboxylate derivatives that have the potential to link 1D coordination polymers (such as **5** and **6**) together to form networks of higher dimensionality.

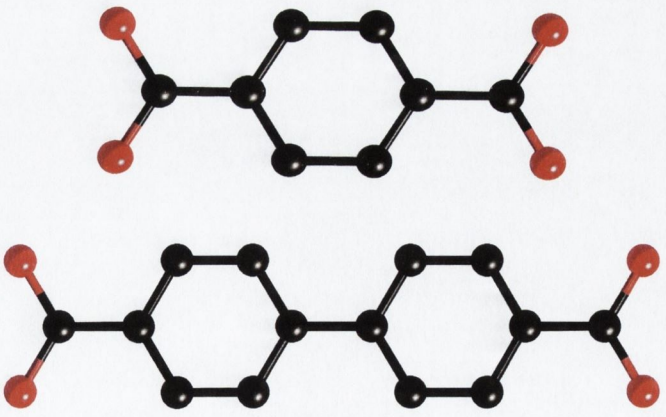

Figure 4.1 – Two potential carboxylate containing derivatives for use in synthesis of coordination polymers. (*Top*: 1,4-benzenedicarboxylate, *bottom*: 4,4'-diphenyldicarboxylate)

The use of aromatic groups which are functionalised with carboxylate groups provides the linkages with a degree of rigidity which would not be present if aliphatic

chains were used. The π-systems present may also potentially favour the inclusion of aromatic guests in the voids within the network.

4.1 Reaction of Cu(II) with 4,4'-bipyridine and 1,4-benzenedicarboxylic acid.

The primary aim to the work reported herein is to connect 1D coordination polymers formed between various metal atoms and 4,4'-bipy. Since the acetate anion was used in previous structures, it was decided to utilise a functionalised acetate moiety (bdc) to attempt to link 1D chains together. Although coordination polymers containing both 4,4'-bipy and bdc have been reported, there are only a few examples.[114, 175, 221]

Continuing in the same vein as the previous chapter, a hydrothermal synthetic approach was adopted. The main reason for this is that H_2bdc has a low solubility in aqueous media. Elevated temperatures and pressures that are present in the digestion bomb may assist in the solubility of this reactant (secondly, previous coordination polymers were synthesised using hydrothermal techniques. In order to minimise the number of experimental variables the procedure used in previous syntheses was adopted). All the heat-cool cycles used in the synthesis of the compounds under discussion are described in Chapter 5.*

4.1.1 Hydrothermal reaction of $Cu(NO_3)_2$ with 4,4'-bipy and H_2bdc (1:1:1).

An aqueous mixture of $Cu(NO_3)_2$, 4,4'-bipy and bdc (1:1:1) was placed in a Teflon®-lined stainless steel vessel, and given a standard heat-cooling cycle. Upon opening the reaction vessel, it was noted that there was a mixture of products. There was a large amount of light blue and green powders present in the reaction vessel. Amongst these various crystalline products could be extracted. Royal blue block-shaped crystals were removed (**9**), as well as pale green and pale blue crystals, (**10**) and (**11**), respectively. It should be noted here that although the reaction was repeated several times, in every case there were differing yields, both in terms of quantity and composition. As a consequence, on certain occasions more powder product would form with less crystalline product, whilst on other occasions the reverse would occur and a (relatively) large amount of crystalline product would be returned by the reaction (the amount of crystalline product ranged from approximately 50% (of total product obtained) to less than 10%). These unpredictable product returns for this reaction made quantifying yield challenging. The yield of **9**, ranged from approximately 60% of crystalline product, to a matter of several crystals. The yields of **10** and **11** were similarly difficult to quantify, and ranged from a matter of several crystals to

---

* See Chapter 5, Section 5.1.7 (page 152) for full details.

approximately 40% of the crystalline product. Compounding the problem of yield, was the fact that **10** and **11** were extremely difficult to separate, due to the size of the crystals. The crystals also were often joined together and could not be separated without destroying each crystal.

Although the yield of the crystalline products was extremely low, the crystals produced were of sufficient quality for an X-ray diffraction study to be performed, enabling a structural determination to be made.

*4.1.2 Crystal structure of [Cu(4,4'-bipy)(bdc)(H_2bdc)]. (**9**)*

Crystallographic details for this structure are given in Table 4.1. This structure was refined in the *C2/c* space group. Figure 4.2 shows the coordination sphere of the Cu(II) centre and atomic numbering of the ligands coordinated to it.

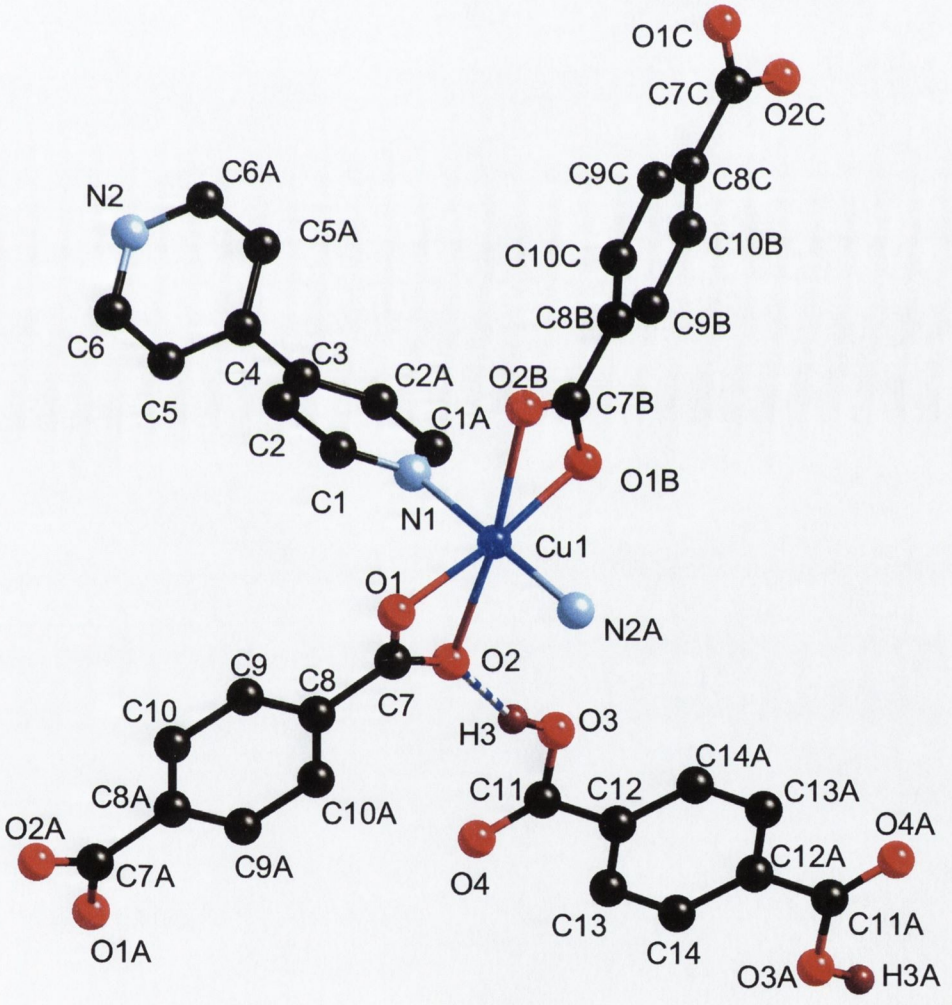

Figure 4.2 – Molecular structure and atomic labelling diagram for **9**. (Non hydrogen-bonding hydrogen atoms omitted for clarity)

The Cu(II) centre adopts a distorted octahedral geometry, with two 4,4'-bipy molecules and two bdc molecules chelating to the metal centre, with like donors arranged *trans* to each other. The bite angle of the chelating acetate is 58.26(4)°. The

axial positions around the Cu(II) centre are occupied by one of the bdc chelating oxygen atoms (Cu1–O2 2.458(1) Å). The equatorial positions are occupied by the remaining oxygen atoms and 4,4'-bipy nitrogen atoms. Selected bond lengths and angles are given in Table 4.2.

The metal centres lie on two-fold rotation axes and are linked by 4,4'-bipy molecules into chains that extend along the crystallographic *b* axis. The bipy molecules themselves are twisted along this axis, with a torsion angle of 65.24(11)° (C2-C3-C4-C5) between the pyridyl rings. The Cu(II) centres are further linked together by chelating bdc groups to form a chain extending along the (101) direction. This connectivity forms 2D (4,4) sheets.

Figure 4.3 shows a single 2D sheet. Adjacent 4,4'-bipy chains are related by inversion centres, which lie at the centre of the chelating bdc molecules. The metal-to-metal distance along the 4,4'-bipy connectors is 11.0979(4) Å, whilst the metal-to-metal distance along the chelating bdc connectors is 10.7285(3) Å.

There is also a hydrogen-bond between a H_2bdc molecule and one of the oxygen atoms O2 of the chelating bdc moieties. This contact is also shown in Figure 4.2 as a blue and white dashed bond (O2···O3 2.593(2) Å). The position of the hydrogen atom (H3) was fixed during the refinement of the solution. The short contact to the chelated oxygen atom *via* the hydrogen-bond occurs at both ends of the H_2bdc molecule, since an inversion centre resides in the centre of the aromatic ring. This connection allows for 2D sheets to be joined together, forming a three-dimensional hydrogen-bonded network. Figure 4.4(a) shows this connection between 2D sheets.

Table 4.1 – Crystallographic data for **9**, **10** and **11**.

Compound	**9**	**10**	**11**
Chemical Formula	$C_{26}H_{18}N_2O_8Cu$	$C_{128}H_{88}N_{20}O_{40}Cu_8$	$C_{14}H_{10}N_3O_5Cu$
Formula Weight	549.96	3054.50	363.79
Crystal System	Monoclinic	Triclinic	Monoclinic
Space Group	*C*2/*c*	*P*-1	*C*2/*m*
a /Å	10.5967(4)	16.859(2)	13.713(3)
b /Å	11.0979(4)	17.760(2)	10.581(2)
c /Å	19.5400(7)	22.178(3)	11.166(2)
α /°	90.00	85.519(2)	90.00
β /°	97.678(1)	88.707(2)	125.116(3)
γ /°	90.00	70.854(2)	90.00
V /Å^3	2277.3(2)	6254.1(13)	1325.3(5)
Z	4	2	4
D_{calc} /g cm^{-3}	1.604	1.622	1.823
μ(Mo-K$_\alpha$) /mm^{-1}	1.017	1.428	1.681
T /K	153(2)	153(2)	153(2)
Crystal Size max /mm	0.25	0.45	0.25
mid /mm	0.20	0.20	0.13
min /mm	0.15	0.13	0.12
$2\theta_{max}$	60.02	50.00	56.70
Min/Max Trans. Factor	0.865/1.000	n/a[†]	0.798/1.000
R_{int}	0.0287	0.1106	0.0265
R_1, wR_2 [I>2σ(I)][a]	0.0317, 0.0885	0.1243, 0.2613	0.0552, 0.1189
R_1, wR_2 (all data)	0.0341, 0.0896	0.1762, 0.2832	0.0581, 0.1202
Reflections: collected	16579	46394	1745
unique	3269	21744	1745
observed	2988	13870	1675

[a] $R_1 = \Sigma||F_o| - |F_c||/\Sigma|F_o|$, $wR_2 = [\Sigma w(F_o^2 - F_c^2)^2/\Sigma w(F_o^2)^2]^{1/2}$

[†] No absorption correction was applied to this data.

Table 4.2 – Selected bond lengths (Å), distances (Å) and angles (°) for **9**.

Cu1 – N1	2.027(2)	N1 – Cu1 – O1	86.57(3)
Cu1 – O1	1.974(1)	N1 – Cu1 – O2	85.77(3)
Cu1 – O2	2.459(1)	O1 – Cu1 – O2	58.26(4)
Cu1 – N2^{i}	2.015(2)	O1 – Cu1 – O2^{ii}	121.14(4)
C7 – O1	1.280(2)	O1 – Cu1 – O1^{ii}	173.14(6)
C7 – O2	1.249(2)	O2 – Cu1 – O2^{ii}	171.54(5)
O2 ··· H3	1.8038	C2 – C3 – C4 – C5	65.3(1)
O2 ··· O3	2.593(2)	O2 ··· H3 – O3	155.92

Symmetry Codes: *i* = x, 1+y, z; *ii* = 1-x, y, 1½-z.

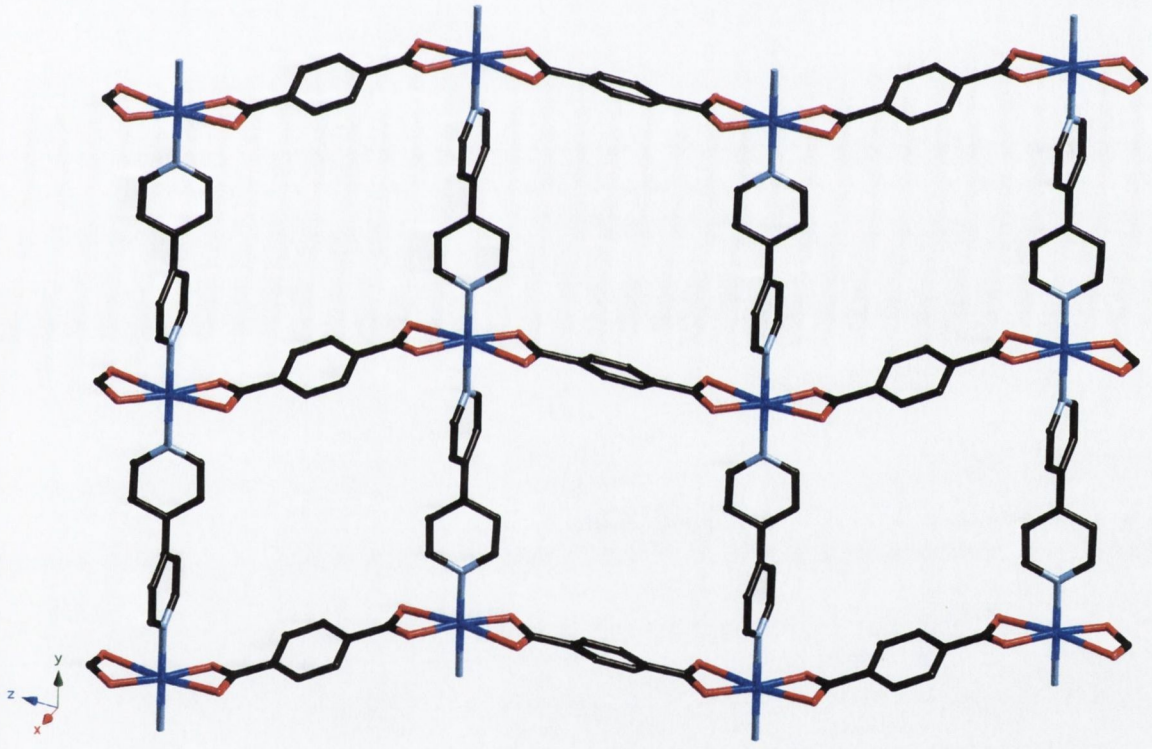

Figure 4.3 – Single 2D sheet of **9** consisting of Cu(II) centres connected by 4,4'-bipy and chelating bdc molecules. (Hydrogen atoms omitted for clarity)

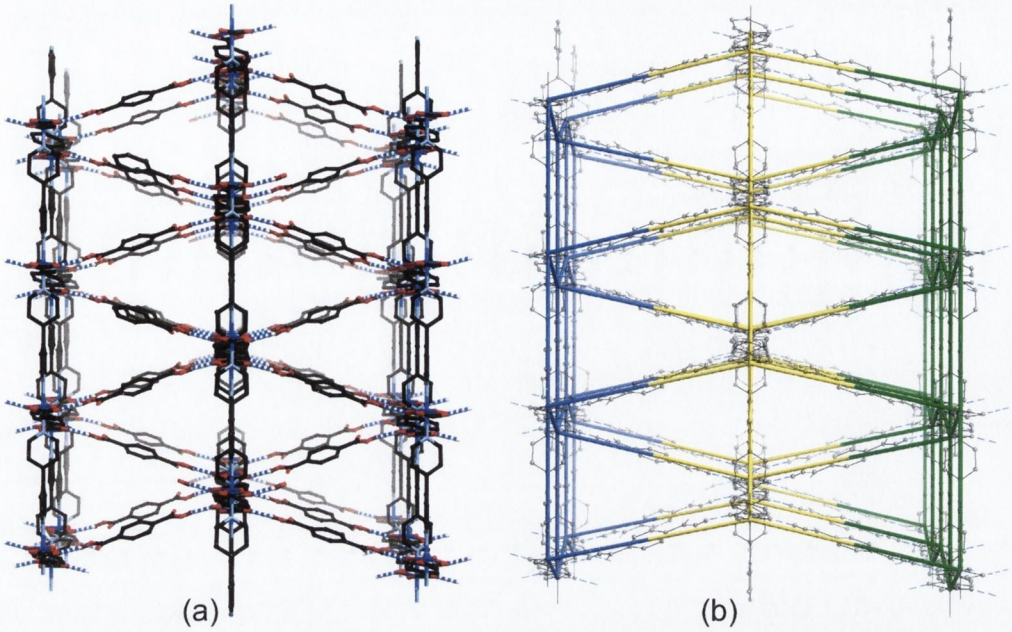

Figure 4.4 – (a) Interconnected (4,4) 2D sheets form a hydrogen-bonded 3D network (view along the (101) direction (i.e. edge on to (4,4) sheets). Hydrogen atoms omitted for clarity). (b) Schematic representation of network formed when metal centres are connected directly (purple/yellow/green connectors)

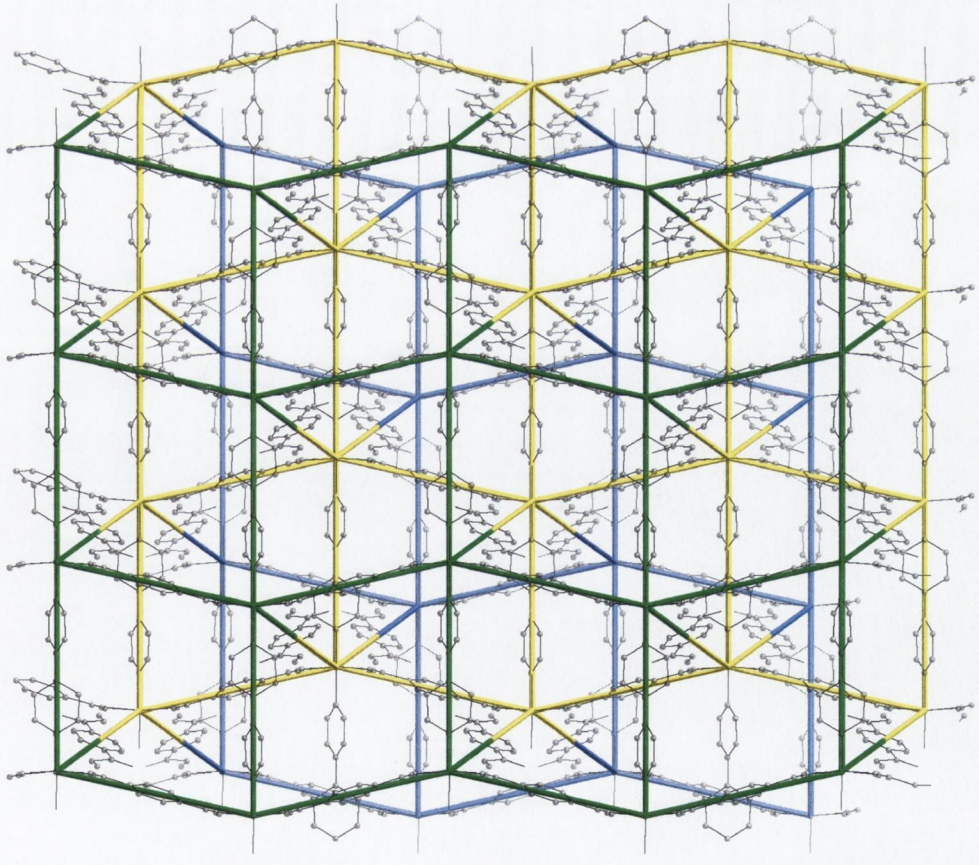

Figure 4.5 – Schematic representation of network superimposed on the actual structure. Note the (4,4) 2D sheets are connected together. Adjacent inter-sheet connections alternate between pointing up- and downwards. (This view is the same as that shown in Figure 4.4(b), but rotated 90° about the vertical axis)

Figure 4.5 shows that the 2D sheets do not pack (along the (101) direction) with the Cu(II) centres on adjacent sheets horizontally aligned. The hydrogen-bonded connectors (H_2bdc), alternate between pointing upwards and downwards along the (101) direction. The metal-to-metal distance along the H_2bdc connector is 15.6780(4) Å. The coordinating ligands can be represented as simple lines between nodes, which in the present case are the Cu(II) centres. Figure 4.4(b) shows a schematic representation of the network that is formed between metal centres, which is superimposed onto the actual network. Figure 4.5 is the structure shown in Figure 4.4(b) rotated through 90° about the vertical axis. The three (4,4) sheets are clearly visible (green (front), yellow (middle) and purple (back) – a single sheet is shown in Figure 4.3). If one follows a sheet in the horizontal direction the connections between sheets alternate between pointing upwards and downwards. Whilst all the nodes within the network are six-connected the overall type of network formed by this compound is different to the commonly reported α-Po type net, and has the Schläfli notation $[4^8.5^4.6^3]$. As far as can be ascertained, there are no other networks with this topology reported, however a private communication from Dr. Stuart Batten (Monash University) indicated that a different compound displaying the same topology has been synthesised but has not yet been published.[222]

A further feature of **9** is that three networks are interpenetrated within themselves. Figure 4.6 shows a section of the three interpenetrated networks. Structure **9** is unique in this feature, since the compound mentioned in the communication from Dr. Batten does not interpenetrate.

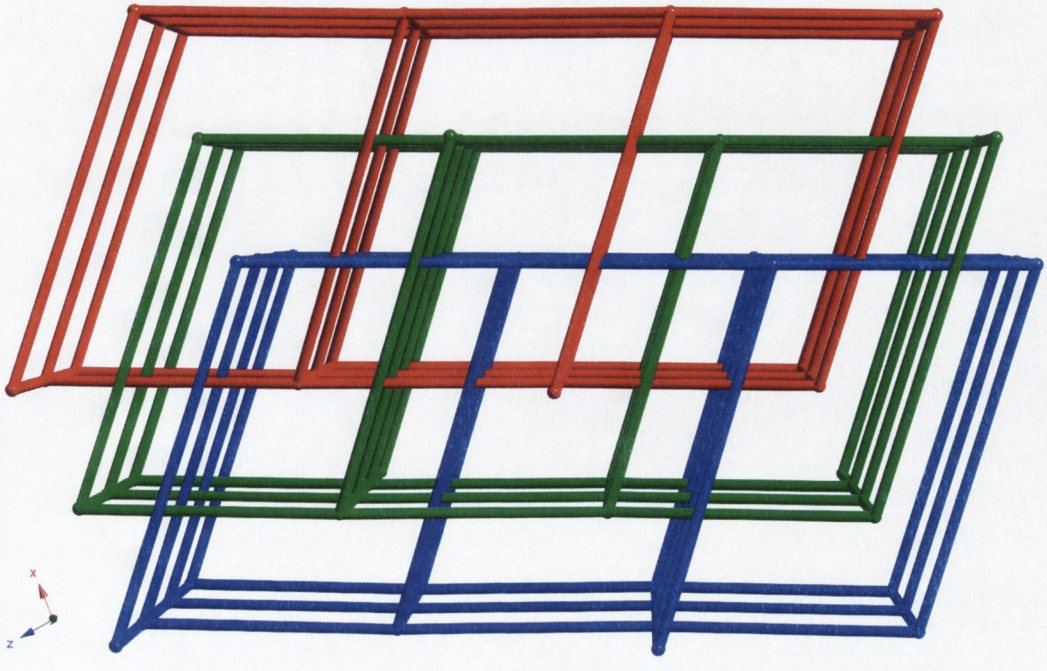

Figure 4.6 – Triply interpenetrated networks of **9** (view along *b* axis).

*4.1.3 Crystal structure of $[Cu_4(4,4'\text{-bipy})_4(bdc)_3(NO_3)_2(H_2O)_2]$ (**10**)*

Data for this structure were collected at Trinity College. Automatic cell indexing failed and inspection of the raw frames indicated that non-merohedral twinning might be present. This was confirmed by the GEMINI program[184] which was able to index two twin domains to the data. The structure solution was obtained using the data from only one component of the twin. Crystallographic details for this structure are given in Table 4.1. The structure was refined in the *P*-1 space group. The asymmetric unit of the structure contains four dimeric pairs of Cu(II) atoms linked together. This mode of coordination leads to an extremely high number of atoms within the asymmetric unit, which is shown in Figure 4.7. It should be noted that (in this figure) the full coordination spheres of each Cu(II) atom are not shown. Due to the complexity of the structure, descriptions of Cu(II) dimeric pairs (Cu1/Cu2, Cu3/Cu4, Cu5/Cu6 and Cu7/Cu8) will be separated and discussed on an individual basis.

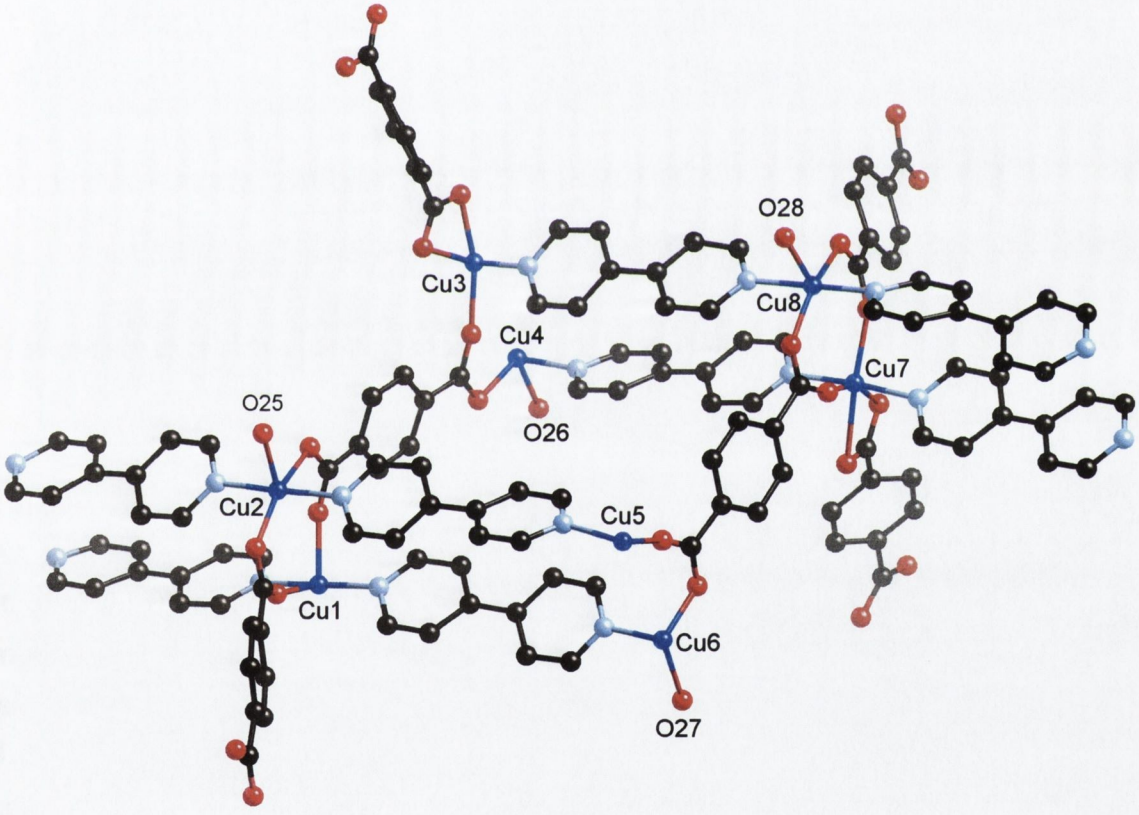

Figure 4.7 – Molecular structure and partial atomic labelling diagram for asymmetric unit of **10**. (Nitrate anions and hydrogen atoms omitted for clarity)

4.1.3.1 Cu1 and Cu2 containing dimeric unit.

Figure 4.8 shows the full coordination sphere of each of the metal centres in the Cu1/Cu2 dimeric unit.

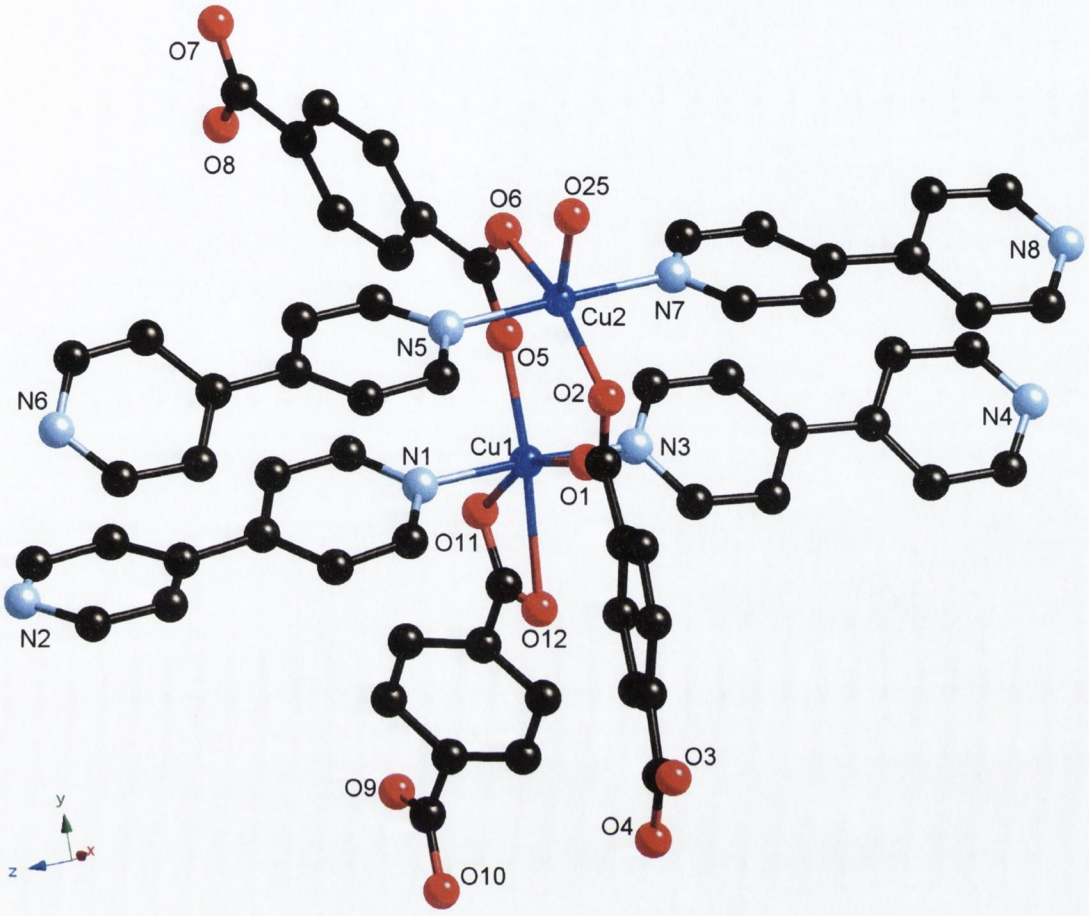

Figure 4.8 – Coordination sphere of the Cu1 and Cu2 containing dimeric unit of **10**. (Nitrate anions and hydrogen atoms omitted for clarity)

As with each of the dimers, one metal centre adopts a distorted octahedral geometry (Cu1), whilst the other adopts a square based pyramidal geometry (Cu2). The metal-to-metal distance of the dimeric unit is 3.820(2) Å. A listing of selected bond lengths and angles for this dimer can be found in Table 4.3. Each Cu(II) centre has two 4,4'-bipy molecules coordinated to it in a *trans* arrangement. This is a feature that is common to all of the dimers and allows for the formation of 1D chains, which extend along the *c* axis. The Cu1 centre has (apart from the 4,4'-bipy molecules) three bdc moieties coordinating to it. Two of the bdc groups bridge between the two metal centres, whilst the other is chelating and coordinates in an axial and equatorial position around Cu1. The bite angle on the chelating bdc group is 57.6(3)°. As can be seen from the bond lengths, the Cu1 centre displays Jahn-Teller distortion, with one of the bonds being considerably longer than the others (Cu1–O12 2.468(9) Å). The Cu2 centre adopts a square-based pyramidal geometry, with the four basal positions occupied by two 4,4'-bipy molecules and two bridging bdc groups, both of which are *trans* to one

another. A coordinated water molecule (O25) occupies the apical position of this metal centre.

Table 4.3 – Selected bond lengths (Å) and angles (°) for **10**.

Cu1 – N1	1.99(1)	N1 – Cu1 – N3	175.8(4)
Cu1 – N3	2.011(9)	N1 – Cu1 – O1	92.5(4)
Cu1 – O1	2.009(8)	N1 – Cu1 – O5	93.7(4)
Cu1 – O5	2.096(8)	N1 – Cu1 – $O11^{i}$	88.2(4)
Cu1 – $O11^{i}$	2.026(8)	N1 – Cu1 – $O12^{i}$	88.7(4)
Cu1 – $O12^{i}$	2.468(9)	$O11^{i}$ – Cu1 – $O12^{i}$	57.6(3)
Cu2 – N5	2.06(1)	O1 – Cu1 – $O11^{i}$	155.4(3)
Cu2 – N7	2.046(9)	O5 – Cu1 – $O11^{i}$	106.7(3)
Cu2 – O2	2.002(8)	O5 – Cu1 – $O12^{i}$	164.1(3)
Cu2 – O6	1.978(8)	N5 – Cu2 – N7	178.3(4)
Cu2 – O25	2.205(9)	O2 – Cu2 – O6	161.3(3)
		O25 – Cu2 – O2	94.8(3)
		O25 – Cu2 – O6	103.4(3)
		O25 – Cu2 – N5	84.9(4)
		O2 – Cu2 – N5	88.9(4)
		C2 – C3 – C4 – C5	14(2)
		C12 – C13 – C14 – C15	8(2)
		C22 – C23 – C24 – C25	27(2)
		C32 – C33 – C34 – C35	22(2)

Symmetry Code: i = -1+x, y, z.

4.1.3.2 Cu3 and Cu4 containing dimeric unit.

The second dimeric unit contains Cu3 and Cu4. As was mentioned earlier, an octahedral (Cu3) and square based pyramidal (Cu4) metal centres are present. Figure 4.9 shows the full coordination sphere of each metal centre within the dimer. It should be noted that not all the atoms in the diagram are part of the asymmetric unit, this is shown in the figure where those atoms outside the asymmetric unit are rendered translucently. Table 4.4 contains selected bond lengths and angles for this dimer, as well as the symmetry operators for those atoms outside the asymmetric unit. The metal-to-metal distance for this dimeric unit is 3.849(2) Å.

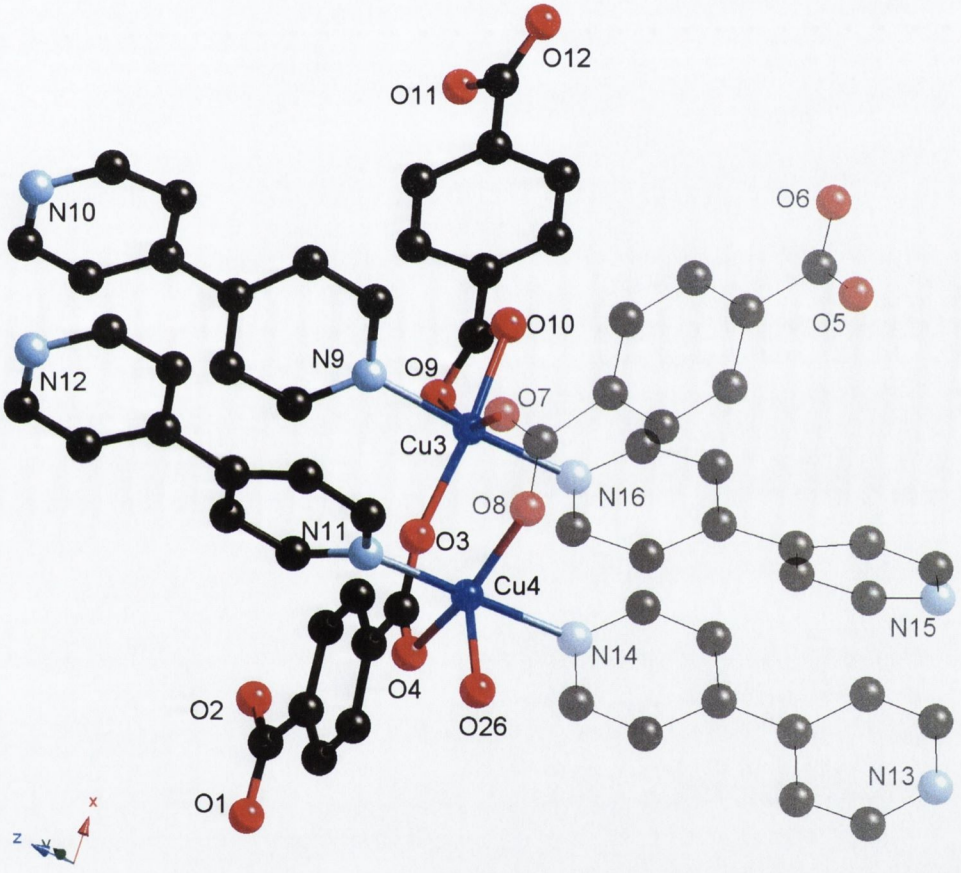

Figure 4.9 –Coordination sphere of the Cu3 and Cu4 containing dimeric unit of **10**. (Those atoms outside the bounds of the asymmetric unit are rendered as translucent. Nitrate anions and hydrogen atoms omitted for clarity)

The Cu3 centre has two 4,4'-bipy molecules coordinated to it in a *trans* orientation, however only one of these is within the asymmetric unit (N(9) to N(10)), the other is symmetry generated (Table 4.4). Four coordinating oxygen atoms occupy the remaining coordination sites, two belonging to a chelating bdc group (O(9) and O(10)), the other two are bridging bdc groups (O(3)/O(4) and O(7)/O(8)). The bridging bdc groups also join dimeric units, for example the bdc molecule containing the oxygen atoms O(1), O(2), O(3) and O(4) connects the four Cu(II) centres Cu1, Cu2, Cu3 and

Cu4. The connectivity of these atoms allows for the formation of dinuclear chains extending in the (-110) direction. Each chain consists of two metal centres bridged by a carboxylate moiety of a bdc molecule. The other carboxylate group (of the bdc molecule) coordinates to another metal-containing dimeric unit. This mode of coordination extends the network formed into a second dimension and thereby allows the formation of a 2D sheet, which extends in the (-110) direction and along the *c* axis (the plane of the sheet has the Miller indices (110)). The metal-to-metal distances across the dimeric connections are 10.073(2) Å (Cu1–Cu4) and 10.048(2) Å (Cu2–Cu3).

Table 4.4 – Selected bond lengths (Å) and angles (°) for **10**.

Cu3 – N9	1.991(9)	N9 – Cu3 – N16^{i}	175.7(4)
Cu3 – N16^{i}	2.020(9)	N9 – Cu3 – O3	91.2(4)
Cu3 – O3	2.001(8)	N9 – Cu3 – O9	87.5(3)
Cu3 – O7^{ii}	2.139(8)	N9 – Cu3 – O10	89.1(3)
Cu3 – O9	2.395(9)	N9 – Cu3 – O7^{ii}	85.1(3)
Cu3 – O10	2.059(8)	O9 – Cu3 – O7^{ii}	85.1(3)
Cu4 – N11	2.017(9)	O3 – Cu3 – O10	160.2(3)
Cu4 – N14^{i}	2.078(9)	O9 – Cu3 – O10	89.1(3)
Cu4 – O4	2.006(7)	N11 – Cu4 – N14^{i}	178.2(4)
Cu4 – O8^{ii}	1.993(7)	O4 – Cu4 – O8^{ii}	159.2(3)
Cu4 – O26	2.192(8)	O26 – Cu4 – N11	93.2(3)
		O26 – Cu4 – O4	100.5(3)
		O26 – Cu4 – O8^{ii}	100.0(3)
		O26 – Cu4 – N14^{i}	85.9(3)
		N11 – Cu4 – O4	92.7(3)
		C42 – C43 – C44 – C45	17(2)
		C52 – C53 – C54 – C55	21(2)

Symmetry Codes: *i* = x, y, -1+z; *ii* = 1+x, -1+y, z; *iii* = x, -1+y, z.

4.1.3.3 Cu5 and Cu6 containing dimeric unit.

The third dimeric unit contains the metal centres Cu5 and Cu6. Figure 4.10 shows the atomic structure and connectivity of the coordination spheres of both metal atoms.

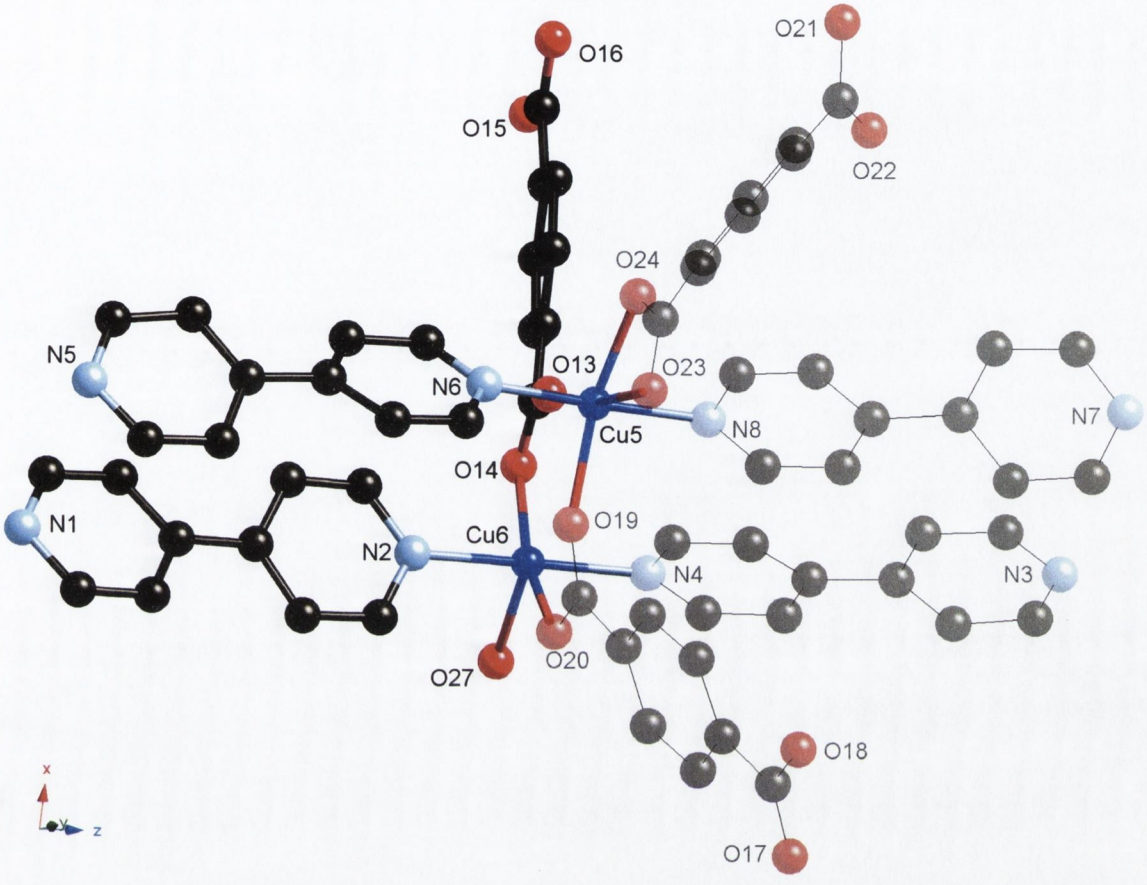

Figure 4.10 – Coordination sphere of the Cu5 and Cu6 containing dimeric unit of **10**. (Those atoms outside the bounds of the asymmetric unit are rendered as translucent. Nitrate anions and hydrogen atoms omitted for clarity)

The mode of bridging between the Cu5 and Cu6 is similar to that seen in the other dimeric units. Two bdc molecules (one in and one outside the asymmetric unit) span between the Cu(II) centres. The metal-to-metal distance within the dimer is 3.909(2) Å. Selected bond lengths and angles for both metal centres are listed in Table 4.5. The Cu5 centre is six-coordinate and has a similar arrangement of ligands as the Cu1, and Cu4 atoms. The Cu6 atom is five coordinate, square-based pyramidal with a water molecule (O27) coordinated in the apical position. The bdc molecule that is chelating to Cu5 also chelates to an adjacent copper centre (Cu7). This linkage connects dimers together, and extends in the (110) direction.

Table 4.5 – Selected bond lengths (Å) and angles (°) for **10**.

Cu5 – N6	1.996(9)	N6 – Cu5 – N8^{i}	177.1(4)
Cu5 – N8^{i}	2.008(9)	N6 – Cu5 – O13	90.9(3)
Cu5 – O13	2.135(8)	N6 – Cu5 – O23^{iii}	88.2(3)
Cu5 – O19^{ii}	2.035(8)	N6 – Cu5 – O24^{iii}	92.5(3)
Cu5 – O23^{iii}	2.519(8)	N6 – Cu5 – O19^{ii}	86.8(3)
Cu5 – O24^{iii}	2.042(8)	O13 – Cu5 – O23^{iii}	171.3(3)
Cu6 – N2	2.011(9)	O19^{ii} – Cu5 – O24^{iii}	151.2(3)
Cu6 – N4^{i}	2.058(9)	O23 – Cu5 – O24^{iii}	85.0(3)
Cu6 – O14	1.973(8)	O13 – Cu5 – O19^{ii}	95.3(3)
Cu6 – O27	2.190(8)	N2 – Cu6 – N4^{i}	179.4(4)
Cu6 – O20^{ii}	2.003(8)	O14 – Cu6 – O20^{ii}	159.5(3)
		O27 – Cu6 – N2	90.5(3)
		O27 – Cu6 – O14	104.0(3)
		O27 – Cu6 – O20^{ii}	96.2(3)
		O27 – Cu6 – N4^{i}	89.3(3)

Symmetry Codes: *i* = x, y, 1+z; *ii* = -1+x, 1+y, z; *iii* = x, 1+y, z.

4.1.3.4 Cu7 and Cu8 containing dimeric unit.

The fourth dimeric unit contains the metal centres Cu7 and Cu8. Figure 4.11 shows the atomic structure and connectivity of the coordination spheres of both metal atoms. Selected bond lengths and angles for this dimeric unit are listed in Table 4.6.

As is the case in the other dimers, one metal centre adopts a distorted octahedral geometry (Cu7) and the other is square-based pyramidal (Cu8) with a metal-to-metal distance of 3.878(2) Å. The metal centre, Cu7, has the same ligand connectivity as Cu1, Cu3 and Cu5, two bridging bdc molecules and one chelating. Two bridging bdc molecules and one water molecule (in the apical position) are coordinated to Cu8. Both metal centres have two 4,4'-bipy molecules coordinated in a *trans* orientation, which forms a chain extending along the *c* axis. All the 4,4'-bipy molecules in the structure are twisted along the central carbon-carbon bond. Torsion angles vary from 3° to 27° and are listed in Tables 4.3 and 4.4. There are also weak π-interactions between adjacent 4,4'-bipy molecules within the chain.

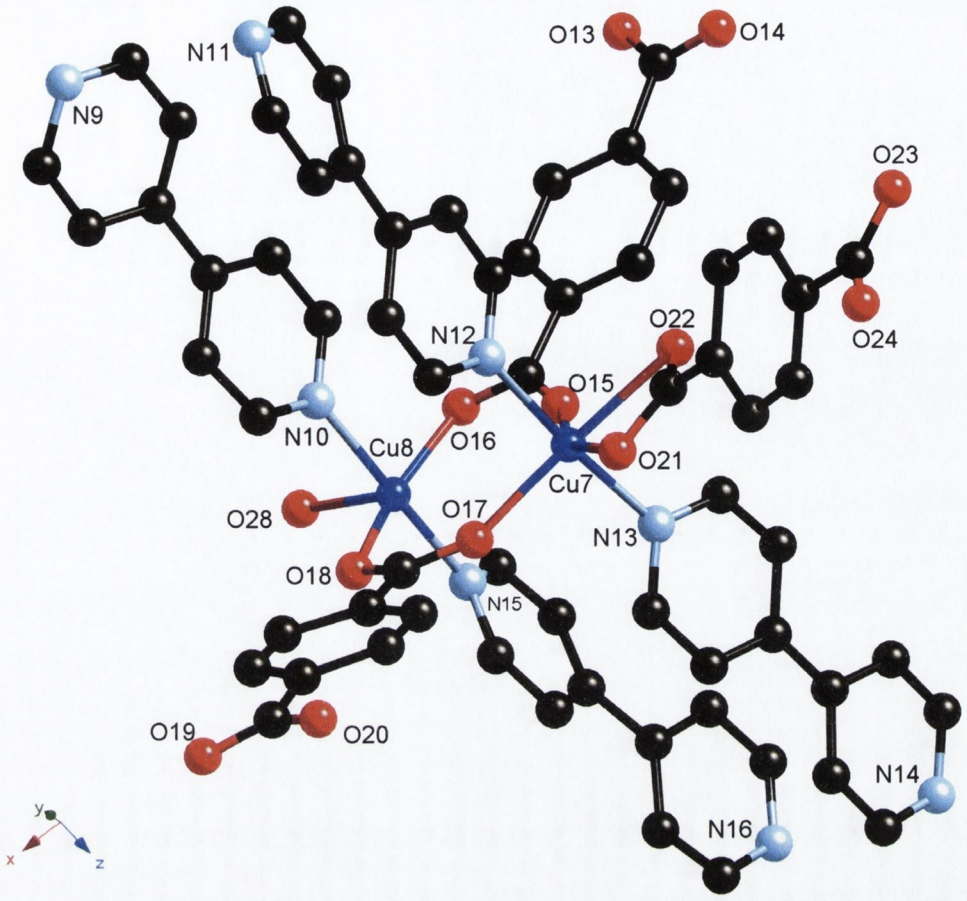

Figure 4.11 – Coordination sphere of the Cu7 and Cu8 containing dimeric unit of **10**. (Nitrate anions and hydrogen atoms omitted for clarity)

The metal centres are bridged *via* carboxylate groups from bdc molecules, which link the double-metal-containing chains together into a 2D sheet, which extends in the (110) plane. The mode of bridging between metals in a dimer is the same as the previous dimeric pairs. The 2D sheets are joined together through the chelating bdc molecules.

Table 4.6 – Selected bond lengths (Å) and angles (°) for **10**.

Cu7 – N12	2.018(9)	N12 – Cu7 – N13	174.8(4)
Cu7 – N13	1.986(9)	N12 – Cu7 – O15	93.3(3)
Cu7 – O15	2.016(8)	N12 – Cu7 – O17	93.0(3)
Cu7 – O17	2.110(7)	N12 – Cu7 – O21	87.4(3)
Cu7 – O21	2.086(8)	N12 – Cu7 – O22	84.4(3)
Cu7 – O22	2.407(8)	O17 – Cu7 – O22	164.9(3)
Cu8 – N10	2.059(9)	O21 – Cu7 – O22	58.9(3)
Cu8 – N15	2.023(9)	O15 – Cu7 – O22	97.6(3)
Cu8 – O16	1.965(8)	O15 – Cu7 – O17	97.4(3)
Cu8 – O18	1.981(7)	N10 – Cu8 – N15	175.6(4)
Cu8 – O28	2.168(8)	O16 – Cu8 – O18	158.8(3)
		O28 – Cu8 – N10	86.2(3)
		O28 – Cu8 – O18	103.9(3)
		O28 – Cu8 – O16	97.1(3)
		O28 – Cu8 – N15	90.7(3)
		N10 – Cu8 – O16	89.0(3)

4.1.3.5 Hydrogen-bonding.

There are four water molecules coordinated directly to metal centres (Cu2, Cu4, Cu6, Cu8). Each water molecule is hydrogen-bonded to two nitrate anions. Figure 4.12 shows the hydrogen-bonding between water molecules and nitrate anions. A coordinated water molecule (O25) occupies the apical position of Cu2. This water molecule hydrogen-bonds to two nitrate anions (N17 and N18), which are represented by the blue and white dashed bonds. The oxygen-to-oxygen distances are listed in Table 4.6. One of the oxygen atoms of the nitrate anions (O34) is hydrogen-bonded to an adjacent water molecule (O26) which is, in turn, coordinated to Cu4 on an adjacent dimeric unit. Those atoms outside the asymmetric unit are rendered translucently, and the symmetry operators are given in Table 4.7. The lower part of Figure 4.12 shows the hydrogen-bonding *via* water molecules and nitrate anions between Cu6 and Cu8. Exactly the same mode of hydrogen-bonding is present, and those atoms outside the asymmetric unit are rendered translucently.

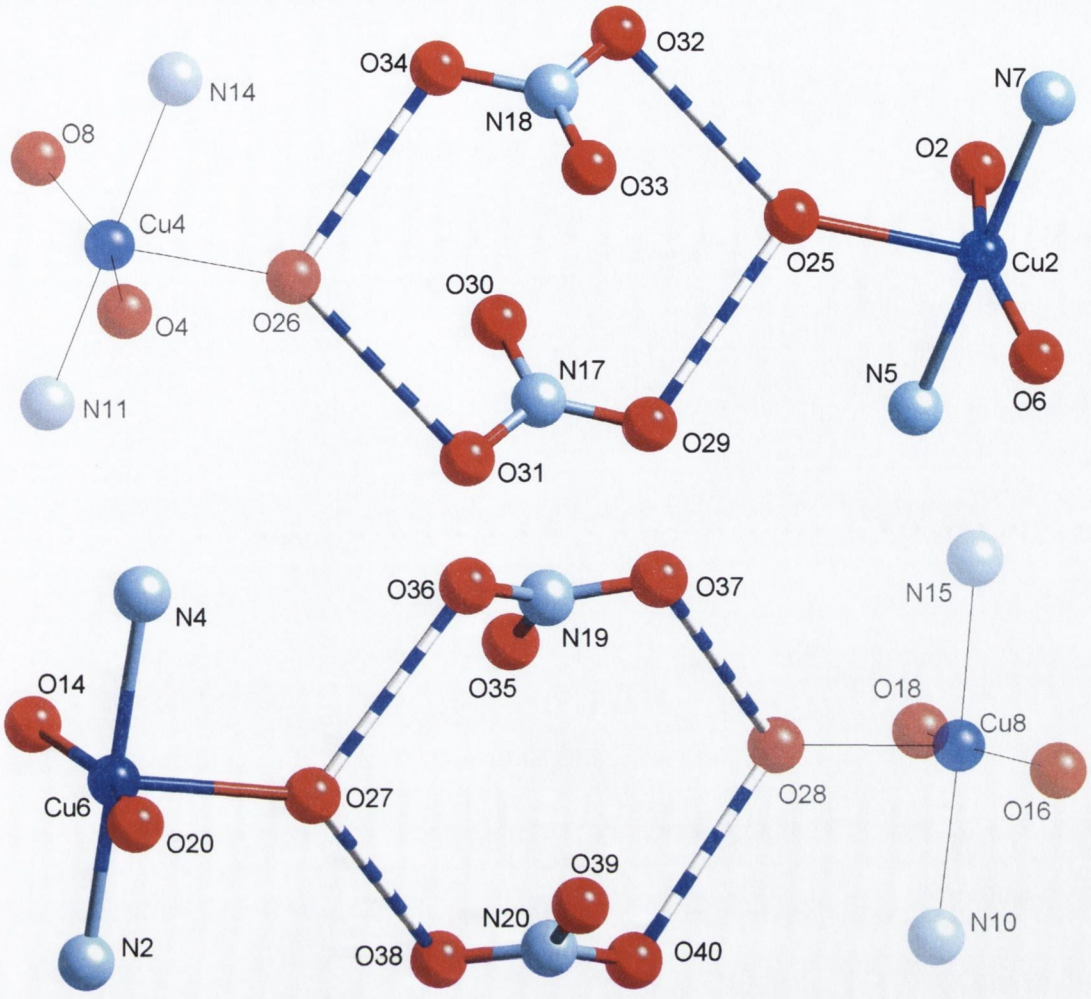

Figure 4.12 – Hydrogen-bonding between coordinated water molecules and nitrate anions. Hydrogen-bonds are represented as blue and white dashed bonds. Translucent atoms are outside the bounds of the asymmetric unit (symmetry operators are listed in Table 4.6)

Table 4.7 – Selected hydrogen-bond distances (Å) for **10**.

O25 ··· O29	2.77(2)	O27 ··· O36	2.773(15)
O25 ··· O32	2.85(2)	O27 ··· O38	2.773(14)
O31 ··· O26^{i}	2.83(2)	O37 ··· O28^{ii}	2.738(15)
O34 ··· O26^{i}	2.79(2)	O40 ··· O28^{ii}	2.743(14)

Symmetry Codes: *i* = x, 1+y, z ; *ii* = -1+x, y, z.

This hydrogen-bonding provides an extra mode of connectivity between metal dimeric pairs. In each of the dimers, one bdc molecule chelates to an octahedral metal centre. As mentioned in Section 4.1.3.3 (page 130) the chelating bdc links 2D sheets together, which creates a 3D coordination polymer. The hydrogen-bonding described above provides an additional connection in the third dimension. Figure 4.13 is a schematic representation of the 3D network formed by these connections. The blue blocks represent the Cu(II) containing dimeric units. The purple blocks represent

4,4'-bipy molecules which form a chain which extends along the *c* axis. The red blocks represent the bridging bdc molecules. Together the purple and red blocks create a 2D sheet in the (110) plane. The green blocks represent the chelating bdc molecules, which link the 2D sheets together. The yellow blocks represent the nitrate containing hydrogen-bonding connection between metal centres. These linkages essentially 'reinforce' the connections between sheets

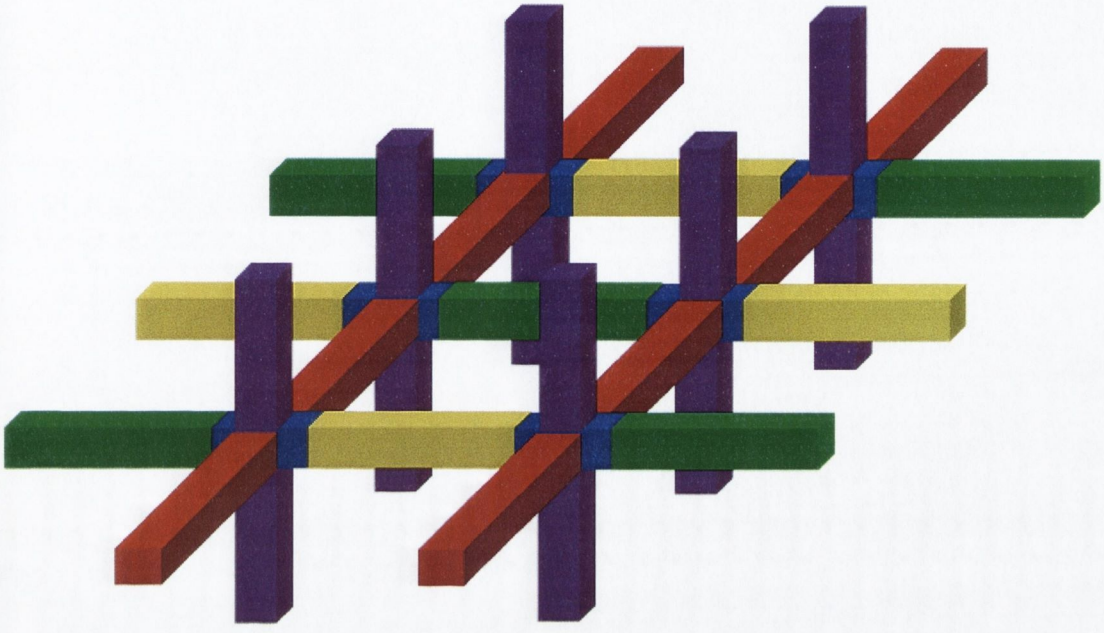

Figure 4.13 – Schematic representation of the linkages between dimeric units. Blue blocks represent metal containing dimers, purple blocks represent the linkage through 4,4'-bipy molecules, red blocks represent the bridging bdc molecules, which form a 2D sheet. The green blocks represent chelating bdc molecules and the yellow blocks represent the nitrate-containing hydrogen-bonding linkage between metal centres.

This mode of connectivity affords the formation of a 3D coordination polymer. Figure 4.14 shows a packing diagram of a single 3D network formed by **10**. The view in the diagram is along the crystallographic *c* axis, with the 4,4'-bipy chains extending out of the projection plane. Metal-to-metal distances along the bridging ligands within the network vary from 9.7 to 11.1 Å. A full listing of internuclear distances can be found in Table 4.8.

If a node is positioned at the mid-point between the copper atoms within each dimeric unit and the connections represented by simple lines or blocks (as in Figure 4.13) it can easily be seen that the network has an α-Po topology. The voids present in the network shown in Figure 4.14 are occupied by a second network, which is interpenetrating the first. Figure 4.15 shows the topology of this net as well as the twofold interpenetration that is present.

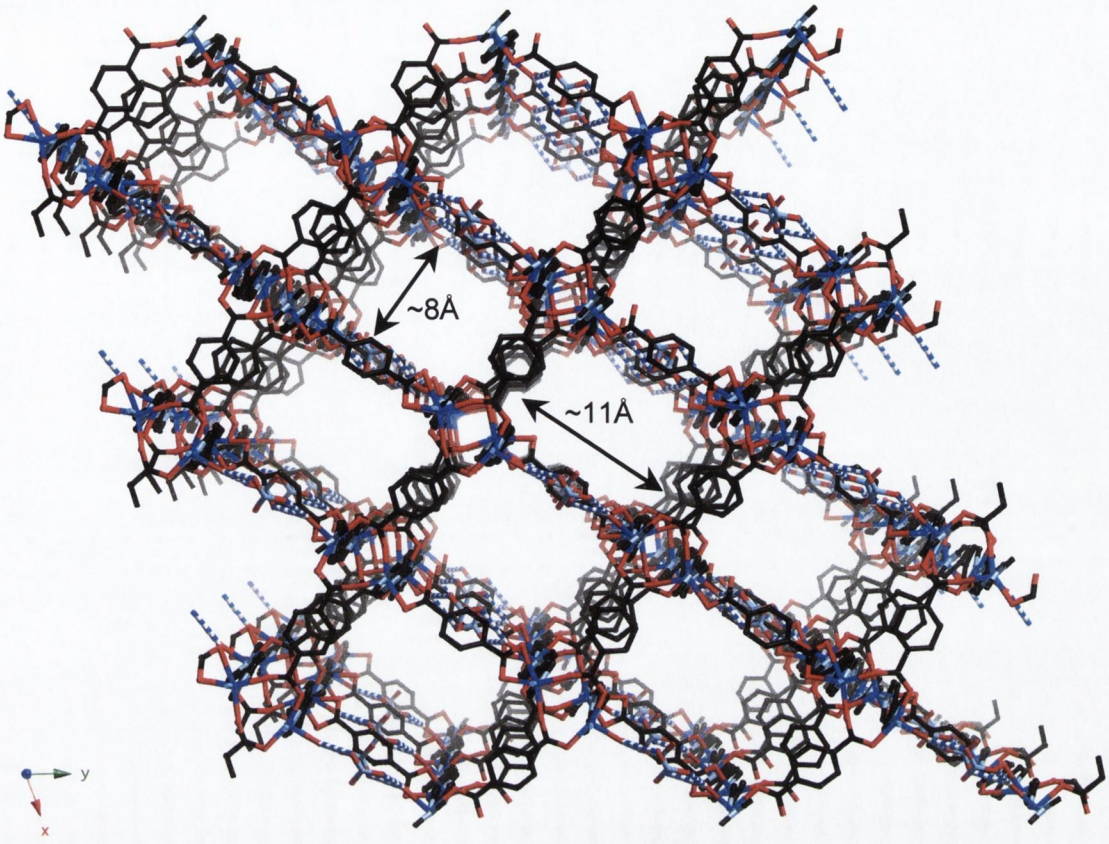

Figure 4.14 – Packing diagram of a single network of **10**. (Approximate dimensions of channels shown, view along *c* axis, hydrogen atoms omitted for clarity)

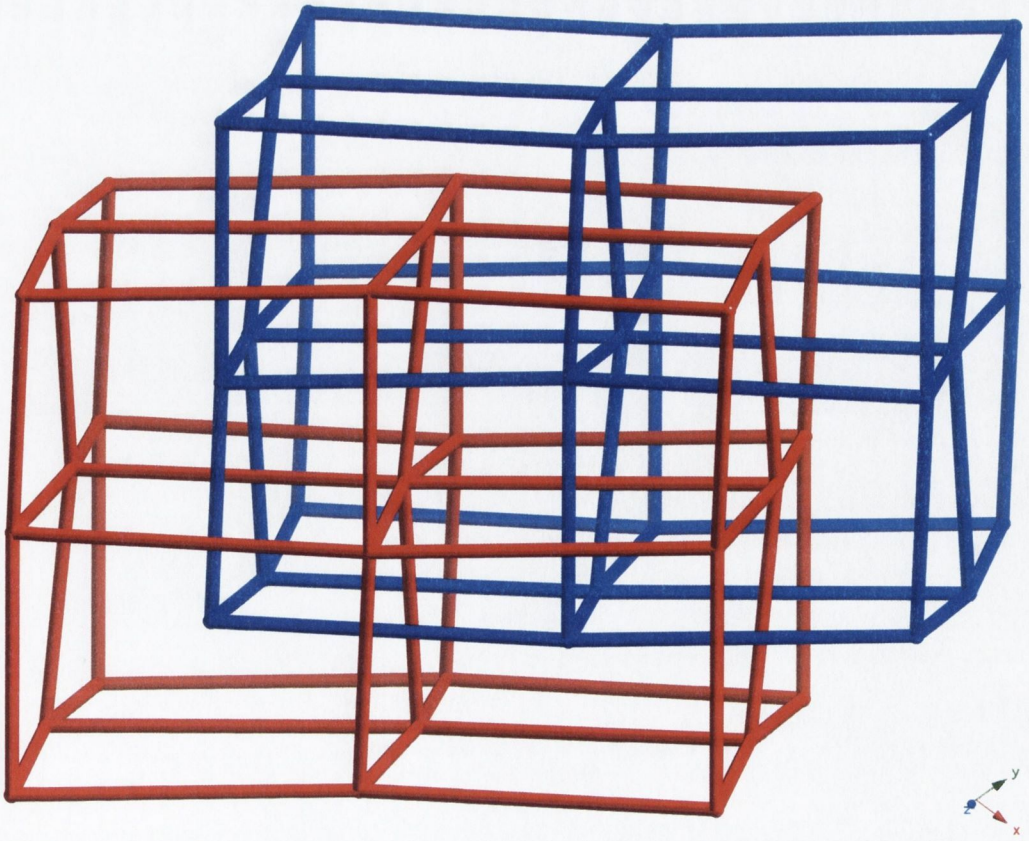

Figure 4.15 – Twofold interpenetration of α-Po-type networks of **10**. (Nodes are located at the mid-point between two Cu(II) centres within each dimeric unit)

Table 4.8 – Selected metal-to-metal distances (Å) for **10**.

Cu1 – Cu2	3.820(2)	Cu3 – Cu4	3.850(2)
Cu5 – Cu6	3.909(2)	Cu7 – Cu8	3.878(2)
Cu1 – Cu6	11.098(2)	Cu2 – Cu5	11.123(2)
Cu1 – Cu6^{iv}	11.127(2)	Cu2 - Cu5^{iv}	11.096(2)
Cu1 – Cu4	10.073(2)	Cu2 - Cu3	10.047(2)
Cu1 – Cu4^{ii}	10.281(2)	Cu2 - Cu3^{ii}	10.281(2)
Cu1 – Cu3^{i}	10.822(2)	Cu2 - Cu4^{viii}	9.980(2)
Cu3 – Cu2^{v}	10.281(2)	Cu4 - Cu7	11.103(2)
Cu3 – Cu8	11.127(2)	Cu4 - Cu7^{iv}	11.109(2)
Cu3 – Cu8^{iv}	11.094(2)	Cu4 - Cu1^{v}	10.281(2)
Cu3 - Cu1^{iii}	10.822(2)	Cu4 - Cu2^{vi}	9.980(2)
Cu5 - Cu2^{vii}	11.096(2)	Cu6 - Cu1^{vii}	11.127(2)
Cu5 - Cu8	10.220(2)	Cu6 - Cu7	10.229(2)
Cu5 - Cu8^{ii}	10.099(2)	Cu6 - Cu7^{ii}	10.118(2)
Cu5 - Cu7^{viii}	10.874(2)	Cu6 - Cu8^{i}	9.796(2)
Cu7 - Cu4^{vii}	11.109(2)	Cu8 - Cu3^{vii}	11.094(2)
Cu7 - Cu6^{v}	10.118(2)	Cu8 - Cu5^{v}	10.099(2)
Cu7 - Cu5^{vi}	10.874(2)	Cu8 - Cu6^{iii}	9.796(2)

Symmetry Codes: *i* = -1+x, y, z; *ii* = -1+x, 1+y, z; *iii* = 1+x, y, z; *iv* = x, y, -1+z; *v* = 1+x, -1+y, z; *vi* = x, -1+y, z; *vii* = x, y, 1+z; *viii* = x, 1+y, z.

*4.1.4 Crystal structure of [Cu(4,4'-bipy)(bdc)(NO_3)] (**11**)*

Data for this structure was collected at Trinity College. Automatic cell indexing failed and inspection of the raw frames indicated that non-merohedral twinning might be present. This was confirmed by the GEMINI program[184] which was able to index two twin domains to the data. The structure solution was obtained using the data from only one component of the twin. As expected the refinement was poor since it did not take into account the overlapping peaks from the other domain. The raw data was then re-integrated, with the latest Bruker SAINT integrating program,[223] and an absorption correction performed using the TWINABS program.[185] The initial solution was then refined against the re-integrated data in HKLF5 format, which gave an good refinement (R_1 = 0.055). The structure was refined in the *C2/m* space group, crystallographic details are listed in Table 4.1.

The structure of **11** contains a dimeric repeating unit. Figure 4.16 shows the atomic labelling and coordination sphere of the dimeric subunit of **11**. The Cu(II) centre adopts a highly distorted geometry, which can be described as approximately mid-way between square-pyramidal and trigonal-bipyrimidal. Analysis of the shape determining angles using the approach of Addison and co-workers[224] yields a τ value of 0.48 for Cu1 (τ = 0 and 1 for perfect square-pyramidal and trigonal-bipyramidal geometries, respectively). There are two 4,4'-bipy molecules coordinated in the axial positions. The three equatorial positions are occupied by two bdc moieties and a coordinated nitrate anion. The carboxylate group of the bdc molecules form a bridge between metal centres allowing for a 3.858(1) Å metal-to-metal distance, this is similar to the dimeric unit seen in the zinc containing compound **6**. Selected bond lengths and angles for **11** are listed in Table 4.9.

The axially coordinated 4,4'-bipy molecules link dimeric units into a polymeric chain, that extends along the crystallographic *c* axis. The 4,4'-bipy molecule shows no twist between pyridyl rings. The offset arrangement of the metal dimer means that the face-to-face π-interactions which exist between bipy molecules are slightly shorter than the metal-to-metal distance (Cu1···Cu1 3.858(1) Å, N3···N3 3.35(1) Å). Polymeric chains are further linked into a second dimension through the connectivity of the bdc molecule. The carboxylate group bridges between the two Cu(II) centres that make up the dimer. There is a two-fold rotation axis that lies midway between the metal centres and extends along the C7–C8 bond. Furthermore the aromatic ring is twisted with respect to each of the carboxylate groups (torsion angles are listed in Table 4.9). This connection links 1D polymeric chains together to form a 2D sheet. Figure 4.17 shows a single sheet, from two perpendicular directions.

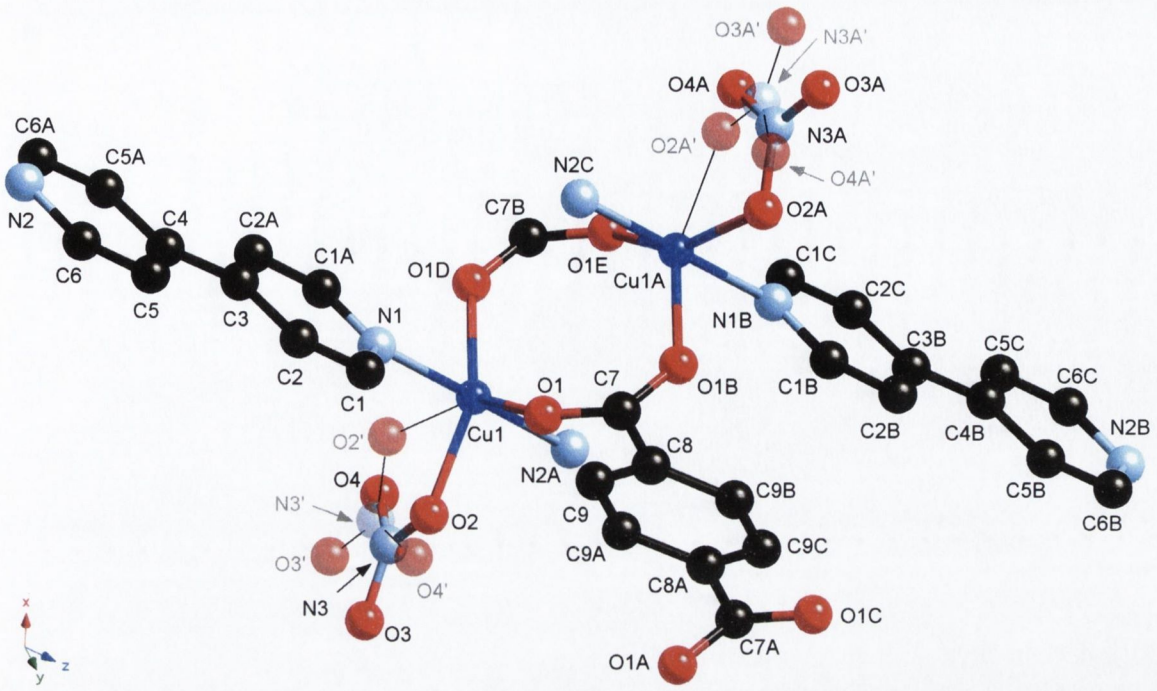

Figure 4.16 – Molecular structure and atomic labelling diagram for **11**. Coordination sphere of a single dimeric unit shown. (Disordered nitrate positions (N3', O2' etc.) shown as translucent atoms, hydrogen atoms omitted for clarity)

Table 4.9 – Selected bond lengths (Å), distances (Å) and angles (°) for **11**.

Cu1 – N1	2.033(4)	N1 – Cu1 – N2A^{ii}	179.7(1)
Cu1 – N2A^{ii}	2.028(4)	N1 – Cu1 – O1	87.7(1)
Cu1 – O1	2.066(3)	N1 – Cu1 – O2	89.5(2)
Cu1 – O1D^{i}	2.066(3)	N1 – Cu1 – O1D^{i}	87.7(1)
Cu1 – O2	1.964(5)	O1 – Cu1 – N2A^{ii}	92.5(1)
C3 ··· C3^{iv}	3.58(1)	O1 – Cu1 – O2	84.0(2)
O3 ··· O4^{v}	2.983(9)	O1 – Cu1 – O1D^{i}	125.0(1)
N3 ··· N3^{v}	3.35(1)	O2 – Cu1 – O1D^{i}	150.7(2)
N3 ··· O3^{v}	3.03(1)	O2 – Cu1 – N2A^{ii}	90.2(2)
N3 ··· O4^{v}	3.560(9)	O1 – C7 – C8 – C9	32.8(2)
Cu1 ··· Cu1A^{iii}	3.858(1)		

Symmetry Codes: *i* = x, 1-y, z; *ii* = x, y, z-1; *iii* = 1-x, 1-y, 1-z; *iv* = 1-x, 1-y, 2-z; *v* = 2-x, 1-y, 2-z.

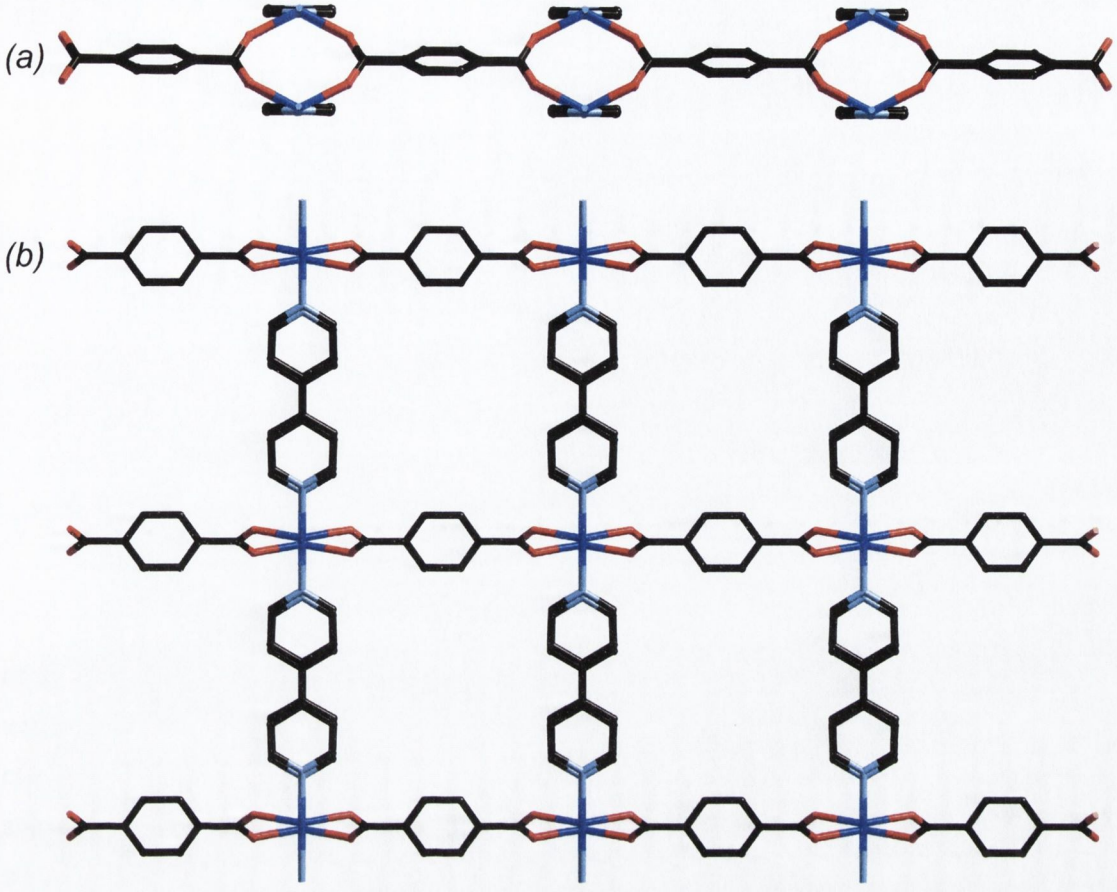

Figure 4.17 – Packing diagram for **11**, showing a (4,4) 2D sheet formed by 4,4'-bipy chains linked with bdc molecules. *(a)* View along *c* axis (4,4'-bipy chains perpendicular to projection plane). *(b)* View along (101) direction (4,4) topology is clearly shown. (Nitrate anions and hydrogen atoms omitted for clarity)

As can be seen in Figure 4.16, there is a nitrate anion coordinated to the Cu(II) centre. This molecule is disordered over two positions, which are depicted by the translucent atoms. Each atom is refined at half occupancy, and a mirror plane relates the two positions. There is a definite contact between the nitrate anions on adjacent 2D sheets, which amounts to an interaction between the delocalised electrons in the nitrate anions. Figure 4.18 shows the two positions (purple and green) of the disordered nitrate anions as well as the contact between them (dashed line, O3···O4 2.983(9) Å). Although this type of contact between anions is unusual, it is not unprecedented. There is a similar contact between adjacent nitrate anions in the crystal structure of $AgNO_3$. Further examples of this type of contact between nitrate anions are given in the Appendix.[225-229]

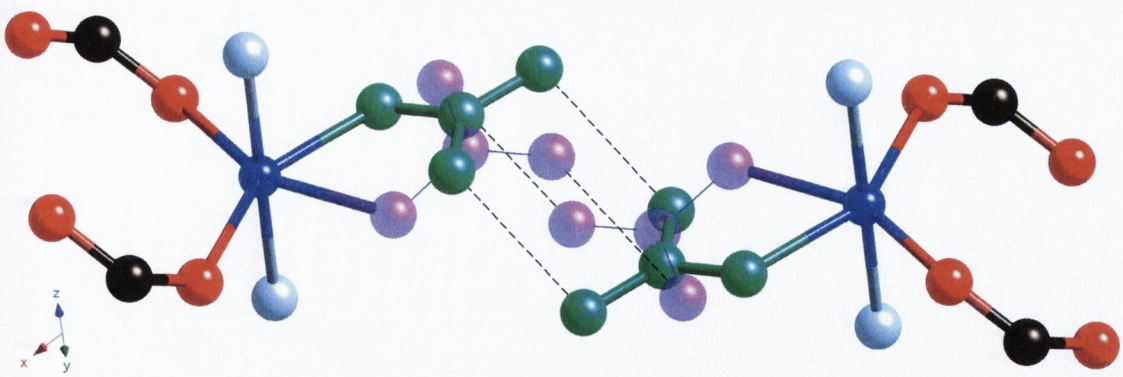

Figure 4.18 – Short contacts between nitrate anions on adjacent 2D sheets. Interactions are shown as dashed lines. Atom positions are refined at half occupancy and exist as shown i.e. when the green nitrate anion is present on the left-hand metal centre the nitrate anion on the right-hand metal centre is present on the opposite side of the mirror plane.

The reason this model was adopted was that when the structure was initially refined in the non-centrosymmetric space group *C*2 the disorder in the nitrate anions was not apparent. Only a single nitrate anion was present in the model, which had contacts to nitrate anions, on adjacent sheets, that were too close to make chemical sense. After the data was re-integrated to account for both twin components and the structure refined in the centrosymmetric space group *C*2/*m*, the disorder in the nitrate anions became apparent and was disordered as shown in Figure 4.16. This allowed the short-contacts between adjacent nitrate anions to make chemical sense (as a delocalised-electron interaction).

The contact between 2D sheets allows for the formation of an α-Po-type 3D network, which is doubly interpenetrated. Figure 4.19 shows the two interpenetrated networks. This mode of interpenetration is the same as was seen in **10**, a schematic of which is given in Figure 4.15. The bridging bdc molecule is twisted out of the plane of either carboxylate group coordinated to the metal centres. The interpenetration of the two networks is further stabilised by a hydrogen-bond which is present between the hydrogen atoms on the aromatic ring of the bdc molecule (H9) of one network, and an oxygen atom (O3) of a nitrate anion of the other network. Figure 4.20 shows the hydrogen-bonds (blue-and-white dashed bonds) between H9 of the bdc molecule and adjacent nitrate anions. The nitrate anions are rendered as translucent since they are part of the second network and are shown in only one of the disordered positions. The hydrogen-bond (O3···H9) length is 2.52(4) Å (O3···C9 3.156(7) Å).

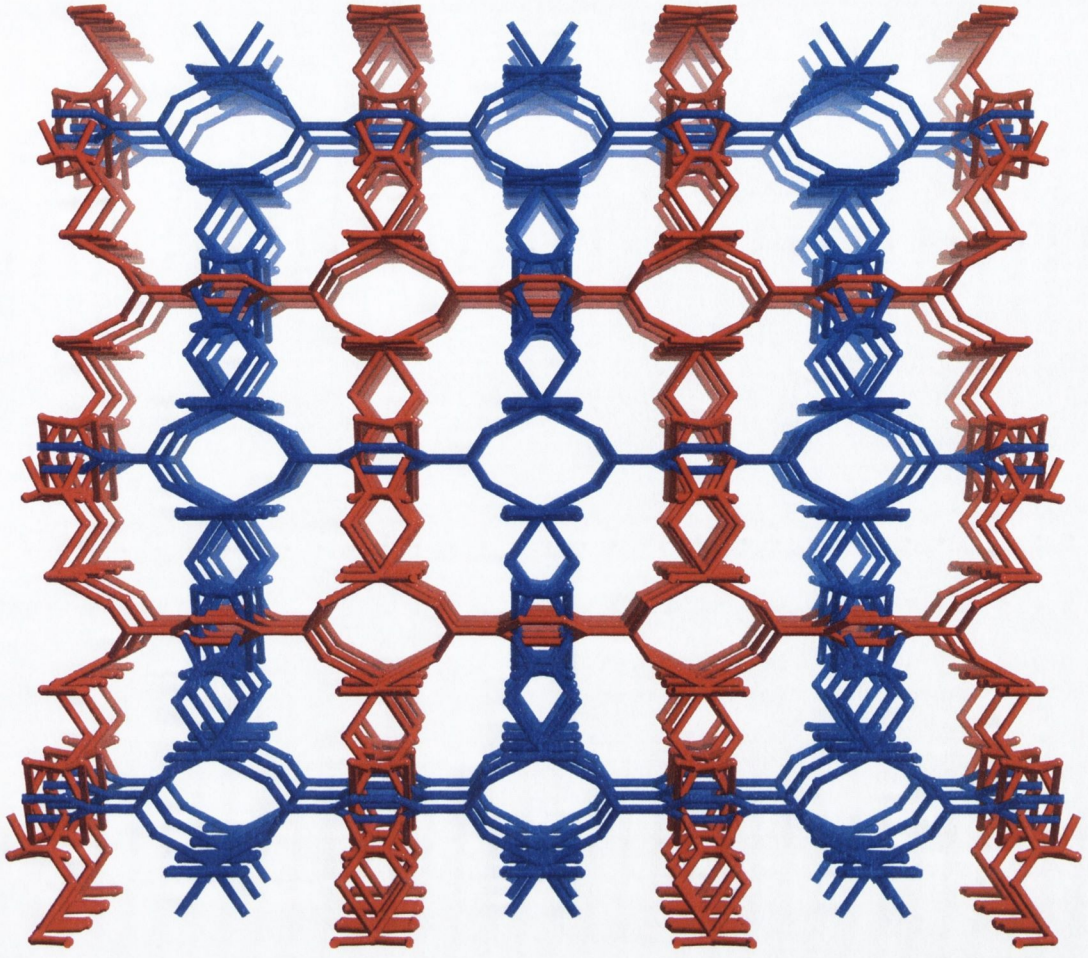

Figure 4.19 – Packing diagram, showing the interpenetration of two α-Po-type networks of **11**. (View along c axis, hydrogen atoms omitted for clarity)

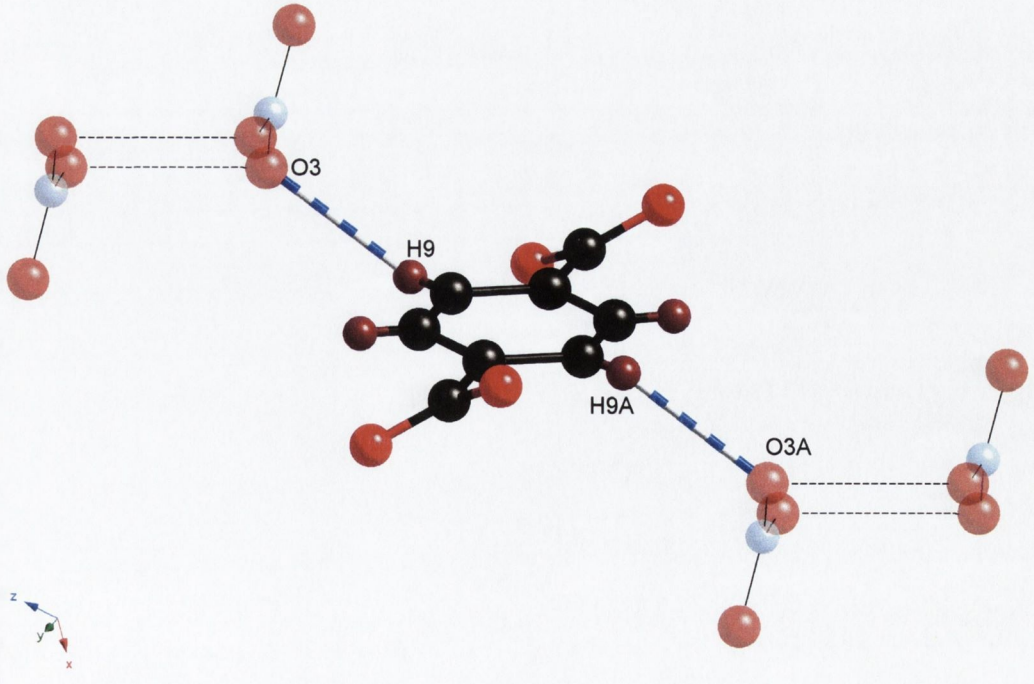

Figure 4.20 – Hydrogen-bonding between bdc molecule and nitrate anions on an adjacent network of **11**. (Nitrates rendered as translucent)

4.2 Reaction of Ni(II) with 4,4'-bipyridine and 1,4-benzenedicarboxylic acid.

Following the positive results obtained with combining Cu(II) with the linear bidentate ligands 4,4'-bipy and bdc, the next metal to be utilised was Ni(II). There are fewer Ni(II) coordination polymers reported than Cu(II) containing polymers in the literature. The success in obtaining various polymeric systems with Ni(II) and 4,4'-bipy (structures **3** and **4**) as reported in the previous chapter was particularly encouraging in this respect. The reaction conditions would be identical to the Cu(II) containing reaction.

4.2.1 Hydrothermal reaction of $Ni(NO_3)_2$ with 4,4'-bipy and H_2bdc (1:1:1).

An aqueous mixture of $Ni(NO_3)_2$, 4,4'-bipy and H_2bdc (1:1:1) was placed in a Teflon®-lined stainless steel vessel, and given a standard heat-cooling cycle. The majority of product was an amorphous powder, however upon inspection under the microscope, small green crystals could be discerned. There was a large quantity of amorphous powder, which appeared to be a mixture of white and green powders. The yield of crystals from the reaction was extremely small and amounted to less that 1% of the total product obtained. A crystal suitable for a structural determination *via* X-ray diffraction was available, and a structure model was obtained. There was an insufficient quantity of crystalline product to obtain microanalytical data. Microanalytical data obtained on the powder could not be matched to the crystal structure requirements.

*4.2.2 Crystal structure of [Ni(4,4'-bipy)(bdc)] (**12**).*

Data for this structure were collected on a Bruker SMART CCD at TCD, and a partial solution found. The crystal was a non-merohedral twin, and the partial solution was based on a cell generated by the GEMINI program.[184] Re-integration of the data by Dr. Simon Parsons at the University of Edinburgh, followed by an absorption correction with the TWINABS program generated an HLKF5 type file, against which the initial solution could be refined. Crystallographic details for this structure are given in Table 4.10. The structure was refined in the space group *C2/m*. Figure 4.21 shows the molecular structure and atomic numbering of the dimeric unit formed by this compound.

The structure consists of a Ni(II) centre which adopts a distorted octahedral geometry. The axial positions are occupied by coordinating 4,4'-bipy molecules which link metal centres to form a chain extending along the crystallographic *c* axis. As can be seen in Figure 4.21 one of the pyridyl rings is disordered over two positions. The atoms C1a, C2a, C1b and C2b have each been refined at half occupancy.

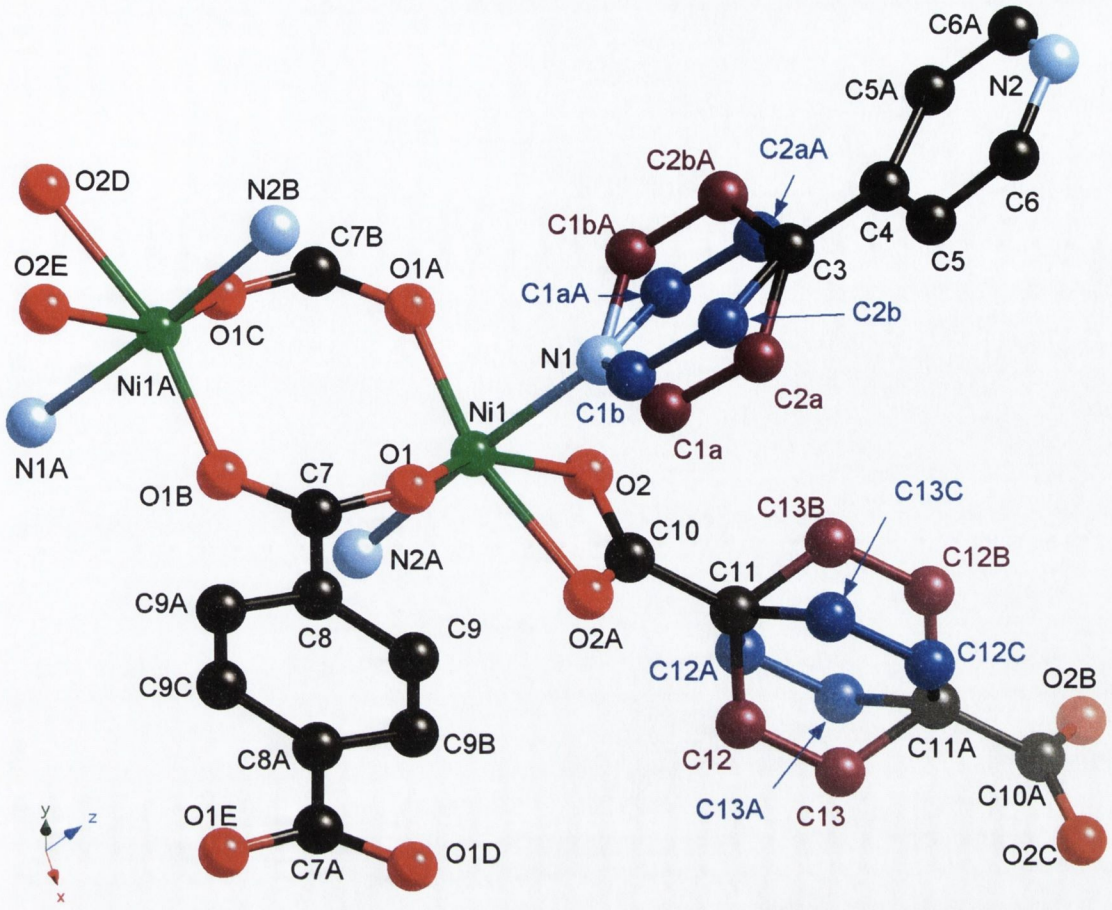

Figure 4.21 - Molecular structure and atomic labelling diagram for **12**. (Note: atoms C1a, C1b, C2a, C2b, C12, and C13 are refined at half occupancy, different coloured atoms (maroon and navy blue) depict the two possible ring positions. Hydrogen atoms omitted for clarity)

The equatorial positions around the Ni(II) centre are occupied by coordinating oxygen atoms, belonging to bdc molecules. As with previous structures seen in this Chapter there are two types of coordination present. The first bdc molecules bridges between two Ni(II) centres, by being mono-coordinate. A listing of selected bond lengths and angles is given in Table 4.11. There are two bridging bdc groups that conjoin two Ni(II) centres, which has the effect of linking the polymeric 4,4'-bipy chains to form a 2D sheet. The metal-to-metal distance within the dimer is 4.205(1) Å. The other carboxylate group chelates the Ni(II) centre, with a bite angle of 61.61(7)°. This connection joins sheets to form a three-dimensional coordination polymer. The network formed by the polymer is an α-Po type network, where the nodes are located at a point midway between the metal centres within the dimeric unit. There are two networks interpenetrated within one another and Figure 4.22 is a packing diagram showing the interpenetrated networks formed by this compound.

Table 4.11 – Crystallographic data for **12**.

Compound	**12**
Chemical Formula	$C_{18}H_{12}N_2O_4Ni$
Formula Weight	379.01
Crystal System	Monoclinic
Space Group	*C*2/*m*
a /Å	16.389(2)
b /Å	10.223(1)
c /Å	11.233(1)
α /°	90.00
β /°	118.479(2)
γ /°	90.00
V /Å^3	1654.3(3)
Z	4
D_{calc} /g cm^{-3}	1.522
μ(Mo-K$_\alpha$) /mm^{-1}	1.198
T /K	153(2)
Crystal Size max /mm	0.23
mid /mm	0.18
min /mm	0.13
$2\theta_{max}$	61.04
Min/Max Trans. Factor	0.738/1.000
R_{int}	0.0552
R_1, wR_2 [I>2σ(I)][a]	0.0384, 0.0815
R_1, wR_2 (all data)	0.0464, 0.0836
Reflections: collected	2816
unique	2816
observed	2413

[a] $R_1 = \Sigma||F_o| - |F_c||/\Sigma|F_o|$, $wR_2 = [\Sigma w(F_o^2 - F_c^2)^2/\Sigma w(F_o^2)^2]^{1/2}$

Table 4.10 – Selected bond lengths (Å) and angles (°) for **12**.

Ni1 – N1	2.088(2)	N1 – Ni1 – N2A^{ii}	175.38(8)
Ni1 – N2A^{ii}	2.072(2)	N1 – Ni1 – O1	88.77(5)
Ni1 – O1	2.0037(12)	N1 – Ni1 – O2	86.81(7)
Ni1 – O1A^{i}	2.0037(12)	O1 – Ni1 – O2	155.00(5)
Ni1 – O2	2.1461(13)	O1 – Ni1 – O1A^{i}	110.90(7)
Ni1 – O2A^{i}	2.1461(13)	O1 – Ni1 – O2A^{i}	93.60(5)
O1 – C7	1.2558(16)	O2 – Ni1 – O2A^{i}	61.61(7)
O2 – C10	1.2558(16)	C2a – C3 – C4 – C5	18.6(5)
		C2b – C3 – C4 – C5	16.4(5)
		O2 – C10 – C11 – C12	56.6(4)
		O2 – C10 – C11 – C12^{i}	126.6(3)

Symmetry Codes: *i* = x, 1-y, z; *ii* = x, y, -1+z.

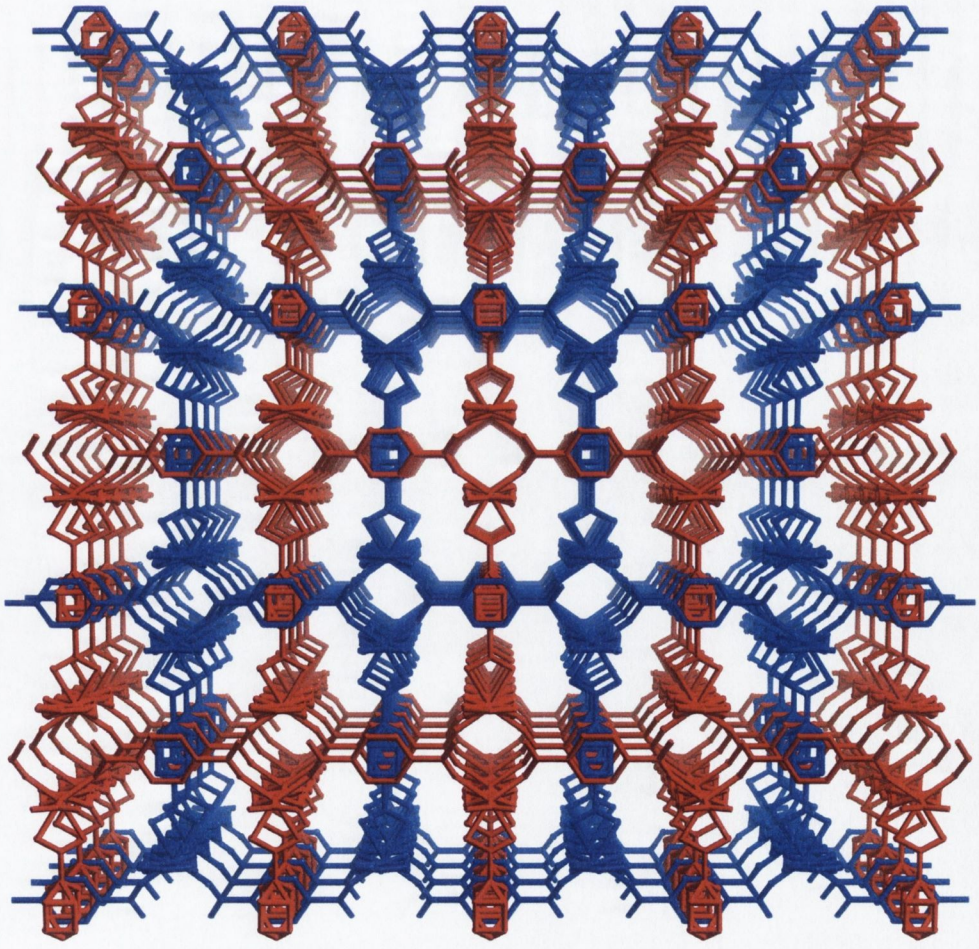

Figure 4.22 – Packing diagram showing two interpenetrated networks of **12**. (View along the *c* axis, hydrogen atoms omitted for clarity)

Figure 4.23 shows a representation of the two interpenetrated networks, where the nodes are points midway between the Ni(II) centres. The dimensions (as depicted in Figure 4.23) are approximately 14.8 Å in the x-direction (horizontally) 10.2 Å in the y-direction (vertically) and 11.2 Å in the z-direction (coming out of the paper).

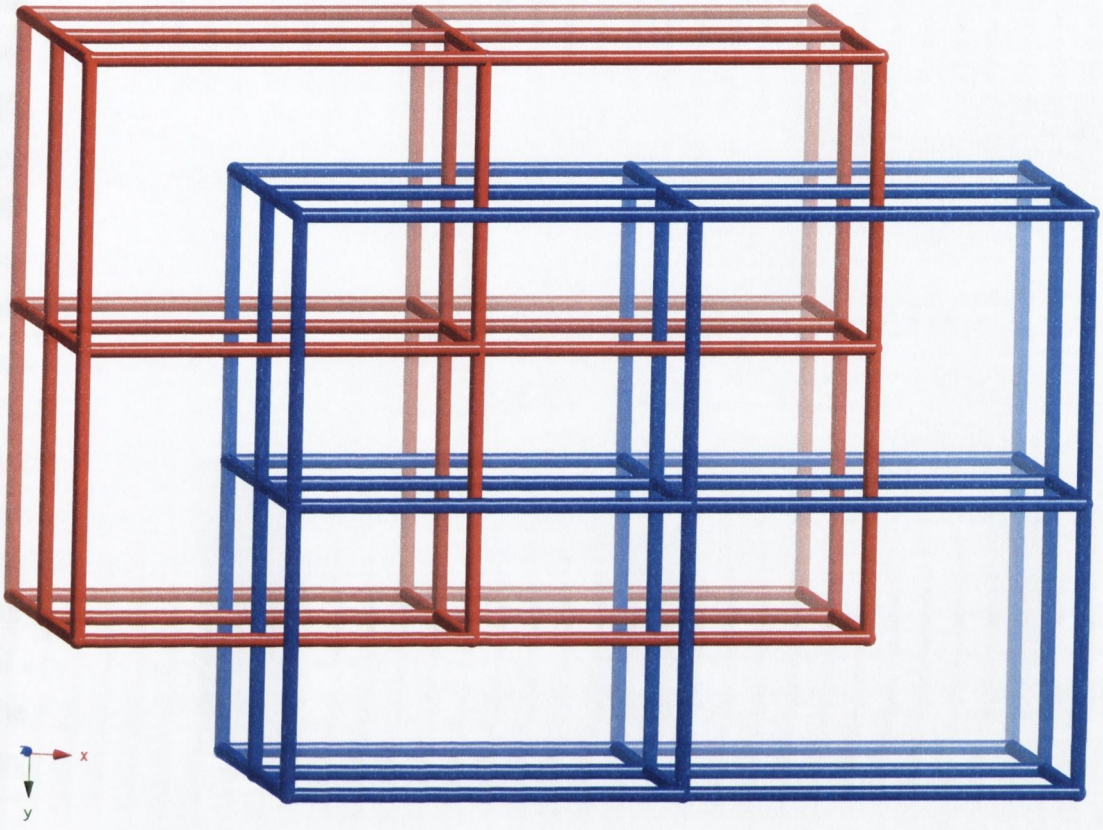

Figure 4.23 – Twofold interpenetration of α-Po type networks of **12**.

The network shown in Figure 4.22 is remarkably similar to that seen in the structure of **11**. The mode of connectivity is similar, having bidentate 4,4'-bipy along with bridging and chelating bdc molecules. In **11** however, there are less chelating bdc groups, with half of them replaced with a nitrate containing hydrogen-bonded bridge.

4.3 Conclusions

As a result of this study various novel coordination polymers have been synthesised. The use of hydrothermal synthetic techniques has both positive and negative aspects. On the positive side it appears to greatly enhance the crystallisation of products. The high pressures and temperatures present in the bomb allow for ligands with low solubility to be forced into solution and are thus able to participate in the reactions. On the negative side, there appears to be much occurring within a single reaction, giving rise to the formation of several products.

The reaction of Cu(II) with 4,4'-bipy and H_2bdc, in a 1:1:1 ratio, gave rise to three different crystalline products. Although the crystalline yields were variable, the

structures of each product were particularly interesting. Structure **9** ([Cu(4,4'-bipy)(bdc)(H_2bdc)]) formed a 2D coordination polymer, which hydrogen-bonds to form a 3D network with an unusual topology (Schläfli notation [$4^8.5^4.6^3$]). Although this network topology is recently known,[222] the threefold interpenetration of such networks is unprecedented. Of the three crystalline products in this reaction, **9** was produced with the most regularity, although amounts formed were variable. Structure **10** ([Cu_4(4,4'-bipy)$_4$(bdc)$_3$(NO_3)$_2$(H_2O)$_2$]) formed a 3D coordination polymer with an α-Po type topology, which shows twofold interpenetration. This compound was the only true 3D coordination polymer formed in the reaction. Although the topology is a fairly common structural feature, interestingly this structure contains a large number of unique atoms (195 non-hydrogen atoms in the asymmetric unit). The asymmetric unit initially appears to have higher symmetry, but analysis with the ADDSYMM feature of the PLATON program[230-232] revealed none. Structure **11** ([Cu(4,4'-bipy)(bdc)(NO_3)]) formed a 2D coordination polymer, which has interactions *via* coordinated nitrate anions, that connect sheets together to form two interpenetrating 3D networks. Although this type of interaction has been seen in inorganic compounds such as $AgNO_3$ and HNO_3 (see Appendix) a search of the CSD did not return any coordination polymers with this mode of interaction. The stabilisation of the interactions and interpenetration is reinforced by the hydrogen-bonding between the nitrate anions and a hydrogen atom on an aromatic ring of a bdc molecule.

In is interesting to note that of the three structures **9**, **10** and **11**, none of them have any solvent molecules in the lattice. All of the structures are very tightly packed with no available space for solvent molecules to sit within the lattice. This is confirmed by the CALCVOID feature of the PLATON program.[230-232]

Structure **12** Ni(4,4'-bipy)(bdc)] was again obtained from data that showed non-merohedral twinning. The compound forms a true 3D coordination polymer, which has an α-Po topology. The bdc molecule has two modes of coordination, bridging and chelating to the Ni(II) centres. Although there is some disorder to the atoms in the structure, the disorder can be modelled successfully (R_1 = 0.0384). The structure itself is similar to structures reported by Chen and co-workers.[114] They report the crystal structures of Co(II), Cd(II) and Zn(II) analogues of **12**. All of the reported compounds are 3D coordination polymers with an α-Po topology, display twofold interpenetration and were synthesised with hydrothermal techniques. The geometry of the dimeric units is the only difference between the complexes of the different metals. Structure **12** is isostructural with the Co(II) containing structure reported by Chen and co-workers.

The formation of "dimeric" chains is a common feature within the structures of **10**, **11** and **12**, and is to be expected since carboxylate has the potential to bridge between two metal centres whilst allowing π-stacking between aromatic linkers such as

4,4'-bipy. The work described in the present chapter has demonstrated that the objective of linking 1D "dimeric" chains of metal centres (such as **5** and **6**) has been achieved. 'Functionalisation' of the acetate bridging group to include a second coordinating site has allowed the formation of 2D sheets and 3D networks.

Chapter Five

Materials & Methods.

Experimental.

5.1 Materials and methods.

5.1.1 Reagents.

All chemicals and solvents were of reagent grade (unless stated) and purchased from Aldrich Chem. Co. Ltd., Fluka Chemika-Biochemica (U.K.), Lancaster Synthesis Ltd. or local solvent suppliers, and were used as received, unless otherwise stated. Water was deionised before use.

5.1.2 Elemental analysis.

Elemental Analysis was carried out at University College, Dublin by Ms. Ann Connelly using a Carlo Erba 1006 automatic analyser. Expected range C, N ± 0.3%, H ± 0.5%

5.1.3 Nuclear magnetic resonance spectroscopy.

NMR spectra were recorded on a Bruker DPX 400 machine operating at 400.14 MHz for ^{1}H, 100.14 MHz for ^{13}C. Samples were run in deuterated solvents and are listed for each spectrum. Standard abbreviations for spectra: s, singlet; d, doublet; t, triplet, m, multiplet; br, broad.

All titration solutions were prepared in a 4:1 $CD_3CN/CDCl_3$ solvent mixture. Titration procedures involved placing the sample in an NMR tube, collecting the spectrum, decanting the sample into a vial, adding an aliquot of metal solution and mixing. The sample was then placed back in the NMR tube and the next spectrum collected. This procedure was continued until the desired metal-to-ligand ratio had been reached.

5.1.4 Infrared spectroscopy.

Infrared spectra were recorded in the range 4000 – 600 cm^{-1} on a Mattson Genesis II FTIR. Samples were run as 8 mm diameter potassium bromide pellets prepared under vacuum. The following abbreviations were used to describe the intensities: vs, very strong; s, strong; m, medium; w, weak; vw, very weak; sh, shoulder; br, broad; vbr, very broad.

5.1.5 Electrospray mass spectrometry.

Electrospray mass spectrometry was carried out on a Micromass LCT Electrospray mass spectrometer. Samples were dissolved in HPLC grade solvent at a concentration of ~2 ng/L. Spectra are reported in the following manner: *m/z* and assignment.

5.1.6 X-ray crystal diffraction.

X-ray analyses for crystals of $[Ru(2,2'\text{-bipy})_2(qpy)][PF_6]_2 \cdot CH_3COCH_3$ and **1** were performed by Dr. Mark Nieuwenhuyzen (Queen's University of Belfast) with a Bruker SMART 1000 CCD diffractometer. X-ray analyses for the remaining crystals were performed by Dr. Paul Jensen (Trinity College Dublin) with a Bruker SMART APEX CCD diffractometer. The candidate was involved in all aspects of structure determination at Trinity College Dublin. The final refinements were performed by the candidate, with assistance provided by Dr. Paul Jensen where necessary.

Both diffractometers utilised graphite-monochromated Mo-Kα radiation (λ = 0.71073 Å). The omega scan method was used to collect either a full sphere or hemisphere of data for each crystal with detector-to-crystal distance of either 5 or 6 cm at temperatures of 153 or 173 K. Data were collected, processed, and corrected for Lorentz and polarisation effects using SMART and SAINT-NT software.[233, 234] Absorption corrections for single crystals were applied using SADABS.[235]The structures were solved using either Patterson or direct methods and refined on HKLF4 data with the SHELXTL program package.[236] Data for twinned crystals (all non-merohedral) were indexed using the GEMINI program[184] rather than the usual SMART routine. The twinned data were processed using the twin output option of SAINT (version 6.22[223]) and corrected for absorption using TWINABS.[185] For **4** and **12** this processing was performed by Dr. Simon Parsons (University of Edinburgh) using a test version of the new software prior to its official release. The twinned structures (all two component) were solved as for the single crystals using HKLF4 data for a single domain containing overlap but were successfully refined on HKLF5 data with a single BASF (twin component) parameter.

All non-hydrogen atoms were refined anisotropically except for the disordered molecules in **1**, on which restraints were also used. Hydrogen atoms (excluding water) were assigned to calculated positions using a riding model with appropriately fixed isotropic thermal parameters. Water hydrogen atoms, however, were located from difference maps and their positions refined with O-H distance restraints (DFIX 0.84 Å) and isotropic thermal parameters fixed at 1.5 times that of the adjoining oxygen atom.

5.1.7 Hydrothermal synthesis – acid digestion bomb.

Hydrothermal synthesis was carried out using a Parr Instrument Company Series 4760/4765 general-purpose digestion bomb employing two different Teflon® inserts (46 ml and 23 ml). Maximum loading of the insert was dependant on reagents used but a typical volume of 20 ml was used for the 46 ml insert, whilst 10 ml was used for the 23 ml insert. The heating cycle used for all reactions involved ramping up to 150°C over a period of 2 hrs, remaining at that temperature for a period of 10 hrs, and

ramping down to 25°C at a rate of 0.1° per minute. All reactions were performed in a Carbolite Model PF200 oven.

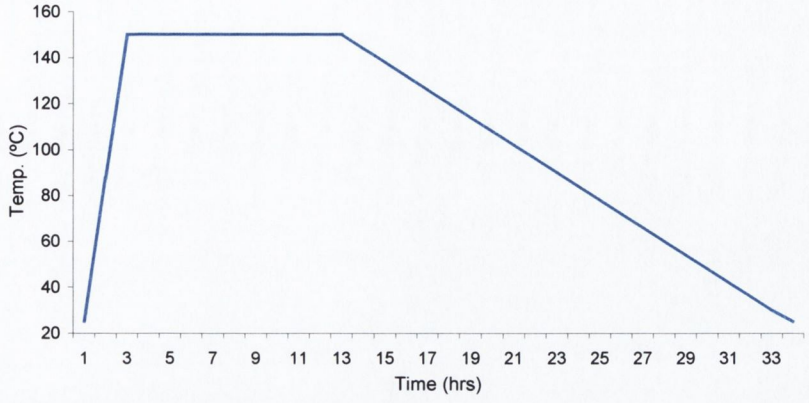

Figure 5.1 – Graphical representation of heating cycle used in hydrothermal reactions.

Figure 5.2 – Photograph of a sealed Parr Instrument general-purpose acid digestion bomb

5.2 Experimental.

5.2.1 Chapter 2.

5.2.1.1 Ligand synthesis (See pullout for ligand structures).

*N,N',N''-tris-pyridin-2-ylmethylene-4,4',4''-triaminotriphenylmethane (**L3**).*

To a chloroform solution (55 ml) of *tris*(4-aminophenyl)methane (**P2**)* (1.001 g, 3.46 mmol) was added a chloroform solution (10 ml) of pyridine-2-carboxaldehyde (0.92 ml, 9.67 mmol) and the mixture was stirred for 4 days. The reaction mixture was dried over $MgSO_4$, filtered and evaporated to dryness. Yield 1.58 g (80%);

* Molecule numbering as given in Figure 2.4 (page 42).

Mpt 201.2 °C; ^{1}H-NMR ($CDCl_3$, 400MHz): δ 8.74(d, 3H, *J* = 4Hz, H_a), 8.66(s, 3H, H_e), 8.22(d, *J* = 8Hz, 3H, H_d), 7.84(t, 3H, H_c), 7.39(t, 3H, H_b), 7.30(dd, 12H, $H_{f,g}$), 5.67(s, 1H, H_h); ^{13}C-NMR ($CDCl_3$, 100MHz): δ 160.2, 154.6, 149.6, 149.1, 142.4, 136.6, 130.2, 125.1, 121.8, 121.3, 55.6; IR (KBr); 1709 (w), 1625(m), 1566(m sh), 1499(s), 1465(m), 1465(m), 1435(m), 1384(w), 1346(w), 1203(m), 1145(w), 1087(w), 1015(w), 992(m), 884(w), 838(w), 809(m), 772(m sh), 741(m), 662(m), 620(m), 573(w), 536(m) cm^{-1}; Found C 78.83; H 5.18; N 14.52%. Required for $[C_{37}H_{28}N_6]\cdot½H_2O$ C 78.56; H 5.17; N 14.86%; ES-MS (MeCN/DCM): 557.02 $[C_{37}H_{29}N_6]^+$.

*N,N',N''-tris-phen-2-olmethylene-4,4',4''-triaminotriphenylmethane (**H_3L4**).*

To a chloroform solution (25 ml) of *tris*(4-aminophenyl)methane (**P2**) (301 mg, 1.04 mmol) was added a chloroform solution (10 ml) of salicylaldehyde (0.300 ml, 2.82 mmol) The mixture was stirred for 4 days after which it dried over $MgSO_4$, filtered and evaporated to dryness. Yield 473 mg (76%); Mpt 158.9 °C; ^{1}H-NMR ($CDCl_3$, 400MHz): δ 13.25 (s, 3H H_k), 8.66 (s, 3H, H_e), 7.57 (m, 3H, H_d), 7.40 (m, 3H, H_b), 7.29 (d, *J* = 6Hz, 6H, H_f), 7.24 (d, *J* = 6Hz, 6H, H_g), 7.04 (m, 3H, H_a), 6.96 (m, 3H, H_c), 5.66 (s, 1H, H_h); IR (KBr): 3051(w br), 1663(w), 1618(vs) 1597(w sh), 1572 (m), 1491(m), 1456(w), 1402(w), 1278(m), 1188(m), 1150(m), 1013(w), 987(w), 910(m), 884(w), 847(w), 816(w), 755(m), 652(w), 523(m) cm^{-1}; Found C 80.03; H 5.47; N 6.85%. Required for $[C_{40}H_{31}N_3O_3]$ C 79.85; H 5.15; N 6.98%.

*N,N'-bis-pyridin-2-ylmethylene-4,4'-diaminodiphenylamine (**L5**).*

To a stirred aqueous solution (25 ml) of recrystallised[†] diaminodiphenyl amine (250 mg, ~0.84 mmol) was added a few drops of concentrated H_2SO_4, followed by a methanolic solution (4 ml) of pyridine-2-carboxaldehyde (160 μl, 1.68 mmol). The mixture was stirred overnight, after which it was neutralised (pH 7) using aqueous 2 M NaOH. The compound was then extracted into dichloromethane (50 ml), dried over $MgSO_4$, and evaporated to dryness under reduced pressure, yielding a brown solid. This solid was taken up in hot ethanol and filtered, slow evaporation of the filtrate yielded golden yellow crystals. Yield 197 mg (62%); Mpt 197.3 °C; ^{1}H-NMR ($CD_3CN/CDCl_3$, 400MHz): δ 8.71 (d, *J* = 4Hz, 2H, H_a), 8.67 (s, 2H, H_e), 8.19 (d, *J* = 8Hz, 2H, H_d), 7.89 (m, 2H, H_c), 7.45 (m, 2H, H_b), 7.38 (d, *J* = 8Hz, 4H, H_f), 7.21 (d, *J* = 8Hz, 4H, H_g), 7.01 (s, 1H, H_h); IR (KBr): 3247(s), 3028(s), 1621(s), 1572(vs), 1325(vs), 838(s) cm^{-1}; ES-MS ($MeCN/CHCl_3$): 189.09 $[C_{24}H_{19}N_5]^{2+}$, 378.17 $[C_{24}H_{19}N_5]^+$; Accurate Mass Analysis: Mass Measured 378.1712 Calculated for $C_{24}H_{20}N_5$ 378.1716 (Tolerance –1.7ppm).

[†] Recrystallisation from boiling water in the presence of activated charcoal.

tris(4-aminophenyl)amine.

To a stirred ethanolic suspension (80 ml) of *tris*(4-nitrophenyl)-amine (1.901 g, 5 mmol) and palladium on carbon (121 mg), under an argon atmosphere, was added, dropwise, an ethanolic solution (10 ml) of hydrazine monohydrate (4 ml, 79 mmol) over approximately 20 mins. The mixture was heated to reflux for 24 hrs, during which time the colour changed from yellow to red/brown. The mixture was filtered whilst hot through a celite pad, and evaporated to dryness, yielding a red/brown coloured microcrystalline solid. Yield 888 mg (61%).

*N,N',N''-tris-pyridin-2-ylmethylene-4,4',4''-triaminotriphenylamine (**L7**).*

To a degassed dichloromethane solution (45 ml) of *tris*(4-nitrophenyl)-amine (400 mg, 1.38 mmol) containing crushed 4Å molecular sieves (1 g) was added a dichloromethane solution (5 ml) of pyridine-2-carboxaldehyde (393 μl, 4.13 mmol). The mixture was stirred under an argon atmosphere for 36 hrs, filtered through a celite® pad and evaporated to dryness. Recrystallisation from methanol yielded an orange powder. Yield 550 mg (72%); Mpt 124.6 °C; ^{1}H-NMR ($CDCl_3$, 400MHz): δ 8.71 (d, J = 4.0 Hz, 3H, H_a), 8.66 (s, 3H, H_e), 8.19 (d, J = 8.0 Hz, 3H, H_d), 7.89 (dd, J = 8.0, 6.0 Hz, 3H, H_c), 7.45 (dd, J = 6.0, 4.0 Hz, 3H, H_b), 7.35 (d, J = 7.0 Hz, 6H, H_f), 7.19 (d, J = 7.0 Hz, 6H, H_g); IR (KBr): 1625(s), 1581(s), 1499(s), 1319(s), 1206(m), 1148(m), 1109(m), 1090(w), 1037(w), 998(w), 883(m), 836(s), 776(m), 743(m), 667(m), 622(w), 581(w), 538(m) cm^{-1}; Found C 72.22;H 4.55; N 16.31%. Required for $[C_{36}H_{27}N_4]\cdot 2¼H_2O$ C 72.28;H 5.30; N 16.39%; ES-MS (MeCN/DCM): 558.24 $[C_{36}H_{27}N_7]^+$.

*N,N',N''-tris-phen-2-olmethylene-4,4',4''-triaminotriphenylamine (**H_3L8**).*

To a degassed dichloromethane solution (20 ml) of *tris*(4-nitrophenyl)-amine (150 mg, 0.52 mmol) containing crushed 4Å molecular sieves (1 g) was added a dichloromethane solution (5 ml) of salicyaldehyde (162 μl, 0.16 mmol). The mixture was stirred under an argon atmosphere for 36 hrs, filtered through a celite® pad and evaporated to dryness. Successive recrystallisations from ethanol and hot toluene yielded orange crystals. Yield 169 mg (54%); Mpt 150.1 °C; ^{1}H-NMR ($CDCl_3$, 400MHz): δ 13.40(s, 3H, H_k), 8.68(s, 3H, H_e), 7.43(m, 6H, H_b/H_d), 7.28(d, J = 8Hz, H_f), 7.21(d, J = 8Hz, H_g), 7.06(d, J = 8Hz, H_a), 6.99(dd, J = 1.0, 7.5Hz, 3H, H_c); IR (KBr); 3465(w br), 1615(vs), 1501(s), 1457(w sh), 1318(m), 1279(s), 1188(m), 1149(w), 1112(w), 1030(w), 907(w), 833(w), 758(m), 729(w sh), 659(w), 524(w) cm^{-1}; Found C 75.48; H 5.63; N 8.05%. Required for $[C_{39}H_{30}N_4O_3]\cdot C_7H_8$ C 75.52; H 5.56; N 8.06%; ES-MS (MeCN/DCM): 302.23 $[C_{39}H_{32}N_4O_3]^{2+}$, 603.23 $[C_{39}H_{31}N_4O_3]^+$.

5.2.1.2 Complex synthesis.

*Ag_3(**L7**)$_2(PF_6)_3$.*

To an acetonitrile solution (5 ml) containing $AgPF_6$ (53 mg, 0.21 mmol), was added a dichloromethane solution (3.5 ml) of **L7** (74 mg, 0.13 mmol). Addition of excess methanolic NH_4PF_6 (15 ml) yielded an orange/red precipitate, which was collected and dried *in vacuo*. Yield 115 mg (55%); Mpt 228.4 °C; ^{1}H-NMR ($CD_3CN/CDCl_3$, 400MHz): δ 8.81(s, 6H, H_e), 8.72 (d, *J* = 5.0Hz, 6H, H_a), 8.13 (dd, *J* = 7.5, 6.0 Hz, 6H, H_c), 7.96 (d, *J* = 7.5 Hz, 6H, H_d), 7.70 (dd, *J* = 6.0, 5.0 Hz, 6H, H_b), 7.32 (d, *J* = 8.5 Hz, 12H, H_f), 7.01 (d, *J* = 8.5 Hz, 12H, H_g); Found: C 46.09; H 3.06; N 10.60. Required for $[Ag_3(C_{36}H_{27}N_7)_2][PF_6]_3$ C 45.86; H 3.53; N 10.40 %; ES-MS (MeCN/DCM): 479.762 $[Ag_3$(**L7**$)_2]^{3+}$.

5.2.1.3 Complexation via ^{1}H-NMR titrations.

*$[Ag_2$(**L5**$)_2][BF_4]_2$.*

A solution of **L5** (5.03×10^{-3} M) was titrated with 20 μl aliquots of a solution of $AgBF_4$ (0.249 M) until 2.0 equivalents of Ag(I) had been added. Excessive broadening of proton resonances made interpretation of the spectrum difficult. ES-MS ($MeCN/CHCl_3$): 337.6 $[Ag_2$(**L5**$)(MeCN)_2]^{2+}$, 378.2 $[C_{24}H_{19}N_5]^+$, 485.1 $[Ag_2$(**L5**$)_2]^{2+}$,

*$[Ag_2$(**L5**$)_2][PF_6]_2$.*

A solution of **L5** (5.03×10^{-3} M) was titrated with 20 μl aliquots of a solution of $AgPF_6$ (0.249 M) until 2.0 equivalents of Ag(I) had been added. Excessive broadening of proton resonances made interpretation of the spectrum difficult. ES-MS ($MeCN/CHCl_3$): 337.6 $[Ag_2$(**L5**$)(MeCN)_2]^{2+}$, 378.2 $[C_{24}H_{19}N_5]^+$, 485.1 $[Ag_2$(**L5**$)_2]^{2+}$.

*$[Cu_2$(**L5**$)_2][BF_4]_2$.*

A solution of **L5** (5.03×10^{-3} M) was titrated with 20 μl aliquots of a solution of $Cu(MeCN)_4BF_4$ (0.205 M) until 2.5 equivalents of Cu(I) had been added. ES-MS ($MeCN/CHCl_3$): 447.1 $[Cu_2$(**L5**$)_2]^{2+}$.

*$[Cu_2$(**L5**$)_2][PF_6]_2$.*

A solution of **L5** (5.03×10^{-3} M) was titrated with 20 μl aliquots of a solution of $Cu(MeCN)_4PF_6$ (0.249 M) until 2.0 equivalents of Cu(I) had been added. ^{1}H-NMR ($CD_3CN/CDCl_3$, 400MHz): δ 8.99(s, 2H, H_e), 8.55 (s, 2H, H_a), 8.11 (t, 2H, H_c), 7.98 (d, *J* = 7.5 2H, H_d), 7.66 (t, *J* = 6.5 Hz, 2H, H_b), 7.43 (d, *J* = 6.5 Hz, 4H, H_f), 7.26(s, 1H, H_h), 7.03 (d, *J* = 6.5 Hz, 4H, H_g); ES-MS ($MeCN/CHCl_3$): 447.1 $[Cu_2$(**L5**$)_2]^{2+}$.

$[Ag_3(\mathbf{L7})_2][BF_4]_3$.

A solution of **L7** (5.02×10^{-3} M) was titrated with 20 μl aliquots of a solution of $AgBF_4$ (0.249 M) until 3.0 equivalents of Ag(I) had been added. ^{1}H-NMR ($CD_3CN/CDCl_3$, 400MHz): δ 8.88(s, 3H, H_e), 8.74 (d, J = 4 Hz, 3H, H_a), 8.16 (t, J = 7.5 Hz, 3H, H_c), 7.96 (d, J = 7.5 3H, H_d), 7.73 (m, 3H, H_b), 7.44 (d, J = 8 Hz, 6H, H_f), 7.11 (d, J = 8 Hz, 6H, H_g); ES-MS ($MeCN/CHCl_3$): 383.1 $[Ag_2(C_{30}H_{24}N_6)^{\ddagger}(MeCN)_2]^{2+}$, 427.8 $[Ag_2(\mathbf{L7})(MeCN)_2]^{2+}$, 479.8 $[Ag_3(\mathbf{L7})_2]^{3+}$.

$[Ag_3(\mathbf{L7})_2][PF_6]_3$.

A solution of **L7** (5.02×10^{-3} M) was titrated with 5 μl aliquots of a solution of $AgPF_6$ (0.249 M) until 2.5 equivalents of Ag(I) had been added. ^{1}H-NMR ($CD_3CN/CDCl_3$, 400MHz): δ 8.81(s, 6H, H_e), 8.72 (d, J = 5.0Hz, 6H, H_a), 8.13 (dd, J = 7.5, 6.0 Hz, 6H, H_c), 7.96 (d, J = 7.5 Hz, 6H, H_d), 7.70 (dd, J = 6.0, 5.0 Hz, 6H, H_b), 7.32 (d, J = 8.5 Hz, 12H, H_f), 7.01 (d, J = 8.5 Hz, 12H, H_g); ES-MS ($MeCN/CHCl_3$): 383.1 $[Ag_2(C_{30}H_{24}N_6)^{\ddagger}(MeCN)_2]^{2+}$, 427.8 $[Ag_2(\mathbf{L7})(MeCN)_2]^{2+}$, 479.8 $[Ag_3(\mathbf{L7})_2]^{3+}$.

$[Cu_3(\mathbf{L7})_2][BF_4]_3$.

A solution of **L7** (5.02×10^{-3} M) was titrated with 20 μl aliquots of a solution of $[Cu(MeCN)_4][BF_4]$ (0.205 M) until 2.5 equivalents of Cu(I) had been added. Excessive broadening of proton resonances made interpretation of the spectrum difficult. ES-MS ($MeCN/CHCl_3$): 435.1 $[Cu_3(\mathbf{L7})_2]^{3+}$, 621.1 $[Cu_2(\mathbf{L7})_2]^{2+}$.

$[Cu_3(\mathbf{L7})_2][PF_6]_3$.

A solution of **L7** (5.02×10^{-3} M) was titrated with 20 μl aliquots of a solution of $Cu(MeCN)_4PF_6$ (0.249 M) until 3.0 equivalents of Cu(I) had been added. Excessive broadening of proton resonances made interpretation of the spectrum difficult. ES-MS ($MeCN/CHCl_3$): 290.4 $[Cu_3(\mathbf{L7})(MeCN)_3]^{3+}$, 382.6 $[Cu_2(\mathbf{L7})(MeCN)_2]^{2+}$, 435.1 $[Cu_3(\mathbf{L7})_2]^{3+}$.

5.2.3 Chapter 3.

$[Ru(2,2'\text{-bipy})_2qpy][PF_6]_2$.

$Ru(2,2'\text{-bipy})_2Cl_2$ (304 mg, 0.62 mmol)[154] and qpy (226 mg, 0.73 mmol) were added to a degassed 1:1 mixture of $EtOH/H_2O$, and heated to reflux for 24 hrs. Upon cooling, the mixture was stirred for a further 48 hrs. Reduction to ⅔ of the original volume by evaporation followed by addition of excess methanolic NH_4PF_6 yielded an orange/brown powder. Purification *via* ion-exchange chromatography afforded the pure product. The

---

‡ $(C_{30}H_{24}N_6)$ = Fragment corresponding to loss of pyridyl arm

crude product was dissolved in MeCN, and loaded onto a Sephadex C-25 column. Elution with a 5:3 0.1 M aqueous NaCl/acetone mixture released the desired product. Yield 45 mg (45%) ^{1}H-NMR (CD_3CN, 400MHz): δ 8.98 (s, 1H), 8.87 (d, 2H), 8.55 (d, 2H), 8.30 (d, 2H), 8.10 (m, 2H), 7.78 (d, 2H), 7.74 (d, 2H), 7.43 (m, 2H); ES-MS (MeCN): 362 $[Ru(2,2'\text{-bipy})_2(qpy)]^{2+}$.

Reaction of $Co(NO_3)_2{\cdot}6H_2O$ with 2,2'-bipy and qpy.

2,2'-Bipy (270 mg, 1.73 mmol) was added to an aqueous solution (50 ml) of $Co(NO_3)_2{\cdot}6H_2O$ (250 mg, 0.86 mmol) and stirred overnight. A methanolic solution (10 ml) of qpy (261 mg, 0.84 mmol) was added dropwise to the stirring solution. The mixture was stirred for a further 4 days, filtered and left to crystallise. A small number of orange crystals formed after several days. Yield 3 mg IR (KBr): 3048 (s vbr), 1598(s), 1535(m), 1488(w), 1407 (m sh), 1361(s br), 1220(m), 1063(m), 1042(w), 999(w), 817(m), 730(w).

*Reaction of $Co(NO_3)_2{\cdot}6H_2O$ with 2,2'-bipy and 4,4'-bipy. (Structure **1**)*

2,2'-Bipy (564 mg, 3.61 mmol) was added to an aqueous solution (50 ml) of $Co(NO_3)_2{\cdot}6H_2O$ (502 mg, 1.72 mmol) and stirred for 9 hrs. A methanolic solution (10 ml) of 4,4'-bipy (281 mg, 1.80 mmol) was then added and the mixture was stirred for 4 days. The solution was filtered and left to crystallise. Orange crystals formed after 1 week. Yield 250 mg (15%). IR (KBr): 3080 (s vbr), 1608 (s sh), 1598(s), 1535(m), 1488(w), 1407 (m sh), 1362(s br), 1326(s sh), 1221(m), 1063(m), 1042(w), 999(w), 817(m), 730(w).

*Hydrothermal reaction of $Co(NO_3)_2$ with 4,4'-bipy. (Structure **2**)*

To an aqueous solution (8 ml) of $Co(NO_3)_2{\cdot}6H_2O$ (504 mg 1.73 mmol) was added 4,4'-bpy (284 mg, 1.83 mmol) and the mixture placed in an acid digestion hydrothermal bomb. A standard reaction cycle was performed (See Section 5.1.7). Large orange crystals were formed, however the reaction mixture and crystalline product was contaminated with black residue. The mother liquor was filtered and left to stand. Small orange crystals formed overnight. Yield 322 mg (25%); Mpt >240 °C; IR (KBr): 3057 (s vbr), 1601(s), 1535(s), 1491(m), 1357(s br), 1218(s), 1065(m), 1042(w), 1000(m), 806(s), 731(w), 621(s), 569(w), 489(w) (the IR of both crystalline products was the same).

*Reaction of $Ni(OAc)_2$ with 2,2'-bipy and 4,4'-bipy. (Structure **3**)*

To stirred aqueous solution (10 ml) of $Ni(OAc)_2{\cdot}4H_2O$ (255 mg, 1.02 mmol) was added 2,2'-bipy (160 mg, 1.02 mmol) and the mixture was stirred overnight. A methanolic solution (5 ml) of 4,4'-bipy (165 mg, 1.06 mmol) was added and the mixture stirred for a

further 5 days, after which it was filtered and left to stand. Blue crystals formed over a week. Yield 48 mg (7%); Mpt 231.5 °C; IR (KBr); 3413(br), 1608(sh), 1578(s), 1541(sh), 1489(m), 1409(s), 1384(sh), 1219(m), 1069(m), 1044(w), 1010(w), 816(m), 732(w), 621(m), 572(w), 500(w) cm^{-1}; Found C 49.98; H 6.45; N 9.38%. Required for $[Ni(C_{10}H_8N_2)_2(CH_3CO_2)_2(H_2O)_2]\cdot 2H_2O\cdot CH_3OH$ C 50.27; H 6.41; N 9.38%.

*Reaction of $Ni(OAc)_2$ with 4,4'-bipy. (Structure **4**)*

To an aqueous solution (20 ml) of $Ni(OAc)_2\cdot 4H_2O$ (256 mg, 1.03 mmol) was added a methanolic solution (5 ml) of 4,4'-bipy (165 mg, 1.06 mmol). The mixture was stirred for 24 hrs, filtered and left to crystallise. Yield 180 mg (47%); Mpt >240 °C; IR (KBr); 3408(s br) 2923(m br), 1611 (s sh), 1552 (s br), 1409 (s br), 1338(w sh), 1223(s), 1141(w), 1073(m), 1046(w), 1019(w), 971(w), 899(m), 826(s), 752(w sh), 728(m), 659(m), 637(w), 560(w), 465(w) cm^{-1}; Found C 45.63; H 4.78; N 7.94%. Required for $[Ni(C_{10}H_8N_2)(CH_3CO_2)_2(H_2O)_2]$ C 45.57; H 4.92; N 7.92%.

*Reaction of $Cu(OAc)_2$ with 4,4'-bipy. (Structure **5**)*

To an aqueous solution (10 ml) of $Cu(OAc)_2\cdot H_2O$ (209 mg, 1.05 mmol) was added 4,4'-bpy (160 mg, 1.02 mmol) and the mixture in a Teflon®-lined digestion bomb and 10 ml water added. The bomb was sealed, placed in a Carbolite oven and a standard heat cycle was run. The bomb was removed from the oven and opened. The reaction mixture consisted of a blue precipitate, amongst which was mixed royal blue crystals. Yield 110 mg (29%). IR (Crystals) (KBr); 3421(s), 1609(s), 1584(s sh), 1491(w), 1414(m br), 1336(w), 1221(m), 1077(m), 1045(w), 1013(w), 925(w), 814(m), 725(w), 676(w), 644(m), 624(w), 475(w) cm^{-1}.

*Reaction of $Zn(OAc)_2$ with 4,4'-bipy. (Structure **6**)*

To an aqueous solution (20 ml) of $Zn(OAc)_2\cdot 2H_2O$ (303 mg, 1.38 mmol) was added a methanolic solution (5 ml) of 4,4'-bipy (215 mg 1.38 mmol) and stirred for 2 days. A white precipitate formed, stirring was halted and the mixture was left for several days during which time the precipitate settled and colourless prism crystals grew as the solvent evaporated. Yield 120 mg (26%); Mpt >240 °C; IR (KBr); 3042(w) 1602(s br), 1586(sh), 1487(w), 1422(s br), 1332(w sh), 1218(m), 1067(m), 1044(m), 1005(m), 931(w), 818(s), 731(w), 673(m), 624(s), 469(w) cm^{-1}; Found C 49.54; H 4.37; N 8.19%. Required for $[Zn(C_{10}H_8N_2)(OAc)_2]$ C 49.51; H 4.15; N 8.25%.

*Hydrothermal reaction of $Cu(NO_3)_2\cdot 3H_2O$ with H_2bdc and 4,4'-bipy. (Structures **7** & **8**)*

$Cu(NO_3)_2\cdot 3H_2O$ (200 mg, 0.828 mmol), 1,4-benzenedicarboxylic acid (274 mg, 1.649 mmol) and 4,4'-bipy (129 mg, 0.826 mmol) were placed in a Teflon®-lined digestion bomb and 10 ml water added. The bomb was sealed, placed in a Carbolite

oven and a standard heat cycle was run. The bomb was removed from the oven and opened. Amongst the powder present two different types of crystals were formed, although the yields of each type varied with each batch of product. Samples of the crystals formed in each batch were analysed by X-ray diffraction to ensure they were the same as previous batches.

Powder residue yield between 95 and 98 %. IR (KBr); 3255(m br), 1687(s), 1612(s), 1562(s), 1510(m sh), 1416(m), 1369(s), 1288(s), 1220(m sh), 1112(w), 1072(w), 1016(w), 936(w), 881(w), 813(m), 754(m), 644(w), 507(w) cm^{-1}.

[Cu(4,4'-bipy)$(NO_3)_2 \cdot 2.5H_2O$] Structure **7** - royal blue prisms)

[Cu(4,4'-bipy)$(NO_3)_2(H_2O)_2$] (Structure **8** - pale blue/green blocks)

Crystalline yield < 5 %

5.2.4 Chapter 4.

*Hydrothermal reaction of $Cu(NO_3)_2$ with 4,4'-bipy and H_2bdc. (Structures **9**, **10** & **11**)*

$Cu(NO_3)_2 \cdot 3H_2O$ (202 mg, 0.836 mmol), 1,4-benzenedicarboxylic acid (145 mg, 0.873 mmol) and 4,4'-bipy (143 mg, 0.916 mmol) were placed in a Teflon®-lined digestion bomb and 10 ml water added. The bomb was sealed, placed in a Carbolite oven and a standard heat cycle was run. The bomb was removed from the oven and opened. Amongst the large amount of powder three different types of crystals were formed, although the yields of each type varied with each batch of product. Samples of the crystals formed in each batch were analysed by X-ray diffraction to ensure they were the same as previous batches. Crystalline yield between 10 and 50 % of product

Powder residue yield between 50 and 90%. IR (KBr); 3091(s vbr), 1679(s), 1612(s), 1562(s), 1510(s sh), 1416(s sh), 1396(s), 1288(a), 1138(w), 1072(w), 1018(w), 936(w), 881(w), 813(m), 754(m), 644(m), 507(m) cm^{-1};

[Cu(4,4'-bipy)(bdc)(H_2bdc)] (Structure **9** - royal blue prisms) IR (KBr); 3064(m br), 1689(s), 1600(s), 1490(s), 1415(s), 1282(s), 1135(w), 1076(w), 1011(m), 939(w), 877(w), 821(m), 781(m), 730(m), 644(m), 565(w), 518(w) cm^{-1};

Yield between <5 to 60% of crystalline product

[Cu(4,4'-bipy)(bdc)$(NO_3)(H_2O)$] (Structure **10** - pale green needles)

[Cu(4,4'-bipy)(bdc)(NO_3)] (Structure **11** - pale blue prisms)

Yield of **10** and **11** between <5 and 40% of crystalline product.

(Crystals could not be separated as they were 'fused' together.)

*Hydrothermal reaction of $Ni(NO_3)_2$ with 4,4'-bipy and H_2bdc. (Structure **12**)*

$Ni(NO_3)_2 \cdot 6H_2O$ (200 mg, 0.6877 mmol), 1,4-benzenedicarboxylic acid (115 mg, 0.6922 mmol) and 4,4'-bpy (129 mg, 0.8259 mmol) were place in a Teflon®-lined digestion bomb and 10 ml water added The bomb was sealed, placed in a Carbolite

oven and a standard heat cycle was run. The bomb was removed from the oven and opened.

Powder residue yield approximately 98 %. IR (KBr); 3270(s br), 1678(m), 1614(s), 1550(s), 1495(m sh), 1419(m), 1359(s), 1292(m sh), 1067(m), 1016(m), 808(s), 752(s), 640(m), 503(m) cm^{-1}.

[Ni(4,4'-bipy)(bdc)] (Structure **12** - pale blue prisms)

Crystalline yield < 2 %

Chapter Six

Future Work.

Future work.

The work described in the preceding chapters can be broadly divided into two areas: the synthesis of novel molecular helicate systems, and the synthesis of novel coordination polymers. Each area will be discussed separately in terms of future research potential.

6.1 Molecular helicates.

Much of the work presented in Chapter 2, whilst novel, is built upon previously established work performed within the Kruger group.[56-58] This provided the basis to make the move from traditional C_2 symmetric ligands to the formation of a C_3 symmetric ligand system. With the chemistry of this system now established there is potential to use the building blocks to form new and potentially interesting compounds. The 'backbone' unit that forms the basis of this potential is shown in Figure 6.1.

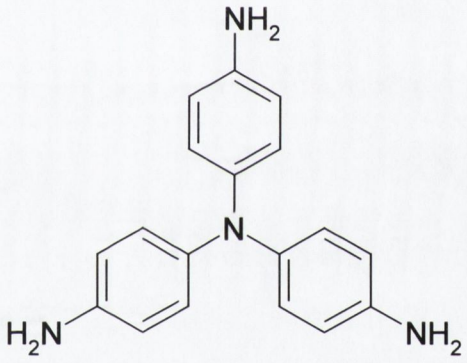

Figure 6.1 – 'Backbone' unit for potential functionalisation in future avenues of research.

One ongoing aspect to the work presented here, was mentioned in the conclusions section of Chapter 2, where collaboration with Dr. J. Lacour is being undertaken. The point of this is to utilise a chiral anion (TRISPHAT) synthesised by Lacour and co-workers.[147] It is hoped that this anion will be able to resolve the ^{1}H-NMR resonance peaks of the helicate system.

The central triphenylamine core is highly adaptable and future research should explore thus avenue. For instance, we have only investigated the amine core thoroughly. Preliminary work using a tetrahedral carbon core (**L3** and **H_3L4**) showed promise this should be elaborated further in an effort to overcome the degradation problems seen by these ligands.

The switch between the trigonal (nitrogen) and tetrahedral (carbon) centre will have a pronounced effect upon the resultant structure of any complex formed. This will provide for an interesting study into the effects the geometry of the bridging atom has on the complexes formed.

A further extension of this work to incorporate other Group 15 atoms within the central core might also be explored. Incorporating larger atoms such as phosphorous and arsenic would allow potential access to the resultant cavity, within the complex to be explored. (Should this change be made, the cavity would of course be larger). In addition incorporating P within the scaffold would provide a further NMR active nucleus to assist in determining the solution structure.

The extremely large library of aldehydes and ketones that can be reacted with the terminal amine groups will allow for the formation of diverse compounds that can be complexed with various transition metals.

6.1.1 Iterative development of dendrimer-like assemblies.

Dendrimers consist of a core molecule, and alternating layers of two monomers. Each pair of monomer layers completes a shell and a generation. The core generally consists of an amine core, although other molecules can be used. It is envisaged that the backbone unit shown in Figure 6.1 could be employed as a core in the development of dendrimer type systems (Figure 6.2).

Once synthesised, each generation (G1, G2, G3....) will be assessed for the ability to coordinate transition metals. Simply changing the precursor mono-aldehyde will lead to the formation of many dendritic systems.

6.1.2 Small molecular entrapment.

The condensation of di-aldehydes, di- or poly-ketones about the trigonal core will possibly yield imino-based 'cryptand' type ligands,[237] whose coordinating ability toward a range of transition metals can then be assessed. These species may also have the ability to encapsulate small molecules within their cavity in addition to metal ions. A simple reduction of the imino group to the corresponding amines will generate the hexa-amino cryptand analogues that can then be screened for their ability to encapsulate anionic guests. These kinds of hosts will have 'dual' entrapment ability, as they possess both a hydrophobic tri-phenyl core and hydrophilic amino periphery. This should allow the entrapment of charged aromatic species within the 'cryptand' cavity.

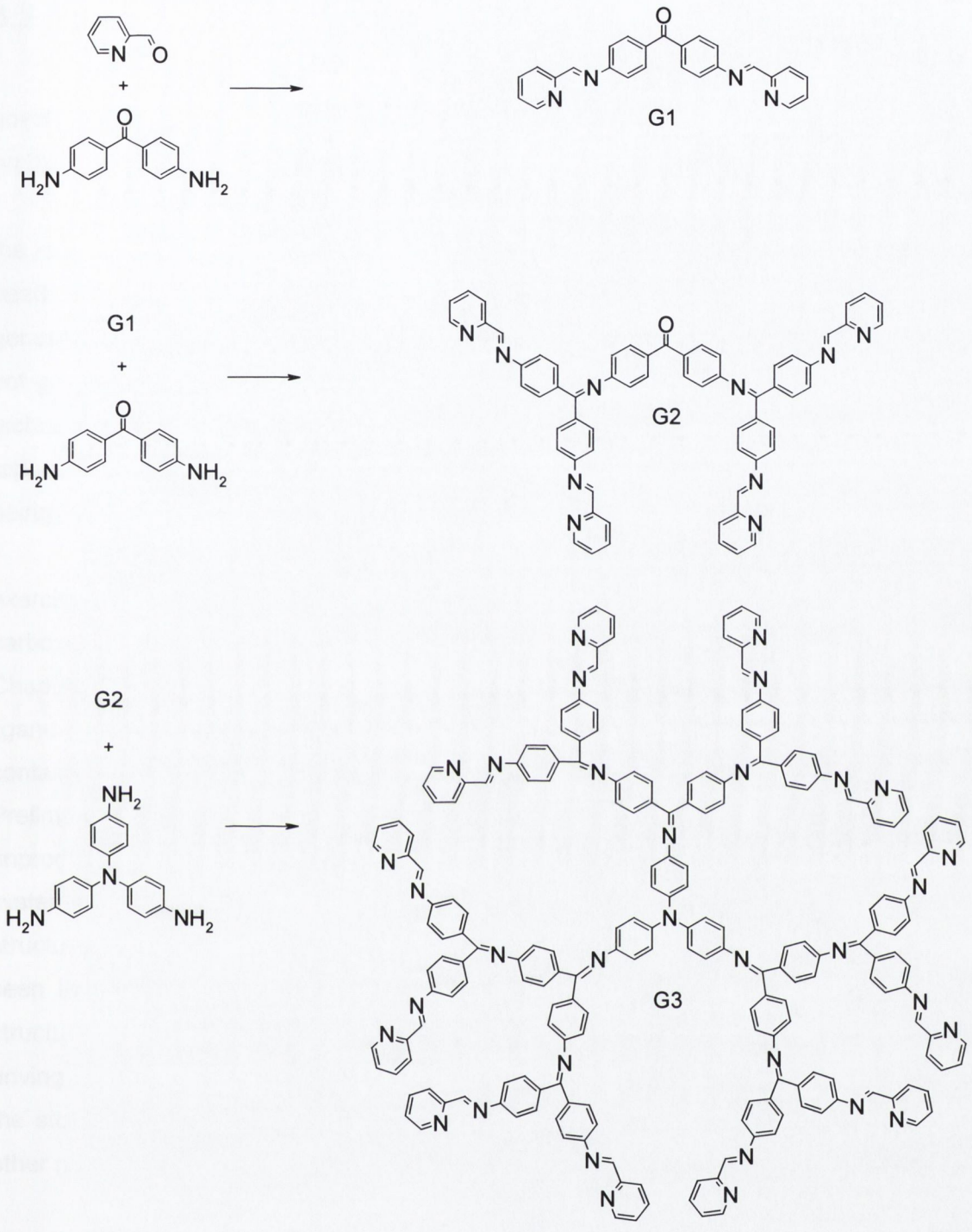

Figure 6.2 – Potential synthesis of dendrimer type molecules using the Schiff-base chemistry reported in previous chapters.

6.2 Coordination Polymers.

Many of the structures presented in Chapters 3 and 4 are both interesting and novel. There remains much scope, in terms of future research, that can be carried out on the basis of what is presented herein.

The most obvious point to start at is an attempt to improve the crystalline yield of the reactions. Linked to this is the goal of forming a single phase of product. Reactions need to be optimised to produce both the maximum yield of product, as well as generating a crystalline product. The presence of powders in the reaction mixtures is not greatly desired, as X-ray powder diffraction techniques are required for analysis (a technique that is not readily available at TCD). The formation of the crystalline products reported in this thesis provides encouragement insofar as the hydrothermal techniques being employed are proving successful.

Variation of the carboxylate coordinating ligands is another option to be fully exercised in this line of research. Although many structures have been reported where carboxylate ligands have been coordinated to metal centres, it has been shown (in Chapter 3) that structures can be formed from basic, well studied and highly utilised ligands, such as 4,4'-bipy. There appears to be no reason why the use of carboxylate containing ligands will not allow for the formation of novel and interesting structures. Preliminary studies involving the use of diphenyl dicarboxylate have thus far proved unproductive. However there is much scope to the work, subtle variations in solvent systems, may prove successful in the formation of crystalline products suitable for structural analysis. One of the main aims is to minimise the degree of interpenetration seen in the resultant networks. Interpenetration, whilst aesthetically pleasing to the structure, is highly problematic when it comes to the usefulness of the compound. The driving force behind forming these types of complexes is to maximise their usefulness in the storage of various gases, and so if the cavities in the networks, are occupied by other networks, the storage potential of the compound will be greatly reduced.

The next point at which to continue study into these compounds are the physical properties. One of the driving forces behind this line of research is the potential that coordination polymers have in the storage of hydrogen gas for use in fuel cells. Amongst others Yaghi and co-workers[98, 104, 116, 117, 238, 239] have reported the properties of the compounds synthesised by them, which far outstrip the storage capabilities of zeolites.[118, 121] Various techniques are used in measuring these types of properties; TGA, DSC, etc are all required. As such, it is these types of studies that remain to be performed on the compounds reported in this thesis.

Appendix

Chapter 1

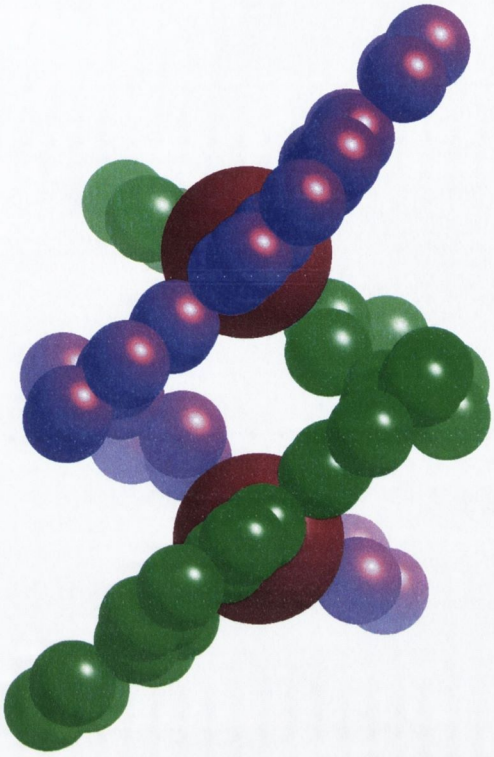

Figure A1 – Space filling diagram of $[Pd_2(quinquepy)_2]^{4+}$ species synthesised by Constable and co-workers.[44] (Separate ligand strand shown in different colours, Pd centres maroon, solvent molecules, counterions and hydrogen atoms omitted for clarity)

Figure A2 – Structure of diamond, consisting of four-connected nodes.

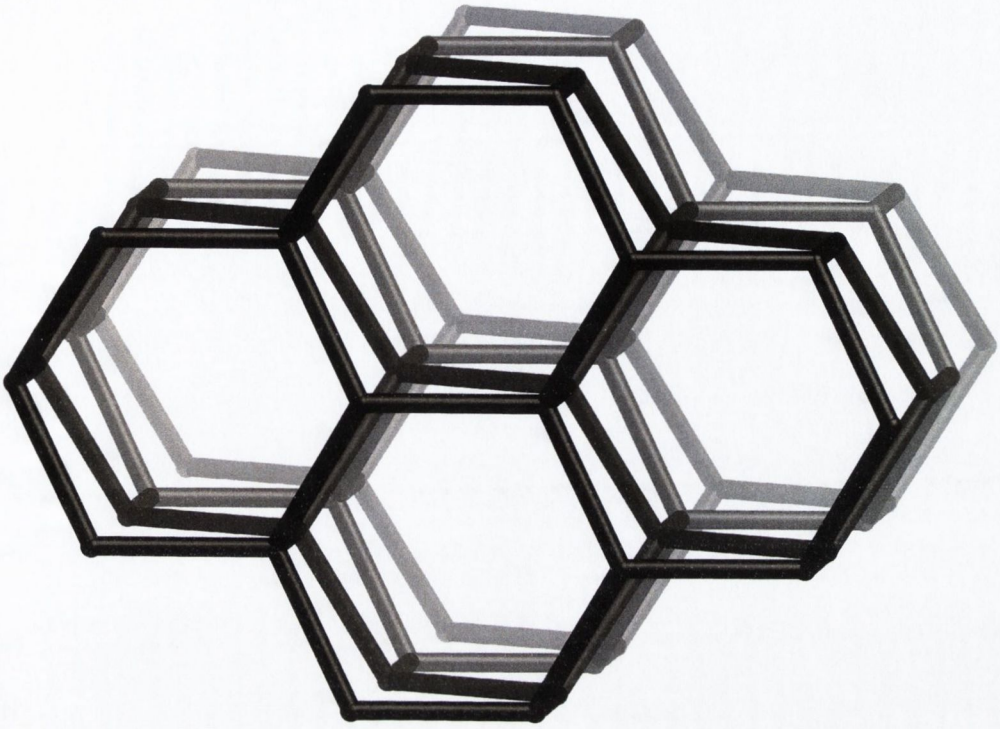

Figure A3 – Structure of lonsdaleite, consisting of four-connected nodes.

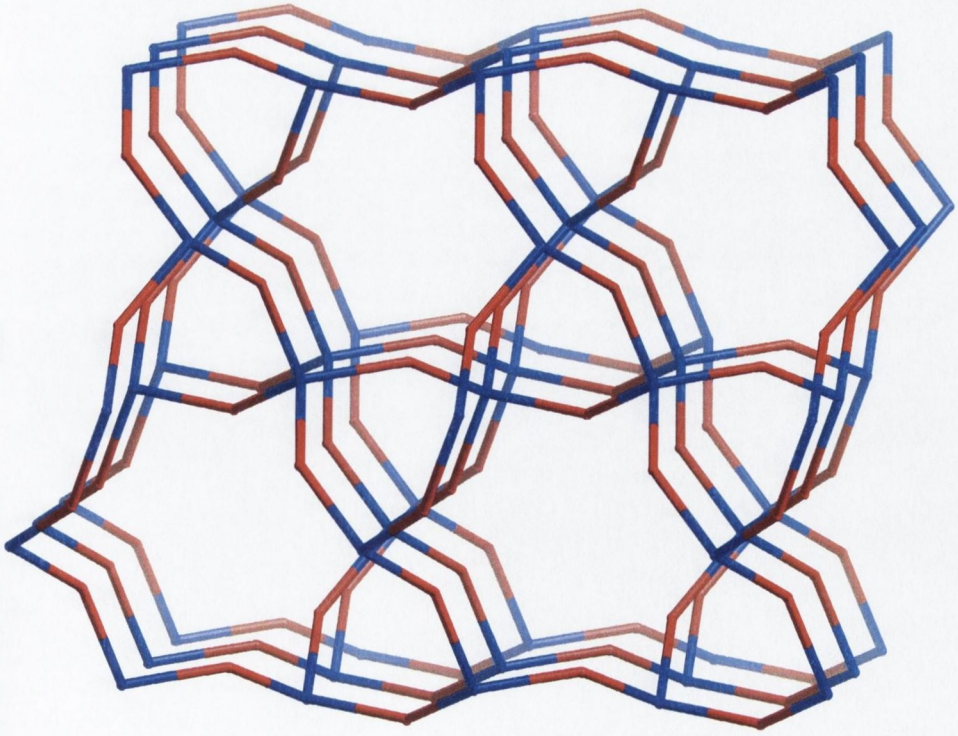

Figure A4 – Structure of quartz, consisting of four-connected nodes and angled bridging connectors.

Chapter 2 – Ligand structures

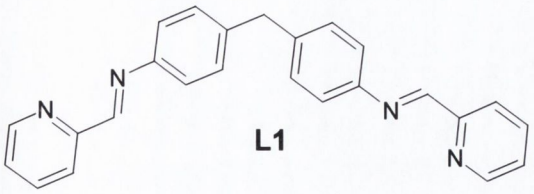

L1

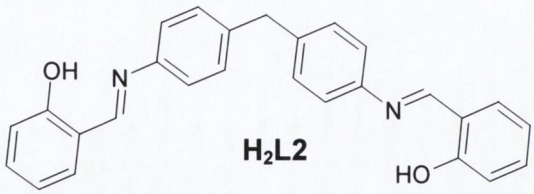

H_2L2

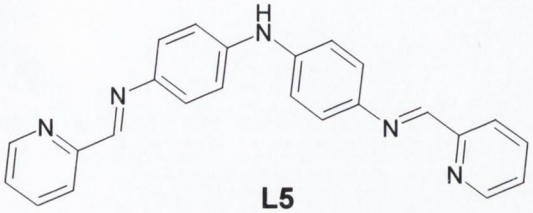

L5

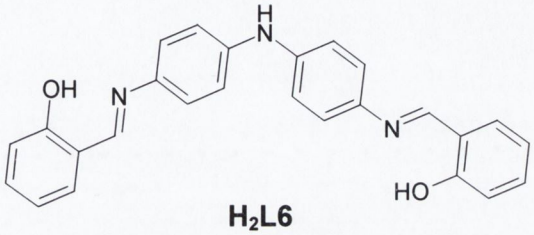

H_2L6

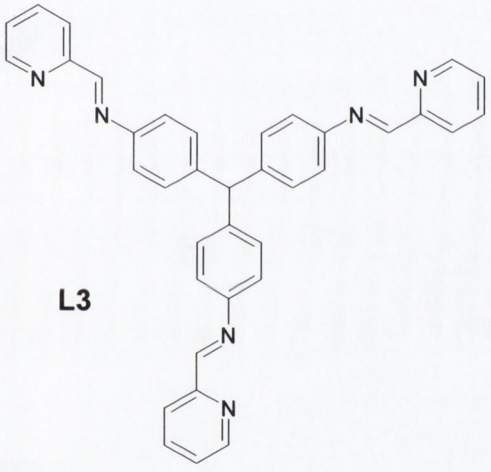

L3

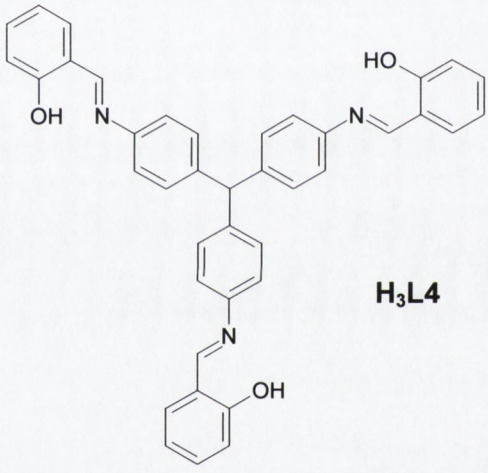

H_3L4

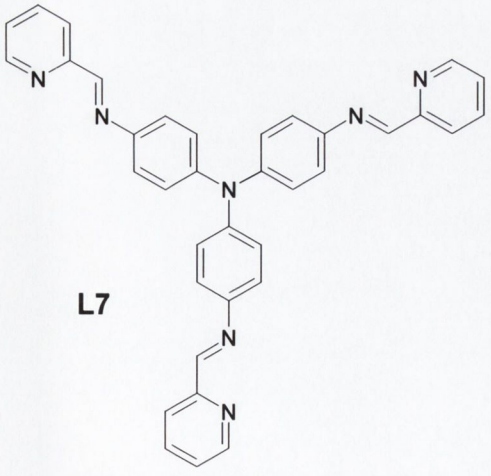

L7

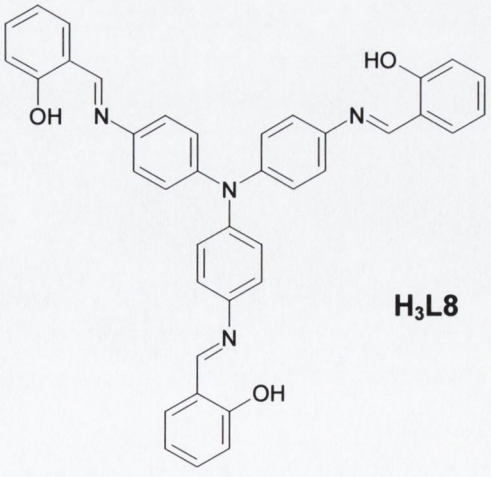

H_3L8

Chapter 3

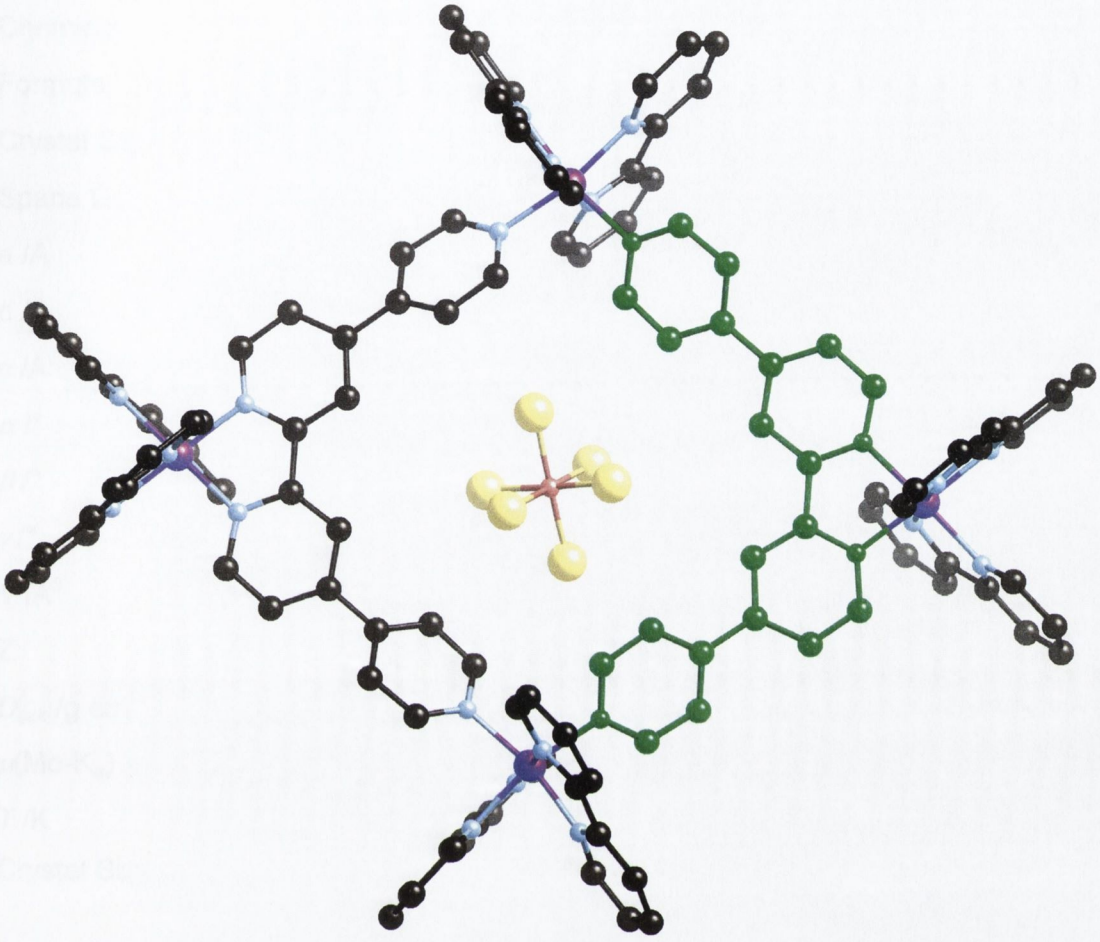

Figure A5 – Proposed structure of Ru_4 containing model of a tetranuclear molecular box showing PF_6^- encapsulation. (This structure is based on a Hyperchem™ model)[129]

Table A1 – Crystallographic data for $[Ru(2,2'\text{-bipy})_2(qpy)][PF_6]_2 \cdot 2(CH_3COCH_3)$.

Compound	$[Ru(2,2'\text{-bipy})_2(qpy)][PF_6]_2$
Chemical Formula	$[Ru(2,2'\text{-bipy})_2(qpy)][PF_6]_2 \cdot 2(CH_3COCH_3)$
Formula Weight	1129.89
Crystal System	Monoclinic
Space Group	$P2_1/c$
a /Å	21.090(2)
b /Å	14.842(1)
c /Å	14.345(1)
α /°	90
β /°	93.798(2)
γ /°	90
V /Å^3	4480.7(5)
Z	4
D_{calc} /g cm^{-3}	1.675
μ(Mo-K$_\alpha$) /mm^{-1}	0.523
T /K	153(2)
Crystal Size max /mm	
mid /mm	n/a*
min /mm	
$2\theta_{max}$	50.00
Min/Max Trans. Factor	n/a†
R_{int}	0.1302
R_1, wR_2 [I>2σ(I)][a]	0.0981, 0.2638
R_1, wR_2 (all data)	0.1567, 0.2919
Reflections: collected	30102
unique	7874
observed	4307

[a] $R_1 = \Sigma||F_o| - |F_c||/\Sigma|F_o|$, $wR_2 = [\Sigma w(F_o^2 - F_c^2)^2/\Sigma w(F_o^2)^2]^{1/2}$

* A selection of crystals (in the mother liquor) were sent to Dr. M Nieuwenhuyzen (QUB).

† This information was not present in the electronic format supplied by Dr. M Nieuwenhuyzen.

Chapter 4

Examples of close contacts between nitrate anions in inorganic systems.

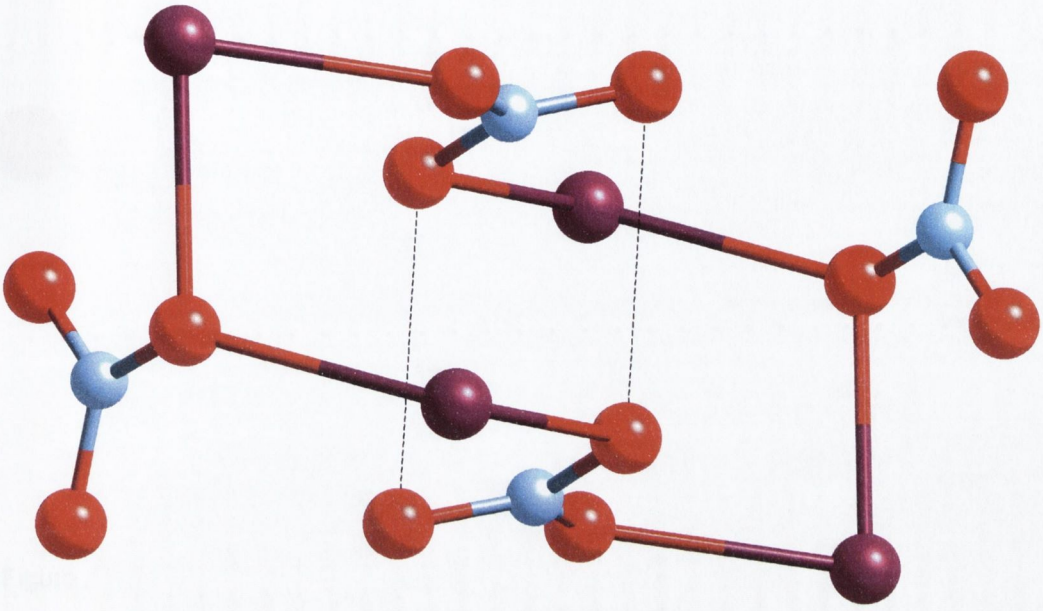

Figure A6 – Interactions between nitrate anions in the $AgNO_3$ structure. Dashed line represent contacts in the range 3.10–3.15Å.[225] (ICSD #28103. Purple atoms represent Ag atoms)

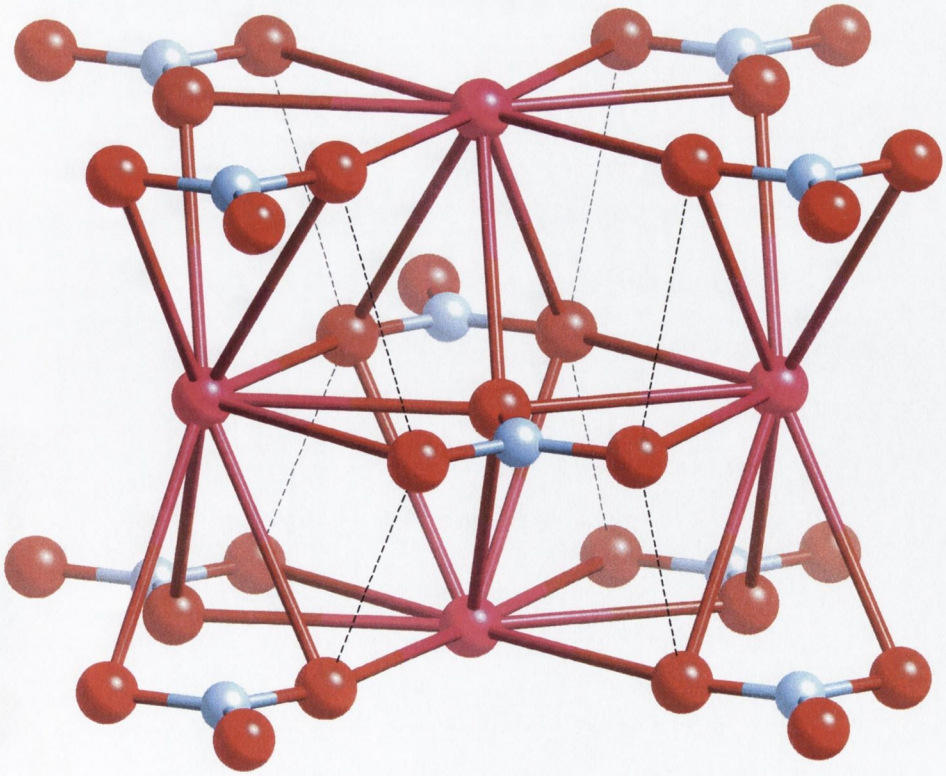

Figure A7 – Interactions between nitrate anions in the $RbNO_3$ structure. Dashed line represent contacts in the range 2.90–3.00Å.[226] (ICSD #16338. Pink atoms represent Rb atoms)

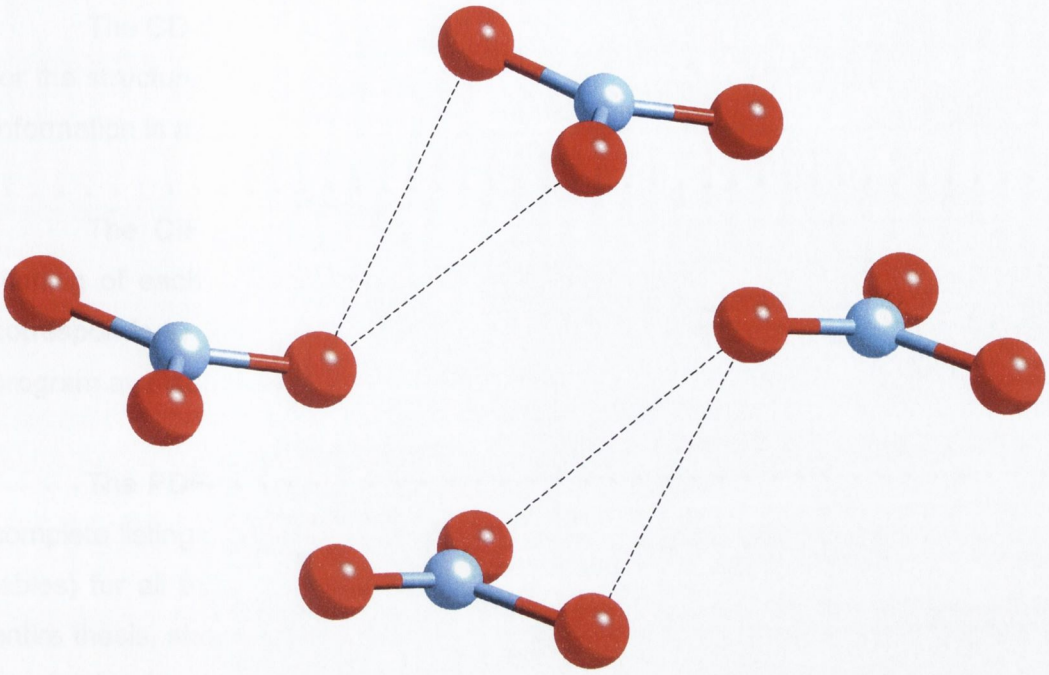

Figure A8 – Interactions between nitrate anions in the HNO_3 structure. Dashed line represent contacts in the range 2.80–3.00Å.[227] (ICSD #30605)

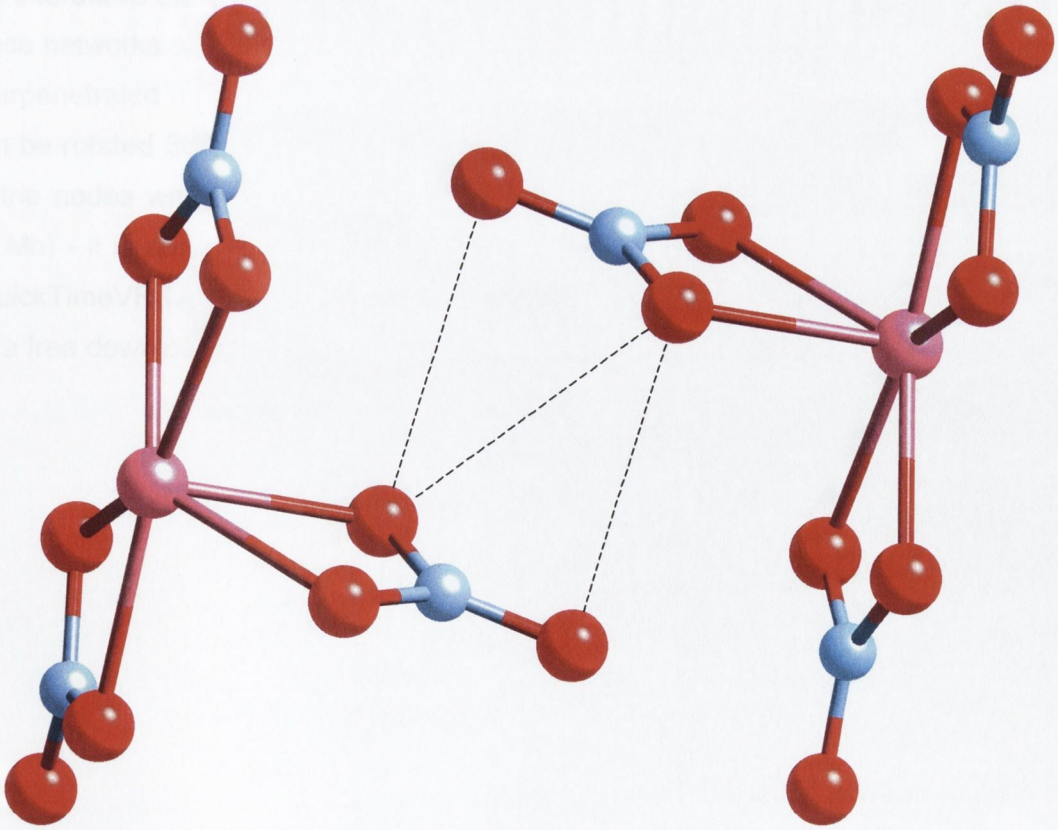

Figure A9 – Interactions between nitrate anions in the $Sn(NO_3)_4$ structure. Dashed line represent contacts in the range 3.00–3.10Å.[229] (ICSD #16873. Pink atoms represent Sn atoms)

Attached CD-ROM

The CD-ROM attached to this thesis contains electronic versions of various files for the structures given in this thesis. There are 3 folders that contain these files. (This information is also given in the ReadMe.txt file on the CD)

The CIF folder contains all the crystallographic information files (*.cif). The naming of each file corresponds to the structure as given in the thesis (e.g. Struct1 corresponds to Structure **1**. CIFs can be viewed in the Mercury program, which is a program available as a free download from the CCDC website (www.ccdc.cam.ac.uk))).

The PDF folder contains portable document format files (*.pdf). These files are complete listings of the crystallographic information (including bond lengths and angles tables) for all the structures presented herein. It also contains a PDF type file of this entire thesis, should the reader require and electronic copy (PDF files can be viewed in the Adobe Acrobat Reader program, which is available as a free download from the Adobe website (www.adobe.com/products/acrobat/readermain.html)).

The QuickTimeVR folder contains 4 QuickTime Virtual Reality files. These files are interactive 3D representations of the networks formed by structures 7 and 9. Both of these networks show interpenetration, and as such, there are both single networks and interpenetrated networks. When the files are opened in QuickTime Player, the networks can be rotated 360 degrees in two axes. This assists in understanding the connectivity of the nodes within the network. NOTE These files are quite large (between 45 and 71 Mb) - it is recommended that they be saved to the local hard drive before opening (QuickTimeVR files can be viewed in the QuickTime Player program, which is available as a free download from the Apple website (www.apple.com/quicktime/download)).

Glossary

Interpenetration	The entanglement of two or more networks, such that the separation of the networks is not possible without the breaking of bonds.
Metal-organic framework (MOF)	An alternative description of coordination polymer. Essentially a MOF is a network consisting of metal centres (or clusters of metal centres) linked together with multidentate organic ligands.
Platonic solid	A platonic solid is a polyhedron all of whose faces are congruent regular polygons, and where the same number of faces meet at every vertex. The best known example is a cube whose faces are six congruent squares.
Polymorph	Polymorphs contain the same chemical components but have a different packing of those components in the solid state.
Pseudopolymorph	A similar situation exists as for polymorphs, with the exception that in a pseudopolymorph, the chemical composition differs only in the amount or type of solvent present in the structure
Schläfli notation	As far as this thesis is concerned, the Schläfli notation is presented in the form $n^{p(p-1)/2}$ where n is the number of nodes in the smallest circuit, and p is the number of connection that radiate from each node. (A full description is given in Chapter 1, page 28).
Topology	Topology is the theory of shapes which are allowed to stretch, compress, flex and bend, but without tearing or gluing. For example, a square is topologically equivalent to a circle, since a square can be continously deformed into a circle. Similarly a doughnut and a coffee cup with a handle are topologically equivalent, since a doughnut can be reshaped into a coffee cup without tearing or gluing.

References

[1.] J.-M. Lehn, *Angew. Chem. Int. Ed.*, 1988, **27**, 90.

[2.] J.-M. Lehn, *Supramolecular Chemistry, Concepts and Perspectives*, VCH Weinheim, 1995.

[3.] C. B. Aakeroy and K. R. Seddon, *Chem. Soc. Rev.*, 1993, 397.

[4.] T. Steiner, *Angew. Chem. Int. Ed.*, 2002, **41**, 49.

[5.] L. Pauling, *The Nature of the Chemical Bond and the Structure of Molecules and Crystals - An Introduction to Modern Structural Chemistry*, Oxford University Press, London, 1940.

[6.] P. W. Atkins, *General Chemistry*, Scientific American Books, New York, 1989.

[7.] T. Zeegers-Huyskens and P. L. Huyskens, *Intermolecular Forces - An Introduction to Modern Methods and Results*, ed. P. L. Huyskens, W. A. P. Luck, and T. Zeegers-Huyskens, Springer-Verlag, Berlin, 1991.

[8.] R. P. D. Doyle, *Early and Late Transition Metal Complexes Incorporating p-Block Oxo-Anions*, Ph.D. Thesis, University of Dublin, Dublin, 2001.

[9.] K. O'Donaghue, *Towards Binuclear Metal Complexes as Probes for DNA: A Study of Bis-Phenanthroline Ruthenium (II) Dipyrido[3,2-d:2',3'-f]quinoxaline and its derivatives.*, Ph.D. Thesis, University of Dublin, Dublin, 2002.

[10.] P. D. Beer, P. A. Gale, and D. K. Smith, *Supramolecular Chemistry*, ed. J. Evans, Oxford University Press, 1999.

[11.] J. W. Steed and J. L. Atwood, *Supramolecular Chemistry*, John Wiley & Sons Ltd., Chichester, 2000.

[12.] C. J. Pedersen, *Angew. Chem. Int. Ed.*, 1988, **27**, 1021.

[13.] J.-M. Lehn, *Angew. Chem. Int. Ed.*, 1990, **29**, 1304.

[14.] D. J. Cram, *Angew. Chem. Int. Ed.*, 1988, **27**, 1009.

[15.] J.-M. Lehn, A. Rigault, J. Seigel, J. Harrowfield, B. Chevrier, and D. Moras, *Proc. Natl. Acad. Sci. USA*, 1987, **84**, 2565.

[16.] D. Philip and J. F. Stoddart, *Angew. Chem. Int. Ed.*, 1996, **35**, 1154.

[17.] P. Sforza, 2001, http://www.ppws.vt.edu/~sforza/tmv/tmv.html

[18.] P. Tecilla, R. P. Dixon, G. Slobodkin, D. S. Alavi, D. H. Waldeck, and A. D. Hamilton, *J. Am. Chem. Soc.*, 1990, **112**, 9408.

[19.] G. M. Whitesides, J. P. Mathias, and C. T. Seto, *Science*, 1991, **254**, 1312.

[20.] S. Leininger, B. Olenyuk, and P. J. Stang, *Chem. Rev.*, 2000, **100**, 853.

[21.] V. Balzani, A. Credi, F. M. Raymo, and J. F. Stoddart, *Angew. Chem. Int. Ed.*, 2000, **39**, 3349.

[22.] M. Asakawa, P. R. Ashton, W. Dehaen, G. L'abbé, S. Menzer, J. Nouwen, F. M. Raymo, J. F. Stoddart, M. S. Tolley, S. Toppet, A. J. P. White, and D. J. Williams, *Chem. Eur. J.*, 1997, **3**, 772.

[23.] H. Ogino, *New J. Chem.*, 1993, **17**, 683.

[24.] M. Fujita, in 'Molecular Catenanes, Rotaxanes and Knots: A Journey Through the World of Molecular Topology' Vol, ed. J.-P. Sauvage and C. Dietrich-Buchecker, Weinheim, 1999, p. 57.

[25.] M. Fujita and K. Ogura, *Coord. Chem. Rev.*, 1996, **148**, 249.

[26.] M. Fujita, F. Ibukuro, H. Seki, O. Kamo, M. Imanari, and K. Ogura, *J. Am. Chem. Soc.*, 1996, **118**, 899.

[27.] M. Fujita, *Acc. Chem. Res.*, 1999, **32**, 53.

[28.] M. Albrecht, *Chem. Rev.*, 2001, **101**, 3457.

[29.] A. F. Williams, *Chimia*, 2000, **54**, 585.

[30.] R. S. Cahn, C. Ingold, and V. Prelog, *Angew. Chem. Int. Ed.*, 1966, **5**, 385.

[31.] E. C. Constable, in 'Comprehensive Supramolecular Chemistry' Vol 9, ed. J. L. Atwood, J. E. D. Davies, D. D. MacNicol, and F. Vögtle, Oxford, 1996, p. 213.

[32.] G. Struckmeier, U. Thewalt, and J.-H. Fuhrhop, *J. Am. Chem. Soc.*, 1976, **98**, 278.

[33.] G. C. Van Stein, H. Van der Poel, G. Van Koten, A. L. Spek, A. J. M. Duisenberg, and P. S. Pregosin, *J. Chem. Soc., Chem. Commun.*, 1980, 1016.

[34.] J.-M. Lehn, J.-P. Sauvage, J. Simon, and R. Ziessel, *Nouv. J. Chim.*, 1983, **7**, 413.

[35.] C. J. Carrano and K. N. Raymond, *J. Am. Chem. Soc.*, 1978, **100**, 5371.

[36.] R. C. Scarrow, D. L. White, and K. N. Raymond, *J. Am. Chem. Soc.*, 1985, **107**, 6540.

[37.] J.-M. Lehn and A. Rigault, *Angew. Chem. Int. Ed.*, 1988, **27**, 1095.

[38.] M. Greenwald, D. Wessely, I. Goldberg, and Y. Cohen, *New J. Chem.*, 1999, **23**, 377.

[39.] A. Lützen, M. Hapke, J. Griep-Raming, D. Haase, and W. Saak, *Angew. Chem. Int. Ed.*, 2002, **41**, 2086.

[40.] B. Hasenknopf, J.-M. Lehn, N. Boumediene, E. Leize, and A. Van Dorsselaer, *Angew. Chem. Int. Ed.*, 1998, **37**, 3265.

[41.] M. Albrecht, *Chem. Eur. J.*, 2000, **6**, 3485.

[42.] J. Xu, T. N. Parac, and K. N. Raymond, *Angew. Chem. Int. Ed.*, 1999, **38**, 2878.

[43.] E. C. Constable, S. M. Elder, J. V. Walker, P. D. Wood, and D. A. Tocher, *J. Chem. Soc., Chem. Commun.*, 1992, 229.

[44.] E. C. Constable, S. M. Elder, J. Healy, M. D. Ward, and D. A. Tocher, *J. Am. Chem. Soc.*, 1990, **112**, 4590.

[45.] E. C. Constable, *Tetrahedron*, 1992, **48**, 10013.

[46.] C. Piguet, G. Bernardinelli, and G. Hopfgartner, *Chem. Rev.*, 1997, **97**, 2005.

[47.] E. C. Constable, M. J. Hannon, P. Harverson, M. Neuburger, D. R. Smith, V. F. Wanner, L. A. Whall, and M. Zehnder, *Polyhedron*, 2000, **19**, 23.

[48.] M. Barley, E. C. Constable, S. A. Corr, R. C. S. McQueen, J. C. Nutkins, M. D. Ward, and M. G. B. Drew, *J. Chem. Soc., Dalton Trans.*, 1988, 2655.

[49.] E. C. Constable, A. J. Edwards, P. R. Raithby, and J. V. Walker, *Angew. Chem. Int. Ed.*, 1993, **32**, 1465.

[50.] M. J. Hannon, C. L. Painting, A. Jackson, J. Hamblin, and W. Errington, *Chem. Commun.*, 1997, 1807.

[51.] C. M. Harris and E. D. McKenzie, *J. Chem. Soc. (A)*, 1969, 746.

[52.] G. C. Van Stein, H. Van der Poel, G. Van Koten, A. L. Spek, A. J. M. Duisenberg, and P. S. Pregosin, *J. Chem. Soc., Chem. Commun.*, 1980, 1016.

[53.] N. Yoshida and K. Ichikawa, *Chem. Commun.*, 1997, 1091.

[54.] N. Yoshida, N. Ito, and K. Ichikawa, *J. Chem. Soc., Perkin Trans. 2*, 1997, 2387.

[55.] N. Yoshida, K. Ichikawa, and M. Shiro, *J. Chem. Soc., Perkin Trans. 2*, 2000, 17.

[56.] J. Keegan, P. E. Kruger, M. Nieuwenhuyzen, and N. Martin, *Cryst. Grow. Design*, 2002, **2**, 329.

[57.] P. E. Kruger, N. Martin, and M. Nieuwenhuyzen, *J. Chem. Soc., Dalton Trans.*, 2001, 1966.

[58.] J. Keegan, P. E. Kruger, M. Nieuwenhuyzen, J. O'Brien, and N. Martin, *Chem. Commun.*, 2001, 2192.

[59.] L. J. Childs, N. W. Alcock, and M. J. Hannon, *Angew. Chem. Int. Ed.*, 2001, **40**, 1079.

[60.] M. J. Hannon, C. L. Painting, and W. Errington, *Chem. Commun.*, 1997, 307.

[61.] M. J. Hannon, C. L. Painting, and W. Errington, *Chem. Commun.*, 1997, 1805.

[62.] J. Hamblin, L. J. Childs, N. W. Alcock, and M. J. Hannon, *J. Chem. Soc., Dalton Trans.*, 2002, 164.

[63.] M. J. Hannon, S. Bunce, A. J. Clarke, and N. W. Alcock, *Angew. Chem. Int. Ed.*, 1999, **38**, 1277.

[64.] N. Yoshida and K. Ichikawa, *Chem. Commun.*, 1997, 1091.

[65.] P. K. Bowyer, K. A. Porter, A. D. Rae, A. C. Willis, and S. B. Wild, *Chem. Commun.*, 1998, 1153.

[66.] S.-P. Yang, X.-M. Chen, and L.-N. Ji, *J. Chem. Soc., Dalton Trans.*, 2000, 2337.

[67.] L. J. Charbonniere, M.-F. Gilet, K. Bernauer, and A. F. Williams, *Chem. Commun.*, 1996, 39.

[68.] S. Rüttimann, C. Piguet, G. Bernardinelli, B. Bocquet, and A. F. Williams, *J. Am. Chem. Soc.*, 1992, **114**, 4230.

[69.] L. J. Charbonniere, A. F. Williams, C. Piguet, G. Bernardinelli, and E. Ruivara-Minten, *Chem. Eur. J.*, 1998, **4**, 485.

[70.] P. J. Stang and S. R. Seidel, *Acc. Chem. Res.*, 2002, **35**, 972.

[71.] P. J. Stang and B. Olenyuk, *Acc. Chem. Res.*, 1997, **30**, 502.

[72.] A. Reichert, H. Ringsdorf, and P. Schuhmuacher, in 'Comprehensive Supramolecular Chemistry' Vol 9, ed. J. L. Atwood, J. E. D. Davies, D. D. MacNicol, and F. Vögtle, Oxford, 1996, p. 313.

[73.] K. Umemoto, K. Yamaguchi, and M. Fujita, *J. Am. Chem. Soc.*, 2000, **122**, 7150.

[74.] C. J. Jones, *Chem. Soc. Rev.*, 1998, **27**, 289.

[75.] M. Fujita, *Chem. Soc. Rev.*, 1998, **27**, 417.

[76.] P. M. Stricklen, E. J. Volcko, and J. G. Verkade, *J. Am. Chem. Soc.*, 1983, **105**, 2494.

[77.] B. Olenyuk, P. J. Stang, and A. Fechtenkötter, *J. Chem. Soc., Dalton Trans.*, 1998, 1707.

[78.] F. M. Romero, R. Ziessel, A. Dupont-Gervais, and A. Van Dorsselaer, *Chem. Commun.*, 1996, 551.

[79.] M. D. Levin and P. J. Stang, *J. Am. Chem. Soc.*, 2000, **122**, 7428.

[80.] M. Fujita, J. Yazaki, and K. Ogura, *J. Am. Chem. Soc.*, 1990, **112**, 5645.

[81.] P. J. Stang and D. H. Cao, *J. Am. Chem. Soc.*, 1994, **116**, 4981.

[82.] P. J. Stang, D. H. Cao, S. Saito, and A. M. Arif, *J. Am. Chem. Soc.*, 1995, **117**, 6273.

[83.] S. Mann, G. Huttner, L. Zsolani, and K. Heinze, *Angew. Chem. Int. Ed.*, 1996, **35**, 2808.

[84.] E. B. Fleischer, *J. Am. Chem. Soc.*, 1964, **86**, 3889.

[85.] P. E. Eaton and T. W. Cole, *J. Am. Chem. Soc.*, 1964, **86**, 3157.

[86.] U. Müller and H. Sinning, *Angew. Chem. Int. Ed.*, 1989, **28**, 185.

[87.] M. R. Ghilardri, S. Midollini, S. Moneti, and A. Orlandini, *J. Chem. Soc., Chem. Commun.*, 1988, 1241.

[88.] A. Sekiguchi, T. Yatabe, H. Kamatani, C. Kabuto, and H. Sakurai, *J. Am. Chem. Soc.*, 1992, **114**, 6260.

[89.] S. Roche, C. Haslam, H. Adams, S. L. Heath, and J. A. Thomas, *Chem. Commun.*, 1998, 1681.

[90.] K. K. Klausmeyer, T. B. Rauchfuss, and S. R. Wilson, *Angew. Chem. Int. Ed.*, 1998, **37**, 1694.

[91.] K. K. Klausmeyer, S. R. Wilson, and T. B. Rauchfuss, *J. Am. Chem. Soc.*, 1999, **121**, 2705.

[92.] S. C. N. Hsu, M. Ramesh, J. H. Espenson, and T. B. Rauchfuss, *Angew. Chem. Int. Ed.*, 2003, **42**, 2663.

[93.] F. Herren, P. Fischer, A. Ludi, and W. Hälg, *Inorg. Chem.*, 1980, **19**, 956.

[94.] D. K. Chand, K. Biradha, M. Fujita, S. Sakamoto, and K. Yamaguchi, *Chem. Commun.*, 2002, 2486.

[95.] A. J. Blake, N. R. Champness, P. Hubberstey, W.-S. Li, M. A. Withersby, and M. Schröder, *Coord. Chem. Rev.*, 1999, **183**, 117.

[96.] P. Jensen, *The Synthesis, Structure and Magnetism of Coordination Polymers Incorporating Dicyanamide*, Ph.D. Thesis, Monash University, Melbourne, 2002.

[97.] S. R. Batten, *Curr. Opin. Solid State Mater. Sci.*, 2001, **5**, 107.

[98.] M. Eddaoudi, D. B. Moler, H. Li, B. Chen, T. M. Reineke, M. O'Keeffe, and O. Yaghi, *Acc. Chem. Res.*, 2001, **34**, 319.

[99.] B. Moulton and M. J. Zaworotko, *Chem. Rev.*, 2001, **101**, 1629.

[100.] K. T. Holman, A. M. Pivovar, J. A. Swift, and M. D. Ward, *Acc. Chem. Res.*, 2001, **34**, 107.

[101.] R. Robson, *J. Chem. Soc., Dalton Trans.*, 2000, 3735.

[102.] P. J. Hagrman, D. Hagrman, and J. Zubieta, *Angew. Chem. Int. Ed.*, 1999, **38**, 2638.

[103.] O. R. Evans, R.-G. Xiong, Z. Wang, G. K. Wong, and W. Lin, *Angew. Chem. Int. Ed.*, 1999, **38**, 536.

[104.] O. Yaghi, H. Li, C. Davis, D. Richardson, and T. L. Groy, *Acc. Chem. Res.*, 1998, **31**, 474.

[105.] C. J. Kepert and M. J. Rosseinsky, *Chem. Commun.*, 1999, 375.

[106.] D. M. L. Goodgame, S. Menzer, A. M. Smith, and D. J. Williams, *J. Chem. Soc., Dalton Trans.*, 1997, 3213.

[107.] L. Carlucci, G. Ciani, D. M. Proserpio, and A. Sironi, *J. Chem. Soc., Chem. Commun.*, 1994, 2755.

[108.] B. F. Hoskins and R. Robson, *J. Am. Chem. Soc.*, 1990, **112**, 1546.

[109.] R. Robson, in 'Comprehensive Supramolecular Chemistry' Vol 6, ed. J. L. Atwood, J. E. D. Davies, D. D. MacNicol, and F. Vögtle, Oxford, 1996, p. 733.

[110.] A. F. Wells, *Three-Dimensional Nets and Polyhedra*, John Wiley & Sons, New York, 1977.

[111.] S. R. Batten and R. Robson, *Angew. Chem. Int. Ed.*, 1998, **37**, 1460.

[112.] Cambridge Structural Database Ver 5.24 (updates April 2003), 2003, CCDC

[113.] I. J. Bruno, J. C. Cole, P. R. Edgington, M. Kessler, C. F. Macrae, P. McCabe, J. Pearson, and R. Taylor, *Acta. Crystallogr.*, 2002, **B58**, 398.

[114.] J. Tao, M.-L. Tong, and X.-M. Chen, *J. Chem. Soc., Dalton Trans.*, 2000, 3669.

[115.] G. Li, C. Davis, T. L. Groy, D. Kelley, and O. Yaghi, *J. Am. Chem. Soc.*, 1998, **120**, 2186.

[116.] H. Li, M. Eddaoudi, M. O'Keeffe, and O. Yaghi, *Nature*, 1999, **402**, 276.

[117.] M. Eddaoudi, J. Kim, N. Rosi, D. Vodak, J. Wachter, M. O'Keeffe, and O. Yaghi, *Science*, 2002, **295**, 469.

[118.] O. Yaghi, M. O'Keeffe, N. W. Ockwig, H. K. Chae, M. Eddaoudi, and J. Kim, *Nature*, 2003, **423**, 705.

[119.] *Chem. Br.*, 2003, **39**, 17.

[120.] B. McEnaney, *Chem. Br.*, 2003, **39**, 24.

[121.] N. Rosi, J. Eckert, M. Eddaoudi, D. Vodak, J. Kim, M. O'Keeffe, and O. Yaghi, *Science*, 2003, **300**, 1127.

[122.] D. Demazeau, *J. Mater. Chem.*, 1999, **9**, 15.

[123.] S. Feng and R. Xu, *Acc. Chem. Res.*, 2001, **34**, 239.

[124.] Ocean_Explorer, 2003, http://oceanexplorer.noaa.gov/explorations/02fire/background/vent_chem/media/chemistry.html

[125.] J. McMurry, *Organic Chemistry*, Brooks/Cole, Belmont, 1992.

[126.] B. S. Furniss, A. J. Hannaford, P. W. G. Smith, and A. R. Tatchell, *Vogel's Textbook of Practical Organic Chemistry*, Addison Wesley Longmann, Harlow, 1996.

[127.] M. J. Hannon, C. L. Painting, and N. W. Alcock, *Chem. Commun.*, 1999, 2023.

[128.] J. Hamblin, A. Jackson, N. W. Alcock, and M. J. Hannon, *J. Chem. Soc., Dalton Trans.*, 2002, 1635.

[129.] HyperChem Standard, Version 7, 2002, HyperCube, Inc.

[130.] P. E. Kruger, B. Moubaraki, and K. S. Murray, *Polyhedron*, 1997, **16**, 2659.

[131.] P. N. W. Baxter, J.-M. Lehn, J. Fischer, and M.-T. Youinou, *Angew. Chem. Int. Ed.*, 1994, **33**, 2284.

[132.] D. Hellwinkel and H. Fritsch, *Chem. Ber.*, 1990, **123**, 2207.

[133.] Fluka, 2003, http://www.sigmaaldrich.com/Brands/Fluka___Riedel_Home/Analytical/Microscopy/Stains_and_Dyes.html

[134.] M. Aygun, S. Ozturk, and F. Aydogan, *Acta. Crystallogr.*, 2002, **E58**, o158.

[135.] M. Aygun, S. Isik, T. Turgut, S. Ozbey, and E. Kendi, *Acta. Crystallogr.*, 1999, **C55**, 1689.

[136.] A. L. Vance, N. W. Alcock, J. A. Heppert, and D. H. Busch, *Inorg. Chem.*, 1998, **37**, 6912.

[137.] V. C. Gibson, C. Redshaw, and M. R. J. Elsegood, *New J. Chem.*, 2002, **26**, 16.

[138.] A. T. Vallina and H. Stoeckli-Evans, *Acta. Crystallogr.*, 2001, **C57**, 489.

[139.] P. E. Kruger, N. Martin, and M. Nieuwenhuyzen, *Unpublished results.*

[140.] K. Senechal, 2002, Personal Communication

[141.] A. Marquis, J. P. Kintzinger, R. Graff, P. N. W. Baxter, and J.-M. Lehn, *Angew. Chem. Int. Ed.*, 2002, **41**, 2760.

[142.] MassLynx™, Version 3.5, 2000, Micromass Ltd

[143.] G. J. Kubas, in 'Inorganic Syntheses' Vol 28, 1990, p. 68.

[144.] B. Conerney, P. Jensen, P. E. Kruger, and C. MacGloinn, *Chem. Commun.*, 2003, 1274.

[145.] S. J. Gaskell, *J. Mass Spectrom.*, 1997, **32**, 677.

[146.] J. Lacour, 2003, Personal Communication

[147.] J. J. Jodry and J. Lacour, *Chem. Eur. J.*, 2000, **6**, 4297.

[148.] H. Ogino, *J. Am. Chem. Soc.*, 1981, **103**, 1303.

[149.] P. J. Stang, B. Olenyuk, J. Fan, and A. M. Arif, *Organometallics*, 1996, **15**, 904.

[150.] M. Fujita, O. Sasaki, T. Mitsuhashi, T. Fujita, J. Yazaki, K. Yamaguchi, and K. Ogura, *Chem. Commun.*, 1996, 1535.

[151.] M. Fujita, S. Nagao, M. Iida, K. Ogata, and K. Ogura, *J. Am. Chem. Soc.*, 1993, **115**, 1574.

[152.] R. J. Morgan and A. D. Baker, *J. Org. Chem.*, 1990, **55**, 1986.

[153.] M. A. Hayes, C. Meckel, E. Schatz, and M. D. Ward, *J. Chem. Soc., Dalton Trans.*, 1992, 703.

[154.] M. E. B. Higgins, *A Study of Hydrogen-Deuterium Exchange on the Photophysical Properties of Ruthenium(II) Polypyridyl Complexes*, Ph.D. Thesis, University of Dublin, Dublin, 2001.

[155.] P. de Wolf, S. L. Heath, and J. A. Thomas, *Chem. Commun.*, 2002, 2540.

[156.] M. Hernández-Molina, F. Lloret, C. Ruiz-Pérez, and M. Julve, *Inorg. Chem.*, 1998, **37**, 4131.

[157.] D. Szalda, C. Creutz, D. Mahajan, and N. Sutin, *Inorg. Chem.*, 1983, **22**, 2372.

[158.] Y. Ohashi, K. Yanagu, Y. Mitsuhashi, K. Nagata, Y. Kaizu, Y. Sasada, and H. Kobayashi, *J. Am. Chem. Soc.*, 1979, **101**, 4739.

[159.] F. H. Allen, *Acta. Crystallogr.*, 2002, **B58**, 380.

[160.] M. J. Zaworotko, *Chem. Soc. Rev.*, 1994, 283.

[161.] J. A. Real, G. De Munno, M. C. Muñoz, and M. Julve, *Inorg. Chem.*, 1991, **30**, 2701.

[162.] L. R. MacGillivray, S. Subramanian, and M. J. Zaworotko, *J. Chem. Soc., Chem. Commun.*, 1994, 1325.

[163.] S. D. Huang and R.-G. Xiong, *Polyhedron*, 1997, **16**, 3929.

[164.] S. R. Batten, J. C. Jeffery, and M. D. Ward, *Inorg. Chim. Acta*, 1999, **292**, 231.

[165.] P. W. Carreck, M. Goldstein, E. M. McPartlin, and W. D. Unsworth, *J. Chem. Soc., Chem. Commun.*, 1971, 1634.

[166.] S. Kitagawa, M. Munakata, and T. Tanimura, *Inorg. Chem.*, 1992, **31**, 1714.

[167.] J. Darriet, M. S. Haddad, E. N. Duesler, and D. N. Hendrickson, *Inorg. Chem.*, 1979, **18**, 2679.

[168.] D. Hagrman, C. Zubieta, D. J. Rose, J. Zubieta, and R. C. Haushalter, *Angew. Chem. Int. Ed.*, 1997, **36**, 873.

[169.] R. W. Gable, B. F. Hoskins, and R. Robson, *J. Chem. Soc., Chem. Commun.*, 1990, 1677.

[170.] F. Robinson and M. J. Zaworotko, *J. Chem. Soc., Chem. Commun.*, 1995, 2413.

[171.] O. Yaghi and H. Li, *J. Am. Chem. Soc.*, 1996, **118**, 295.

[172.] M. Kondo, T. Yoshitomi, K. Seki, H. Matsuzaka, and S. Kitagawa, *Angew. Chem. Int. Ed.*, 1997, **36**, 1725.

[173.] M.-L. Tong, B.-H. Ye, J.-W. Cai, X.-M. Chen, and S. W. Ng, *Inorg. Chem.*, 1998, **37**, 2645.

[174.] S.-J. Chen, X.-T. Chen, Z. Xue, J.-H. Zhou, J. Li, J.-M. Hong, and X.-Z. You, *J. Mater. Chem.*, 2003, **13**, 1132.

[175.] S. M.-F. Lo, S. S.-Y. Chui, F. L.-Y. Shek, C. Z.-J. Lin, X. X. Zhang, G.-H. Wen, and I. D. Williams, *J. Am. Chem. Soc.*, 2000, **122**, 6293.

[176.] J. Y. Lu, C. Norman, K. A. Abboud, and A. Ison, *Inorg. Chem. Commun.*, 2001, **4**, 459.

[177.] O. Yaghi, H. Li, and T. L. Groy, *Inorg. Chem.*, 1997, **36**, 4293.

[178.] H. W. Park, S. M. Sung, K. S. Min, H. Bang, and M. P. Suh, *Eur. J. Inorg. Chem.*, 2001, 2857.

[179.] B. Moulton, E. B. Rather, and M. J. Zaworotko, *Cryst. Eng.*, 2001, **4**, 309.

[180.] K. Biradha, K. V. Domasevitch, B. Moulton, C. Seward, and M. J. Zaworotko, *Chem. Commun.*, 1999, 1327.

[181.] K. Biradha, A. Mondal, B. Moulton, and M. J. Zaworotko, *J. Chem. Soc., Dalton Trans.*, 2000, 3837.

[182.] K. Biradha, K. V. Domasevitch, C. Hogg, B. Moulton, K. N. Power, and M. J. Zaworotko, *Cryst. Eng.*, 1999, **2**, 37.

[183.] K. Biradha and M. Fujita, *Chem. Commun.*, 2001, 15.

[184.] GEMINI, Autoindexing Program for Twinned Crystals, Version 1.02 Release 5/2000, 1999, Bruker-AXS Inc.

[185.] TWINABS, Version Beta Test, 2003, Bruker-AXS Inc.

[186.] Y.-S. Zhang, G. D. Enright, S. R. Breeze, and S. Wang, *New J. Chem.*, 1999, **23**, 625.

[187.] J. Lu, C. Yu, T. Niu, T. Paliwala, G. Crisci, F. Somosa, and A. J. Jacobson, *Inorg. Chem.*, 1998, **37**, 4637.

[188.] P. Chaudhuri, K. Oder, K. Wieghardt, S. Gehring, W. Haase, B. Nuber, and J. Wiess, *J. Am. Chem. Soc.*, 1988, **110**, 3657.

[189.] M.-L. Tong, X.-M. Chen, X.-L. Lu, and T. C. W. Mak, *J. Chem. Soc., Dalton Trans.*, 1998, 5.

[190.] B.-Q. Ma, H.-L. Sun, S. Gao, and G.-X. Xu, *Inorg. Chem.*, 2001, **40**, 6247.

[191.] A. J. Blake, S. J. Hill, P. Hubberstey, and W.-S. Li, *J. Chem. Soc., Dalton Trans.*, 1997, 913.

[192.] S.-I. Noro, R. Kitaura, M. Kondo, S. Kitagawa, T. Ishii, H. Matsuzaka, and M. Yamashita, *J. Am. Chem. Soc.*, 2002, **124**, 2568.

[193.] J. Lu and A. M. Babb, *Chem. Commun.*, 2001, 821.

[194.] A. J. Blake, N. R. Champness, A. Khlobystov, D. A. Lemenovskii, W.-S. Li, and M. Schröder, *Chem. Commun.*, 1997, 2027.

[195.] P. de Meester, S. R. Fletcher, and A. C. Skapski, *J. Chem. Soc., Dalton Trans.*, 1973, 2575.

[196.] L. Carlucci, G. Ciani, D. M. Proserpio, and A. Sironi, *J. Chem. Soc., Dalton Trans.*, 1997, 1801.

[197.] J. Tao, M.-L. Tong, J.-X. Shi, X.-M. Chen, and S. W. Ng, *Chem. Commun.*, 2000, 2043.

[198.] M. Sasa, K. Tanaka, X.-H. Bu, M. Shiro, and M. Shionoya, *J. Am. Chem. Soc.*, 2001, **123**, 10750.

[199.] C.-D. Wu, C.-Z. Lu, D.-M. Wu, H.-H. Zhuang, and J.-S. Huang, *Inorg. Chem. Commun.*, 2001, **4**, 561.

[200.] J.-G. Mao, Z. Wang, and A. Clearfield, *New J. Chem.*, 2002, **26**, 1010.

[201.] S.-I. Noro, M. Kondo, I. Tomohiko, S. Kitagawa, and H. Matsuzaka, *J. Chem. Soc., Dalton Trans.*, 1999, 1569.

[202.] S.-I. Noro, M. Kondo, S. Kitagawa, T. Ishii, and H. Matsuzaka, *Chem. Lett.*, 1999, 727.

[203.] J. Lu, T. Paliwala, S. C. Lim, T. Niu, and A. J. Jacobson, *Inorg. Chem.*, 1997, **36**, 923.

[204.] R. Carballo, A. Castineiras, B. Covelo, and E. M. Vazquez-Lopez, *Polyhedron*, 2001, **20**, 899.

[205.] B.-Q. Ma, S. Gao, T. Yi, and G.-X. Xu, *Polyhedron*, 2001, **20**, 1255.

[206.] M. Kondo, M. Shimamura, S.-I. Noro, T. Yoshitomi, S. Minakoshi, and S. Kitagawa, *Chem. Lett.*, 1999, 285.

[207.] L.-M. Zheng, X. Fang, K.-H. Lii, H.-H. Song, X.-Q. Xin, H.-K. Fun, K. Chinnakali, and I. A. Razak, *J. Chem. Soc., Dalton Trans.*, 1999, 2311.

[208.] C.-H. Huang, L.-H. Huang, and K.-H. Lii, *Inorg. Chem.*, 2001, **40**, 2625.

[209.] O. Yaghi, G. Li, and T. L. Groy, *J. Am. Chem. Soc.*, 1996, **118**, 9096.

[210.] C. J. Kepert and M. J. Rosseinsky, *Chem. Commun.*, 1998, 31.

[211.] T. Whitfield, L.-M. Zheng, X. Wang, and A. J. Jacobson, *Solid State Sciences*, 2001, **3**, 829.

[212.] B. Gomez-Lor, E. Gutierrez-Puebla, M. Iglesias, M. A. Monge, C. Ruiz-Valero, and N. Snejko, *Inorg. Chem.*, 2002, **41**, 2429.

[213.] S. W. Lee and J. Y. Baeg, *Inorg. Chem. Commun.*, 2003, **6**, 313.

[214.] O. Ermer and L. Lindenberg, *Helv. Chim. Acta*, 1988, **71**, 1084.

[215.] S. C. Hawkins, R. Bishop, I. G. Dance, T. Lipari, D. C. Craig, and M. L. Scudder, *J. Chem. Soc., Perkin Trans. 2*, 1993, 1729.

[216.] R. Bishop, I. G. Dance, and S. C. Hawkins, *J. Chem. Soc., Chem. Commun.*, 1983, 889.

[217.] S. C. Hawkins, R. Bishop, D. C. Craig, I. G. Dance, A. D. Rae, and M. L. Scudder, *J. Chem. Soc., Perkin Trans. 2*, 1993, 1737.

[218.] L. Carlucci, N. Cozzi, G. Ciani, M. Moret, D. M. Proserpio, and S. Rizzato, *Chem. Commun.*, 2002, 1354.

[219.] R. H. Groenemann, L. R. MacGillivray, and J. L. Atwood, *Inorg. Chem.*, 1999, **38**, 208.

[220.] C. S. Hong and Y. Do, *Inorg. Chem.*, 1997, **36**, 5684.

[221.] W. Mori, F. Inoue, K. Yoshida, H. Nakayama, S. Takamizawa, and M. Kishita, *Chem. Lett.*, 1997, 1219.

[222.] S. R. Batten, 2003, Personal Communication

[223.] Bruker SAINT-NT, Version 6.22, 2003, Bruker-AXS Inc.

[224.] A. W. Addison, T. N. Rao, J. Reedijk, and G. C. Verschoor, *J. Chem. Soc., Dalton Trans.*, 1984, 1349.

[225.] C. S. Gibbons and J. Trotter, *J. Chem. Soc. (A)*, 1971, 2058.

[226.] M. S. Kalliomäki and V. P. J. Meisalo, *Acta. Crystallogr.*, 1979, **B35**, 2829.

[227.] V. Luzzati, *Acta. Crystallogr.*, 1951, **4**, 120.

[228.] P. F. Lindley and P. Woodward, *J. Chem. Soc. (A)*, 1966, 123.

[229.] C. D. Garner, D. Sutton, and S. C. Wallwork, *J. Chem. Soc. (A)*, 1967, 1949.

[230.] A. L. Spek, PLATON - A Multipurpose Crystallographic Tool, 10M - Ver. 70403, 2003,

[231.] A. L. Spek, *Acta. Crystallogr.*, 1990, **A46**, C34.

[232.] L. J. Farrugia, Platon for Windows Taskbar, Ver. 1.07, 2003,

[233.] Bruker SMART, Version 5.625, 1997-2001, Bruker-AXS Inc.

[234.] Bruker SAINT-NT, Version 6.02a, 1997-2001, Bruker-AXS Inc.

[235.] SADABS, Version 2.03, 1999, Bruker-AXS Inc.

[236.] G. M. Sheldrick, SHELXTL, Version 5.1, 1998, Bruker-AXS Inc.

[237.] M. G. B. Drew, D. Farrell, G. G. Morgan, V. McKee, and J. Nelson, *J. Chem. Soc., Dalton Trans.*, 2000, 1513.

[238.] M. Eddaoudi, J. Kim, J. Wachter, H. K. Chae, M. O'Keeffe, and O. Yaghi, *J. Am. Chem. Soc.*, 2001, **123**, 4368.

[239.] T. J. Barton, L. M. Bull, W. G. Klemperer, D. A. Loy, B. McEnaney, M. Misono, P. A. Monson, G. Pez, G. W. Scherer, J. C. Vartuli, and O. Yaghi, *Chem. Mater.*, 1999, **11**, 2633.